

Trade-off in building with soft soils

A framework to assess the impact of optimizations on Production Estimating or Reclamation Engineering on project costs

Master's Thesis

C.P.W.A. Smeenk

Delft University of Technology

Trade-off in building with soft soils

A framework to assess the impact of
optimizations on Production Estimating or
Reclamation Engineering on project costs

by

C.P.W.A. Smeenk

to obtain the degree of Master of Science

at the Delft University of Technology,

to be defended publicly on Wednesday January 15th, 2024 at 14:00.

Student number:	4679101	
Project duration:	May, 2024 – December 2024	
Thesis committee:	Prof. dr. ir. M. van Koningsveld,	TU Delft (chair), Van Oord
	Dr. C. Chassagne,	TU Delft (supervisor)
	ir. M. de Geus,	Van Oord (supervisor)
	Dr. ir. C. Hoffmann,	Van Oord (supervisor)
	ir. I. Myouri,	TU Delft (supervisor)

This thesis is confidential and cannot be made public.

An electronic un-classified version of this thesis is available at <http://repository.tudelft.nl/>.

Preface

Before you lies a master's thesis "A trade-off in building with soft soils", written to obtain the *MSc Civil Engineering* degree at Delft University of Technology (TU Delft). This thesis marks the end of an exciting last 8 months into the world of dredging and land reclamations at Van Oord. I am truly thankful for the opportunity to complete my graduation project at this outstanding company. What stood out to me the most was the company mentality and the helpfulness of every colleague I met. Thanks to the support and kindness of everybody at Van Oord, I was able to further develop my interest in the dredging world. Most importantly, I was able to have a fantastic time throughout the graduation process.

Thanks to the support and kindness of everyone at Van Oord, I was able to further develop my interest in the dredging industry and, most importantly, have a fantastic time throughout the graduation process.

First and foremost, I want to thank Martin de Geus for the many hours we spent discussing the production model and the overall topic of graduation. I enjoyed diving into the details with you, as I have made big personal steps in the past half year. Your enthusiasm for the dredging industry has inspired me and started my own passion for dredging industry and production estimation. I also appreciate your availability and the way you have always assisted quickly in answering any of my questions or requests. I am very grateful that you took me along on this journey into the world of dredging.

I would also like to thank Christian for everything I learned from our discussions and your approach to solving land reclamation and geotechnical challenges. You always took the time to explain geotechnical concepts clearly, and your passion for the field has left a big impression on me. I also really enjoyed our personal conversations and appreciated how you made time for me, even when you were working from Spain or during your holidays in Uruguay. Your dedication, help and expert judgment has helped made personal steps over the past half year.

Next, I want to thank Claire Chassagne and Ismail Myouri for the valuable insights you shared during our meetings. You were always available for feedback and discussions, which really helped me move forward. Claire, I especially enjoyed our trip to Eindhoven, where you showed me the NMR equipment in action. Both of you brought so much energy and enthusiasm to your research and the academic world, and that enthusiasm inspired me as well. I truly enjoyed working with you and learning from your personal insights during the past half year.

I would like to thank Mark for arranging and giving me the opportunity to start my graduation thesis at Van Oord. From the very beginning, I enjoyed our discussions, from the initial topic brainstorming to the later stages where you helped me stay on track. Your detailed feedback throughout the process was invaluable and greatly helped me to improve my work.

Finally, I would like to thank my parents, Sis and Pieter Smeenk, for all their guidance and trust over the past 20 years. Thanks to you I have been able to come to the point where we are at now. I am deeply grateful for the encouragement you provided during both the easy and challenging times. Your belief in me has always inspired me to stay positive, work hard, and strive to achieve my goals. Thank you for enabling me to bring out the best in myself.

*C.P.W.A. Smeenk
Rotterdam, January 2025*

Abstract

Sand utilization has increased over the past decades and is getting a scarce resource globally. In Singapore, no sand is available for construction purposes or land reclamation projects. The increasing scarceness of “suitable” sandy building materials around the world forces the dredging industry to consider the usage of alternative “complex” materials for land reclamation purposes. However, working with these kinds of “complex” materials introduces operational and technical challenges on the estimation of project duration and costs, due to their low permeability, high compressibility and complex consolidation behaviour of this slurry material.

The main involved departments on land reclamation projects are the production department and the geotechnical department. The production department is responsible for “Production Estimation” and estimates the rate of which soil can be produced by transporting it from the dredging area to the reclamation area, considering specific equipment choices and costs. The geotechnical department is responsible for “Reclamation Engineering” and handles the engineering of the soil brought in by production to be formed into a soil which is eventually usable for the client.

Two reclamation projects of the past; the “Scandinavia” and “Black Sea” project have proven that Production Estimation and Reclamation Engineering are closely connected when working with “complex” material. While working with “suitable” sandy materials primarily focuses on minimizing project costs through optimizing Production Estimation, the effects of Reclamation Engineering optimizations increases significantly when dealing with “complex” materials. This is due to their long duration of consolidation and the potentially high costs of soil improvements required before the asset can be delivered to the client. In this context, optimizing Production Estimation by dredging at low initial density comes at the expense of Reclamation Engineering as low initial density often results in longer and more costly consolidation, and vice versa. Therefore, it can be concluded that a trade-off exists in optimizing for Production Estimation and Reclamation Engineering in minimizing project costs.

It becomes evident from the literature review that no specific research is dedicated to investigating the effect of the trade-off between optimizing Production Estimation or Reclamation Engineering in minimizing project costs. Therefore, the main research objective of this thesis is to answer the question:

*“How can project costs be minimized by explicitly balancing the trade-off between optimizing for **Production Estimation and Reclamation Engineering**?”*

This thesis provides a new framework for evaluating the effects of the trade-off between Production Estimation and Reclamation Engineering optimizations on total project costs, in order to answer the main research question. This framework couples production estimation models to geotechnical estimation models by OpenCLSim and a large-strain consolidation model. This integral approach enables the simulation of the continuous reclamation construction process, including filling, self-weight consolidation and long-term consolidation under the effect of ground improvement methods. The proposed framework is subjected to a case-study to assess how optimizations on Production Estimation and Production Engineering affect consolidation behaviour and project costs. In this analysis optimizations are implemented by varying initial density coming with hydraulic and mechanical dredging work methods. This thesis evaluates these optimizations in three stages; single production cycle, production - self-weight consolidation analysis, and a full scale case study including long-term consolidation under the effect of ground improvement methods. The full-scale case study is evaluated using a hydraulic work method of 1100 kg/m³ and a mechanical work method of 1300 kg/m³. The production and reclamation models are calibrated by the material characteristics from the case-study, whereas the large-strain consolidation method is calibrated and validated by physical samples from the project site.

Results from the full scale case-study show that utilizing a mechanical method at 1300 kg/m³ (aimed at optimizing Reclamation Engineering) results in a **1,86 more expensive** project than using a hydraulic method at 1100 kg/m³ (aimed for optimizing Production Estimation). Almost no differences occur be-

tween Reclamation Engineering costs for the two dredging work methods as the case-study material quickly consolidates and converges to a similar compaction profile within a similar time-frame. Consequently, the potential advantage of achieving a higher initial density using the mechanical method is diminished by its lower production rates and high costs. By converging to a similar compaction state within the same duration creates no significant differences between the ground improvement methods needed to force the profile to comply to design requirements. This will lead to almost no differences in costs for Reclamation Engineering. As a result, only optimizations in Production Estimation can lead to minimization of the project costs for the considered case-study material.

Nevertheless, it can be concluded that it is possible to get insights on how to minimize project costs based on the trade-off between Production Estimation and Reclamation Engineering when using a framework which couples their interactions through self-weight (large-strain) consolidation and Open-CLSim. The existence of the trade-off and its magnitude on minimizing project costs depends on the soil type used in the project. “Complex” materials that tend towards relatively “well-consolidating” seem to reduce the magnitude of the trade-off, while it is believed that more “poor-consolidating” materials enhance the magnitude of the trade-off. Therefore, the predictability of the trade-off between Production Estimation and Reclamation Engineering optimizations is closely related to the understanding of production effects (varying initial density and varying duration between layer stacking) on the consolidation behaviour of the slurry material.

The proposed framework in this thesis is believed to be a first step in estimating project costs and duration based on a physics-based approach, compared to the current “empirical estimations” that are used to represent physical processes such as large-strain consolidation. The proposed framework could lead to a more integrated understanding between Production Estimation and Production Engineering when using “complex” material and more insights on how optimizations between the two departments can minimize project costs.

Contents

Preface	i
Abstract	ii
1 Introduction	1
1.1 Evolution in land reclamation projects	1
1.2 Work method trade-off	1
1.3 Problem description	3
1.4 Research objective	3
1.5 Research scope	3
1.6 Research structure	4
2 Literature Review	5
2.1 Production Estimating	6
2.2 Reclamation Engineering	6
2.3 Production Estimation - Reclamation Engineering coupling	7
2.4 Company experience	8
2.5 Literature review statement	10
3 Theoretical framework & Case-study	11
3.1 Theoretical framework	11
3.1.1 Production Estimation	12
3.1.2 Reclamation Engineering	16
3.1.3 Coupling Production - Reclamation	19
3.2 Case-Study	21
3.2.1 Overview	21
3.2.2 Framework Calibration	27
3.2.3 Framework Validation	30
3.2.4 Optimizations Production Estimation - Reclamation Engineering	31
4 Results	33
4.1 Production - single dredging cycle analysis	33
4.2 Production - self-weight consolidation analysis	34
4.3 Full scale case-study	39
5 Discussion	45
5.1 Interpretation of results	45
5.2 Research limitations	48
5.3 Research implications	50
6 Conclusion	52
7 Recommendations	57
References	60
A Production Estimation	63
A.1 Soil cutting	63
A.2 Sailing: Holtrop & Mennen method	70
A.3 Hydraulic production	75
A.3.1 Trailing Production	76
A.3.2 Sailing	83
A.3.3 Discharge production	83

A.3.4	Power Utilization	87
A.4	Mechanical production	90
A.4.1	Loading production	90
A.4.2	Sailing	98
A.4.3	Discharge production	99
A.4.4	Power utilization	99
A.5	Costs	101
A.6	Production Estimation calculations	107
A.6.1	Hydraulic production	107
A.6.2	Mechanical production	109
B	Reclamation Engineering	111
B.1	Reclamation process	111
B.2	Fill material	112
B.3	Consolidation	116
B.3.1	Large-strain consolidation	116
B.3.2	Small-Strain consolidation	123
B.4	Design requirements	127
B.5	Ground improvement methods	127
B.6	Costs	129
B.7	Large-Strain consolidation: numerical computations	130
B.8	Small-Strain consolidation: numerical computations	135
C	Soil sample analysis	138
C.1	Laboratory experiments	138
C.1.1	Settling column tests	138
C.1.2	Grain size distribution	140
C.1.3	Attenberg limits	141
C.2	Calibration tests	143
C.2.1	Carrier & Beckham calibration	143
C.2.2	Analytical solution calibration	144
C.3	Discussion: calibration method testing	146

1

Introduction

1.1. Evolution in land reclamation projects

Land reclamation projects heavily rely on sand, since sand is the best building material for the creation of new land, due to its favourable engineering properties. Sand utilization has increased over the past decades to 50 metric tons, and is getting a scarce recourse globally (UNEP, [2022](#)). In the Netherlands, the demand for sand has surged due to rising sea levels and the increasing need for sand in coastal defense projects. Meanwhile, in Singapore, no sand is available locally for construction or land reclamation purposes, as all surrounding countries have exhausted their sand resources (RTL, [2024](#)). This situation has significant consequences for land reclamation projects in regions where sand is not widely available. In addition to the worldwide scarcity of sand, increased environmental awareness and stricter regulations on sediment spill are imposing additional constraints on dredging companies, as sediment overflow can harm marine ecosystems. This has consequences for dredging companies because overflow of sediment is used to segregate “unsuitable” material from the “suitable” material in a hopper. The combination of sand scarcity and environmental restrictions has forced the industry to consider the use of alternative “complex” materials for reclamation purposes in order to comply with the environmental scope of the client and the availability of sand resources.

“Complex” materials have the property that they consist of high fines fraction. This means that the material used, consists of a soil structure where small grain-sized particles dominate its engineering properties. Several important physical properties are the result of this high fines fraction, including low permeability and high compressibility. Fine-grained soil bodies consist of very small continuous pore spaces between the particles, creating low permeability. High compressibility occurs because of the materials ability to compact significantly under loading. These material properties may lead to settlement and consolidation time-frames of years to even decades when these particles are mixed with water during dredging and placed in a reclamation (Van Rijn, [2019](#)).

For dredging companies, transitioning from working with “suitable” sandy materials to “complex” fine grained materials introduces operational and technical challenges. These include managing bulking, high time-frames for self-weight consolidation and high compaction of the slurry (IADC, [2020b](#)), and potentially high costs for ground improvement measures to improve the soil. Addressing these challenges requires innovative approaches to project execution strategies to ensure a reliable end product and maintain the economic viability of these kind of projects.

1.2. Work method trade-off

The main involved departments on land reclamation projects are the production department and the geotechnical department. The production department is responsible for “Production Estimation” and estimates the rate of which soil can be produced by transporting it from the dredging area to the reclamation area, considering specific equipment choices and costs. The geotechnical department is responsible for “Reclamation Engineering” and handles the engineering of the soil brought in by production to be formed into a soil which is eventually usable for the client. In this process, soil improvement

strategies, duration of consolidation and costs before the asset can be delivered to the client are important. The geotechnical department must work with the soil as delivered by the production department, where factors such as initial density and segregation caused by placement methods significantly influence its consolidation behavior. These production-related effects often dictate how the geotechnical department processes the material to transform it into a usable product for the client. Conversely, the consolidation behavior of the material influences the quantity of material that the production department needs to deliver. Therefore, production and geotechnical aspects are closely interconnected. Where in the past production costs dominated the total project costs, now geotechnical costs are getting more important, since more engineering is needed to obtain a good quality asset with “complex” material. Efficient interconnection between the production and geotechnical departments is needed to ensure a strong business case for land reclamation tenders. It is often assumed that optimizations in one department, such as production (favoring lower initial density), do not align with the interests of the geotechnical department (favoring higher initial density) and vice versa.

The relation between *Production Estimation* and *Reclamation Engineering* raises the following question at engineering departments of dredging companies: *How does optimizing production estimation or reclamation engineering affect our business case when we are forced to work with “complex” materials?* One potential solution could involve alternating dredging work methods; hydraulic dredging aimed at optimizing production aspects and mechanical dredging focused on optimizing geotechnical aspects.



Figure 1.1: “Suitable” building materials vs “complex” building materials for land reclamation application.

The two main dredging work methods are hydraulic dredging and mechanical dredging. These methods are often used in capital dredging projects. Hydraulic dredging uses suction heads that suck the seabed material and mix it with water in order to transport it through pipelines. Mechanical dredging often considers backhoe or clamshell excavation of the sea-floor material and transportation by barges.

Hydraulic dredging is generally considered to be the relatively fastest and cheapest dredging method. This dredging method optimizes the costs of the Production Estimation phase, due to its relatively high production rate. However, the downside of the hydraulic method is that it mixes the dredged soil with water in order to transport it through pipelines. The material will end up with a relatively low density in the reclamation. Low initial density generally disfavours consolidation behaviour of “complex” material. The hydraulic dredging method will generally lead to longer consolidation time-frames and an increase of Reclamation Engineering costs, because more ground improvement methods are required to obtain a soil profile which complies with the design requirements of the client.

Mechanical dredging can be more expensive and more time consuming compared to hydraulic dredging, depending on the case. This dredging method generally disfavours the costs of the Production Estimation phase, due to its relatively low production rates. In a general sense, the mechanical dredging method has the advantage of conserving more of the in-situ properties of the dredged material by not mixing it with additional water. This is because the material is lifted mechanically by the backhoe bucket through the water column. The material will end up with a relatively high density in the reclamation. High initial density generally favours consolidation behaviour of “complex” material. The mechanical dredging method will generally lead to shorter consolidation time-frames and a decrease

of Reclamation Engineering costs, because less ground improvement methods are needed in order to obtain a soil profile which complies with the design requirements of the client.

The aim of a dredging company is to optimize the complete project on costs, leading to the best business case for the company and the best chance to win a project tender. The above considerations of the different dredging methods illustrate that the fastest and cheapest dredging method may not necessarily lead to the fastest and cheapest consolidation phase, especially when using “complex” materials. In addition, the above also suggests that choosing different dredging work methods can optimize either production costs (making them cheaper or faster) or reclamation costs (by reducing consolidation time-frames). This makes it evident that a trade-off exists between the choice of optimization between *Production Estimation* and *Reclamation Engineering* in relation to the project costs.

1.3. Problem description

Quantifying the trade-offs between production and geotechnical optimization is a present-day topic for dredging companies. Historically, working with sand introduce minimal challenges, allowing production costs to dominate over geotechnical costs due to the material's favourable engineering properties. However, the shift to working with “complex” materials has created new challenges, demanding a different strategy for project cost and project duration planning. In some cases, prioritizing geotechnical optimization over production efficiency may lead to a stronger business case. This highlights the need for innovative strategies to address the new challenges created by using these “complex” materials.

The following main challenges have been identified when working with “complex” materials, according to company experts:

- A framework is missing which includes the integral approach between Production and Geotechnics for realizing land reclamations with “complex” soils.
- A quantification of optimization effect on either *production estimation* or *reclamation engineering*, by altering hydraulic and mechanical dredging work methods is missing.
- The current way of estimating engineering parameters of soil is based on empirical databases. A estimation tool, characterizing soil properties based on physics is missing.

1.4. Research objective

The main research objective is to answer the following research question: *How can project costs be minimized by explicitly balancing the trade-off between optimizing for **Production Estimation** or **Reclamation Engineering**?*

To answer the main research question, several sub-questions (SQ's) are formulated.

- SQ1. How can a quantitative framework be developed to assess the impacts of *Production Estimation* and *Reclamation Engineering* optimizations on project costs?
- SQ2. Which *Production Estimation* related factors affect the duration and costs of hydraulic and mechanical dredging work methods?
- SQ3. Which *Reclamation Engineering* related factors do affect the duration and costs of the consolidation phase of placed material?
- SQ4. How can the cost and duration of *Production Estimation* for hydraulic and mechanical work methods, along with the costs and duration for *Reclamation Engineering* be modeled?
- SQ5. What are the main effects of production-reclamation interactions on consolidation behavior, and how do these interactions influence consolidation?
- SQ6. How do production-reclamation optimizations influence project duration and costs?

1.5. Research scope

This thesis aims to propose an initial framework for estimating project costs, focusing on the integral relationship between Production Estimation and Reclamation Engineering. The framework simplifies physical processes into numerical models by introducing assumptions to simplify complex calculations.

Production Estimation will be modeled using simplified, physics-based approaches aimed at approximating production duration and costs. Production is assumed to be a continuous process, neglecting workability factors and environmental constraints such as emissions and sediment spill associated with specific equipment use. Cost estimates for production are limited to weekly vessel costs and fuel expenses, excluding commercial and other cost aspects.

Reclamation Engineering assumes that the consolidation process is one-dimensional, neglecting two-dimensional effects caused by high-energy placement techniques and segregation. The consolidating slurry or soil is assumed to be homogeneous. Cost considerations are restricted to the quantity of ground improvement methods used.

Figure 1.2 shows the aim of this thesis to develop a framework that can scale from micro-scale to meso-scale and then to macro-scale. This scaling process is based on the assumption that the material's behavior observed in laboratory experiments will remain consistent when applied to larger scales.

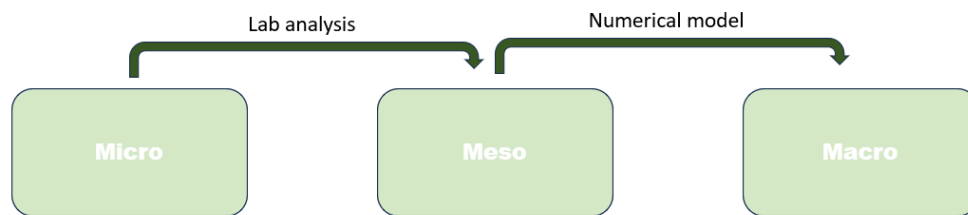


Figure 1.2: Upscaling process

1.6. Research structure

This research adopts the structure as demonstrated in Figure 1.3 to ensure clarity and readability. The *Introduction* presents the research topic, outlines the main objectives, and defines the scope. The *Literature Review* provides a summary of existing knowledge and identifies critical gaps of knowledge that this research aims to address. The *Methods, Models, and Materials* section explains the methodology used to answer the research questions and explains the general structure of the models that form the new framework. The outcomes of the simulations and experiments are presented in the *Results* section. These implications and limitations of these findings are further analyzed in the *Discussion*. The key insights are presented in the *Conclusion*, summarizing the main findings of this thesis. Finally, the thesis ends with *Recommendations* for future research.

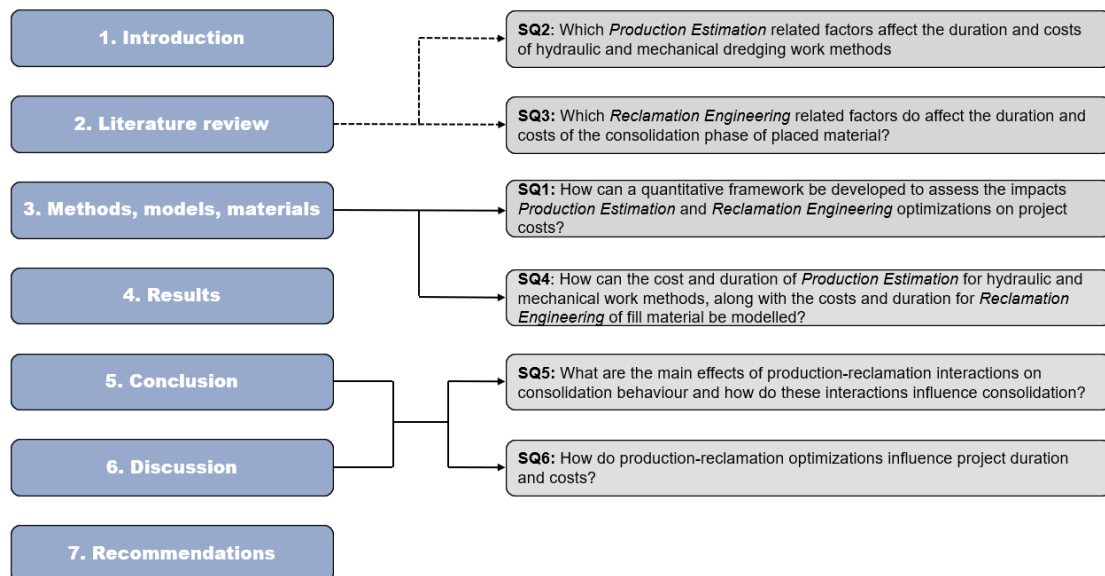


Figure 1.3: Research structure

2

Literature Review

The goal of this literature review is to analyse existing research and knowledge related to *Production Estimating* and *Reclamation Engineering* with a focus on the connection between these two aspects in land reclamation projects. By reviewing academic studies, relevant industry insights and expert judgement, this section aims to provide a comprehensive understanding of the current state of knowledge related to ***Production Estimating, Reclamation Engineering*** and ***Production-Reclamation coupling***. These three pillars of knowledge are considered the main drivers for addressing the complexities of the main research question, as they surround the technical, economic, and integrative aspects essential for optimizing land reclamation processes.

This section starts with an overview of the main scientific and practical expertise that exists within each of the three pillars of knowledge. After that, the company's own experiences are shared. This section ends with an identification of the key knowledge gaps associated with each pillar and the main takeaways from company experiences. The knowledge gaps identified in this review of the literature form the basis for understanding the challenges in integrating *Production Estimating* and *Reclamation Engineering* in land reclamation projects. Addressing these gaps is essential for developing innovative approaches to optimize production-reclamation coupling, which is central to the main research question of this thesis.

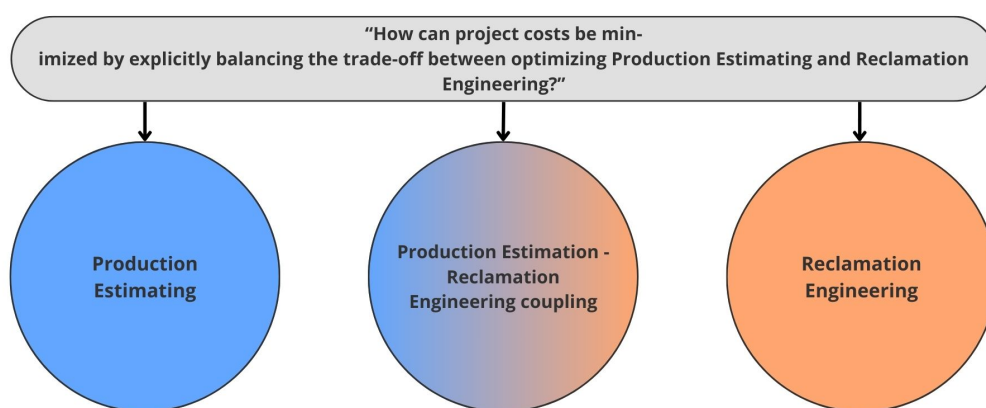


Figure 2.1: Relevant area's of knowledge for answering the main research question

2.1. Production Estimating

This section presents the theory of *Production Estimation* for estimating the duration and costs for production. Additionally, the characteristic effects of different dredging work methods on the soil properties is provided.

Production Estimation of hydraulic dredging work methods is extensively illustrated by the books of Schrieck (2021) and Vlasblom (2005a), providing the fundamental working principles of the dredging cycle of a Trailing Suction Hopper Dredgers (TSHD) such as trailing/loading, workability and discharging. Details of pump-pipeline interaction during trailing and discharging, as well as pump-drive interaction is widely described in the work of VBKO (1998a), VBKO (1998c) and Schrieck (2021). This is the main theory behind estimation of loading and discharge stages of hydraulic dredging. The theory of soil jetting production and cutting production of rock, clay and sand are extensively described by S. Miedema (2014). Combining soil cutting and jetting production is modeled by S. Miedema (2019). The body of public work outlined above and with expert judgement from the company, provides knowledge for creating a framework for estimating the production rates of hydraulic dredging methods.

Production Estimating of mechanical dredging work methods is mainly described by the work of Vlasblom (2005b) and VBKO (1998b), providing the main theory behind the working principles of a Backhoe Dredger (BHD). Internal research at Van Oord is performed by De Wit (2013) on increasing the accuracy of production estimations by extensively modeling of the cutting forces generated by a BHD bucket while cutting sea-floor material. The body of public work outlined above and the expert judgement of the company provides the knowledge for creating a framework for estimating the production rates of mechanical dredging methods.

The effects of hydraulic and mechanical production work methods on soil properties is widely researched. The difference in water content of the dredged material between the two work methods is described in the work of Van Rijn (2019) and USACE (2015). In addition to the water content, VBKO (1998c) and VBKO (1998b) provide values for the bulking factors for estimating the bulk density for different kind of soils dredged by hydraulic or mechanical work methods. The Hydraulic Fill Manual of Van 't Hoff and Van Der Kolff (2012) states that utilizing mechanical dredging methods favour the preservation of in-situ soil properties such as density and shear strength, which is considered to be best for soft soil reclamation realization.

Sailing is a main part of the dredging cycle and is important in estimating production duration. Sailing velocities for ships can be estimated with the methods of Van der Kaa (1978) and Holtop and Mennen (1982). These theories estimate sailing velocities based on installed vessel power and the hull resistance. Here, the Holtop and Mennen (1982) method is a empirical approach.

In addition to public sources on production estimations, this review incorporates internal company knowledge for the analysis of production work methods. This knowledge is acquired based on centuries of dredging experience and on dredging research coming from acknowledged researchers (e.g. Van Rhee, Miedema, Vlasblom) which have worked with Van Oord and Delft University of Technology. Internal knowledge is converted to the author of this thesis by company production and energy expert (M. de Geus).

2.2. Reclamation Engineering

This section presents the main knowledge on *Reclamation Engineering* for estimating the duration and costs for the reclamation works.

The details and working principles of Reclamation Engineering is described in extensive detail by the *Hydraulic Fill Manual* of Van 't Hoff and Van Der Kolff (2012). This work elaborates on all aspects of land reclamations, e.g. reclamation work methods, reclamation contracts, design requirements, effect of ground improvement methods, asset delivery, construction time-lines and the utilization of “complex” materials in reclamation projects.

According to The *Hydraulic Fill Manual* (Van 't Hoff and Van Der Kolff, 2012), the small-strain consolidation theory can be used when working with “high quality” granular fill material for estimations of settlement and shear stress resistance. The small-strain consolidation theory is explained in detail in the work of Verruijt (2012), Schofield and Wroth (1968), Zeitoun and Wakshal (2013) and Chassagne

(2021). However, the work of Van 't Hoff and Van Der Kolff (2012) also acknowledges the potential problems of working with “complex” soft material and states that in this case, the small strain theory may not be applicable anymore for accurately estimating consolidation.

Besides the work of Van 't Hoff and Van Der Kolff (2012), other work has reported on working with soft soils in reclamation projects. The work of Chu et al. (2009) describes how ultra-soft clay was used successfully for land reclamation purposes in Singapore. The high compressibility and low permeability properties of fine clay particles during self-weight consolidation is acknowledged by IADC (2020b). Deltares (2016) and Xu et al. (2012) both highlight the importance of considering large-strain consolidation during self-weight consolidation of mud in land reclamations.

The *Hydraulic Fill Manual* of Van 't Hoff and Van Der Kolff (2012) describes that large-strain consolidation theories get important when dealing with highly compressible soils (high fines content), where soil parameters can not be considered to be constant. The effect of fines on compressibility and permeability is widely researched by Fan et al. (2022). This work describes the non-linear evolution of these soil parameters at different particle void ratios. Ahmed et al. (2023) describes that small strain consolidation assumptions are not valid for slurries that undergo large strains in soft soil tailing facilities.

According to the work of De Lillis et al. (2020) and Agapito and Bareither (2018); the use of large-strain consolidation models provides reliable estimates for hydraulically dredged material utilized in land reclamation applications. In addition, the work of Myouri (In prep), Chassagne (2021), Van Rijn (2019) Barciela Rial (2019) and Ito and Azam (2013) prove that the physical consolidation behaviour of slurries can be relatively accurately modeled by numerical large strain consolidation approaches.

The effects and modeling of ground improvement methods on the consolidation of soils are extensively researched for PVD's by Townsend and McVay (1990), Nguyen and Kim (2019), Chai et al. (2001) and Ni and Geng (2022) and theoretically described by Van 't Hoff and Van Der Kolff (2012) and Hazirbaba and Mughieda (2019).

The large-strain consolidation theory is originally described by Gibson et al. (1967) and is extensively described by the work of Chassagne (2021) and Merckelbach (2000). Estimations of the non-linear properties of compressibility and permeability are researched by Merckelbach (2000), who obtained a physical method based on the 'fractal approach of flocs'. Znidar et al. (2011) and Carrier and Beckman (1984) have obtained empirical power laws for fitting the non-linear properties of compressibility and permeability.

In addition to public sources on reclamation engineering, this review incorporates internal company knowledge. This knowledge is acquired based on decades of experience in realizing land reclamation projects. Internal knowledge is converted to the writer of this thesis by company geotechnical experts (C. Hoffmann).

The body of public work outlined above and the expert judgement of the company provides the knowledge for creating a framework for estimating the consolidation behaviour corresponding to *Reclamation Engineering* and its corresponding costs.

2.3. Production Estimation - Reclamation Engineering coupling

The effects of how choices for dredging work method translate into are briefly described by Van 't Hoff and Van Der Kolff (2012) and Van Rijn (2019). This work states that mechanical work methods could favour consolidation of soft soil reclamation's due to its higher bulk density. Both of these publications acknowledge the trade-off between dredging work method and consolidation behaviour exists. However, the extent to which one work method is more favorable than another in terms of project cost and duration is not addressed in these publications.

The costs of each Production and Reclamation is also not widely present in literature. The Hydraulic Fill Manual describes on the main cost components of land reclamation projects. This work also includes that “Low quality fill material” will lead to extra costs for ground improvement methods necessary for meeting design requirements. Van Rijn (2019) gives general cost estimates of the utilization of mechanical and hydraulic work methods for dredging and dumping in land reclamation projects. The publication CIRIA (2009) proposes a method for estimating the costs for utilization of dredging equipment. The

proposed method which is used between dredging companies when working in joint venture projects for first cost estimations.

Costs aspects of projects belong to the competitive position of companies. All the knowledge on costs of production and reclamation aspects are known within the company. However, according to company experts, the optimization trade-off between production and reclamation costs is not researched. The current way of working is to optimize project costs based on a production work method chosen.

2.4. Company experience

According to company experts, the current workflow could be potentially optimized by increasing the understanding and coordination between Production and Geotechnical departments of dredging companies. Research related to this topic could start a internal discussion that there might be potential innovations by alternating the conventional working strategy when dealing with complex materials in reclamation projects. Company experts acknowledge that this can potentially lead to providing a better business case for the company.

Company experts acknowledge that working with complex materials brings different challenges compared with ordinary sandy material. In the past decade, material with high fines fraction was considered unsuitable for reclamation purposes. The current approach based on “guessing” bulking values based on experience works sufficient when working with ideal material, but starts to be insufficient when working with more complex materials as explained in the intermezzo below. Increasing the understanding of physical behaviour of these materials could provide insights in how to handle them to be usable in reclamation works. This could bring some soils from the “unsuitable” label to “suitable”. Large-strain consolidation models could provide more physical understanding of transient material developments during self-weight consolidation. This could be essential knowledge during the tender or execution phase of such reclamation works.

Intermezzo: Current way of working

The current estimation approach for estimating material behaviour in a hydraulic fill is based on bulking and small strain consolidation. The bulking principle is essential in estimating the initial shrinkage of the material after placement in the reclamation area. This value helps estimating the amount of material that is needed from Production for filling of the reclamation (IADC, 2020a). Estimating bulking values of material is currently based on experience which the company obtained during the past century of working in the dredging industry.

The bulking principle is often used in land reclamation projects to estimate the evolution of the volume or density of the material from in-situ conditions to the conditions after filling when self-weight consolidation ends. This method is convenient when using sands, which settle fast and self-consolidate quickly. After self-weight consolidation, small strain consolidation methods are used to estimate the long term consolidation effects (including ground improvement methods). Here the bulking principle is the proper method to estimate the filling with, because the time-frame between settling and the end of self-weight consolidation is almost instantaneous.

Because of negligible timeframes for settling and self-weight consolidation when working with “suitable” material, no gap exists between layer construction by production and the small strain consolidation estimations of the geotechnical department (Figure 2.2). The “large-strain” behaviour of the material exists for a short period of time and can be approximated with a constant value for shrinkage (bulking) without any transient considerations.

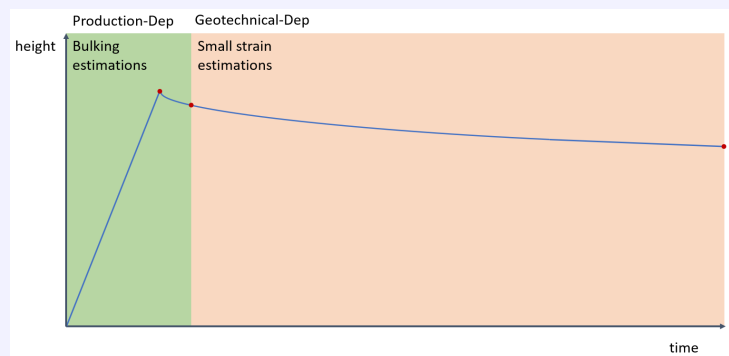


Figure 2.2: No knowledge gap: filling and consolidation of 1 layer of sandy soil

However, when working with “complex” materials, consisting mainly of silt or clay, slurries occur which comes with high deformations and do not quickly consolidate under its own weight. This is due to their relatively low permeability, high compressibility and high water retaining capacity. In fact, settling and self-weight consolidation of these materials could take months to years, due to unfavourable material properties (Van Rijn, 2019). Here, the bulking principle is not the proper method to estimate the filling with, because the time-frame between settling and the end of self-weight consolidation can not be neglected, but takes significant proportion of the total project duration, as illustrated in Figure 2.3.

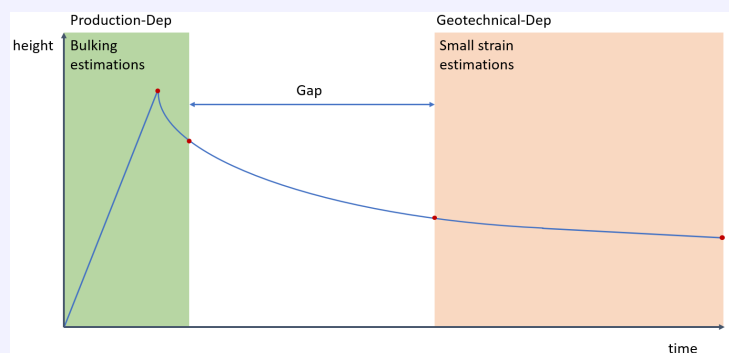


Figure 2.3: Major knowledge gap: filling and consolidation of 1 layer of silty/clayey soil

Creating a method that simulates the filling stages of a reclamation could provide the company with more accurate predictions on the evolution of self-weight consolidation of the slurry in the filling stage, leading to better predictions on the overall project costs and duration.

The company has experience with building with “Complex” materials from the past. Two projects of the past are highlighted in this context, the **Scandinavia** project and the **Black Sea** project.

The first project originates from **Scandinavia**, where complex soils were dredged and used for land reclamation. The heavily over-consolidated material was dredged and completely disintegrated during hydraulic dredging, resulting in very low hopper densities. In contrast, gentle mechanical excavation produced material with higher strength and higher barge density, which was beneficial for consolidation activities. This project highlighted the interaction between production rates and consolidation rates.

The second project originated in the **Black Sea** area. In this project, clay was dredged and completely disintegrated into low-density fill material through hydraulic dredging. Due to the “complex” soil composition and the very low initial density, consolidation rates were slow. As a result, the fill material gained little strength in relatively long time periods. The low shear strength development of the slurry made it difficult to build up layers over time, which diminished the financial advantages of hydraulic dredging work method. Consequently, expensive ground improvement methods were required to artificially enhance soil properties to deliver the asset to the client.

The first project emphasizes that hydraulic and mechanical dredging methods each have its own characteristic effects on soil properties. Mechanical dredging, in particular, was employed to achieve more favorable soil properties for consolidation. The experience from the second project highlights that optimizing for production by choosing the most cost-effective dredging method does not always result in the most economical overall solution when working with complex soils. Experience from both projects using “complex” material, emphasize that the connection between *Production Estimation* and *Reclamation Engineering* is vital to obtain the most economical solution to a “complex” project.

2.5. Literature review statement

From this literature review can be concluded that a lot of knowledge exists in the individual fields of *Production Estimating* and *Reclamation Engineering*. In addition, knowledge on costs is also profound in literature and within the company. However, a significant gap emerges from the literature. There is no knowledge in current literature on the interaction between Production Estimation and Reclamation Engineering, and the optimization trade-off between the two to minimize land reclamation project costs. Some publications include some minor statements regarding the connection between the two aspects, but do not dedicate it their scientific attention. Company experiences from past projects emphasize that bringing together knowledge in fields of Production Estimation and Reclamation Engineering, including the optimization trade-off of these two pillars are needed to determine the most cost-effective execution method for land reclamation projects using “complex” materials.

A secondary research gap can be established from this literature review. Currently, self-weight consolidation is not included in the reclamation workflow when working with “complex” materials. The utilization of a large-strain model in estimating the physical behaviour of a reclamation consisting of “complex” material is proven to be important for the estimation of self-weight consolidation behaviour of slurry material in land reclamation application. Meanwhile, the company has encountered several projects with “complex” materials where they have experienced difficulties when working with these kinds of materials. As a result, company experts acknowledge the value of such large-strain model and state that a large-strain model could bridge the gap between Production Estimating and Reclamation Engineering when working with fine grained, “complex” material. Providing an estimation framework which includes self-weight consolidation by large-strain models could improve project costs and duration estimations. Consequently, the trade-off of optimizations on Production Estimation and Reclamation Engineering can be assessed by this framework.

This literature review confirms the research gaps that this thesis wants to answer. It becomes evident that no specific research is dedicated to investigating the effect of the trade-off between optimizing Production Estimation and Reclamation Engineering in minimizing project costs, forming the basis of the main research question. The second research gap is on including self-weight consolidation estimations by a large-strain model in a new estimation framework. The second research gaps focuses on improving the connection between Production Estimation and Reclamation Engineering by including self-weight consolidation estimations by a large-strain model in a new estimation framework. This research gap is addressed by the sub-questions in this thesis.

Theoretical framework & Case-study

This thesis aims to provide insights in how optimizations on either Production Estimation and Reclamation Engineering can minimize project costs. The literature review reveals that when dealing with complex materials, knowledge gaps start to occur in the estimation sequence for reclamation projects. This section proposes a framework which has the potential to bridge the gap between Production Estimation and Reclamation Engineering. This framework is based on the knowledge presented in the literature study and the input of experts from the industry and scientific experts involved in this thesis.

3.1. Theoretical framework

In this research, optimizations on either Production Estimation or Reclamation Engineering for minimizing project costs are evaluated. This analysis is performed through a new proposed framework which includes a large-strain consolidation model to fill the knowledge gap between Production Estimation and Reclamation Engineering as indicated from the literature study. The new proposed framework consists of a production module and a reclamation module. The reclamation module consists of a large-strain consolidation model to represent self-weight consolidation and a small-strain consolidation model to represent long-term consolidation under the effect of ground improvement methods. The production module consists of hydraulic and mechanical production estimation model. The framework illustrated in Figure 3.1 shows the coherence between the modules. This section will elaborate on input parameters, the working principles behind the models, and output in more detail.

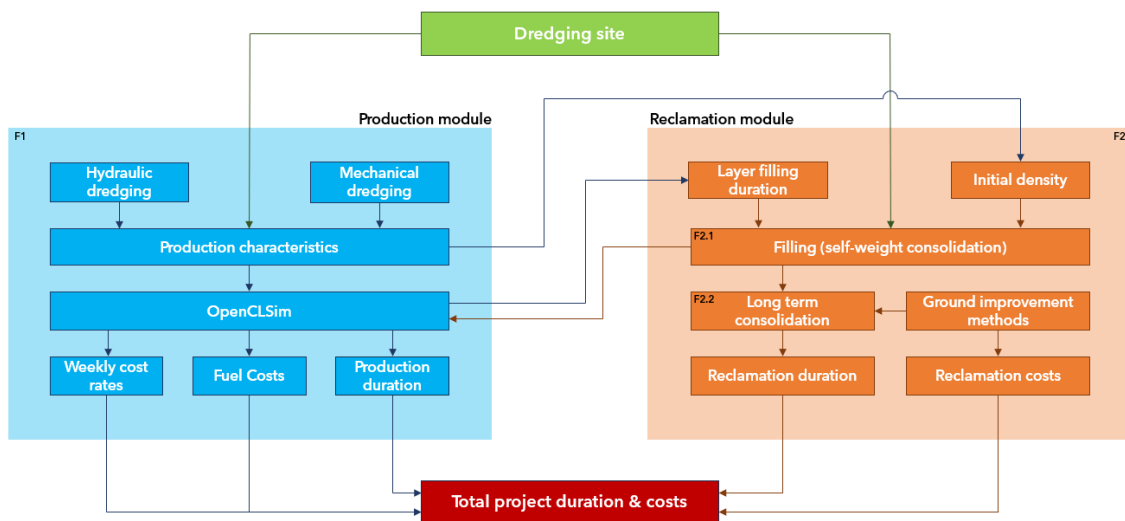


Figure 3.1: *Production Estimation - Reclamation Engineering integrated framework: model interactions*

The production module is connected with the large-strain model through “OpenCLSim” and “Production characteristics”. Production characteristics can be seen as a part of the model that estimates the duration and energy used during the dredging cycle components of hydraulic and mechanical work methods. Production characteristics and OpenCLSim govern the duration between layer placement and the initial density of the material after placement in the reclamation. The large-strain model indicates to the production model how the material will consolidate. Besides consolidation behaviour, the large-strain model will indicate to production how much material is needed to comply with a certain design level. OpenCLSim will estimate the total amount of cycles needed to deliver the required material, including production costs and duration based on case-study and equipment parameters. The large-strain model will eventually transfer into a small strain model at the moment when filling is complete and a sand crust can be placed to make the reclamation accessible for equipment. Small strain consolidation models are used in this framework to include the effect of ground improvement methods to accelerate consolidation. The large-strain model will provide the density profile at the moment that the crust needs to be placed and models are shifted from large-strain to small strain. Each module of this framework will contribute to costs and duration of the complete project. This is the output of the framework in order to analyse the optimizations on Production Estimating and Reclamation Engineering effects on project costs.

The author of this thesis encourages the reader to consult Appendix A and Appendix B for the theoretical profundity and a quantitative description of the Production and Reclamation models.

In the appendices, the theoretical background is explained and the numerical calculation steps of the models are indicated. The appendices are recommended if the reader wants more insight in the working principles behind Production Estimating and Reclamation Engineering.

3.1.1. Production Estimation

The production rates of Van Oord equipment will be represented by physics-based models. These models are created for this thesis based on current literature obtained from the literature review and expert judgement from the company. The Production Estimation model will account for hydraulic dredging with a Trailing Suction Hopper Dredger and mechanical dredging with a Backhoe Dredger in combination with barges. Each method has its own characteristic impacts on (slurry) material properties, production rates, project duration, and costs. The objective of the model is to demonstrate how optimizing production can influence costs, duration, and soil characteristics. Additionally, the model is designed to produce outputs that integrate with the inputs of reclamation models as illustrated in Figure 3.1. These production models aims to provide reliable estimates production-related costs and duration. The modeling approach is illustrated in Figure 3.2.

The model estimates the duration and power utilization of each component of the dredging cycle in “Production Characteristics”: dredging/loading, sailing when full, discharging, and sailing when empty. Here, each dredging method provides its own unique input parameters of vessel characteristics such as cutting power, lifting capacity, pump output, and hopper volume for dredging/loading, along with in-situ soil characteristics such as; dredging depth, cutting depth, density, shear strength, and soil type. Estimating sailing speeds requires data on engine power, transmission efficiency, and vessel geometry for both loaded and unloaded conditions. For discharging, factors as the selected discharge method (rainbowing, pipeline discharge, or bottom-door opening), the discharge pump capacity and discharge duration play a role. Each stage of the dredging cycle is estimated in “Production characteristics” and are linked to duration, weekly operation costs and fuel costs.

OpenCLSim is used to scale up the estimations of duration and costs of “Production characteristics” from one dredging cycle to duration and costs for the total production stage, based on the amount of cycles required to fill the reclamation. The amount of cycles needed is based on the total amount of material needed to fill the reclamation until a specified design level, including its consolidation behaviour. The quantity of material needed is based on outcomes of the large-strain consolidation model, which estimates the deformation of the material after self-weight consolidation. For this thesis, a plugin is created in OpenCLSim to estimate the total production duration and costs for which a reclamation can be filled. Additionally, OpenCLSim estimates the duration between layer stacking by estimating how much time the hydraulic and mechanical methods need to provide 1 meter of material at initial density in the reclamation.

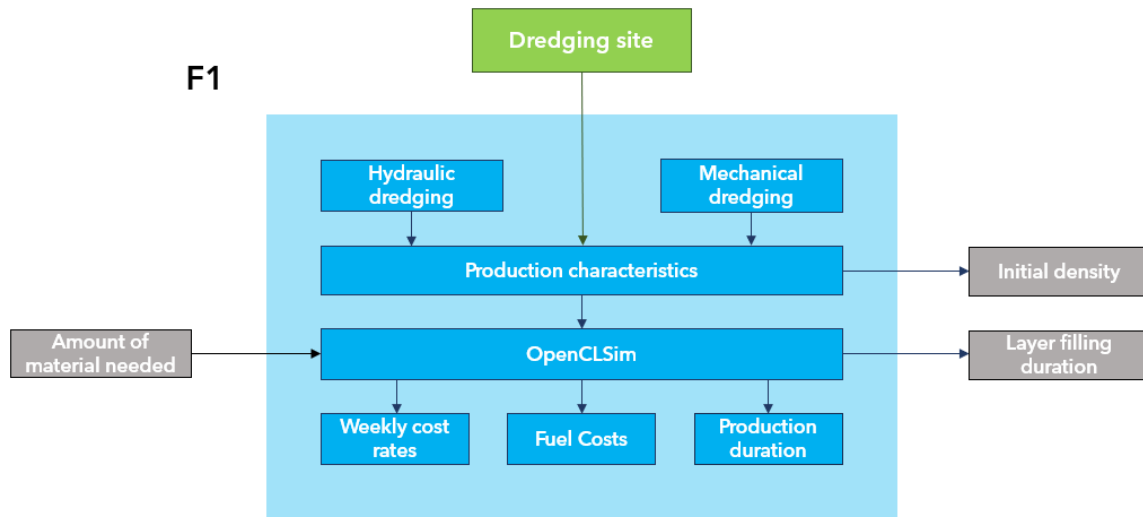


Figure 3.2: Production estimation modeling philosophy

This section provides a brief qualitative explanation of the theory behind the hydraulic and mechanical production models, their input parameters, model operations and output parameters. A detailed quantitative explanation of the complete model is provided in Appendix A.

Hydraulic production

The “Production characteristics” phase in Figure 3.2 is modeled based on a production estimation model. This model estimates the duration and utilized power of each component of the dredging cycle as shown in Figure 3.3. The components in this thesis consist of; dredging - sailing empty - discharging - sailing full, back and forth between dredging site and placement site.

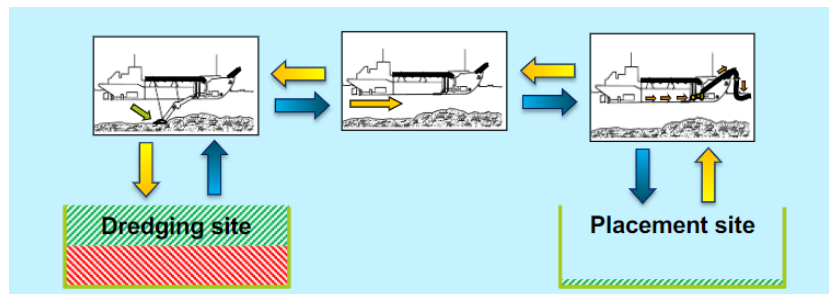


Figure 3.3: Dredging cycle TSHD, obtained from Dredging Technology (CIEM5300)

The “dredging” component for a TSHD consists of soil cutting production and loading production. In context of a TSHD, the soil is cut by the cutting teeth mounted on the draghead. Soil cutting production is based on the theory of S. A. Miedema (2016) and expert judgement from the company. This theory determines the force needed to fail sand, clay or rock. The force that the TSHD is able to transfer depends on the installed power, the velocity during cutting and the force needed to fail the material. The production model for the hydraulic method calculates the force required to fail the in-situ material with the assumption for a cutting velocity of 2 knots. The geometry of the draghead, the soil cutting velocity, cutting depth and the in-situ soil conditions enables the model to calculate the soil cutting production and the energy required to fail the material during the “dredging” phase.

After the material is cut, it is mixed with water in order to be transported through pipeline. The loading production is estimated by modeling the pump-pipeline interactions (VBKO, 1998a) (VBKO, 1998c) (Schrieck, 2021). Here the available pump power, pipeline geometry and required density of the slurry results in an equilibrium between driving forces and resistance created by flow through a pipeline. This

equilibrium corresponds to a pipeline flow-rate which determines the loading duration of the hopper. The model estimates the equilibrium flow-rate before the pump, which is driven by the under-pressure (vacuum) that the pump can create, as well as the equilibrium flow-rate after the pump, which is driven by the over-pressure created (pump head). The model ensures conservation of mass through the pump by calculating the pump impeller RPM for which the equilibrium velocity before the pump equals the equilibrium velocity after the pump. The model estimates the duration of loading and energy required for loading based on the RPM of the pump, the installed pump power, hopper volume and the equilibrium flow during loading.

For efficient dredging, the soil cutting production needs to be in balance with the loading production. To make this process efficient, the model calculates the cutting depth required to achieve the same soil cutting production as the loading production based on a cutting velocity of 2 knots and the target initial density. Furthermore, the energy used for both soil cutting and loading is added up to obtain the total energy used during “dredging”. The total duration of dredging is determined with the time it takes to fill up the hopper volume of the TSHD.

The model estimates sailing velocity based on the Holtrop & Mennen method (Holtrop and Mennen, 1982) for the “sailing full” and “sailing empty” stage. This is an empirical method estimating the sailing velocity based on hull resistance and the efficiency between the drive-train and the propeller. These parameters are all obtained from in-house vessel data of Van Oord. The energy during sailing can be estimated by the power installed for sailing, the estimated sailing velocity obtained from H&M and the duration of sailing. This method is the same for estimating the sailing velocity empty and its required energy. Here, the hull resistance factors are different due to different orientation of the hull of the vessel in the water during sailing full and sailing empty. The model calculates the duration for sailing and its corresponding required energy.

During the “discharge” phase, the hopper is emptied at the placement site. The discharge production is estimated by modeling the pump-pipeline interaction in the same way as the loading production. During discharging, the pipeline geometry is different compared to the loading stage. Besides that, 500 meter of additional floating pipeline is used to pump the material from the hopper to the reclamation. During this discharge process, the TSHD uses 2 centrifugal pumps in a series connection. This enables to overcome the resistance of such long floating pipeline length during discharging. The model estimates the duration of discharge and energy required for discharging based on the RPM of the pumps, the installed pump power, hopper volume and equilibrium flow during discharging.

The output of this model consists of the total duration it takes for the TSHD to complete one dredging cycle and the energy that is used along one dredging cycle that come with dredging a certain density slurry. Furthermore, fuel costs are calculated based on the total energy required and the fuel source of the vessel's drive-trains. Together with the weekly cost rates of CIRIA (2009) for utilizing the equipment, the costs of one dredging cycle is estimated.

Mechanical production

For the mechanical dredging work method, the “Production characteristics” phase in Figure 3.2 is modeled based on a production estimation model. This model estimates the duration and utilized power of a Backhoe dredger in combination with a barge of each component of the dredging cycle as shown in Figure 3.4. The dredging cycle of the mechanical method consists of; dredging - sailing full - discharging - sailing empty, back and forth between dredging site and placement site.

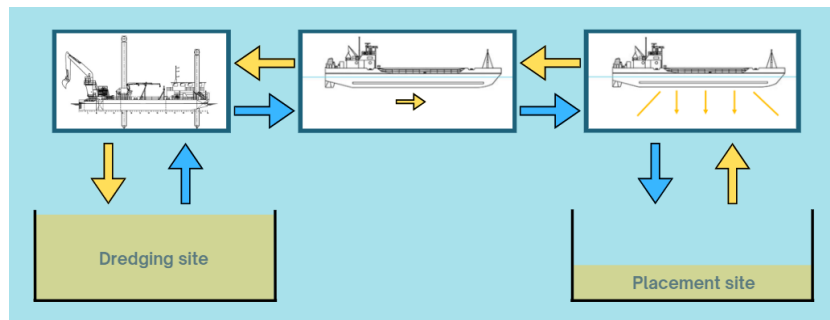


Figure 3.4: Dredging cycle Backhoe + barge

The “dredging” component for a BHD consists of soil cutting production and loading production. In the context of a BHD, the bucket teeth will cut the in-situ material and the hydraulic pumps of the backhoe will drive the loading production. The soil cutting production is also based on the theory of S. A. Miedema (2016). The production model uses excavation graphs to determine how much force the backhoe can exert at certain depth on the in-situ sea-floor material. This available force needs to exceed the force required, to successfully cut the material.

After the material is cut, backhoe operations are needed to transfer it from the sea-floor to the barge. The backhoe operations during loading consist of; cutting, lifting, swing, release, swing, and lowering. The production model estimates the cutting velocity by the installed power of the backhoe and the amount of force required to fail the in-situ material. The other loading operations are assumed to take 60 seconds (De Wit, 2013). The “dredging” duration is estimated by adding the cutting duration to assumed 60 seconds of the other backhoe operations. The model performs a lifting check, based in lifting graphs. This lifting check estimates if the backhoe can lift up the bucket content from the sea-floor to the barge. The energy required for the “dredging” component is calculated based on the installed power and the duration of the backhoe operations.

After the backhoe has finished loading the barge, the barge will sail full to the placement site. Again, the Holtrop & Mennen method (Holtrop and Mennen, 1982) is used to estimate the velocities of sailing full and empty, based on the vessel characteristics of the barge considered. The energy during sailing can be estimated by the power installed for sailing, the estimated sailing velocity obtained from H&M and the duration of sailing. This method is exactly the same as for the hydraulic method.

During the “discharge” phase the hopper of the barge is emptied at the placement site. The production model calculates the discharge production based on the assumption of bottom-door-opening which takes 30 minutes (company experts). During the placement duration, it is assumed that 100% of the installed power of the auxiliary engine is used for discharging. Based on these assumptions, the model calculates the required energy and the duration of the “discharge” component of the BHD dredging cycle.

The output of this model consists of the total duration it takes for the BHD+barge to complete one dredging cycle and the energy that is used along one dredging cycle that come with dredging a certain density slurry. Furthermore, fuel costs can be calculated based on the total energy required and the fuel source of the drive-trains of the backhoe and barge. Together with the weekly cost rates of CIRIA (2009), the costs are estimated of one dredging cycle.

OpenCLSim

After the production models have calculated the duration, energy required and the weekly cost rates of one single dredging cycle, logistical software of Van Oord, OpenCLSim (De Boer et al., 2023) is used to scale up the process of Production Estimation from single-cycle analysis to a multi-cycle analysis on global project scale. OpenCLSim is able to estimate the duration it takes to transport a prescribed amount of material from location A to location B. The self-weight consolidation model of Reclamation Engineering provides feedback to OpenCLSim on the amount of material that is needed from Production. By using this software, the models of Production Estimation and Reclamation Engineering can be

coupled and OpenCLSim can calculate the duration and costs for Production that are needed to deliver the right amount of material to the reclamation.

3.1.2. Reclamation Engineering

In Reclamation Engineering, consolidation behaviour is represented by physics based models. Self-weight consolidation and long-term consolidation under the effect of ground improvement methods will be estimated by numerical models. Consolidation starts in the reclamation when the first layer is placed. Consolidation is a continuous process during the filling stages. The process of filling is a dynamic consolidating process, where new layers are placed by Production after fixed time-increments on top of the already consolidation material present in the reclamation. Specially for “complex” materials consisting of high fines content, the self-weight consolidation phase of the material can be extensive due to the unfavourable properties of this material (e.g. low permeability and high compressibility). These properties are highly non-linear during self-weight consolidation due to fast changing density as a consequence of high settlements. Long term consolidation is taken into account by a small-strain consolidation model where ground improvement methods are used to densify the soil further beyond self-weight consolidation. This is important to prepare the fill material for bearing the design requirement loads. Material properties here are assumed to be constant due to the relatively low settlements that occur in this phase. The objective of the models in Reclamation Engineering is to demonstrate how different initial densities coming from hydraulic and mechanical work methods will affect the consolidation process. The reclamation models aims to provide reliable estimations of self-weight consolidation during filling, long term consolidation by ground improvement methods and costs and duration until the asset can be delivered to the client.

The model philosophy is shown in Figure 3.5. A large-strain consolidation model is used for estimating the self-weight consolidation of a slurry in a reclamation, based on the numerical method obtained from (Chassagne, 2021) and (Myouri, *In prep*). This numerical method is modified to be specially applicable to reclamations, by including a step-wise layer filling method where new layers of slurry are added to the reclamation over time. Here the complete consolidation, consisting of already consolidating material and newly added material is included. As a input of the model, initial density and the duration between placement of two consecutive layers is provided by the production models. Small-strain consolidation theories are applicable after self-weight consolidation (Chassagne, 2021). This is modeled in D-Settlement software of Deltares and estimates the long term settlements under the effect of ground improvement methods (surcharge & PVD's) (Deltares, 2016). The duration of consolidation is estimated until the reclamation complies with the design-requirements and can be delivered to the client. The amount of surcharge and PVD's needed determine the costs coming with Reclamation Engineering. The cost coming with ground improvement methods used and the duration until the asset can be delivered to the client are output of these models.

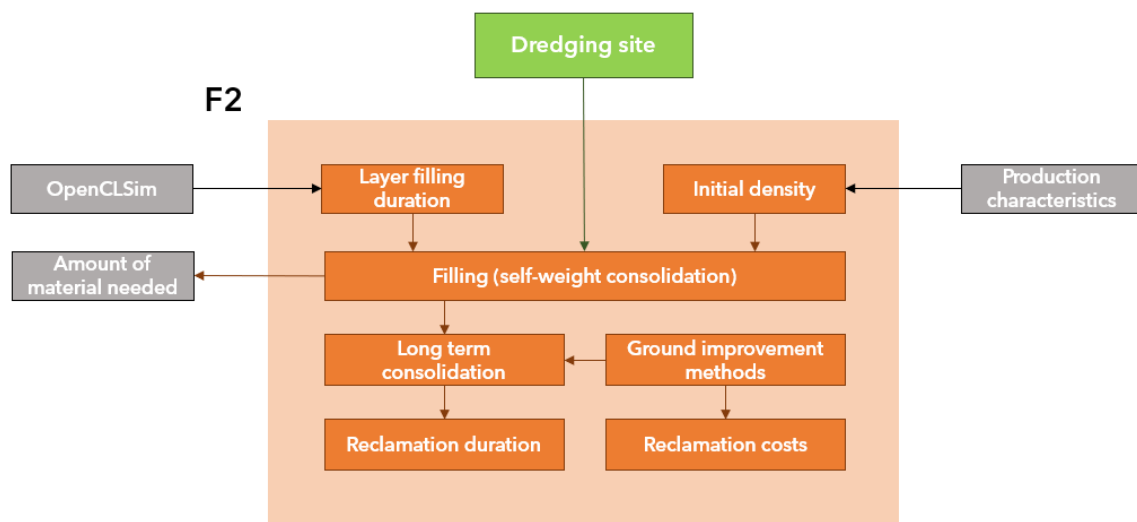


Figure 3.5: Reclamation engineering modeling philosophy

This section provides a brief qualitative explanation of the theory behind the large and small strain consolidation models, their input parameters, model operations and output parameters. A detailed quantitative explanation is provided in Appendix B.

Large Strain model

The "Filling (Self-Weight consolidation)" phase of the proposed framework in Figure 3.5 is simulated by a 1-D numerical large-strain consolidation method, based on the theory of Gibson et al. (1967). This method is obtained and modified into a numerical approach which enables to simulate filling stages of a reclamation. Important activities in the large-strain domain are shown in Figure 3.6. This section explains how the large-strain method is used to estimate the consolidation behaviour of fill material while filling and for full self-weight consolidation.

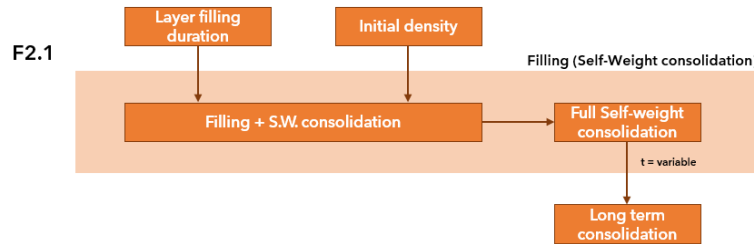


Figure 3.6: Filling and self-weight consolidation activities

The material is placed in the reclamation by Production as a homogeneous soil body with an initial density over the height of the layer. This body of slurry with initial density will consolidate under its own weight. Here, due to the low initial densities, high deformations are observed. The filling duration of one layer is important in this context because this is the time that the material can consolidate under its own weight until the new layer is placed on top. The time-frame between two consecutive layer placements is controlled by duration for which Production can deliver the material. This will be different for different dredging work methods. When the second layer is placed, the already consolidating soil body of layer 1 plus the new homogeneous layer placed on top will consolidate, as indicated in Figure 3.7. This process is repeated by the model until sufficient layers are placed, which will eventually correspond to the design level after settlements. The placement of a new layer on top changes the physical properties of the newly created soil body, increasing mass and drainage length of the column, which also affects the self-weight consolidation duration.

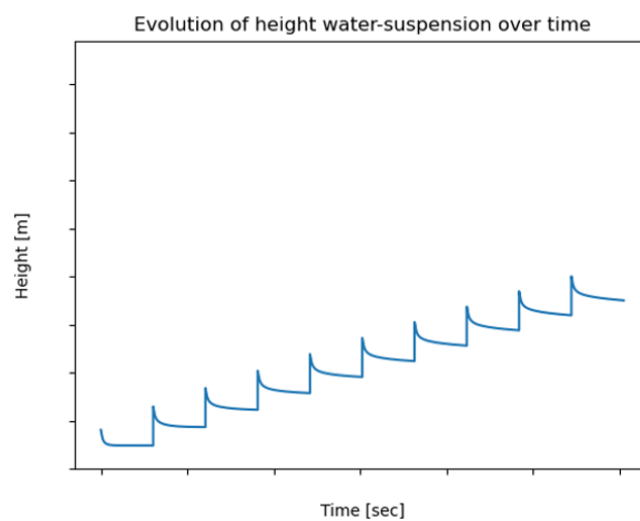


Figure 3.7: Large-strain modeling: self-weight consolidation of complete soil body

When the filling of the layers is complete, the entire slurry body is left to consolidate under its own weight for a period, allowing the soil properties to evolve in stiffness. This process leads to an increase in density and effective stresses. The longer the slurry is allowed to consolidate, the denser the soil becomes. Eventually, the soil reaches a compacted state where it no longer consolidates under its own weight. Naturally, the most compacted soil is found at the bottom of the column, while the top contains less compacted material. This arrangement occurs because the particles at the bottom bear more weight, resulting in higher effective stresses and, therefore, greater compaction after self-weight consolidation. This evolution of soil properties during consolidation, as well as the interface between suspension and water is modeled using the large-strain consolidation model.

In this model, the duration of “full self-weight consolidation” continues until the sand crust is placed on top, marking the start of the first phase of “long-term consolidation” under the effect of ground improvement methods. During crust placement, the soft material at the surface of the fill is assumed to be drained off. Significant loss of soil due to drainage is undesirable, as it increases production costs and generates more waste material. Therefore, the duration of self-weight consolidation is defined as the time required for the soft upper layer to reduce to a thickness equal to the height of the crust being placed. Once the crust is in place and only the compacted material remains, the process of consolidation transitions into the small-strain domain. In this stage, small-strain parameters derived from oedometer tests are assumed to represent the material’s consolidation behavior accurately.

The output of the large-strain model will be the self-weight consolidation duration until the crust can be placed and the evolution of the soil properties of the material in the fill over time. In addition, utilization of the large-strain consolidation proposed in this study could add value by giving a physical estimation of parameters as; shear strength development, bulking values, volume of material that is needed for reclamation, required height of surrounding bunds of reclamations and height evolution of the reclamation interface.

Small Strain model

After the “filling and self-weight consolidation” stage, small-strain consolidation theory is used to estimate “Long term consolidation”. As mentioned before, the transition between the two is characterized by the time when a sand crust is placed on top of the filled material to make the reclamation accessible for equipment. Small strain consolidation is estimated using D-Settlement software and the 1D small strain consolidation theory of Terzaghi. This software will estimate the consolidation behaviour of the material when subjected to external loads (surcharge) and Pre-fabricated Vertical Drains (PVD). The input of this small strain model are based on soil properties from the large-strain model and the **Scandinavia** report. Important construction activities in the small strain domain are shown in Figure 3.8. This section explains the activities needed in the small-strain domain to estimate the duration and costs before handing over the asset to the client.

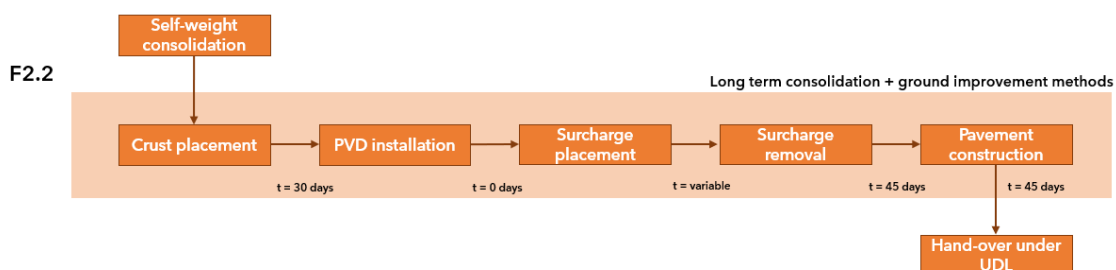


Figure 3.8: Long term consolidation and ground improvement activities

After the self-weight consolidation stage, several steps must be completed to prepare the asset for handover to the client (Figure 3.8). First, a crust of sand is placed to provide sufficient bearing capacity, ensuring safe access for equipment on the reclamation. Once accessible, PVD’s and surcharge can be installed. After the surcharge has served its purpose, it is removed, and a pavement layer is constructed at the design level. After completion of the pavement layer, the reclamation is handed over to the client under UDL (Uniformly Distributed Load) conditions. During this stage, the reclamation must

meet the client's design requirements, particularly regarding acceptable settlements under UDL loading, as illustrated in Figure 3.8. Due to the differences in duration created by the filling method and the total fixed duration of the project, different time-frames are left to conduct the ground improvements in for each dredging method. This will lead to different amounts of ground improvements needed to comply with the design requirements in time. These steps and corresponding loads are modeled in D-Settlement.

The required crust height is calculated according to the bearing capacity formula's of Terzaghi. The height of the sand layer that needs to be placed on top of the filled material to provide enough bearing capacity for equipment to access the reclamation can be calculated according to this method. The required thickness of the sand "crust" layer is determined by the weight of the equipment that will operate on it under undrained conditions. Important parameters in this calculation are the soil parameters of the fill material, such as undrained shear strength and density. Additionally, the calculation incorporates the soil parameters of the sand crust itself, including its friction angle, density and water table level. The required crust height is calculated by in-house software of Van Oord.

For this model, the steps outlined in Figure 3.8 are assumed to be carried out at fixed times, except for the surcharging stage. The sand crust is placed immediately and remains in place for 30 days before both the PVD's and the surcharge are fully installed. The surcharge is then left on the reclamation and will be stripped off 90 days before hand-over. The pavement layer is constructed 45 days before the asset is handed over to the client under UDL conditions, as specified in the design requirements.

The available duration for surcharge is determined by the total project duration (fixed) minus the time required for filling, self-weight consolidation, ground improvement installation and removal, and construction of the pavement layer. When less time is available for soil improvement (because filling or self-weight consolidation takes long), more surcharge and PVD's are needed to drain excess pore pressure and achieve sufficient consolidation. Conversely, when more time is available for improving the soil, smaller quantities of ground surcharge and PVD's are needed. This means that the available duration of soil improvement influences the height of the surcharge needed to over-consolidate the soil, ensuring it can handle UDL conditions at handover. Additionally, the number of PVD's required to drain excess pore pressures generated by the surcharge depends on the available surcharging time.

The output of the small strain model consists of the quantity of ground improvements needed and their corresponding costs to deliver the asset in time to the client. This is estimated by the D-Settlement software.

3.1.3. Coupling Production - Reclamation

This sub-section highlights the continuous Production - Reclamation capabilities of the proposed framework. Additionally, the parameters which govern the coupling between the production and reclamation module are emphasized.

Continuous Production - Reclamation process

The continuous Production - Reclamation process which can be estimated by this framework is visualized in Figure 3.9.

The filling stage can be characterized by filling of the reclamation in step 1 of Figure 3.9. Here, a layer of slurry mixture is placed at a homogeneous initial density by Production. The slurry mixture present in the reclamation will consolidate under its own weight. After the next layer is placed, all the material present in the reclamation will again consolidate under its own weight. This layer stacking process is repeated until sufficient material is placed. The duration between layer stacking is governed by OpenCLSim and is dependent on the production rate at which the dredging work method can deliver the material to the reclamation. The initial density of the slurry mixture is determined by the "Production Characteristics", coming with the dredging work method chosen and the in-situ soil conditions.

After sufficient material is placed to comply with the design requirements of the client after settlements, the complete slurry mixture is left to consolidate under its own weight in step 2 of Figure 3.9. This process is governed by large deformations (strains) due to the high water content of the slurry mixture which needs to drain to gain stiffness. This process continues until sufficient stiffness has been developed to bear a sand crust on top of the slurry mixture. The sand crust provides bearing capacity for

equipment to start ground improvements.

The long term consolidation under the effect of ground improvement methods starts in step 3 of Figure 3.9. This process starts with installation of the sand crust layer, the pre-fabricated vertical drains and the surcharge to further compact the filled material in order to bear design loads. During this process small deformations (strains) are expected. In this stage the models switch from large-strain consolidation estimations (variable soil engineering properties) to small strain consolidation estimations (constant soil engineering properties).

After the reclamation material is sufficiently improved and complies with the future design requirements of the client, the asset will be delivered in step 4 of Figure 3.9.

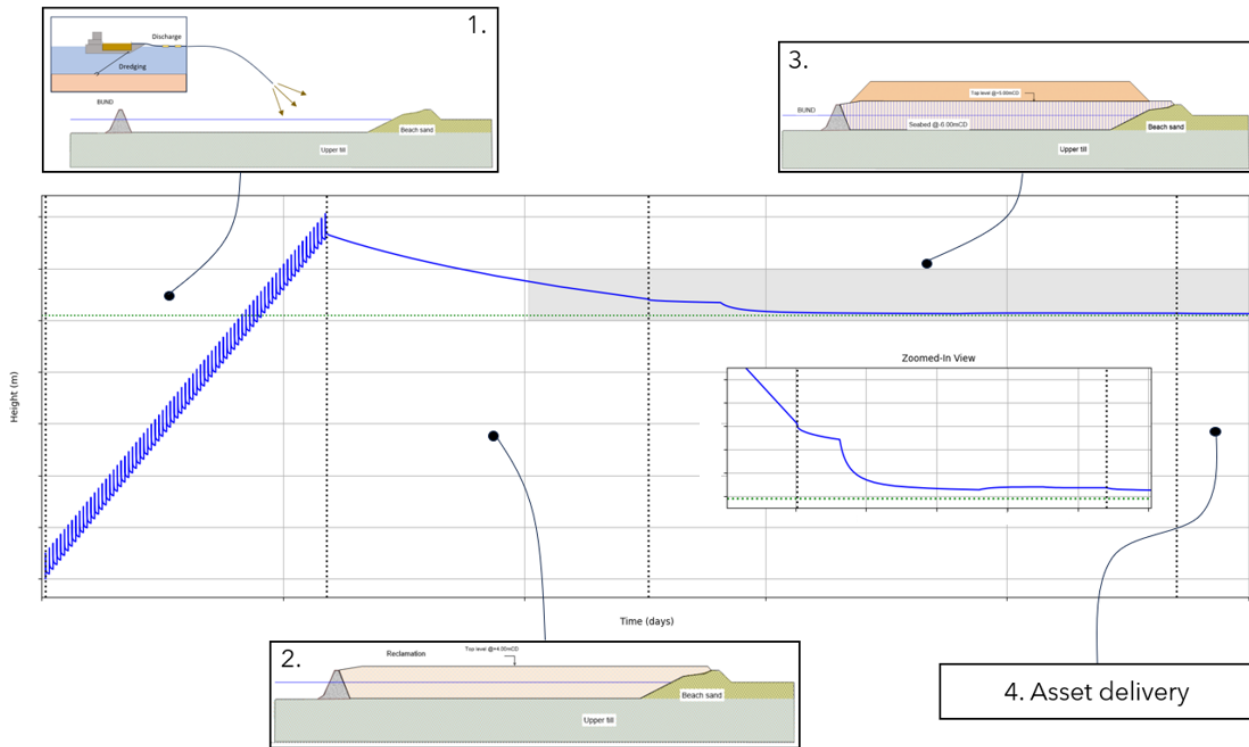


Figure 3.9: Infographic: Continuous land reclamation process

Self-weight consolidation coupling

From Figure 3.9 can be observed that the coupling between Production Estimation and Reclamation Engineering is governed by the process of self-weight consolidation.

The process of self-weight consolidation of "complex" slurry material is highly non-linear. One can expect high permeability and low effective stresses between particles when the volume fraction of solids is initially low (large void spaces exist between particles which makes drainage of water relatively fast). Due to consolidation, where the outflow of water will lead to an increase of packing density, material properties as permeability and effective stress are affected (small void spaces exist between particles which makes drainage relatively slow). Therefore, it can be concluded that during the process of self-weight consolidation, the properties of permeability and effective stresses change significantly for increasing volume fraction of solids. The developments of these properties are visualized in Figure 3.10.

Changing soil properties for different volume fractions of solids are called the "constitutive relations" of the fill material. This is an input for the Gibson et al. (1967) large strain theory. The constitutive relations can be extracted by analyzing the self-weight consolidation process of the slurry mixture in a settling column in laboratory conditions. Correctly and accurately capturing the constitutive relations is essential for reliable outcomes from the large-strain numerical model. The constitutive relations

between volume fraction of solids and hydraulic conductivity and effective stress are approximated by fitting exponential power-laws to the observed consolidation behaviour of the slurry from the settling column. Various methods can be utilized to extract the power-law fits of the constitutive relations from experimental settling column data (Chassagne, 2021) (Ahmed et al., 2023). The constitutive relations obtained from settling column tests of one layer are scaled up by the numerical model to represent the filling of multiple layers during the construction process of a land reclamation.

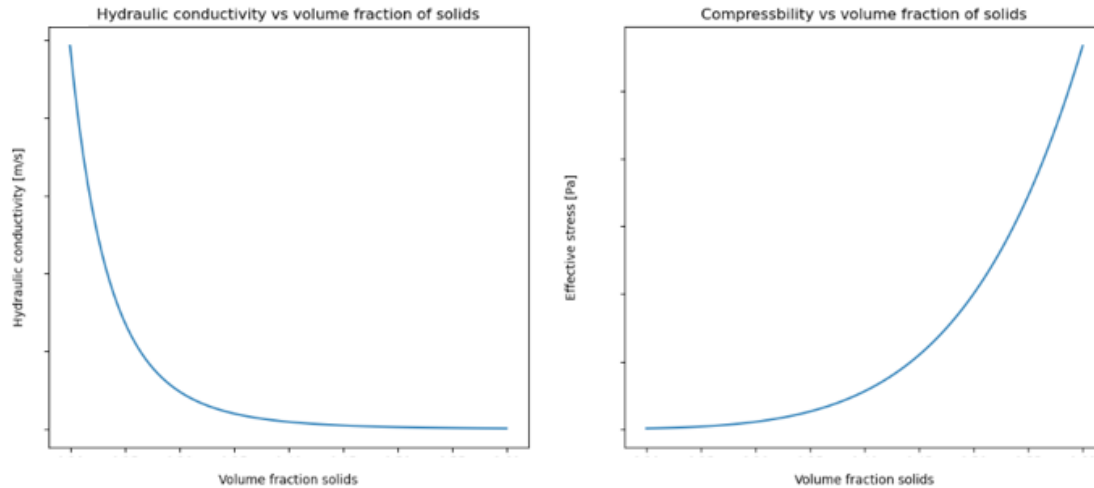


Figure 3.10: Constitutive relations from Merckelbach fitting from NMR data

3.2. Case-Study

Optimizations on Production Estimation and Reclamation Engineering are assessed based on the framework proposed in Figure 3.1 by using a case-study. This case study represents the main challenges of this thesis by presenting a land reclamation project utilizing “complex” material dredged by the hydraulic and mechanical work method. This section presents first an overview of the case-study, including the used equipment, sailing distance, reclamation geometry and the soil material. Next, the tuning of model parameters to represent the case-study material and equipment is presented. This includes a method to use a state-of-the-art calibration technique for capturing the constitutive relations for self-weight consolidation. Finally, the methodology is represented to assess optimizations in Production Estimation and Reclamation Engineering to answer the main research question.

3.2.1. Overview

The case study consists of a dredging area and a reclamation area, separated by 10 kilometers of distance. Dredged material is dredged and transferred to the reclamation site where the material will consolidate. The process of dredging, sailing and discharging is performed by one vessel in the hydraulic method (Trailing Suction Hopper Dredger). For the mechanical method, a stationary backhoe pontoon is used for dredging the material. For the mechanical method, sailing and discharging are performed by 2 split hopper barges. A schematic overview of the case-study is illustrated in Figure 3.11.

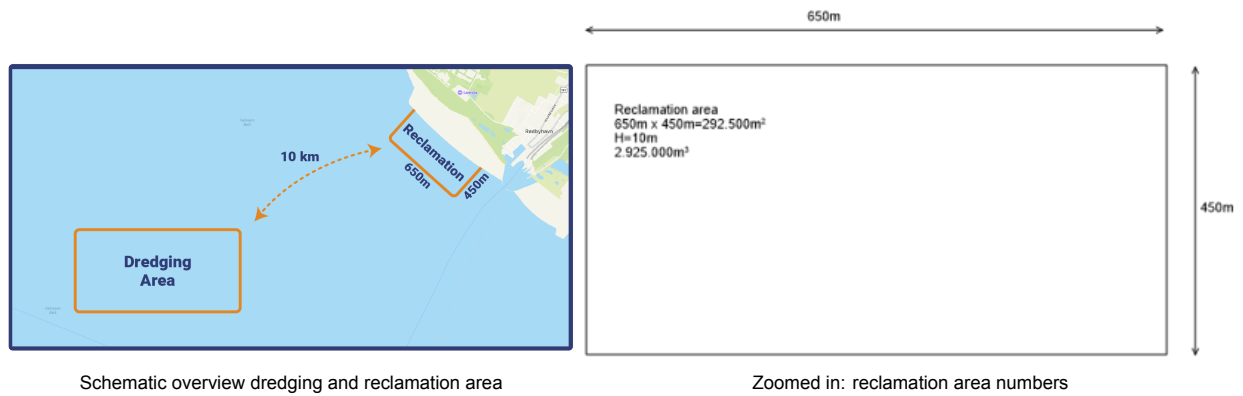


Figure 3.11: Case-study top overview

The reclamation consists of a surface area of 292.500 square meters (650m x 450 m). The filled height consists of upper till material and must be filled from -6 meters to +4 meters, which will make the required volume after consolidation 2.950.000 cubic meters. This is shown in the reclamation cross-section as presented in Figure 3.12. The seawater level is considered to be located at +2 meters.

The soil material used in this thesis is obtained from the **Scandinavia** project named in the literature review. This material, consisting of very over-consolidated in-situ fine material is dredged at a depth of 16 meters at the dredging site. It is assumed that the production model keeps extracting material from 16 meters, no deepening effects are taken into account for this case-study.

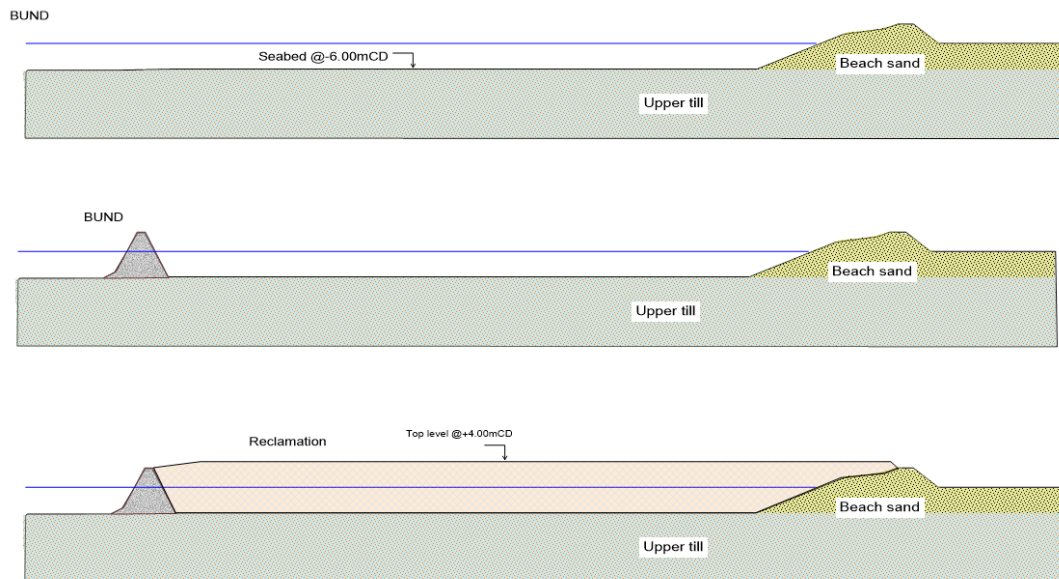


Figure 3.12: Case-study cross-section

Post-delivery, only minimal settlements are permitted under UDL loading. This is included for the design requirement of allowable settlements under loading. Another project requirement is that the total project must be finished in 470 days. The design requirements applied for the full-scale case-study are presented in Table B.3 and Table B.2.

Table 3.1: Settlement requirements under loading

Load condition	Requirement
75 kPa UDL	200 mm over 50 years

Table 3.2: Additional settlement requirements

Settlement value [mm]	Time
50	2 years
100	5 years
150	20 years
200	50 years

Equipment

This section outlines the equipment used in the case-study. The equipment listed down in this section is used to represent the work method of hydraulic dredging and mechanical dredging. The parameters given here are used to calculate production characteristics in Appendix A.

Hydraulic method The hydraulic working method is represented by the Trailing Suction Hopper Dredger “Vox Amalia”. The Vox Amalia consists of a hopper and dredging pumps, by which it can pump up material from the sea-floor to the hopper. This vessel performs all components of the dredging cycle; loading - sailing full - discharging - sailing empty. In contrast to the mechanical dredging method, the hydraulic dredging method moves material at relatively low costs and low densities. The duration and fuel costs for the components of the hydraulic dredging cycle are calculated through the Production Module. The specifications of the Vox Amalia for this case study are illustrated in Table 3.3.

Parameter	Value
Power Installed	<input type="text"/> [kW]
Power pumps	4700 [kW]
Power sailing	14400 [kW]
Trailing velocity	2 [knots]
Draghead width	<input type="text"/> [m]
Dredging depth	16 [m]
Hopper Volume	18900 [m3]
Sailing Velocity (Empty)	<input type="text"/> [knots]
Sailing Velocity (Full)	<input type="text"/> [knots]
Weekly Cost Rate	<input type="text"/> [EUR]
Fuel Usage	<input type="text"/>

Table 3.3: Vox Amalia parameters**Figure 3.13:** Vox Amalia (obtained from Van Oord database)

Mechanical method In this thesis, the mechanical dredging cycle is represented by the Backhoe Dredger “Goliath” in combination with split hopper barges. The Goliath is a backhoe mounted on a semi-

stationary pontoon and is able to dredge the material in circular motion around its axis. The Backhoe loads barges at the dredging site. In contrast to the hydraulic dredging method, the mechanical method moves material at relatively high costs and high densities. The duration and fuel costs for the components of the mechanical dredging cycle are calculated through the production module. The specifications of the Goliath for this case study are illustrated in Table 3.4.

Table 3.4: Goliath parameters

Parameter	Value
Power Installed	3800 [kW]
Volume bucket	<input type="text"/> [m3]
Bucket width	4.3 [m]
Dredging depth	16 [m]
Cutting length	6 [m]
Lifting height	9 – 10 [m]
Weekly Cost Rate	<input type="text"/> [EUR]
Fuel Usage	<input type="text"/>



Figure 3.14: Goliath (obtained from Van Oord database)

The Pieter Caland and Cornelis Lely barges are used to transfer material from the dredging site to the reclamation site. The Pieter Caland and Cornelis Lely are barges with identical specifications. These split hopper barges use bottom-door-dumping for disposing the material in the reclamation. Adding two barges to the dredging cycle will speed up production. The duration and fuel costs for the Pieter Caland and Cornelis Lely for this case study are illustrated in Table 3.5.

Table 3.5: Pieter Caland and Cornelis Lely parameters

Parameter	Value
Power installed	3239 [kW]
Power discharge	<input type="text"/> [kW]
Hopper Volume	2853 [m3]
Sailing Velocity (Empty)	<input type="text"/> [knots]
Sailing Velocity (Full)	<input type="text"/> [knots]
Weekly Cost Rate	<input type="text"/> [EUR]
Fuel Usage	<input type="text"/>



Pieter Caland

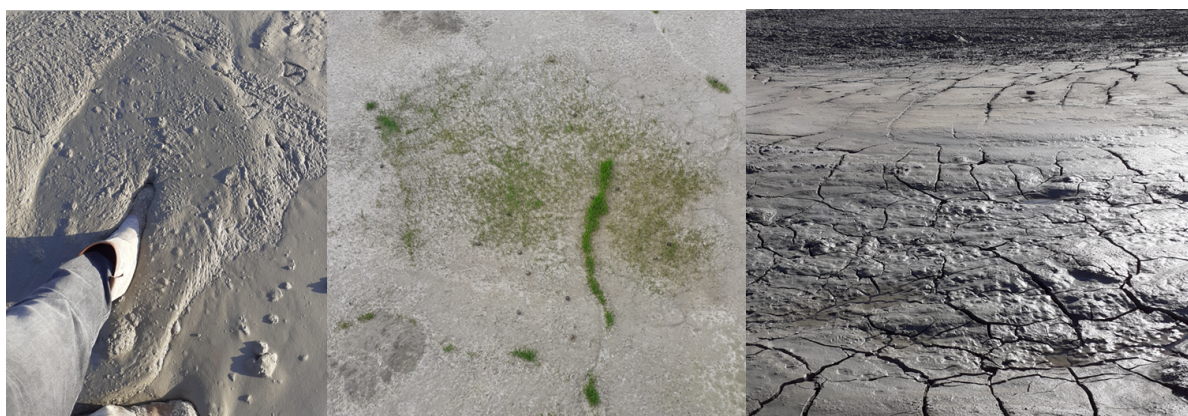


Cornelis Lely

Figure 3.15: Split hopper barges (obtained from Van Oord database)

Materials

The soil material used for this case-study is based on the **Scandinavia** project, which utilizes “complex” materials for reclamation purposes. The general parameters representing the “complex” soil properties are presented in this section.

**Figure 3.16:** “Complex” Scandinavia material (C.Hoffmann)

A physical soil sample is received from the project site for the settling column analysis of the self-weight consolidation process, which is used to calibrate the large-strain model. This soil sample is sampled somewhere in the reclamation. For this case-study, this soil sample is assumed to be representable for all slurry material. The soil properties corresponding to small-strain behaviour are obtained from in-house data reports of the **Scandinavia** project, based on Oedometer tests. These soil properties are representable for the bulk material used in the reclamation. It is assumed that the physical samples used for large-strain calibration represents the same bulk material as the small-strain soil properties obtained from the in-house report. Parameters presented in this section are used as input for the Production and Reclamation modules. More details can be found in Appendix C.

Large-strain material

The physical material used for calibration of the large strain model is analysed in the lab for its index properties as liquid limit (LL) and plastic limit (PL). In addition, the grain-size distribution is measured. The constitutive relations of the large-strain model are obtained by a settling column analysis of the physical material received, as indicated in Figure 3.17. The large strain material is tested in the lab on index properties and its grain-size distribution as presented in Table 3.6.

Table 3.6: Soil parameters for physical soil samples (re-handled material)

clay [%]	silts [%]	sands [%]	gravel [%]	PL [%]	LL [%]
8.06	74.41	17.53	0	20.8	38.6



Settling column tests C0 = 660 g/L



Soil samples

Figure 3.17: Testing of the large-strain material

Small-strain material

The in-situ properties of the material and the small-strain compression properties of the re-handled material are based on **Scandinavia** project information. Table 3.7 represents the material parameters important for soil cutting at the dredging site. Table 3.8 represents re-handled material parameters obtained from the **Scandinavia** project. These parameters are assumed to be representable for the fill material after the placement of the crust in the case-study.

Table 3.7: Soil parameters for in-situ material at dredging site

$\gamma_{sat} [kg/m^3]$	$\varphi [^\circ]$	$UCS [kPa]$	$PL [-]$	$LL [-]$
2300	33	1480	11.5+-15.8	20.8+-21.7

Where:

- γ_{sat} = density [kg/m³]
- φ = friction angle [°]
- UCS = Unconfined compressive strength [kPa]
- PL = Plastic limit [-]
- LL = Liquid limit [-]

Table 3.8: Soil parameters for re-handled material after self-weight consolidation

$\gamma_{sat} [kg/m^3]$	$CR [-]$	$RR [-]$	$C_a [-]$	$C_v [m^2/s]$	$S_u [kPa]$	$\varphi [^\circ]$	$C [kPa]$
1930	0.080	0.008	0.001	3e-06	15	28	0

Where:

- CR = compression ratio [-]
- RR = recompression ratio [-]
- C_a = secondary compression [-]

- C_v = coefficient of consolidation [m²/s]
- S_u = undrained shear strength [kPa]
- C = cohesion [kPa]

The imported sand functioning for the crust and surcharge placed on top of the fill material consists of a saturated unit weight of 20 kN per square meter and a friction angle of 33 degrees. The imported sand has an unsaturated unit weight of 18 kN per square meter.

3.2.2. Framework Calibration

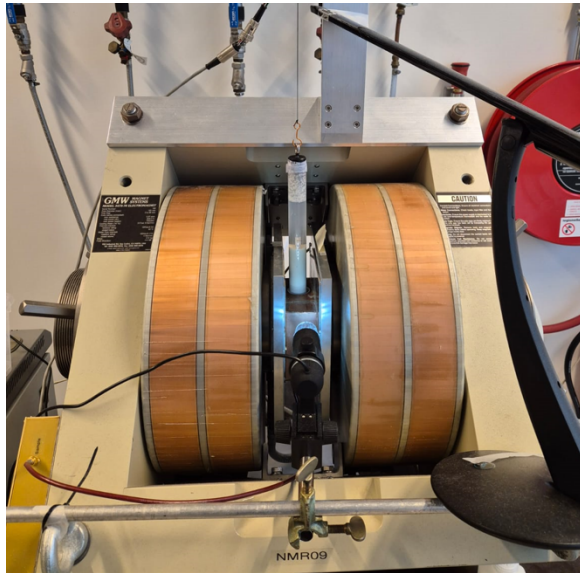
This section describes the calibration strategy of the framework models to this case-study. A detailed explanation of the calibration techniques used can be found in Appendix A for production models and in Appendix B for the reclamation models.

Production Estimation

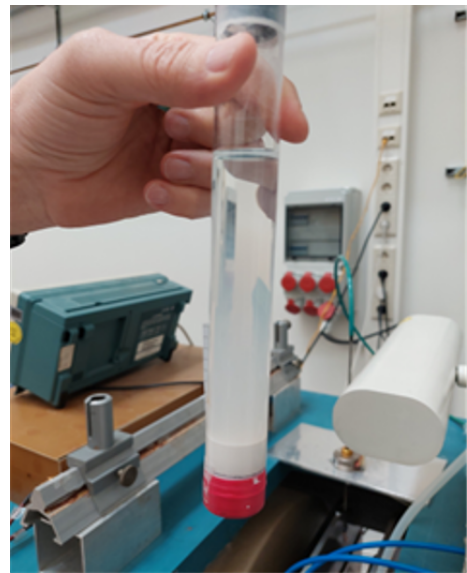
The production models for both hydraulic and mechanical dredging are tuned with vessel and case-study parameters which are essential in estimating the production rates. For Production Estimation, only the dredging pumps for the hydraulic method are calibrated to fit the real-life performance of the specific pumps on board of the Trailing Suction Hopper Dredger. The dredge pumps are calibrated through the affinity rules for pump head and for Net Pressure Suction Head required. More detailed information on the tuning and calibration of the production model parameters can be found in Appendix A.

Reclamation Engineering

In this thesis case study, the constitutive relations representing the self-weight consolidation process of the slurry material in the settling columns are determined using a state-of-the-art calibration technique known as Nuclear Magnetic Resonance (NMR). The NMR technique is chosen because of its potential to provide highly accurate predictions of the self-weight consolidation behaviour of the slurry material. The NMR method can be used to measure water content of the material in a settling column. The water content inside the pores of the slurry can be measured by making a settling column prone to a strong magnetic field. The water content fraction of the slurry material can be determined by detecting the electromagnetic signals of the hydrogen atoms in the sample after absorption of radio-waves, when the sample is prone to a magnetic field. From the measurements of water content fraction, the solid content ϕ_s can be determined indirectly as well as the density of the material. From this method, density profiles can be obtained along the settling column over time. The NMR setup is shown in Figure 3.18.



NMR device



Settling column

Figure 3.18: Nuclear Magnetic Resonance (NMR) setup at TU/e

The calibration constants of constitutive relations that need to be fitted are K_σ , n , and K_k , as shown

in Equation 3.1 and Equation 3.2. These power-law approximations are based on the theory of Merckelbach (2000). Here, Equation 3.1 represents the constitutive relation of hydraulic conductivity and equation 3.2 represents effective stress.

$$\sigma_{sk}(z, t) = K_\sigma [\phi_s(z, t)]^n - K_{\sigma 0} \quad (3.1)$$

$$K(z, t) = K_k [\phi_s(z, t)]^{-n} \quad (3.2)$$

The fitting parameters used to calibrate the constitutive relations are derived from the density profiles and the evolution of the water-suspension interface over time, obtained by the NMR. This makes it an indirect method for capturing the constitutive relations of hydraulic conductivity and effective stress. The calibration constants can be obtained by the following steps (Myouri, [In prep](#)):

1. Determination of n and K_σ based on the final profile of the volume fraction of solids at the end of self-weight consolidation
2. Determination of K_k based on numerically fitting the water-suspension evolution over time.

According to Chassagne (2021), combining the theories of Merckelbach (2000) and Gibson et al. (1967) reduces the original Gibson formulation of Equation 3.3 to Equation 3.4. This shows that the final profile of the volume fraction of solids after self-weight consolidation is only dependent on K_σ and n . These parameters can be obtained by using non-linear fitting algorithms to fit the right side of Equation 3.4 to the last volume fraction of solids profile. This method is convenient and fast. Another option to obtain the K_σ and n parameters is to directly adjust these parameters in the numerical computations of the Gibson equation and adjust these values until the numerical solution of volume fraction of solids obtains the same final profile as observed from experimental data.

$$\frac{\partial \phi_s}{\partial t} = \frac{\partial}{\partial z} \left(K \frac{(\rho_s - \rho_w)}{\rho_w} \phi_s^2 + \frac{K}{g \rho_w} \phi_s \frac{\partial \sigma_{sk}}{\partial z} \right) \quad (3.3)$$

$$\phi_s(t \rightarrow \infty, z) = \left[\frac{(\rho_s - \rho_w)g}{n K_\sigma} (n - 1)(h_\infty - z) \right]^{\frac{1}{n-1}} \quad (3.4)$$

Where:

- Φ_s = volume fraction of solids [-]
- K = hydraulic conductivity [m/s]
- σ_{sk} = effective stress [Pa]
- z = height [m]
- ρ_w = density of water [kg/m³]
- ρ_s = density of solid grains [kg/m³]
- g = gravitational acceleration [m/s²]
- h_∞ = final height after consolidation [m]
- K_σ = fitting constant [-]
- $K_{\sigma 0}$ = fitting constant [-]
- n = fitting constant [-]

The parameter of K_k can be obtained by directly fitting the water-suspension interface as recorded from the settling column by the NMR method, based on the found parameters for K_σ and n . The numerical solution of the Gibson equation is computed for different K_k until a perfect fit is found between the numerical solution and the observed values of the water-suspension interface.

Figure 3.19 represent the results of experimental data compared to the numerical computations after tuning of the model parameters of the slurry material used in this case-study. Here, the numerical computation of large-strain consolidation based on the complete set of K_k , n and K_σ corresponds to the physical behaviour of the settling column as captured by NMR. The benefit of this state-of-the-art NMR method is to obtain accurate density profiles over time of the tested material. This gives the

advantage to directly validate the numerically intermediate density profiles to the intermediate density profiles observed from the physical material.

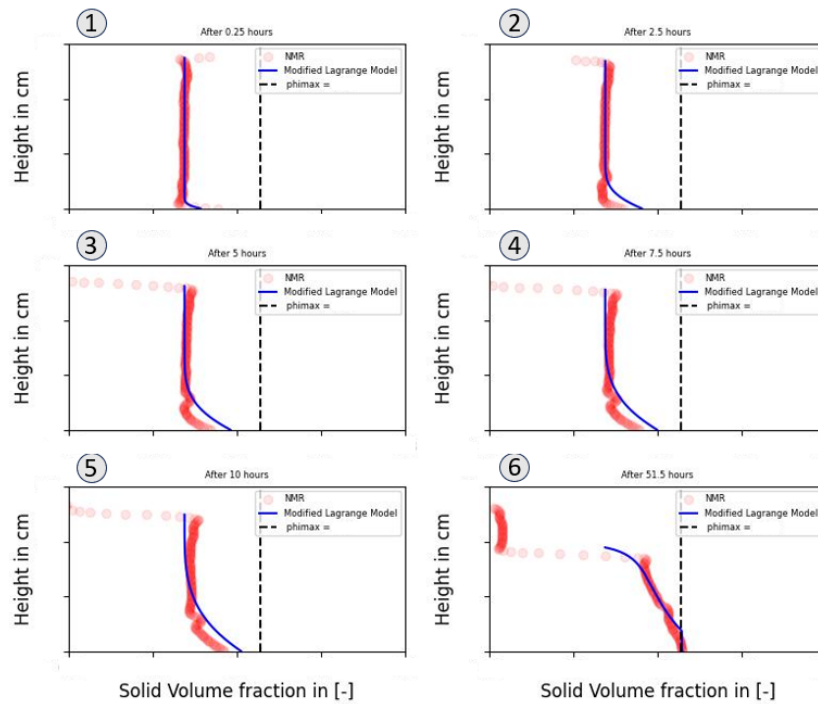


Figure 3.19: Gibson equation fitted to density profile data obtained by Nuclear Magnetic Resonance (NMR) analysis

More details on methods to obtain the constitutive relations and the parameters of the case-study material can be found in Appendix B.

Several calibration techniques are tested in this thesis to try to make the proposed framework applicable in early stages of tenders when no soil information is available. The performance of the numerical model calibrated by these techniques are compared to the data of an external settling column of the physical material, tested in the laboratory. Besides the NMR method, other calibration methods are considered; the "Carrier & Beckham" method and the "Analytical Solution" method. The calibration method of Carrier & Beckham is an empirical method which estimates the constitutive relations based on index properties such as, plastic limit (PL), liquid limit (LL), plasticity index (PI) and activity (act). The analytical solution of Gibson's equation enables to make an analytical estimation of the fitting parameters, using settling column data.

Table 3.9: Calibration methods for Large and Small strain consolidation models

ID	Consolidation model	Calibration method	Constitutive model
1	Large Strain	Nuclear Magnetic Resonance (NMR)	Merckelbach
2	Large Strain	Carrier & Beckham index test	Carrier & Beckham
3	Large Strain	Analytical solution & settling column	Merckelbach
4	Small Strain	Oedometer	NEN-Bjerrum

Long term consolidation is estimated with the small strain model based on the consolidation theory of Terzaghi. This model assumes constant material parameters for permeability and compressibility. These values can be estimated from testing physical samples by Oedometer tests. In this test, a sample is compressed in a 1D Oedometer cell. Here, a relation between stress and strain is obtained by recording the settlements at each stress increment. From these measurements, important information can be obtained for the determination of compressibility and permeability. In this thesis, no Oedometer

tests are conducted directly; instead, the results from Oedometer tests are obtained from the **Scandinavia** soil report, as indicated in Table 3.8. Here, it is assumed that the properties of the soil from the obtained Oedometer data is representable for the physical sample that is tested for the large-strain model.

3.2.3. Framework Validation

This section will elaborate on the verification and validity of the framework models calibrated to this case-study. More detailed information on the validity of the large-strain consolidation calibration methods can be found in Appendix C.

Production Estimation

The production module of both the hydraulic and mechanical work methods are verified by company experts, acknowledging that the right physical principles are used in both the hydraulic and mechanical production models for estimation of production rates, cycle duration and costs. The outcomes of the production models for the case-study material are validated in-house at Van Oord. Due to intellectual property (IP), this validation procedure can not be shared in this thesis.

The conclusion of the production model validation process is that the outcomes for production rates, cycle duration, corresponding hopper densities and costs fall within the range of values that Van Oord would expect during a project for which the case-study material in this thesis is used.

Reclamation Engineering

The reclamation module consisting of the large-strain models to estimate self-weight consolidation and small-strain models to estimate consolidation under effect of ground-improvement methods are verified by company experts and research experts. For validity assessment of the numerical estimations based on the Gibson formulation based on the field material used in this thesis, settling column tests are used. Figure 3.20 compares the performance of the numerical estimation based on the proposed calibration method to the data recorded from an independent settling column of 500 mL containing slurry material.

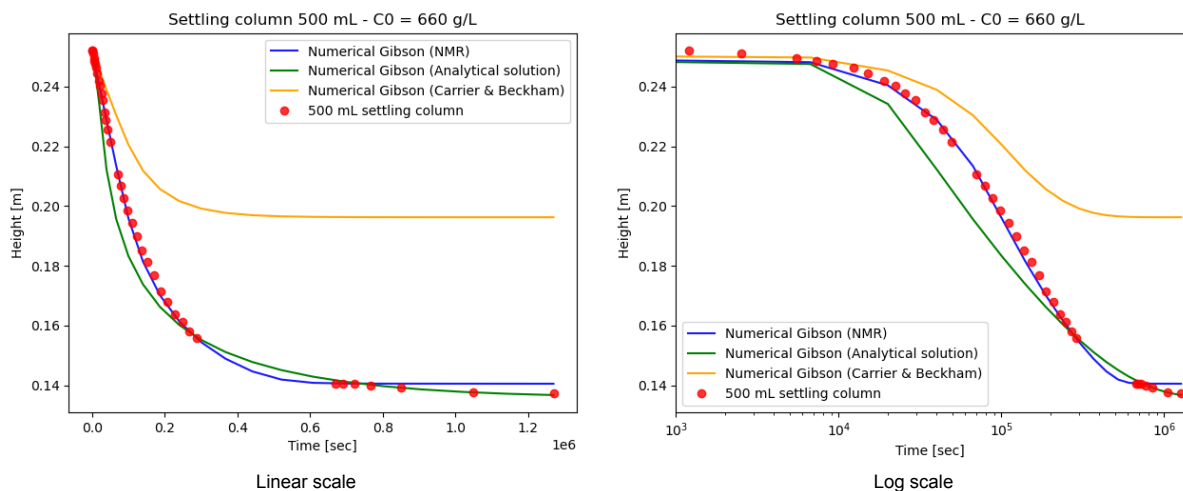


Figure 3.20: Scandinavia material: settling column data and numerical Gibson solution for different calibration methods

Figure 3.20 shows that the Nuclear Magnetic Resonance (NMR) method provides an accurate prediction of the real-life interface evolution in the settling column. However, the final values of the time-series deviate from the observed data due to a sudden leakage that occurred during testing, resulting in an increased uncertainty for the last values. Furthermore, the calibration method proposed by Carrier & Beckham has been shown to be highly inaccurate. Based on the index properties tested in the laboratory, this method significantly underestimates the consolidation behavior of the material. Calibration using the analytical solution overestimates consolidation during the initial stages but converges to accurate estimates in the later stages of consolidation. The numerical estimations based on the NMR method are used in the rest of this thesis for the generation of consolidation data.

Myouri (In prep) has shown that large strain estimations based on the Nuclear Magnetic Resonance (NMR) approach in this thesis is accurate and applicable for a wide range of concentrations. He performed an excellent sensitivity analysis providing proof that the numerical solution of the Gibson equation gives reliable estimations for Kaolinite suspensions at a wide range of initial densities. Besides the perfectly followed suspension interface over time in Figure B of 3.21, also the density profiles at the end of consolidation do match accurately as shown in Figure A of 3.21. The work of I. Myouri provides a base-line, demonstrating that this numerical approach for large-strain consolidation can be applied across a wide range of initial concentrations. In the context of this thesis, the model proves to be applicable for both low initial concentrations typical of hydraulic production methods and high initial concentrations associated with mechanical production methods.

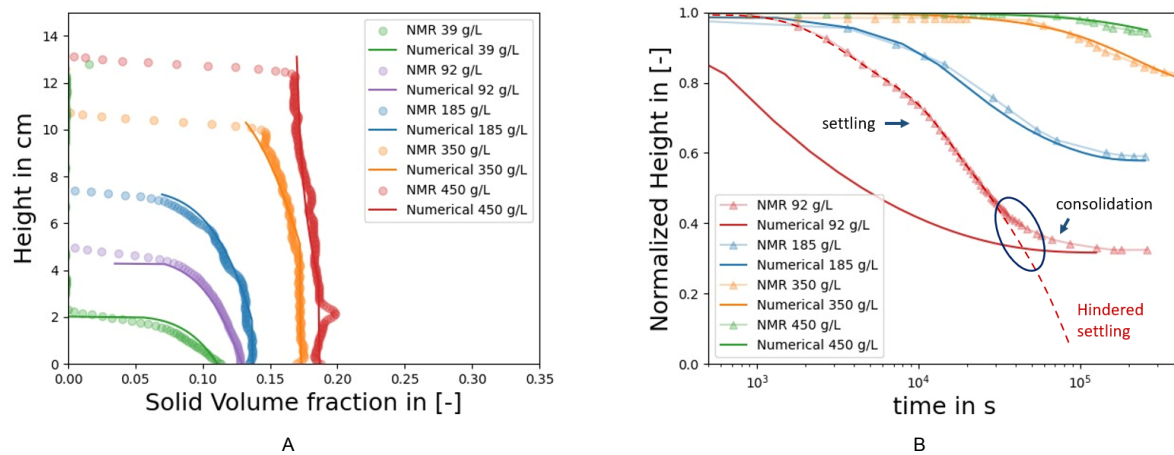


Figure 3.21: Koalinite suspension: sensitivity analysis numerical solution vs settling column obtained from Myouri (In prep), part of “Sediment to Soil” (S2S).

The numerical approach driven by Gibson’s theory is validated in this section for consolidation of one layer of field material. However, this thesis extends the numerical Gibson approach to a transient layer stacking method. This method is capable of stacking time-dependent layers on top of each other with a constant time-interval. This method is completely based on Gibson’s large strain consolidation theory which is widely validated. The validation of the transient layer stacking is hard to validate in the lab in the time duration for this thesis. It is not easy to stack multiple layers on top of each other in a settling column. However, the numerical method adopted for the layer stacking conserves mass throughout the layer stacking process. Deltares has developed a numerical multilayer Gibson method in the past, called *Delcon*. The multilayer approach created in this thesis is matching in results with the results coming from *Delcon*. The *Delcon* code can not be used in this thesis due to intellectual property (IP) reasons. The matching results between both models indicate that the multi-layer approach taken in this thesis is capable of approximating real-life practical cases.

3.2.4. Optimizations Production Estimation - Reclamation Engineering

In this case-study, optimizations on Production Estimation and Reclamation Engineering are implemented by adjusting the initial density of the slurry. The initial slurry density is strongly linked to production and serves as the basis for the self-weight consolidation process. Since initial density and the duration between layer stacking forms the foundation of both models, these parameters can be used to experiment with the trade-off between Production Estimation and Reclamation Engineering optimization on project costs. The trade-off optimizations will be analysed through the framework by the case study in three steps:

1. Single cycle production analysis (only Production)
2. Production - self-weight consolidation analysis (excluding small strain)
3. Full scale case-study (including: production - large strain - small strain analysis)

Single cycle production analysis in the first step will assess the costs and duration of a single dredging

cycle consisting of; dredging - sailing full - discharging - sailing empty, for different initial densities. This will be performed for typical densities coming with the hydraulic and mechanical work methods. Single-cycle production analysis is essential for obtaining initial insights into the “production characteristics” of each dredging method. It highlights power utilization, costs, and cycle duration when the specific work method is applied exclusively to one single dredging cycle through the case study.

The production - self-weight consolidation analysis in the second step will demonstrate the connection between production and large strain consolidation. Here the amount of material that is required for reaching a design level and the duration of self-weight consolidation of the material is analysed. This analysis will highlight the effect of optimizations in Production Estimation or Reclamation Engineering by alternating initial density and the duration between layer stacking. Here, one layer of material placed is defined as 1 meter of homogeneously distributed material across the whole reclamation. This is assumed to be placed instantaneously. The duration between layer the placement of two consecutive layers is determined by logistical software OpenCLSim which estimates the duration it takes to bring in such quantity of material. The results of this analysis indicate what variations in initial density and dredging work method will lead to the lowest production costs considering both production placement and the self-weight consolidation ability of the material. Additionally, effects of initial density and layer stacking duration variations on self-weight consolidation behaviour can be quantified.

Finally, one hydraulic configuration consisting of 1100 kg/m³ initial density and one mechanical configuration consisting of 1300 kg/m³ are tested using the full framework, which includes small-strain estimations for ground improvement methods. Subjecting the framework to a complete case-study will demonstrate how Production Estimation or Reclamation Engineering optimizations will affect the project costs. For “complex” materials it is expected that hydraulic dredging potentially optimizes costs of Production Estimation, due to its high production rates and relatively low costs. The mechanical method is expected to potentially optimize for Reclamation Engineering by achieving a higher initial density, which could lead to improved consolidation of the material. This may decrease the need for extensive ground improvement measures which could reduce Reclamation Engineering costs. With the total project duration fixed for both dredging methods, the differing filling times between the two approaches will result in varying time-frames available for ground improvements. Consequently, the extent of ground improvement required to force the soil properties to the desired state to comply with design requirements varies between each dredging method, directly influencing the overall costs corresponding to Reclamation Engineering

4

Results

This section shows the results of the case-study analysis through the proposed framework in chapter 3. The first part of the results section indicates the effects of optimizations on a single production cycle by varying initial density. The second part of this results section illustrates the connection between production and self-weight consolidation of the material. This part indicates the first results on how optimizations on production or optimizations on self-weight consolidation affects production costs by varying the initial density. The last part of this section subjects the framework to a full-scale case-study, including production, self-weight consolidation, and small strain consolidation including ground improvement methods. This part demonstrates the effects of production optimization or reclamation optimizations on the costs before the asset can be delivered to the client, by alternating between hydraulic and mechanical work methods. Answers can be provided to the research questions by analysing the results of this case-study.

4.1. Production - single dredging cycle analysis

This section provides the dredging cycle parameters for a single dredging cycle analysis. This section is based on the calculations from the production models as presented in Appendix A. For each dredging method the effect of increasing hopper density is shown on the parameters for one dredging cycle. The "Cycle duration" represents the duration it takes to dredge, sail full, discharge, and sail back empty. This duration is obtained from OpenCLSim. "Flow" represents the volume of slurry mixture that is transported over the cycle duration. "Production" represents the amount of tons of solid material that is transported over the cycle duration. "Energy" represents the amount of energy that is utilized by the vessel during the dredging cycle and "Costs" represents the cost coming for one dredging cycle and the costs per transported ton solid material. The results obtained are presented in Table 4.1 and Table 4.2.

Table 4.1: Vox Amalia - Production analysis of one dredging cycle

Density [kg/m ³]	Flow [m ³ /min]	Cycle duration [min]	Production [ton/min]	Energy [kWh]	Costs [EUR]	Costs [EUR/ton]
1050	<input type="text"/>	<input type="text"/>	<input type="text"/>	<input type="text"/>	<input type="text"/>	<input type="text"/>
1100	<input type="text"/>	<input type="text"/>	<input type="text"/>	<input type="text"/>	<input type="text"/>	<input type="text"/>
1150	<input type="text"/>	<input type="text"/>	<input type="text"/>	<input type="text"/>	<input type="text"/>	<input type="text"/>
1200	<input type="text"/>	<input type="text"/>	<input type="text"/>	<input type="text"/>	<input type="text"/>	<input type="text"/>
1250	<input type="text"/>	<input type="text"/>	<input type="text"/>	<input type="text"/>	<input type="text"/>	<input type="text"/>
1300	<input type="text"/>	<input type="text"/>	<input type="text"/>	<input type="text"/>	<input type="text"/>	<input type="text"/>

Table 4.2: Goliath & Pieter Caland - Production analysis of one dredging cycle

Density [kg/m ³]	Flow [m ³ /min]	Cycle duration [min]	Production [ton/min]	Energy [kWh]	Costs [EUR]	Costs [EUR/ton]
1200	<input type="text"/>	<input type="text"/>	<input type="text"/>	<input type="text"/>	<input type="text"/>	<input type="text"/>
1300	<input type="text"/>	<input type="text"/>	<input type="text"/>	<input type="text"/>	<input type="text"/>	<input type="text"/>
1400	<input type="text"/>	<input type="text"/>	<input type="text"/>	<input type="text"/>	<input type="text"/>	<input type="text"/>
1500	<input type="text"/>	<input type="text"/>	<input type="text"/>	<input type="text"/>	<input type="text"/>	<input type="text"/>

The Vox Amalia transports 18900 cubic meters of material per dredging cycle. Here, in Table 4.1 can be observed that a increase in (slurry) density leads to a increased cycle duration, leading to a lower rate of transported slurry mixture per minute, "Flow". Consequently, cycle costs are increasing due to longer production duration and because more energy is used to pump a higher density mixture. However, the costs per transported tons solid material go down because significantly more solid material is moved per cycle for increased hopper density.

The Goliath plus barge transfers 2856 cubic meters per dredging cycle. Here, in Table 4.2, the same trend can be observed where an increase in (slurry) density leads to longer cycle duration, leading to lower "Flow". Cycle costs go up due to the increased cycle duration and more energy is needed to transport the material. However, the costs per transported tons solid material go down because significantly more solid material is moved per cycle for increased hopper density.

4.2. Production - self-weight consolidation analysis

The production analysis illustrates how adjustments in production decisions influence not only production duration and costs but also the self-weight consolidation of the material. The initial density affects the amount of material required to reach the specified design height which is determined by the deformation of the material after self-weight consolidation. This section connects production estimations (Appendix A) with large-strain consolidation estimates (Appendix B) for materials with varying initial densities. It expands on the single-cycle analysis from Section 4.1 to a multi-cycle analysis, where production is directly coupled with consolidation behavior. This process is depicted in Figure 4.1.

This section up-scales the single dredging cycle analysis of section 4.1 to represent the amount of single dredging cycles needed to obtain 1 meter of material across the reclamation area. The "single layer cycle" is indicated in Figure 4.1. Multiple of these "single layer cycles" are used to place sufficient material to obtain the design height after self-weight consolidation. With the Vox Amalia transferring 18900 cubic meters in one single dredging cycle and the Goliath plus barge transferring 2853 cubic meters in one single dredging cycle, OpenCLSim is used to scale up the duration and cost parameters to account for the number of cycles needed to achieve a 1 meter layer across the entire reclamation area. This duration is represented as the time required in between layer stacking, denoted as "Single layer cycle" in Figure 4.1.

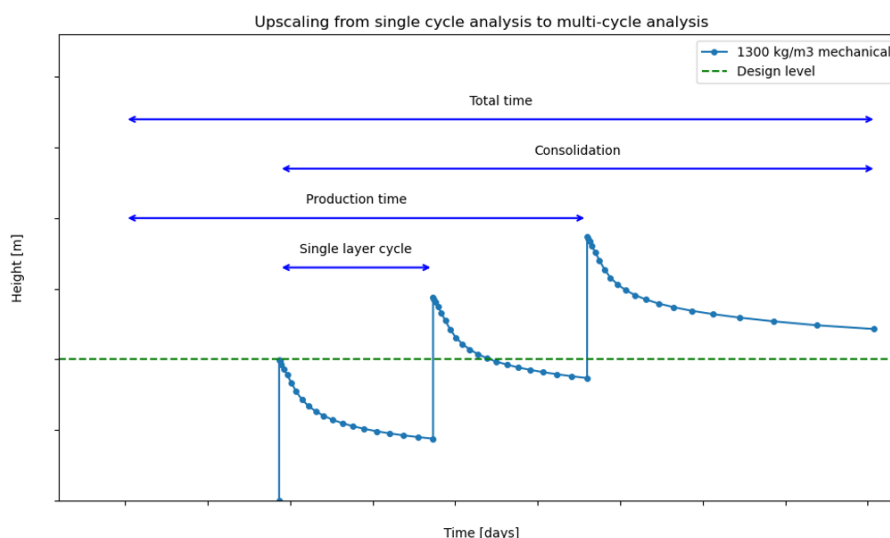


Figure 4.1: Upscaling from single cycle to multicycle analysis

For this analysis, the quantity of material with an initial density needed from production to reach the design level after self-weight consolidation is calculated using both the production and large-strain consolidation models, governed by OpenCLSim. The production costs for dredging and layer placement are based on the number of layers required. The consolidation timeframe is defined as the period from when the first layer begins consolidating until self-weight consolidation is complete. Production time is calculated as the time needed to dredge and place each layer, while total time accounts for all activities from the start of dredging to the end of consolidation. These variables are visualized in Figure 4.1. These calculations are performed for hydraulic dredging with a initial density of 1100 kg/m³ and 1200 kg/m³ in Table 4.3. This is also performed for the mechanical dredging method with a initial density of 1300 kg/m³ and 1400 kg/m³ in Table 4.4.

The material is placed by production in homogeneous layers of 1 meter at the specified initial density, meaning that each layer placed corresponds to a volume of 292,500 cubic meters of dredged material. The duration for placing this amount of material determines the time between layer placements. This analysis considers the material required to reach minimum design levels of 1, 2, or 3 meters after self-weight consolidation, with the number of layers rounded to whole numbers. This results in slight variations in the exact amount of solid mass placed, because it is not possible to end up with the exact design level when using whole layers. For this approach, the overall magnitude of results corresponding to duration and costs will be consistent. The number of layers placed and the corresponding material amount to reach the design level after self-weight consolidation are indicated in the "material" column of Table 4.3 and Table 4.4.

Table 4.3: Production and self-weight consolidation - Hydraulic dredging

Design level [m]	Density [kg/m ³]	Material [m ³]	Prod. Costs [EUR]	Prod. time [days]	Consolidation [days]	Total time [days]
1m	1100	2.340.000 (8)	<input type="text"/>	<input type="text"/>	<input type="text"/>	<input type="text"/>
2m	1100	4.387.500 (15)	<input type="text"/>	<input type="text"/>	<input type="text"/>	<input type="text"/>
3m	1100	6.727.500 (23)	<input type="text"/>	<input type="text"/>	<input type="text"/>	<input type="text"/>
1m	1200	1.170.000 (4)	<input type="text"/>	<input type="text"/>	<input type="text"/>	<input type="text"/>
2m	1200	2.340.000 (8)	<input type="text"/>	<input type="text"/>	<input type="text"/>	<input type="text"/>
3m	1200	3.510.000 (12)	<input type="text"/>	<input type="text"/>	<input type="text"/>	<input type="text"/>

Table 4.4: Production and self-weight consolidation - Mechanical dredging

Design level [m]	Density [kg/m ³]	Material [m ³]	Prod. Costs [EUR]	Prod. time [days]	Consolidation [days]	Total time [days]
1m	1300	877.500 (3)	<input type="text"/>	<input type="text"/>	<input type="text"/>	<input type="text"/>
2m	1300	1.462.500 (5)	<input type="text"/>	<input type="text"/>	<input type="text"/>	<input type="text"/>
3m	1300	2.340.000 (8)	<input type="text"/>	<input type="text"/>	<input type="text"/>	<input type="text"/>
1m	1400	585.000 (2)	<input type="text"/>	<input type="text"/>	<input type="text"/>	<input type="text"/>
2m	1400	1.170.000 (4)	<input type="text"/>	<input type="text"/>	<input type="text"/>	<input type="text"/>
3m	1400	1.755.000 (6)	<input type="text"/>	<input type="text"/>	<input type="text"/>	<input type="text"/>

The effects of increasing density for hydraulic dredging on self-weight consolidation are presented in Table 4.3. Increasing the density from 1100 kg/m³ to 1200 kg/m³, increases the amount of solids in the slurry with 100 percent. As a result, about 50 percent less material is needed for reaching every design level. Due to the decrease of material needed, the amount of layers needed and therefore the costs reduce as well. This comes with a cost reduction of 50 percent as well. The amount of consolidation days needed to bring the 1100 kg/m³ and 1200 kg/m³ material to the design level by self-weight consolidation is about equal between same design levels. The production timeframe is on average 37 percent of the total duration for 1100 kg/m³ while the production timeframe is 20 percent of the total duration for 1200 kg/m³.

The effects of increasing density for mechanical dredging on self-weight consolidation are presented in Table 4.4. Increasing the density from 1300 kg/m³ to 1400 kg/m³, increases the amount of solids in the slurry with 30 percent. Increasing the density for the mechanical method reduces the required material on average with 30 percent for each design level. Therefore, the amount of cycles required and the costs of production to reach design level are reduced on average with 30 percent as well. Additionally, the amount of consolidation days needed to bring the 1300 kg/m³ and 1400 kg/m³ material to the design level by self-weight consolidation is about equal between same design levels. Across different design levels, production time takes on average 68 percent of the total duration for 1300 kg/m³ while the production time is 51 percent of total duration for 1400 kg/m³.

Table 4.5: Production costs for design level of 3 meters

Method	Density [kg/m ³]	Prod. costs [EUR/m ³]	Prod. costs [EUR/day]
Hydraulic	1100	<input type="text"/>	<input type="text"/>
Hydraulic	1200	<input type="text"/>	<input type="text"/>
Mechanical	1300	<input type="text"/>	<input type="text"/>
Mechanical	1400	<input type="text"/>	<input type="text"/>

Water-suspension interface

The water-suspension interface development over time is illustrated in Figure 4.2, highlighting the impact of increasing initial density on the consolidation process of the hydraulic dredging method. This figure visualizes the data presented in Table 4.3. The 1100 kg/m³ hydraulic method is placed at a duration of hours in between layers while the 1200 kg/m³ takes hours between layer placement. It can be seen that the consolidation rate of the 1200 kg/m³ method is slower than the 1100 kg/m³ method in between layer placements. The same trend is evident when scaling the design level from 1 meter to 3 meters. The hydraulic method for 1100 kg/m³ material needs days of full self-weight consolidation after placement of the last layer while the hydraulic method for 1200 kg/m³ material needs days after placement of the last layer to meet the design level of 3 meter.

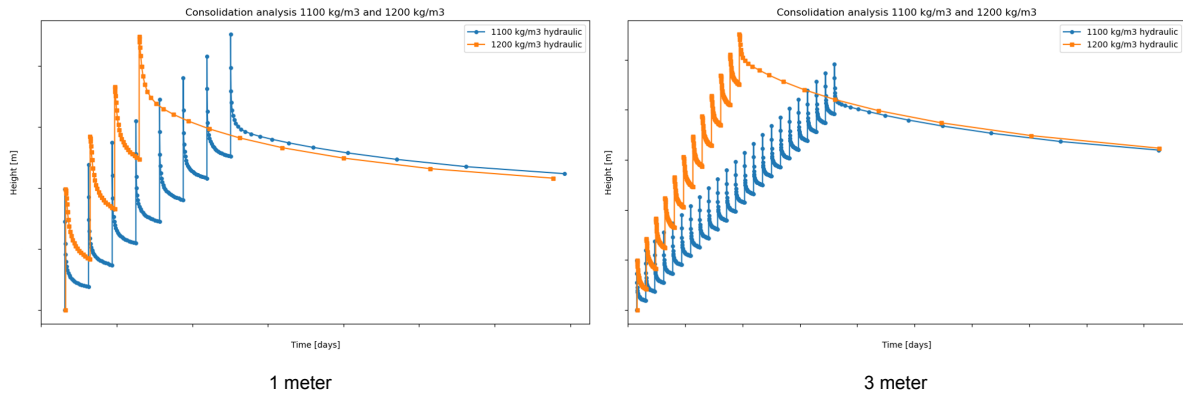


Figure 4.2: Production - reclamation interaction for hydraulic optimization (interface)

Figure 4.3 illustrates development of the water-suspension interface between the hydraulic method for 1100 kg/m³ and the mechanical work method for 1300 kg/m³. The figure highlights how variations in layer filling duration and initial density of hydraulic and mechanical dredging methods influence the consolidation process to meet the same design requirements after self-weight consolidation. This figure visualizes the data presented in Table 4.3 and Table 4.4. Layers of the 1100 kg/m³ hydraulic material are produced at intervals of hours, whereas the 1300 kg/m³ mechanical material requires hours per layer. This extended production duration makes the mechanical method slower in achieving the design requirement. The same trend is evident when scaling the design level from 1 meter to 3 meters. Furthermore, the duration of full self-weight consolidation after the final layer is placed differs significantly: days for the 1100 kg/m³ hydraulic material compared to days for the 1300 kg/m³ mechanical material to meet the 3-meter design requirement.

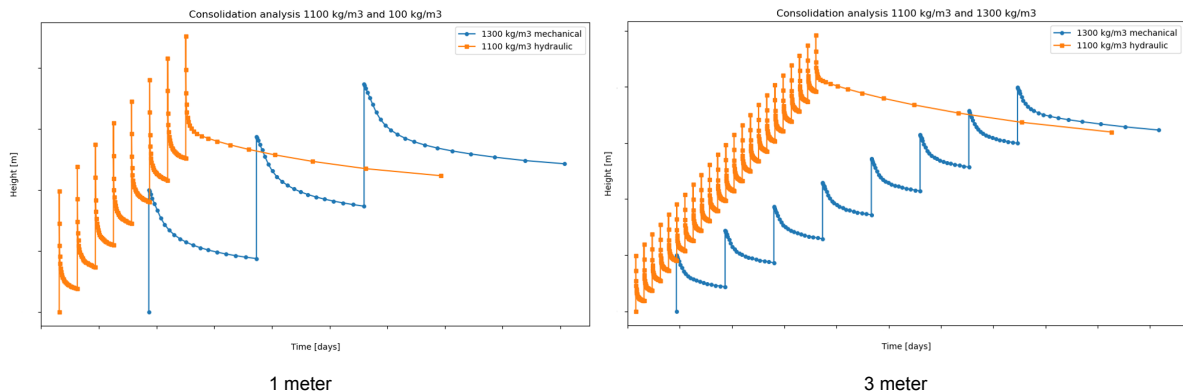


Figure 4.3: Production - reclamation interaction for hydraulic vs mechanical work method (interface)

Density profiles

Where the first part of this section analyses the water-suspension interface over time, this part of the section will dive into what happens underneath the interface with the density developments of the slurry. The density profiles that are obtained and the duration it takes to consolidate are a result of the nature of the material tested, including its compaction and drainage ability behaviour based on NMR analysis in the laboratory. The density profiles presented in this part of this section show the volume fraction of solids over height, after placement of each new layer. This process starts when consolidation starts at $t=0$. In this context, density is indirectly represented by the volume fraction of solids.

This section starts with the analysis of consolidation of a single layer of 1 meter in height for initial densities coming with hydraulic dredging of 1100 kg/m³ and 1200 kg/m³, illustrated in Figure 4.4. The material is allowed to consolidate over the timeframe between the addition of successive layers, hours for the 1100 kg/m³ material and hours for the 1200 kg/m³ material. It is observed that the

1100 kg/m³ material achieves a similar density profile over the bottom part of the 1200 kg/m³ material. However, the 1200 kg/m³ material has a thicker layer of softer material at the top due to more mass deposited in a single layer, which has not the time to consolidate. It seems that on the short term (□□ and □□ hours), the lower density material consolidates more efficiently, while if the material is left to consolidate longer (□□ hours), the higher density material will obtain a more compacted profile at the bottom, due to more weight that pressures consolidation.

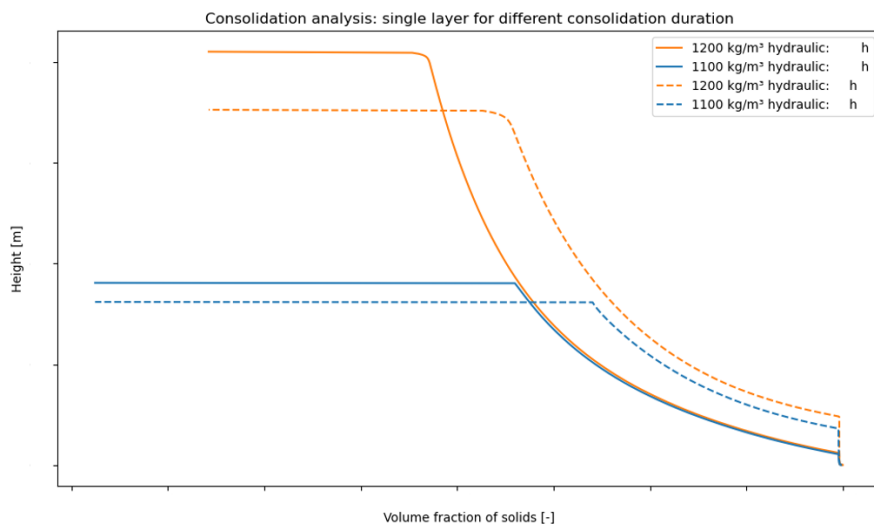


Figure 4.4: Density profile after layer placement duration for a single initial layer of 1 meter at 1100 kg/m³ and 1200 kg/m³

The density profile evolution over time is presented for hydraulic dredging at 1100 kg/m³ and hydraulic dredging at 1200 kg/m³ in Figure 4.5, based on the values in Table 4.3. Significant differences can be observed from this figure. The lowest blue lines in both graphs show the consolidation development of the first layer. It can be observed that the 1100 kg/m³ layer consolidates to below □□ meters while the 1200 kg/m³ layer consolidates to □□ meters, due to more mass that is placed in one layer for the 1200 kg/m³ initial density compared to the 1100 kg/m³ initial density. It can be observed, when comparing the upper pink line for 1100 kg/m³ material to the upper green line for 1200 kg/m³ material that the latter consists of smaller fraction of solids over its top part of the height after placement of the last layer. This means that the upper part of the height of the 1200 kg/m³ material consists of more "soft", lower density material which has the ability to compact relatively more than the profile of the 1100 kg/m³ material, which consists of a smaller top part with soft material after placement of the last layer. This effect is observed in Figure 4.2, where the water-suspension interface of 1200 kg/m³ (orange) material settles more in the full self-weight consolidation regime than the 1100 kg/m³ (blue) material.

During the placement activities, it can be observed that adding more material at small production time intervals lead to "stretching" of the density profile. The "stretching" of the density profile represents the phenomena that more relatively new material with low initial density is placed faster than that the material can consolidate and compact, leading to a density profile where the height of the "soft" material (represented by the curved part of the density lines between □□ and □□ on x-axis) increases after placement of each layer. This "stretching" behaviour is observed more for the 1200 kg/m³ material than the 1100 kg/m³ material in Figure 4.5.

In addition, it can be observed that the profiles densify towards a maximum densification in this consolidation process. This is observed as that the particles obtain eventually a vertical profile at the volume fraction of solids of □□, for both the hydraulic and mechanical dredging methods. This value for volume fraction of solids corresponds with a density of □□ kg/m³. It can be observed in Figure 4.2 that both profiles end up fully at the maximum densification ability over the height, which means that the material stops with self-weight consolidation and does not settle further under its own weight. This happens for both the 1100 kg/m³ and 1200 kg/m³ hydraulic configuration at around the same time. The occurrence of the maximum densification behaviour can be described as "modified Gibson behaviour".

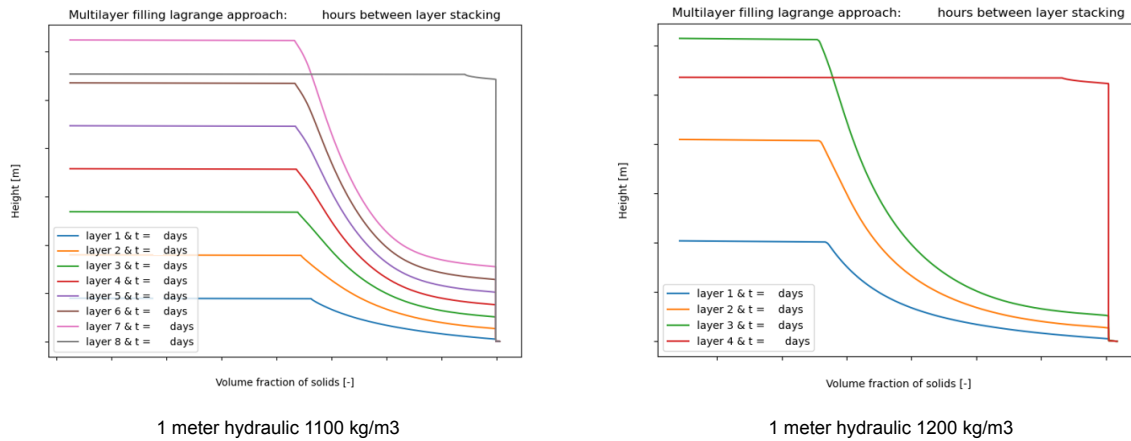


Figure 4.5: Density profile hydraulic dredging 1100 kg/m3 vs 1200 kg/m3

The density profile evolution over time is presented for hydraulic dredging at 1100 kg/m3 and mechanical dredging at 1300 kg/m3 in Figure 4.6, based on the values from Table 4.3 and Table 4.4. Here, triple the mass is placed in one layer for the mechanical method (1300 kg/m3) than the hydraulic method (1100 kg/m3). The extensive production time for placement between two layers for the mechanical method gives the material more time to consolidate to a dense profile before the next layer is placed relatively to the hydraulic material. At the end of consolidation of both materials under its own weight, both obtain its maximum densification profile over almost the entire height. The duration of the mechanical method takes \square days longer than the hydraulic method to obtain this profile.

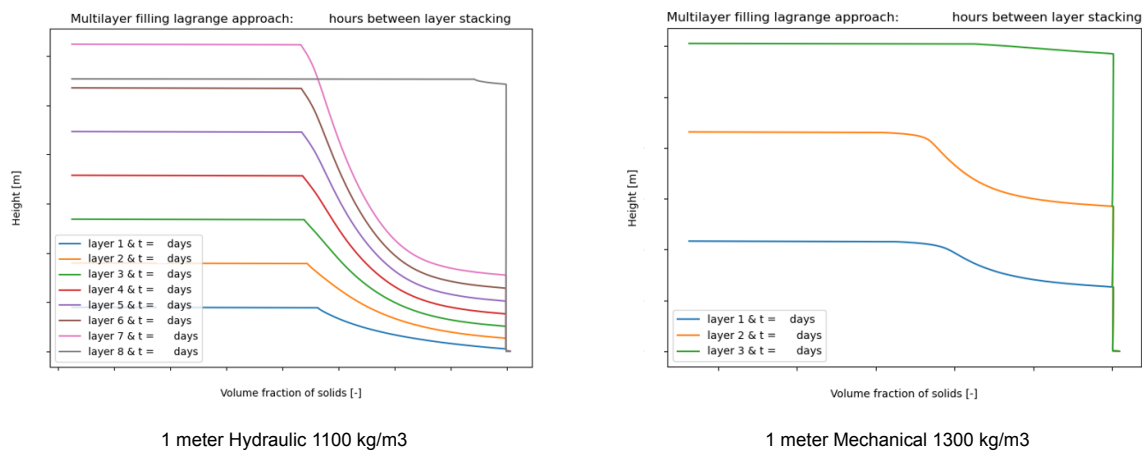


Figure 4.6: Production - reclamation interaction: density profile evolution by consolidation)

The material tested in the lab has been proven to behave differently in the field. The material tested in the laboratory, densified under its own weight to a homogeneous density of \square kg/m3 over height. In practice it was found to compact to \square kg/m3 over height.

4.3. Full scale case-study

This full scale case-study is performed to get more insights in the trade-off between Production Estimation and Reclamation Engineering. This section demonstrates the difference in executing the case-study via hydraulic dredging and mechanical dredging, including both Production and Reclamation costs. This full case-study simulates the filling and self-weight consolidation by the large-strain numerical method. The computation is transitioned to the small-strain domain of D-Settlement at the moment the crust is placed. The total project is to be delivered in 470 days for both work methods.

Hydraulic case-study

The Vox Amalia (Trailing Suction Hopper Dredger) is used to represent the hydraulic method for filling up this reclamation of 292.500 square meters at a design level of 10 meters. The continuous process of filling and consolidation is shown in Figure 4.7. This mechanical method places layers of 1 meters consisting of a homogeneous slurry of 1100 kg/m³ at a duration of [] hours between the placement of two consecutive layers.

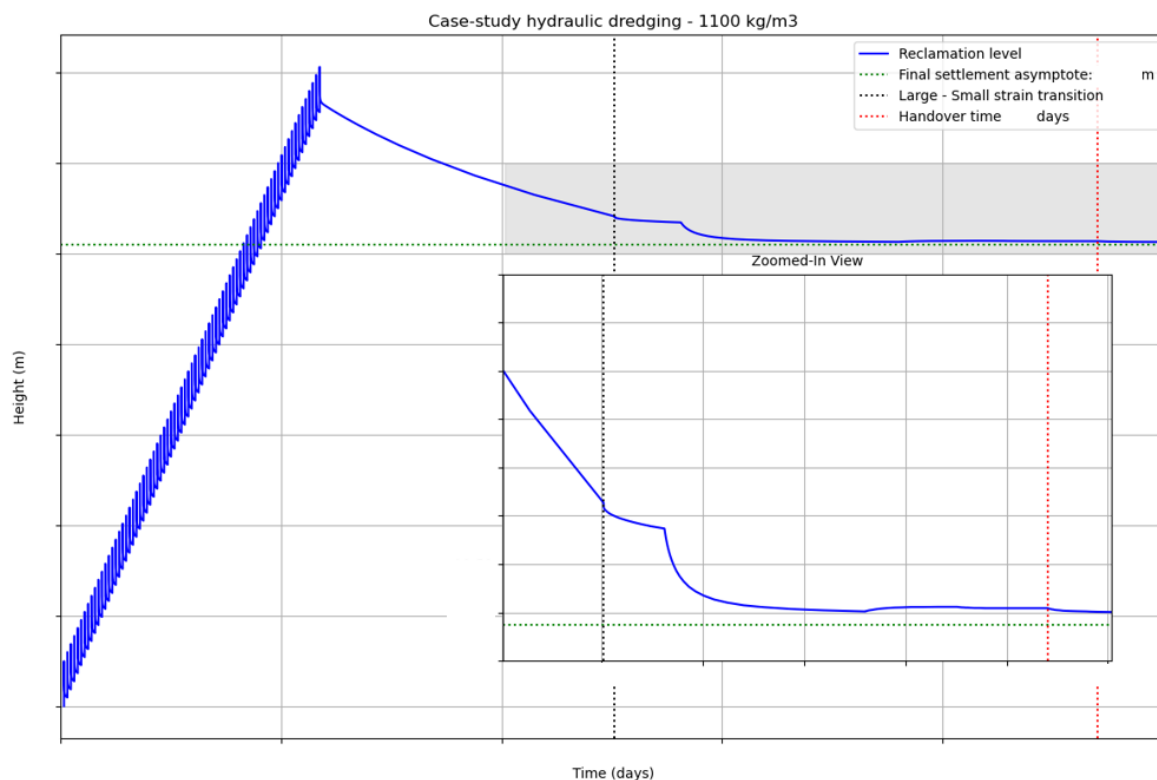


Figure 4.7: Hydraulic case-study: complete reclamation evolvement over time

To fill up this reclamation, 75 layers are needed to place sufficient mass. The filling reaches a maximum of [] meters. The stage of filling takes [] days, resulting in production costs of [] euros for utilization of the Vox Amalia. After placement of the last layer, [] days of self-weight consolidation are needed to consolidate the material until 2 meters of soft material is left on top (see Figure 4.8). After a total of [] days, this soft layer of 2 meters is replaced by a two meter sand crust. The crust thickness of 2 meters is required to provide bearing capacity for the equipment to access the reclamation and install the surcharge and PVD's needed to comply with the design requirements. This calculation is based on bearing capacity equations of Terzaghi.

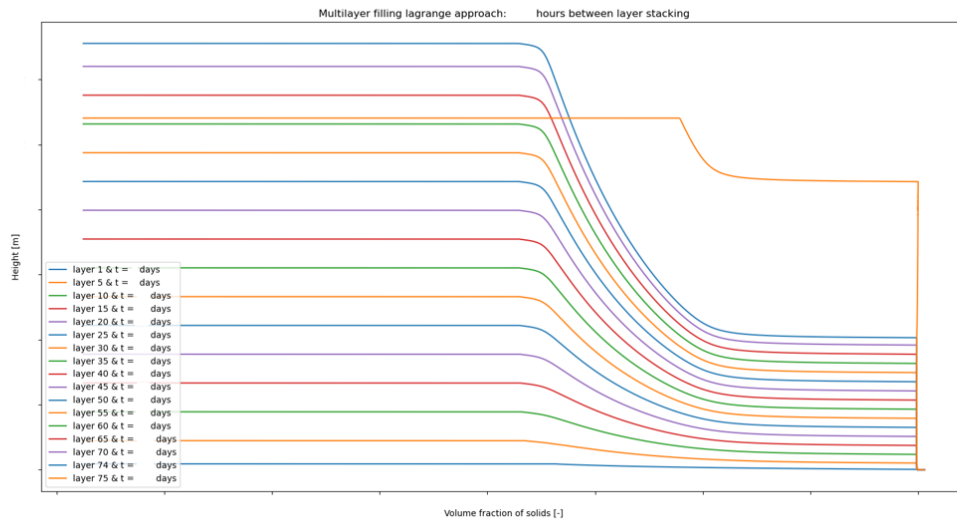


Figure 4.8: Density development in between layer placement after first layer is placed defined as $t=0$

In the small strain domain, the filled material is subjected to ground improvement methods. The loading scheme of the fill material is shown presented in Figure 4.9. Hence, the x-axis starts here at $t=0$, which is marked at the beginning of loading in the small-strain domain. The total days left for the ground improvements methods is days before handover. Here the load starts with 36 kPa, due to a 2 meter crust consisting of 18 kN/m² weight. At day 30, the surcharge installed, increasing the total load up to 133 kPa. At day 129, 90 days before hand-over of the asset to the client, the surcharge is stripped off, whereaes the load decreases back to 36 kPa. 45 days before hand-over, a pavement layer is installed of 22 kPa, to provide a rigid reclamation surface for the client to use. After handover at day 470, the UDL load is installed, after which the improved reclamation needs to comply with the design requirements. It can be found in the left of Figure 4.9 that the design requirements are met under effect of the presented loading scheme.

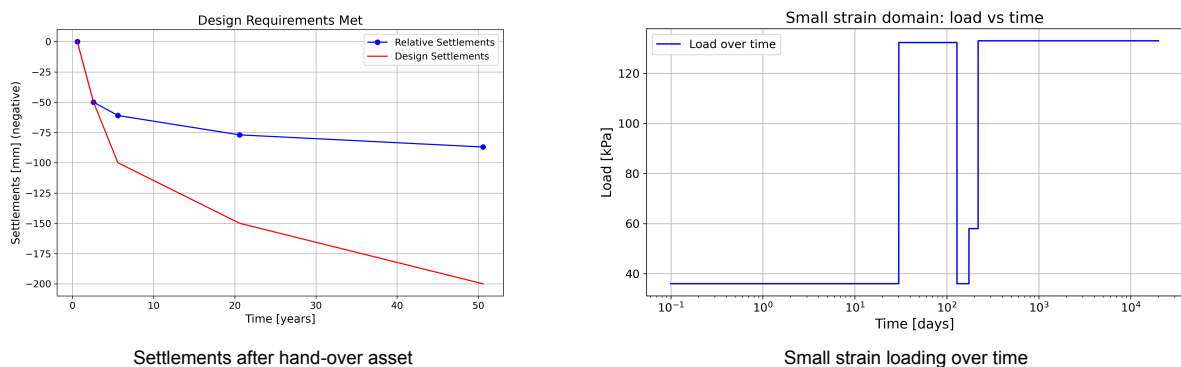


Figure 4.9: Hydraulic case-study: small strain loading

The required quantity of surcharge that needs to be installed was a crust layer of 2 meters, at a weight of 18 kN/m³. The surcharge on top of the crust layer was required to be 5.35 meters at a weight of 18 kN/m². This results into a required volume of 2.149.875 qubic meters, which results into costs of euros based on a price of euros per qubic meter.

The required quantity of Pre-fabricated Vertical Drains needed to increase the draining was a center-to-center distance of 1.8 meters. This brings the total amount of length of PVD's needed to 2.819.794

meters across the whole reclamation. This results in costs of euros based on a variable price of euros per meter PVD and a constant price of euros.

This brings the costs of the total reclamation to euros, including production costs and costs for ground improvement methods as presented in Table 4.6.

Table 4.6: Complete project costs hydraulic work method.

Item	Cost [EUR]
Pre-fabricated Vertical Drains (PVD)	<input type="text"/>
Surcharge + Crust	<input type="text"/>
Hydraulic Production	<input type="text"/>
Total	<input type="text"/>

Mechanical case-study

The Goliath (backhoe) in combination with the Pieter Caland and Cornelis Lely (barges) represent the mechanical method for filling up this reclamation of 292.500 square meters at a design level of 10 meters. The continuous process of filling and consolidation is shown in Figure 4.10. This mechanical method places layers of 1 meters consisting of a homogeneous slurry of 1300 kg/m3 at a duration of hours between the placement of two consecutive layers.

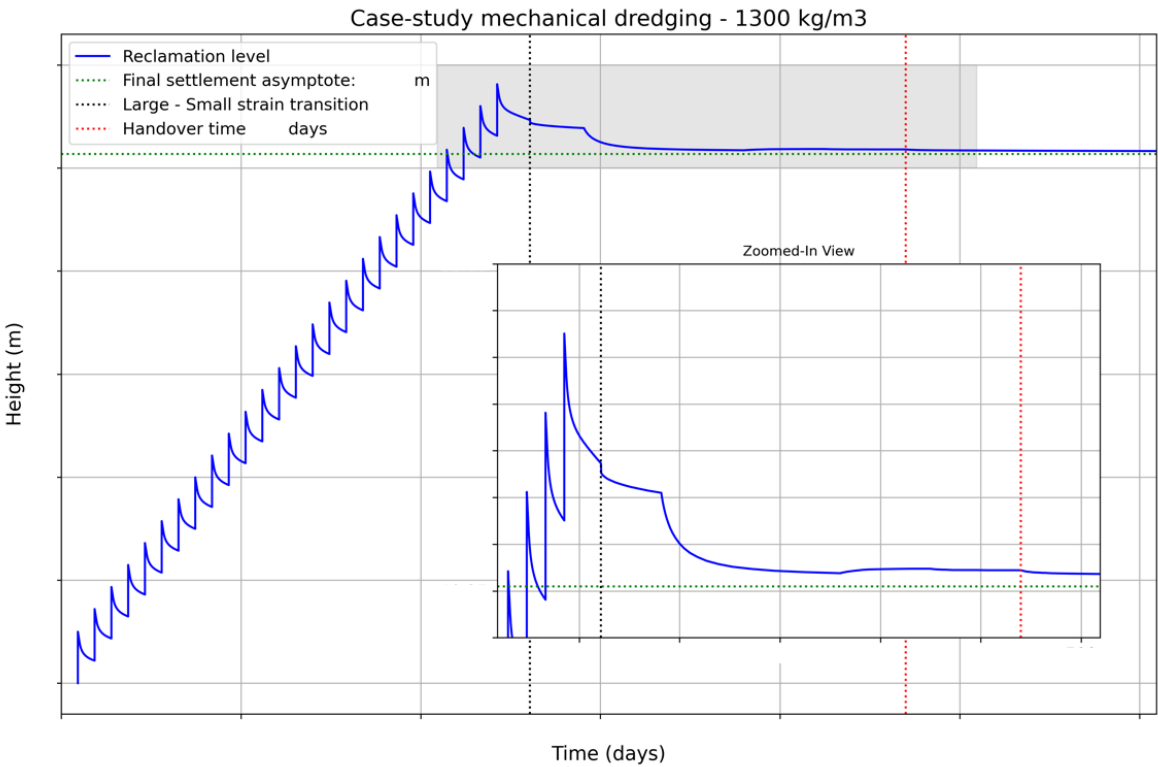


Figure 4.10: Mechanical case-study: complete reclamation evolution over time

To fill up this reclamation, 26 layers are needed to place sufficient mass. The filling reaches a maximum of meters. The stage of filling takes days, resulting in production costs of euros for the combined utilization of the Goliath, Pieter Caland and Cornelis Lely. After placement of the last layer, days of self-weight consolidation are needed to consolidate the material until only 2 meters of soft material is left on top (see Figure 4.11). After a total of days, this soft layer of 2 meters is replaced by a two meter sand crust. The crust thickness of 2 meters is required to provide bearing capacity for the equipment to access the reclamation and install the surcharge and PVD's needed

to comply with the design requirements. This calculation is based on bearing capacity equations of Terzaghi.

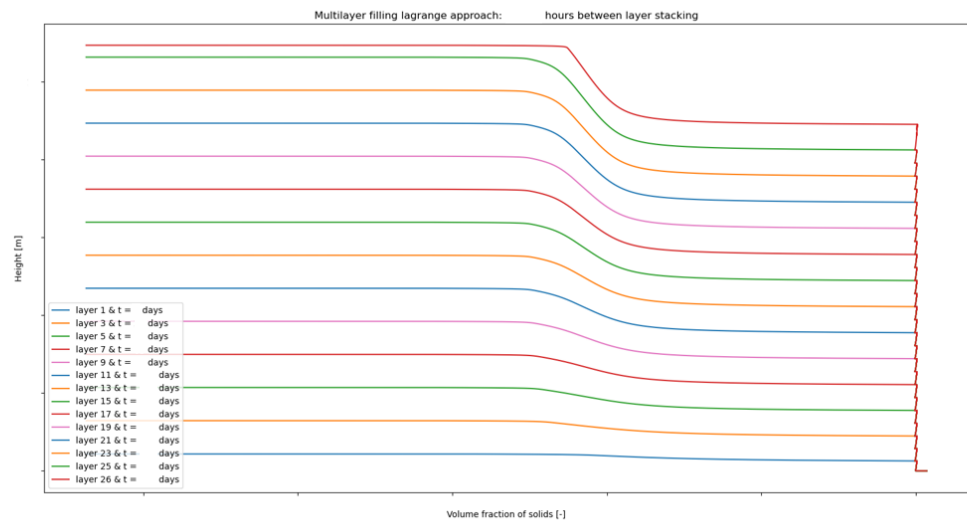


Figure 4.11: Density development in between layer placement after first layer is placed defined as t=0

In the small strain domain, the filled material is subjected to ground improvement methods. The loading scheme of the fill material is shown presented in Figure 4.12. Hence, the x-axis starts here at t=0, which is marked at the beginning of loading in the small-strain domain. The total days left for the ground improvements methods is days before handover. Loading starts with 36 kPa, due to a 2 meter crust consisting of 18 kN/m2 weight. At day 30, the surcharge installed, increasing the total load up to 135 kPa. At day , 90 days before hand-over of the asset to the client, the surcharge is stripped off, wheraes the load decreases back to 36 kPa. 45 days before hand-over, a pavement layer is installed of 22 kPa, to provide a rigid reclamation surface for the client to use. After handover at day 470, the UDL load is installed, after which the improved reclamation needs to comply with the design requirements. It can be found in the left of Figure 4.12 that the design requirements are met under effect of the presented loading scheme.

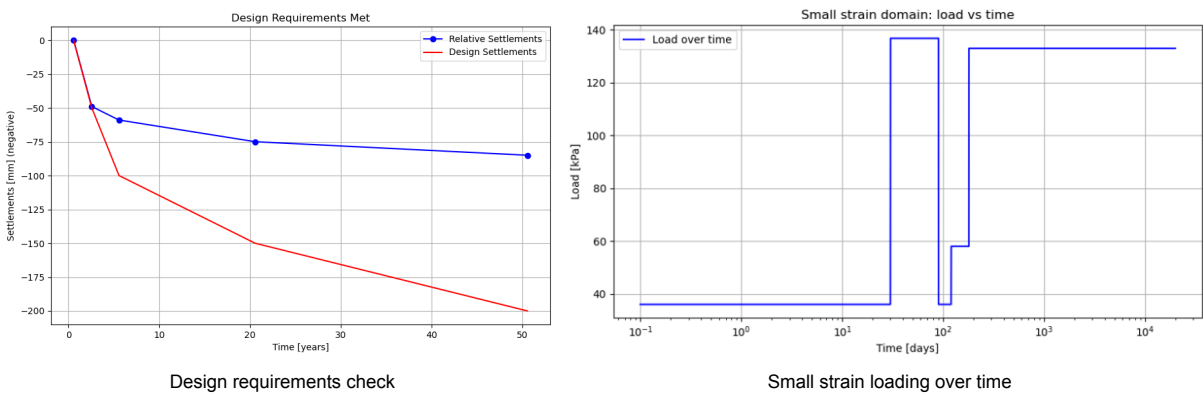


Figure 4.12: Mechanical case-study: small strain loading

The required quantity of surcharge that needs to be installed was a crust layer of 2 meters, at a weight of 18 kN/m3. The surcharge on top of the crust layer was required to be 5.50 meters at a weight of 18 kN/m2. This results into a required volume of 2.193.750 qubic meters, which results into costs of euros based on a price of euros per qubic meter.

The required quantity of Pre-fabricated Vertical Drains needed to increase the draining was a center-to-center distance of 1.8 meters. This brings the total amount of length of PVD's needed to 2.843.249 meters across the whole reclamation. This results in costs of euros based on a variable price of euros per meter PVD and a constant price of euros.

This brings the costs of the total reclamation to euros, including production costs and costs for ground improvement methods as presented in Table 4.6.

Table 4.7: Complete project costs mechanical work method.

Item	Cost [EUR]
Pre-fabricated Vertical Drains (PVD)	<input type="text"/>
Surcharge + Crust	<input type="text"/>
Mechanical Production	<input type="text"/>
Total	<input type="text"/>

5

Discussion

5.1. Interpretation of results

Single production cycle

When comparing the hydraulic dredging method to the mechanical dredging method for a single cycle, notable differences can be observed. An increase in initial (slurry) density results in a longer cycle duration, higher energy consumption to lift the material, greater production of solids, and lower costs per ton of dredged solid material. If the hopper density must be higher, more power is needed to increase the soil cutting production and pumping power of the slurry for the hydraulic method. For the mechanical method, more power is needed for soil cutting and for lifting of the slurry to the barge. This leads to an increase of duration of the "dredging" and "discharge" component of the dredging cycles of the two methods. The opposite effect applies for decreasing the initial density. It can be concluded that initial density affects the absolute duration and costs of a single dredging cycle.

This can be observed for both hydraulic and mechanical dredging methods in the case-study. The hydraulic method stands out by transporting approximately **10 times more volume (flow)** per minute than the mechanical method and being **11 times more cost-effective** per ton of solid material, when comparing both 1200 kg/m³ and 1300 kg/m³ results. These findings align with company expert expectations and theoretical principles, which indicate that increasing the density of dredged material requires more energy and higher cycle durations, therefore increasing costs per cycle. Furthermore, the observed cost advantage and significantly faster production time-frame of the hydraulic work method compared to the mechanical work method are expected and consistent with findings of company experts.

Production - Reclamation interaction

Significant differences are observed when comparing the results of hydraulic and mechanical dredging methods in the context of production interactions with self-weight consolidation behaviour. The hydraulic method requires more volume of material in the reclamation with lower initial density compared to the mechanical method, which needs less volume of material with higher initial density. Additionally, the total time to reach the design level is longer for mechanical dredging compared to hydraulic dredging due to the extensive production duration of the mechanical method. Most important, the hydraulic work method is on average **3,12 times more cost-effective** than the mechanical work method when comparing the performance at 1100 kg/m³ to 1300 kg/m³ across different design levels. The beneficial effect of a higher initial density which comes with the mechanical methods seems to be diminished by the extensive production duration and high equipment costs. Furthermore, the hydraulic work method proves to be on average **4,31 times more cost-effective** than the mechanical work method when comparing 1200 kg/m³ to 1400 kg/m³ across the design levels. It can be observed that increasing initial density for the hydraulic work method, seems to lead to higher costs and cycle duration per individual dredging cycle. However, the amount of cycles needed to fill the reclamation reduce because more mass is added in each layer placement. This makes that an increase of initial density leads to a cheaper total production phase for both the hydraulic and mechanical work method. Hence, it is not always possible for the hydraulic work method to increase initial density in practice due to production constraints.

occurring from dredging the in-situ material. Sometimes it is only possible to increase initial density by switching from the hydraulic to the mechanical work method. This impacts the business case.

Additionally, it can be observed that consolidation behaviour is dependent on initial density and layer stacking duration. When considering the hydraulic work method, placing more mass in a shorter amount of time leads to a relatively increased fill height containing more "soft" material. As a result, this material will consolidate more after the last layer is placed. This can be seen in Figure 4.2, where the 1200 kg/m³ material needs more time to consolidate after placement of the last layer compared to the 1100 kg/m³ material. Gradually placing the same mass over more layers over a longer time via a lower initial density seems to make the material consolidate more efficiently and leads to a smaller required consolidation duration after the last layer is placed.

The observation of the fact that the lower initial density material consolidates more efficiently than the higher initial density material can be explained according to Figure 4.4. It can be observed that the material with a lower initial density eventually reaches a consolidation profile similar to that of the lowest part of the higher initial density material. A potential explanation is that in the first hours, less excess pore pressure is created by the presence of less mass, but is able to drain faster to the high deformations while the higher initial density material creates higher excess pore pressures due to more mass presence, but does drain slower due to relatively smaller deformations in the first hours. Only after hours between layer stacking the effect of faster compaction due to extra mass is starting to dominate. From these results could be stated that the lower initial density consolidates more efficiently in the first 38 hours compared to the higher initial density, while these benefits start to disappear when the layer stacking duration reaches hours. The same behaviour is observed when comparing the 1300 kg/m³ material to the 1400 kg/m³ material for the mechanical dredging method.

Full scale case-study

From the full scale case-study is found that executing the project with a hydraulic dredging method (initial density of 1100 kg/m³) will lead to a **46 percent decrease** in project costs compared to project execution with a mechanical work method (initial density of 1300 kg/m³). However, these differences in project costs are only created due to the smaller production costs coming with the hydraulic method. It is found that the self-weight consolidation behaviour of the full scale case-study shows significant difference in self-weight consolidation behaviour while almost no difference can be found in the absolute duration until self-weight consolidation is finished and the crust is placed. Consequently, the transition to the small-strain domain will be at almost the same time and starts also from the same initial profile corresponding to the maximum densification behaviour observed from the NMR. As a result, both small strain domain duration and costs are almost equal for both the hydraulic and mechanical work method.

The small differences from the small-strain domain lead to the fact that the trade-off which is referred to in the main research question and introduction diminishes for this specific case-study when considering a hydraulic method of 1100 kg/m³ and a mechanical method of 1300 kg/m³ for this type of material. This shows that increasing the initial density by means of a mechanical method does not lead to a smaller consolidation duration but leads to a more expensive project instead. The hydraulic work method outperforms the mechanical work method on costs for both Production Estimation and Reclamation Engineering. When there are no production constraints, increasing the hydraulic density from 1100 kg/m³ to 1200 kg/m³ will decrease the production costs and subsequently project costs even more.

The reason behind the small differences in absolute duration before self-weight consolidation ends could be in the material used. Material used in this thesis can be quantified towards "well consolidating" because two different initial densities compact to a similar density profile in a similar duration. This process is expected to be slower when using more "complex" materials which consolidate less fast.

Table 5.1: Full scale case-study for hydraulic and mechanical work methods

Item	Hydraulic Case [EUR]	Mechanical Case [EUR]
Pre-fabricated Vertical Drains (PVD)	<input type="text"/>	<input type="text"/>
Surcharge + Crust	<input type="text"/>	<input type="text"/>
Production	<input type="text"/>	<input type="text"/>
Total	<input type="text"/>	<input type="text"/>

Results contextualization

In the context of the proposed framework, the results of this case-study need to be put in perspective. The material tested in this study consolidates relatively quickly, putting it more towards the "well-consolidating" materials in Figure 5.1. For this case-study material, the permeability from the constitutive relations was found to be $5.269\text{E-}07$ at the state of maximum densification after self-weight consolidation. This is in between the semi-permeable state of $10\text{E-}5$ and $10\text{E-}8$ according to Chassagne (2021), corresponding to silty material. When considering more clayey material in the range of a permeability between $10\text{E-}8$ and $10\text{E-}12$, the material is believed to move more to the left towards "poor consolidating" material in figure Figure 5.2. Consolidation under its own weight to reach a density of 1700 kg/m^3 of these kinds of materials can take up to 5 to 10 years according to Van Rijn (2019). For these kinds of more "complex" materials, more differences between work methods and consolidation behaviour are expected which makes the trade-off between Production Estimation and Reclamation Engineering more profound.

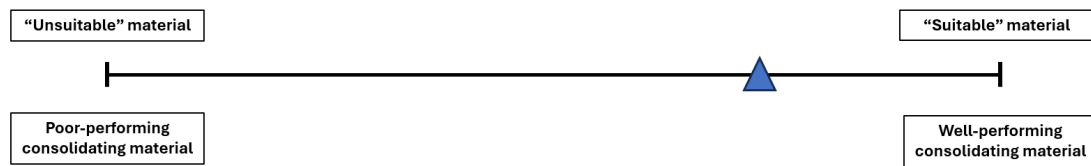


Figure 5.1: Material parameter space: Well performing consolidating material

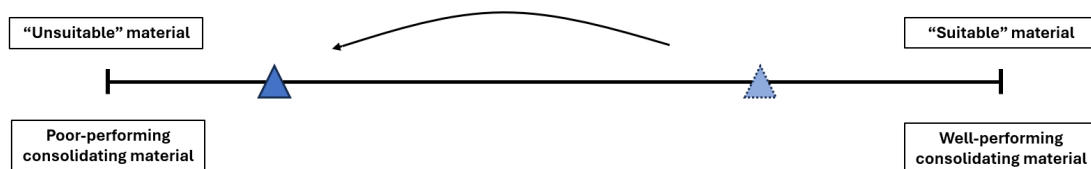


Figure 5.2: Material parameter space: Poor performing consolidating material

When the nature of the material behaves more as "poor consolidating" and the in-situ density is more fluffy (less dense), more differences are expected between the hydraulic and mechanical work method in the initial density that they can retrieve from the in-situ material. According to company experts, the hydraulic method will likely transport less dense material (order 1050 kg/m^3), while the mechanical method will still be able to achieve relative high densities (order $1300 - 1400\text{ kg/m}^3$). It is expected that in this case the mechanical dredging method could be more beneficial than the hydraulic method if it is able to put in more mass in a shorter amount of time, despite its lower production rate. This is a relevant effect because the hydraulic method will then transport 6 times less mass than the mechanical method, which reduces the in-equality between the two work methods for the total time to deliver the same amount of mass to the reclamation. In addition, it is likely that a higher initial density leads to more efficient consolidation when considering more "poor consolidating" materials with extensive consolidation time-frames. Therefore, more differences in the quantity of ground improvements are expected between the two work methods. In these cases, when the material is really challenging and the differences between the hydraulic and mechanical method are bigger, the optimization trade-off between Production Estimation and Reclamation Engineering will be more pronounced.

This hypothesis can be confirmed by analysing the material obtained from the dissertation of Barciela Rial (2019) in the self-weight consolidation stage. The material parameters used of the fines fraction of the Markermeer sediment is used in the numerical approach of this thesis to indicate the behaviour of material behaving more towards "poor consolidating". Figure 5.3 shows the consolidation behaviour of 1 meter homogeneous material for similar initial densities and layer stacking duration used in the case-study of this thesis. This short analysis gives a first indication that a higher initial density enhances self-weight consolidation in the short term as well as the long term. It can be observed that lower initial density material here consolidates to a less dense profile compared to the higher initial density profiles. This indicates that placing more mass in one layer for this "poor consolidating" material leads

to more efficient consolidation. On the long term, differences between the obtained density profiles after self-weight consolidation are significant. These differences will eventually be enhanced if production constraints lead to lower initial densities coming with the hydraulic work method (1050 kg/m³) and the mechanical work method initial density stays constant (1300 kg/m³).

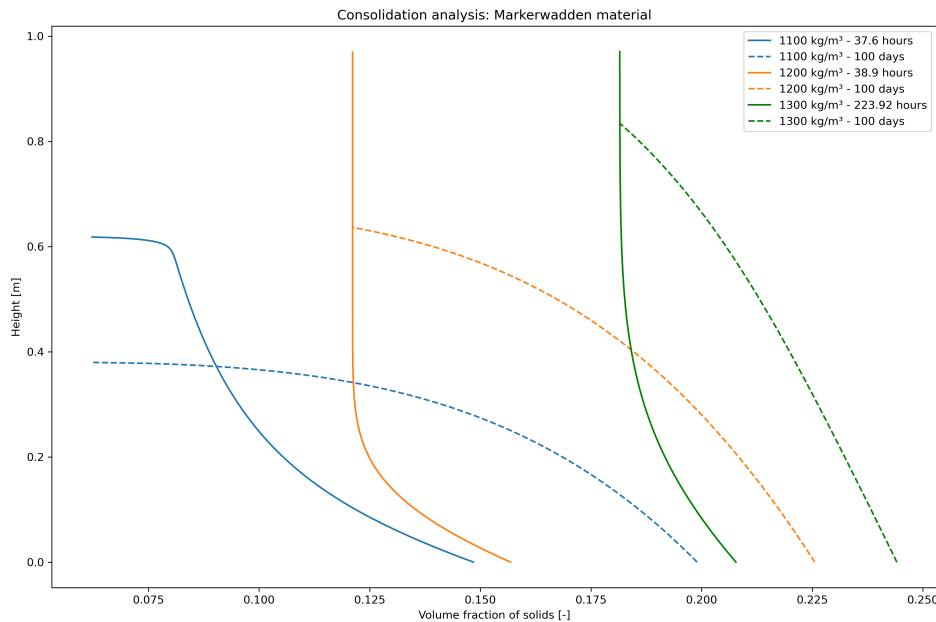


Figure 5.3: Markerwadden "poor consolidating" material: $K_k = 1.11e - 11$, $K_\sigma = 6.25e + 06$ and $n = 2.63$ obtained from SIC200 material of Barciela Rial, [2019](#)

This self-weight consolidation behaviour implicates that the mechanical work method could significantly optimize Reclamation Engineering costs. This because the weaker density profiles obtained with the hydraulic work method need more ground improvements after self-weight consolidation to comply with the design requirements of the client compared to the mechanical work method, which now naturally produces stronger density profiles after self-weight consolidation. This validates the hypothesis earlier in this section that the advantages coming with high initial density of the mechanical method become more pronounced with more "poor consolidating" materials. As a result, the trade-off between Production Estimation and Reclamation Engineering optimizations on minimizing project costs will be more relevant for this case.

5.2. Research limitations

Production Estimation limitations

It can be observed from the results that the increase of cycle duration and energy used coming with increased barge densities for the mechanical method are minor. This is due to a lack of knowledge on how to model the duration of Backhoe operations which transfer the material from the sea-floor to the barge by; lifting, swinging, release, swinging and lowering. The Backhoe operations in this study are assumed to be \square seconds, based on current literature and expert judgement. However, in reality this value could significantly differ due to the material that is dredged and the pilot that operates the Backhoe dredger, introducing potentially high uncertainty on the fixed duration assumption. In addition, the energy utilized for all Backhoe operations is assumed to be equal for every density. Due to the complex working principles behind the backhoe (several pistons which require different energy to complete the operation and transfer the material), this value is assumed to be constant based on expert judgement.

The hydraulic production model does not take into account the pump+drive limitations that occur when the drive can not generate the required torque to keep the impeller spinning at the required rate. This limitation will lead to the fact that working points differ with some uncertainty from reality when working

with high densities and high flow-rates. This has affect on the loading and discharge duration of the hydraulic work method.

The material discharged by the production models is assumed to end up with the hopper or barge density at the reclamation floor. This is a major assumption, neglecting the dispersion effects which dilute the material when dumped through a water column. This effect increases when the distance from the discharge point to the reclamation bottom increases, as more space is available for dispersion effects. During this thesis, it is assumed that a spraying pontoon is used which could spray this material close to the reclamation bottom, neglecting major dilution effects for hydraulic dredging. For mechanical dredging it is assumed that the bottom-door-dumping discharge method is close to the reclamation bottom, neglecting big dispersion effects.

Bottom-door-dumping is the assumed discharging method for the mechanical production cycle. This is performed by split hopper dumping barges. However, in this thesis it is assumed that the discharging method is used along the whole filling process. This is a clear limitation, since the reclamation bottom-height will eventually be smaller than the draft of the vessel, which makes this discharge method impossible. This discharge method is assumed to take 30 minutes. In practice, when the material can not be dumped through bottom-door-dumping, backhoes at the reclamation site need to be used to empty the hopper, which will increase duration for discharging. This limitation affects the discharge duration and energy of the mechanical work method.

Reclamation Engineering limitations

The numerical approach used in this large-strain method excludes the effect of possible segregation during placement of the layers or during consolidation. This model assumes that the placed layers consist of homogeneous material, excluding the segregation effect created by 3D effects during placement. These effects are most pronounced near the pipe where significant hydrodynamic activity is present. Additionally, the physics related to mass exchange during high-energy placement methods are excluded in this approach. Mass exchanges can occur when the material remains highly diluted for extended periods, allowing the heavier particles to segregate from the finer fractions in the slurry. Such segregation may also result from forces exerted on the lower layers during material placement, whether through pipelines or bottom-door dumping. These effects of segregation and mass exchange between layers are neglected in this thesis, enabling the application of simplified stacking of layers. However, segregation can lead to a less efficiently structured soil skeleton, ultimately reducing the density of the fill material. Forces experienced due to placement methods, could in potential slow the consolidation process down locally. A way forward in this field is to include the simulation of two different layers in the large-strain domain, which enables the simulation of possible fractions of segregation. This is possible by implementing the two layer method of **I. Myouri** in the layer stacking approach of this thesis.

The switch between large-strain estimations and small-strain estimations is marked for this case-study by the maximum densification behaviour observed from the self-weight consolidation behaviour observed from the settling columns and NMR calibration method. For the calibration of the small-strain model, Oedometer data is obtained from the project soil investigation report, which is based on bulk behaviour from the soil at the site. This makes the transition between large-strain and small-strain consolidation less evident, as different soil samples are used for calibration. The data analysed in the Oedometer starts at higher densities than the density corresponding to the maximum densification profile. This will likely result in an underestimation of the consolidation deformations in the small strain domain. This can be made more efficient by performing Oedometer tests with the material at a density corresponding to the maximum densification profile. However, when using materials without the maximum densification profile, the transition point between the large-strain and small-strain domains may be less clear. Therefore, it is recommended to add the effect of pre-loading and PVD's into the large-strain formulations of Gibson et al. (1967) and Merckelbach (2000) to make the consolidation process a continuous process. By doing this, also the effect of squeezing of the less dense upper part of the fill material by pre-loading can be estimated. This is already performed in several large-strain estimations used in the mining industry.

The large-strain model is replicating the behaviour of the physical sample material in the settling column sufficiently. However, the density obtained after self-weight consolidation obtained of 1736 kg/m³ differs from the density observed in the field after self-weight consolidation of 1400-1500 kg/m³. According

to company experts, the possible difference in density could be due to segregation, which causes a decrease in density. Another reason could be the effect of testing the material in tap water. By doing this, no flocculation occurs whereas flocculation leads to a decrease in density over the column, due to the fact that they retain more water according to Hijman (2012). Another possible reason could be the effect of organic matter degradation. The work of Shakeel et al. (2021) found that degradation of organic matter leads to clear differences in rheological properties of the material. Here samples that are exposed to air tend to decrease their rheological properties over time. A decrease in strength of the particles means that it can densify more easily, which could be the reason why we find a high density in the lab under self-weight consolidation. The sample used for this thesis case was exposed to air for a unknown, but long time (order of weeks to months). To put the results of the calibration into context, a major dredging company (competitor of Van Oord) has also used a large-strain model for modeling self-weight consolidation and has also found high densities coming with high plasticity and intermediate plasticity materials, compared to expected values. One should have a clear calibration plan in order for the settling column analysis to completely represent the project site conditions.

5.3. Research implications

A lot of knowledge exists in the field of Production Estimation and Reclamation Engineering. However, the interaction between these aspects and their integral contribution to project costs in land reclamation projects was still unknown. The main contribution of this thesis in contrast to available literature is the creation of a framework which integrates the existing bodies of knowledge on Production Estimation and Reclamation Engineering into a framework which can estimate project costs based on including self-weight consolidation estimations. Results from this thesis show that the self-weight consolidation behaviour of “complex” material can change significantly based on changes in Production characteristics. These results confirm that bridging the gap between Production Estimation and Reclamation Engineering by a large-strain consolidation model in combination with OpenCLSim is a step forward compared to the current consolidation estimations based on empirical “guesses”. The limitations named in this chapter can take this framework forward and make it applicable to more practical problems. The framework provides added value for the production department on how much material is needed to comply with design requirements and information on how their material will behave in the reclamation during placement and consolidation. The framework provides added value for the geotechnical department on the duration before the soil is stiff enough to start the ground improvement phase, the quantity of ground improvements needed and potentially the bund height requirements to contain all the slurry material.

Another contribution to existing literature is that results of the case-study demonstrates that a optimization trade-off between Production Estimation and Reclamation Engineering exists. This provides evidence to literature statements of Van Rijn (2019) and Van 't Hoff and Van Der Kolff (2012). The magnitude of the trade-off depends on the “complexity” of the material used for reclamation purpose and the production characteristics of the hydraulic and mechanical work method. The proposed framework in this thesis enables the evaluation of the optimization trade-off between Production Estimation and Reclamation Engineering, to obtain the most overall cost-effective project solution. As a result, results found by using the framework for analysing the optimization trade-off fills the research gap found in the first chapters of this thesis. Implementation of a framework could eventually lead to more integrated understanding between the two departments responsible for Production Estimation and Reclamation Engineering and could lead to more insights on the effect they both together have on complete project costs. Hence, this framework adds value when the estimation gap is high between Production Estimation and Reclamation Engineering, in case of “complex” materials. When the estimation gap is big, when using “suitable” materials, the added value of this framework is less, as Production costs will dominate the total costs.

An equally important contribution is that testing of various calibration methods highlights the importance of proper calibration techniques to accurately determine the constitutive relations. This is essential to obtain reliable computations of the self-weight consolidation process. The chosen calibration method therefore impacts the reliability of the outcomes of the framework estimations. However, advanced techniques like NMR are costly and time intensive, requiring high expertise for equipment operation and maintenance. A possible alternative approach is using a settling column equipped with pressure

sensors (Merckelbach and Kranenburg, 2004). Potentially a non-destructive density measurement system can be added for extra accuracy (Chassagne, 2021). This method could offer a more practical and cheaper calibration solution. This method can potentially obtain similar results to the NMR and effectively estimate density profiles during self-weight consolidation, based on the pore pressures measured and the measured density profiles. This thesis wants to emphasize that one can not always assume full Gibsonian behaviour, as the material in this thesis compacts to a maximum densification profile which shows behaviour which can only be estimated with the modified Gibson approach (Myouri, [In prep](#)). In situations where minimal information is available, the Analytical Solution method can serve as a valuable tool for obtaining initial estimates of the material's self-weight consolidation behavior, which is only based on the data obtained from a settling column.

This thesis narrows down the broad question, "How can the gap between production and geotechnics be bridged?", into more specific, detailed sub-questions such as:

- How can 3D segregation effects be included in the large-strain model?
- How can we include more gradual filling representing in the large-strain code?
- How can the large-strain model be calibrated effectively at the scale of large projects?
- How can strength parameters as undrained shear-strength be determined from the large-strain results?
- How can large-strain consolidation be efficiently coupled with small-strain consolidation using a single calibration method?
- How can the dredging cycle of a backhoe dredger be modeled in terms of loading duration and energy consumption
- How does the trade-off look like when workability and sediment spill restrictions are applied?

This research highlights how the findings and limitations of this thesis open the door to new research opportunities and discussions. Each new question asked could be a potential master thesis on its own. To come back to the introduction of this thesis; new research and discussions are needed to capitalize on the challenges that come with the scarceness of "suitable" building materials and increased environmental restrictions in order to provide high-quality land reclamation projects in the future.

6

Conclusion

A lot of knowledge exists in the field of Production Estimation and Reclamation Engineering. However, the interaction between these aspects and their integral contribution to project costs in land reclamation projects was still unknown. The interactions between these two aspects are getting more important when working with “complex” materials, as the engineering properties of these materials makes building with them more difficult. The main aim of this thesis was to provide an integrated framework which enables the assessment of the optimization trade-off between Production Estimation and Reclamation Engineering on minimizing project costs. This section will answer the sub-questions presented in the introduction of this thesis and concludes with the answer to the main research question.

1. How can a quantitative framework be developed to assess the impact of *Production Estimation* decisions on *Reclamation Engineering* outcomes and overall project costs?

The proposed framework consists of a integrated approach with estimation models for Production Estimation and Reclamation Engineering. The framework is proposed based on literature found in the literature study, company experts and research experts knowledge. Production Estimation is estimated with a physical based numerical approach, describing the duration and costs coming with the dredging cycle components for hydraulic and mechanical dredging. Reclamation Engineering is estimated with a numerical approach describing the duration and costs for consolidation of the filled material under the effect of ground improvement methods. Therefore, the framework is able to cover the complete reclamation process starting from dredging the material in-situ to the delivery of the asset to the client after consolidation.

The gap as identified in the literature review between the two main components of this framework is bridged with a large-strain consolidation model and OpenCLSim. The large-strain model enables the simulation of self-weight consolidation of the filled material during layer placement until the slurry has developed sufficient stiffness to be accessible for equipment. The utilization of a large-strain consolidation model for bridging this knowledge gap is acknowledged by company experts and widely acknowledged in the literature review of this thesis. By including the large-strain consolidation model in the framework makes it capable of bridging the knowledge gap by providing feedback to Production Estimation on how much material is needed and Reclamation Engineering on how long it takes until the reclamation can be made accessible for implementing ground improvement methods. This enables the framework to demonstrate how choices made in the Production phase affect the Geotechnical aspects of the material in the fill.

As a result, the framework returns a timeline of project duration as indicated in Figure 6.1 and the total costs coming with the project.

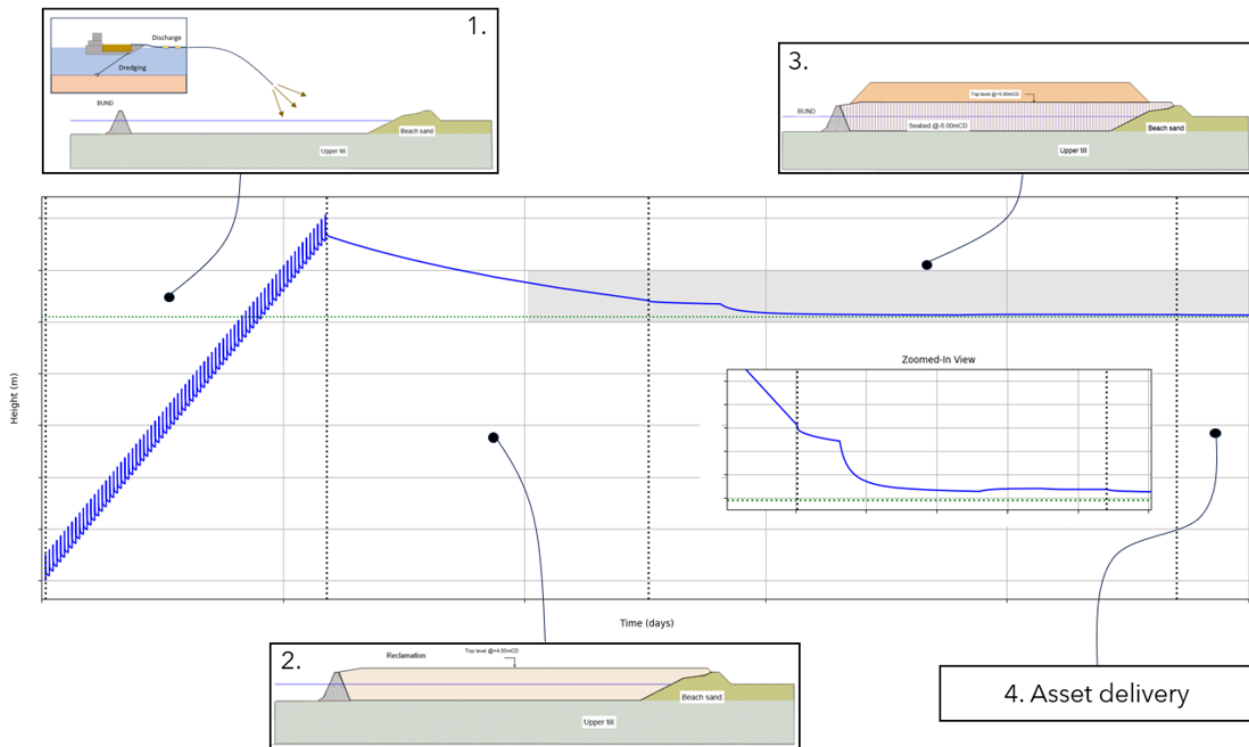


Figure 6.1: Infographic: Continuous land reclamation process

2. Which **Production Estimation** related factors affect the duration and costs of hydraulic and mechanical dredging work methods?

The main contributions on duration of Production Estimation is the time required to complete a dredging cycle. Each component of the dredging cycle; dredging - sailing full - discharging - sailing empty, contributes to duration. The duration of Production Estimation is dependent on the case-study and equipment characteristics.

An increase in (slurry) density results in a longer cycle duration, higher energy consumption to lift the material, greater production of solids, and lower costs per ton of dredged solid material. This can be observed for both hydraulic and mechanical dredging methods in the single dredging cycle case-study. The hydraulic method stands out by transporting approximately **10 times more volume (flow)** per minute than the mechanical method and being **11 times more cost-effective** per ton of solid material, when comparing both 1200 kg/m³ and 1300 kg/m³ results. However, increasing the initial density will lead to the placement of more mass in the reclamation, resulting in less cycles needed from production to place the same amount of mass, reducing total production costs.

The duration and costs of total production are significantly influenced by the in-situ material conditions and the equipment characteristics, as these determine the difference in maximum initial density between the hydraulic and mechanical methods. Additionally, the compaction behavior of the filled material plays a critical role in determining the mass required for reclamation. Therefore it can be concluded that the equipment parameters, initial density, in-situ soil conditions and compaction behaviour of the material are the main contributors to the duration and costs corresponding to Production Estimation.

3. Which **Reclamation Engineering** related factors do affect the duration and costs of the consolidation phase of placed material?

The duration for complete consolidation comprises of two stages of consolidation; self-weight consolidation in the large-strain domain and consolidation under the effect of ground improvement methods in the small-strain domain. The consolidation nature of the used material and the initial density combined with the duration between layer stacking of Production affect the self-weight consolidation duration. Additionally, the duration of self-weight consolidation in combination with the total available duration for

the project determines the time left for consolidation under the effect of ground improvement methods.

The costs considered for this research are the costs for ground improvement methods needed to force the soil profile into the desired state which complies with the design requirements of the client. The amount of ground improvement needed depend on the behaviour of the material under loading, the strength evolution of the filled material under self-weight consolidation and the amount of time available to finish the complete project. Self-weight consolidation does not come with direct costs, it does only affect the crust height needed to provide bearing capacity for the equipment. The less time the material has to consolidate under its own weight, the more soft it will be on the top, the thicker and more expensive the crust layer will be. Therefore it can be concluded that the self-weight consolidation phase contributes indirectly to costs and the consolidation phase under the effect of ground improvement methods contributes directly to costs for Reclamation Engineering.

In conclusion, the costs and duration for Reclamation Engineering are dependent on initial density of the material in the fill, the duration of self-weight consolidation and the consolidation of the material under ground-improvement methods. The costs are dependent on the quantity of ground improvement methods required to be able to deliver the asset to the client.

4. How can the cost and duration of the dredging cycle for hydraulic and mechanical work methods, along with the costs and duration for consolidation behavior of fill material be modeled?

Production Estimation can be modeled by providing duration and costs estimations for every component of the dredging cycle: dredging - sailing full - discharge - sailing empty. For the hydraulic dredging method, dredging and discharging duration can be estimated with modeling pump-pipeline interactions according to VBKO (1998a) and Schrieck (2021). For the mechanical dredging method, dredging is modeled by the duration of loading of the backhoe and movements of the backhoe pontoon Vlasblom (2005b). Discharge is modeled by estimating duration for the bottom-door-dumping method of split hopper barges. For both the hydraulic and mechanical work method, sailing full and empty velocities are estimated according to the Holtop and Mennen (1982) method, based on in-house vessel data. Sailing duration can be estimated for the sailing velocity in combination with a sailing distance. Soil cutting of sand, clay and rock during dredging for both hydraulic and mechanical methods can be estimated with the theory of S. A. Miedema (2016). The model for estimating Production Estimation is validated and verified by in-house knowledge of Van Oord and company expert judgement.

For each component of the dredging cycle of the hydraulic and mechanical method, the energy used is calculated based on power installed for dredging, discharging and sailing and the efficiency components between required installed engine power and installed power. Based on the weekly cost rates of CIRIA (2009) and the fuel costs needed to provide the required energy in each stage of the dredging cycle, the total costs for production can be estimated.

Reclamation Engineering can be modeled by the small strain theory of Terzaghi in geotechnical software D-Settlement (Deltares, 2016). This method enables the utilization of pre-loading and Pre-fabricated Vertical Drains (PVD's) to improve the fill material. The quantity of ground improvement methods needed form the costs for improvement of Reclamation Engineering. This model returns the duration and consolidation behaviour in the small strain domain until the asset can be delivered to the client. This method is calibrated by Oedometer data.

The models for Production Estimation and Reclamation Engineering can be coupled by a large-strain consolidation model for estimating self-weight consolidation behaviour and by OpenCLSim. The logistical software OpenCLSim (De Boer et al., 2023) is used to scale up the Production model to estimate the production duration and the production costs until the reclamation is filled, as well as the duration between layer stacking. The large-strain theory of Gibson et al. (1967) is modeled with a finite difference approach and gives OpenCLSim feedback on how many cycles are needed from Production to obtain the required amount of soil in the reclamation. The large-strain consolidation model is validated by comparing the numerical results to settling column tests in the laboratory. The numerical layer stacking approach proposed in this thesis is proven to be consistent with outcomes of the *Delcon* numerical approach of Deltares which is proven to be reliable and is widely used in practice for similar problems.

5. What are the main effects of production-reclamation interactions on consolidation behavior, and how do these interactions influence consolidation?

From this research results that Production - Reclamation interacts through the initial density of the material in the fill delivered by Production and the duration between the placement of two consecutive layers. From the results can be observed that both initial density and the layer stacking duration plays a role in the observed consolidation behaviour of the material.

For hydraulic dredging, placing a higher initial density reduces the material and cycles needed, allowing more mass to be placed in shorter time. However, this leads to less efficient consolidation in between layer stacking, resulting in softer material in the top part of the placed layers and extending the duration of self-weight consolidation after placement of the final layer. In contrast, placing lower-density material more gradually over more layers improves consolidation between layers stacking and reduces the self-weight consolidation duration after the final placement, for the material considered in this case-study.

In contrast, using the mechanical method comes with extensive periods between layer stacking due to low production rates in combination with a relatively high initial density. As a result of the extensive duration between placement of two consecutive layers, it will take a relatively long time until all the mass is placed. This will lead in combination with relatively fast consolidation of the material to a longer duration until the end of consolidation is reached compared to the hydraulic work method. This means that the benefit of the high initial density material of the mechanical work method is diminished by the extensive period between layer stacking.

It can be concluded that the initial density of the material as well as the duration between stacking of the layers has impact on the observable consolidation behaviour during layer placement and after placement of the last layer when the material consolidates purely under its own weight.

6. How do production-reclamation optimizations influence project duration and costs?

The material used in this thesis case study is initially dredged as rocky material but disintegrates completely into a slurry that consolidates relatively quick into a well compacted state. Significant differences can be observed during the production phase, where differences in hydraulic and mechanical dredging methods result in variations in initial density and the time between layer stacking. However, due to the material's "well-consolidating" behavior, these initial differences diminish during the reclamation phase as the material quickly consolidates and converges to a similar compaction profile within a similar time-frame. Consequently, the potential optimization for Reclamation Engineering of achieving a higher initial density using the mechanical method is diminished by its lower production rates. This results in the effect of not creating significant differences between the ground improvement methods needed to force the profile to comply to design requirements.

As a result, the trade-off between costs for Production Estimation and Reclamation Engineering for using this material is less pronounced, because the hydraulic method outperforms the mechanical method during both production and consolidation. The hydraulic work method proposes a **1.86 times as costs-effective** solution than the mechanical work method for execution of the complete project. Therefore it can be concluded that for this case-study, optimizations in Production Estimation costs, by using hydraulic dredging, do not lead to trade-off effects with Reclamation Engineering costs. Consequently, only Production Estimation optimizations have the potential to reduce project costs in this case-study.

When moving more to the "poor consolidating" materials, it is expected that the high initial density of the mechanical method starts to flourish in the consolidation phase, despite its low production rate and high costs. Therefore moving more to "poor consolidating" materials increases the presence of the trade-off, because the production characteristics of the hydraulic and mechanical method will create greater differences in consolidation behaviour. Consequently, optimizations on either Production Estimation or Reclamation Engineering have both the potential to minimize project costs.

Closing statement

The main aim of this thesis to provide a answer to the following research question: *"How can project costs be minimized by explicitly balancing the trade-off between optimizing for **Production Estimation** or **Reclamation Engineering** ?"*

All things considered, a quantitative and a qualitative answer can be provided to the main research question.

The qualitative answers is that this thesis proves that it is essential to utilize a physics based framework to be able to understand the interactions between Production Estimation and Reclamation Engineering when considering "complex" materials. It is possible to get insights on how to minimize project costs based on the trade-off between Production Estimation and Reclamation Engineering when using a framework which couples their interactions through self-weight consolidation and OpenCLSim. The existence of the trade-off and its magnitude on minimizing project costs depends on the soil type used in the project. "Complex" materials that tend towards relatively "well-consolidating" seem to reduce the magnitude of the trade-off. As a result, only optimizations on Production Estimation are likely to minimize project costs. Meanwhile, it can be concluded that more "poor-consolidating" materials enhance the magnitude of the trade-off. The predictability of the trade-off between Production Estimation and Reclamation Engineering optimizations is closely related to the understanding of production effects (varying initial density and varying duration between layer stacking) on the consolidation behaviour of the slurry material.

The quantitative part of the answer is based on the case-study performed in this thesis. It can be concluded that the differences between the hydraulic and mechanical methods are significant in duration and costs for the production phase. Additionally, the initial density and the duration between layer stacking creates a significant difference at the beginning of self-weight consolidation between the two work methods. These differences diminish in the last stage of self-weight consolidation. Therefore, the "complex" material used in this thesis can be classified towards "well-consolidating". As a result, only optimizations in Production Estimation can lead to minimization of the project costs. It can be concluded from the case-study of this thesis that the trade-off Production Estimation and Reclamation Engineering is not fully explored yet. The effect of changing ground improvement costs was not significantly present in this study. However, this thesis has proven that project costs can be minimized by using the hydraulic dredging work method when relatively "well-consolidating" material is used. When moving to more "poor-consolidating" material, it is likely that the mechanical dredging method will provide more cost-effective project solutions.

7

Recommendations

This section proposes recommendations for further research, based on the experiences gathered in this thesis from the discussion and conclusion sections. This thesis combines the fields of existing knowledge of *Production Estimation* and *Reclamation Engineering* and brings it together in one framework with the aim to assess the effect on optimizations of these aspects on minimizing project costs. The answer to the main research question raises more detailed sub-questions about the coherence between the existing bodies of knowledge. These new, detailed questions are reflected in the studies limitations where due to time-constraints in this thesis, assumptions were needed to exclude or simplify certain physics. This opens the doors for potential new research and discussions to improve and assess the practical applicability of the proposed framework.

It is recommended to further optimize the framework in the following two different research branches:

- Framework physical & practical refinements
- Framework testing (micro - meso - macro scale)

Framework physical & practical refinements

1. Production module: make the models more suitable to specific project conditions during production. This can be achieved by including workability and sediment spill down-time in the production cycle. Including these aspects make the applicability of the framework wider and more project specific. This aspects can be included by OpenCLSim and will affect the production duration and the production costs.
2. Production module: refine the hydraulic and mechanical production models by reducing the amount of assumptions. This will increase the accuracy of the duration and costs estimations of the production models. A first step is to include the pump+drive limitations in the hydraulic production model. This will increase the accuracy of the loading and discharge durations as well as the power utilization during these phases. First steps in the mechanical production model is to refine the estimation method for the duration and power utilization of the backhoe operations of lifting, swinging, lowering and releasing, based on in-situ soil conditions and the weight of the material in the bucket. This can be done by researching backhoe power and time data for each backhoe component. Another major improvement is to refine the placement techniques for the mechanical work method. Including more types of placement from the barges will increase the accuracy of the placement estimations. Currently, the statistics are used of duration and energy for bottom-door-dumping for placement above the waterline and below the waterline. This can be refined by alternating between different placement techniques for placement below the waterline and above the waterline. These aspects will increase the estimation of duration and costs of the production module.
3. Production module: increase the costs detail of the production phase. Currently only fuel costs and maintenance+repair and depreciation+interest costs are incorporated. Costs estimations can

be improved by including other major costs aspects to the production phase. This can be done by including costs aspects accounting for; (de)mobilization, workability, personnel and environment.

4. Reclamation module: Research the transition between the large-strain and the small-strain consolidation models. This can be achieved by introducing the principles of surcharging and PVD's in the large-strain expression. This will enable to capture the squeezing effect when the surcharge layer is placed on top of the still soft material during or after self-weight consolidation. This can facilitate the transition between large-strain and small-strain models by reducing the physical uncertainty for the deformation that occurs when the soft material is pre-loaded. As a result, accuracy increase in duration and costs for the reclamation module can be expected. It is recommended to research if the whole continuous process of consolidation (large and small strain) can be simulated in one numerical model based on the theory of Gibson and the effect of ground improvement methods.
5. Reclamation module: Refine the large-strain consolidation model by reducing the amount of assumptions. This will increase the application of the framework in practical project settings. A first step is to introduce the ability to simulate the effect of segregation during filling of the reclamation. This is possible by modifying the numerical two-layer approach of **I. Myouri** to the layer stacking principle proposed in this thesis. By doing this, the numerical approach would be applicable to simulate the effect of different amounts of segregation during the tender phase. Another step to increase the practical application of the large-strain model is to refine the filling method from large-placement steps of 1 meter of material to more smooth gradual filling process. By doing this,
6. Reclamation module: increase the costs detail of the reclamation phase. Currently only the costs of the ground improvement methods are included. Costs estimations can be improved by including other major costs contributions to the reclamation phase costs. This can be done by including costs aspects accounting for; engineering, monitoring, personnel, exploitation and environment.

Framework testing (micro - meso - macro scale)

1. Research a wide variety of "complex" soils ranging from "well-consolidating" to "poor-consolidating" by state-of-the-art calibration methods. This is recommended to assess the trade-off between *Production Estimation* and *Reclamation Engineering* on project costs and duration for different kinds of materials. This is important to get insights on how big the gap between optimization on production and optimization on geotechnics can be on project costs when working with different kinds of "complex" materials. Additionally, increasing the amount of tests performed on a single soil sample at different initial densities can create more knowledge on consolidation behaviour at different initial densities and its corresponding calibration uncertainties when applying the framework to a full scale project.
2. Research and propose a calibration plan to capture physical behaviour of the sample with the most costs effective and accurate calibration approach and should be able to scale up the numerical approach. Since the sophisticated NMR method is too complex to be operated and maintained by a normal organization, more practical and costs effective calibration methods should be considered. A first step would be to start testing with a settling column equipped with pressure sensors with possibly a non-destructive density measurements. Additionally, a calibration plan is needed in order to capture major physical processes affecting the consolidation behaviour, such as slurry fluid from the site and organic matter. Therefore it is also recommended to study the effect of organic matter and flocculation in the lab affecting the consolidation of "complex" materials. Furthermore, the calibration plan should include on how large-strain calibration methods, capturing the non-linear soil properties at low effective stress conditions can be combined with small-strain oedometer calibration methods, capturing the soil properties under high effective stress conditions. By including this in the calibration plan, a more smooth transition can be facilitated between the large-strain and small-strain calibration methods. This could lead to increase of accuracy in duration and costs of the reclamation module.
3. Validate the up-scaling by the numerical model from laboratory conditions to large-scale field conditions (meso - macro transition). This is important to assess the validity of the model when applied at large scales than the laboratory. It is recommended to scale up the problem from small

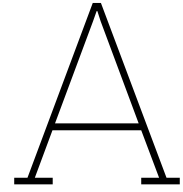
settling columns to larger settling columns in the lab to assess the reliability of the calibration methods when up-scaling the numerical method to larger scale in the lab. During this first step, the layer stacking approach can be tested in a settling column in the lab. This can be performed in bigger settling columns for which it will be possible to drain off top part of the water and add new material without disrupting the already placed material. Additionally, a measurement plan is recommended to gather data from full-scale reclamation project sites to validate the model and highlight potential improvements. By doing this, more practical insights and limitations of the model can be facilitated. This can help with further improvements for scaling up the reclamation module. Furthermore, large-scale field testing is recommended to test the consolidation behaviour of stacked layers at difference densities and placement duration intervals for hydraulic and mechanical dredging. This can assess the validity of the frame-work proposed and help to further improve its applicability.

References

- Agapito, L. A. and C. A. Bareither (2018). "Application of a one-dimensional large-strain consolidation model to a full scale tailings storage facility". In: *Minerals Engineering* 119, pp. 38–48. DOI: <https://doi.org/10.1016/j.mining.2018.01.013>.
- Ahmed, M., N. A. Beier, and H. Kaminsky (2023). "A Comprehensive Review of Large Strain Consolidation Testing for Application in Oil Sands Mine Tailings". In: *Minerals Engineering* 119, pp. 34–48. DOI: <https://doi.org/10.3390/mining.3010008>.
- Barciela Rial, M. (2019). "Consolidation and drying of slurries: A Building with Nature study for the Marker Wadden (dissertation)". In: *TU Delft repository*. DOI: [10.4233/uuid:ae11c3e7-86f2-4c6a-8d53-ee8781d56a72](https://doi.org/10.4233/uuid:ae11c3e7-86f2-4c6a-8d53-ee8781d56a72).
- Carlton, J.S. (1994). *Marine Propellers and Propulsion*. Second edition. Netherlands: Elsevier.
- Carrier, W. D. and J. F. Beckman (1984). "Correlations between index tests and the properties of remoulded clays". In: *Geotechnique* 34, pp. 211–228.
- Chai, J. et al. (2001). "Simple Method of Modeling PVD-Improved Subsoil". In: *Journal of Geotechnical and Geoenvironmental Engineering* 127, pp. 965–972.
- Chassagne, C. (2021). *Introduction to colloid science*. TU Delft Open eBooks. DOI: <https://doi.org/10.3464/mg.16>.
- Chu, J., M. W. Bo, and A. Arulrajah (2009). "Reclamation of a slurry pond in Singapore". In: *Proceedings Of The Institution Of Civil Engineers* 162.1, pp. 13–20. DOI: [10.1680/geng.2009.162.1.13](https://doi.org/10.1680/geng.2009.162.1.13).
- CIRIA (2009). *A guide to cost standards for dredging equipment*. C684. CIRIA.
- De Boer, G.J. et al. (2023). "Simulating for sustainability: alternative operating strategies for energy efficiency". In: *Terra et Aqua* 170. URL: https://www.iadc-dredging.com/wp-content/uploads/2023/06/Terra-et-Aqua_170-Summer-2023-TECHNICAL-double-pages.pdf.
- De Lillis, A., G. M. Rotisciani, and S. Miliziano (2020). "Numerical investigation of the behaviour of hydraulically dredged fine-grained soils during and after filling of the containment facility of the port of Gaeta". In: *Elsevier*.
- De Wit, W. (2013). "Modelling of the cutting forces on a backhoe's bucket in saturated sand". In: *TU Delft repository*.
- Deltares (2016). "D-Settlement user manual". In: 16.1.
- Fan, J., R. K. Rowe, and R. W. Brachman (2022). "Compressibility and permeability of sand-silt tailings mixtures". In: *Canadian Geotechnical Journal* 59, pp. 1348–1357. DOI: [dx.doi.org/10.1139/cgj-2021-0356](https://doi.org/10.1139/cgj-2021-0356).
- Gibson, R. E., G. L. England, and M. J. L. Hussey (1967). "The Theory of One-Dimensional Consolidation of Saturated Clays." In: *Geotechnique* 17, pp. 261–273.
- Hazirbaba, K. and O. Mughieda (2019). "A Comparative Study of Targeted Ground Improvement Alternatives during Site Reclamation". In: *Jordan Journal Of Civil Engineering* 13.

- Hijman, R.M. (2012). "The effect of flocculant on the sedimentation and consolidation of fine tailings". In: *TU Delft Repository*.
- Holtop, J. and G.G.J. Mennen (1982). "An approximate power prediction method". In: *International Shipbuilding Progress*. MARIN.
- IADC, International Association of Dredging Companies (2020a). *Bulking*. URL: <https://www.iadc-dredging.com/subject/dredging-terminology/bulking/> (visited on 08/10/2020).
- (2020b). *Soft Clays*. URL: <https://www.iadc-dredging.com/subject/dredging-terminology/soft-clays/> (visited on 08/12/2020).
- Ito, M. and S. Azam (2013). "Large-strain consolidation modeling of mine waste tailings". In: *Environmental Systems Research (Heidelberg)* 2.1, p. 7. DOI: [10.1186/2193-2697-2-7](https://doi.org/10.1186/2193-2697-2-7).
- ITTC (2002). "Resistance uncertainty analysis, example for Resistance Test". In: *International Towing Tank Conference* 23.
- MAN (2023). *Basic principles of ship propulsion*. Issue 2023. Netherlands: MAN Energy Solutions.
- McKinsey (2022). *Prime Numbers: Markets will be markets: An analysis of long-term returns from the SP 500*. URL: <https://www.mckinsey.com/capabilities/strategy-and-corporate-finance/our-insights/the-strategy-and-corporate-finance-blog/markets-will-be-markets-an-analysis-of-long-term-returns-from-the-s-and-p-500> (visited on 12/24/2020).
- Merckelbach, L. (2000). "Consolidation and strength evolution of soft mud layers (Dissertation)". In: *TU Delft Repository*. URL: <https://resolver.tudelft.nl/uuid:0f3a28e2-d652-4162-a980-116a4f616be4>.
- Merckelbach, L. and C. Kranenburg (2004). "Determining effective stress and permeability equations for soft mud from simple laboratory experiments". In: *Geotechnique* 54, pp. 581–591.
- Miedema, S. A. (2016). *Slurry Transport: Fundamentals, A Historical Overview & The Delft Head Loss & Limit Deposit Velocity Framework*. 2nd ed. IOS Press.
- (2014). *The Delft Sand, Clay & Rock Cutting Model*. 3rd edition. Delft University Press.
- (2019). "Production estimation of water jets and cutting blades in drag heads". In: *Proceedings of Western Dredging Association: Dredging summit and Expo '19*.
- Myouri, I. (In prep). "Experimental and theoretical investigation on the consolidation of kaolinite suspensions in demiwater". In.
- Nguyen, B. and Y. Kim (2019). "Radial consolidation of PVD-Installed normally consolidated soil with discharge capacity reduction using large-strain theory". In: *Geotextiles And Geomembranes* 47.2, pp. 243–254. DOI: [10.1016/j.geotexmem.2019.01.008](https://doi.org/10.1016/j.geotexmem.2019.01.008).
- Ni, J. and X. Geng (2022). "Radial consolidation of prefabricated vertical drain-reinforced soft clays under cyclic loading". In: *Transportation Geotechnics* 37, p. 100840. DOI: [10.1016/j.trgeo.2022.100840](https://doi.org/10.1016/j.trgeo.2022.100840).
- Roh, M. and K. Lee (2018). *Computational ship design*. Seoul National University. Springer. URL: <https://doi.org/10.1007/978-981-10-4885-2>.
- RTL (2024). *Een quadriljoen zandkorrels op onze planeet en toch dreigt een tekort: "Alles begint bij zand"*. URL: <https://www.rtl.nl/nieuws/editienl/artikel/5480071/zand-zandtekort-quadriljoen-planeet> (visited on 11/12/2024).
- Schofield, A. and P. Wroth (1968). *Critical State Soil Mechanics*. Cambridge University.

- Schriek, Van Der (2021). *Dredging Technology Book1*. Issue 2021. Delft University of Technology. Netherlands: Van Der Schriek BV.
- Shakeel, A. et al. (2021). "Effect of organic matter degradation in cohesive sediment: a detailed rheological analysis". In: *Journal of soils and sediments* 22, pp. 2883–2893. DOI: <https://doi.org/10.1007/911368-022-03156-5>.
- Townsend, F.C. and M.C. McVay (1990). "SOAs LARGE STRAIN CONSOLIDATION PREDICTIONS". In: *Journal of Geotechnical Engineering* 116.
- UNEP, United Nations Environment Programme (2022). *Sand and Sustainability: 10 strategic recommendations to avert a crisis*. Issue 2022. Nairobi 00100, Kenya: UNEP Geneva. URL: <https://unepgrid.ch/en/resource/2022SAND>.
- USACE (2015). *Dredging and Dredged Material Management*.
- Van 't Hoff, J. and A.N. Van Der Kolff (2012). *Hydraulic Fill Manual*. In CRC Press eBooks.
- Van der Kaa, E.J. (1978). "Power and speed of push-tow units in canals". In: *rpc/ Symposium on Aspects of Navigability of Constraint Waterways including Harbour entrances*. Delft Hydraulics publication.
- Van Rijn, L. C. (2019). *Land reclamations of dredged mud; consolidation of soft soils*. URL: <https://www.leovanrijn-sediment.com>.
- Van Koningsveld, M. et al. (2021). *Ports and Waterways: Navigating the changing world*. Issue 2021. Delft University of Technology. Netherlands: TU Delft OPEN. DOI: <https://doi.org/10.5074/T.2021.004>.
- VBKO (1998a). *VOUB deel 3: Baggerpomp en Aandrijving*. 1998th ed. Voortgezette opleiding uitvoering waterbouwwerken. Netherlands: Smits drukkerij.
- (1998b). *VOUB deel 4: Emmerbaggermolen / Baggerkraan / Winzuiger / Bakkenzuiger*. 1998th ed. Voortgezette opleiding uitvoering waterbouwwerken. Netherlands: Smits drukkerij.
- (1998c). *VOUB deel 5: Sleephopperzuiger*. 1998th ed. Voortgezette opleiding uitvoering waterbouwwerken. Netherlands: Smits drukkerij.
- Verruijt, A. (2012). *Soil Mechanics*. Delft University of Technology. TU Delft Open Courseware. URL: <https://ocw.tudelft.nl/wp-content/uploads/SoilMechBook.pdf>.
- Vlasblom, W. J. (2005a). *Chapter 2: Trailing suction hopper dredger*. TU Delft Open Courseware. URL: <https://ocw.tudelft.nl/courses/design-of-dredging-equipment/#1499175318191-95f2683b-ff2e>.
- (2005b). *Chapter 8: The backhoe or Dipper dredger*. TU Delft Open Courseware. URL: <https://ocw.tudelft.nl/courses/design-of-dredging-equipment/#1499175318191-95f2683b-ff2e>.
- Woud, H.K. and D. Stapersma (2002). *Design of Propulsion and Electric Power Generation Systems*. Issue 2018. Netherlands: IMarEST.
- Xu, G. et al. (2012). "Sedimentation Behavior of Four Dredged Slurries in China". In: *Marine Georesources and Geotechnology* 30, pp. 143–156. DOI: <https://dx.doi.org/10.1080/1064119x.2011.602382>.
- Zeitoun, D.G. and E. Wakshal (2013). *Land subsidence analysis in urban areas*. Springer.
- Znidar, D. et al. (2011). "Consolidation Testing of Oil Sand Fine Tailings". In: *Proceedings Tailings and Mine waste*. DOI: <https://dx.doi.org/10.14288/1.0107745>.



Production Estimation

This appendix will provide detailed information about *Production Estimation*. The physical basis of the hydraulic and mechanical production models will be explained, as well as the theoretical contents on costs estimation. The theory described in the hydraulic and mechanical production section as well as the theory in the costs section form the hydraulic and mechanical production models. The physical and practical principles explained in this section are formed into a numerical model in python. This appendix will end off with Production Estimation calculations based on the theory that is described earlier in this appendix.

This appendix adheres to the following structure. First the general soil cutting theory is explained. Next, the Holtrop & Mennen method is explained which estimates the sailing velocity of a vessel full and empty. This theory is used in both the hydraulic en mechanical models. After this general theory, the dredging cycle components of the hydraulic and mechanical models are explained. This section includes calculations that represent the case-study for this thesis, including soil cutting and estimation of sailing velocities. Finally, the costs section is explained which couples the production models to cost rates.

A.1. Soil cutting

Sediment needs to be disentangled from the sea-floor in order to transport it through pipeline. Sand, clays and rock differ in the energy that is needed to disentangle the material. For each soil type, different disentangling methods can be applied. The main methods are cutting, jetting and eroding. This section will explain the basics of cutting of sand, clay and rock and the principle of jetting.

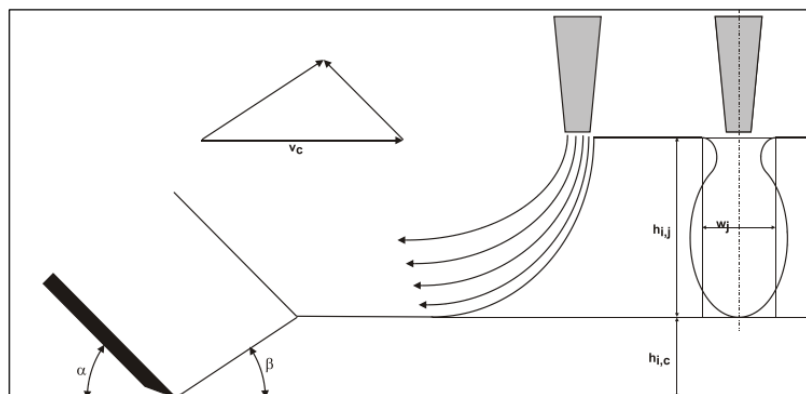


Figure A.1: Cutting by blade & Jetting by nozzles obtained from S. Miedema, [2019](#).

The energy in order to cut one cubic meter of soil is known as the specific energy E_{spec} . This parameter

is material dependent where strong soils require more energy to be disentangled compared to weaker soils. According to VBKO (1998c), the specific energy can be interpreted as "the amount of kilowatts needed to cut one cubic meter of soil per second". This is represented in formula form in equation A.1. In this formula, F_{cut} is the cutting force needed to overcome the shear resistance of the material. The cutting velocity of the blade is represented as V_{cut} . The shear resistance and the corresponding cutting force required to disentangle the sea-floor material is different for each type of soil.

$$E_{spec} = \frac{F_{cut} \cdot V_{cut}}{h \cdot b \cdot V_{cut}} \quad (A.1)$$

$$Q_{situ} = \frac{F_{cut} \cdot V_{cut}}{E_{spec}} \quad (A.2)$$

Where:

- E_{spec} = Specific energy [kPa]
- F_{cut} = Cutting force [kN]
- h = Cutting depth [m]
- b = Cutting width [m]
- V_{cut} = Cutting velocity [m/s]

Cutting Sand

In cutting theory of **sand**, soil is sheared by the horizontal motion of the blade over the sea-floor. Shearing of the sea-floor material will lead to a volume increase due to the re-arrangement of the grain structure from dense to loose (dilatancy) near the failure plane. The sudden increase of pore spaces lead to local under-pressures (Schriek, 2021). Due to the saturated conditions under water, water will flow to these newly created pore spaces. The inflow of water needs to happen at the same rate of the newly created pore spaces to neutralize under pressures quickly. The more resistance the water experiences for flowing into these spaces, the lower the resulting under-pressure will be (Schriek, 2021). The resistance of inflowing water depends on the permeability of the material and the shearing velocity of the material. The occurring under-pressure can reach vapour pressure in extreme cases whereby cavitation will occur, leading to very high required cutting forces and possible blade damage due to collapse of vapour bubbles. According to S. Miedema (2014), dilatancy effects dominate the cutting forces for sand. Therefore, other contributions due to adhesion, cohesion and gravitation can be neglected.

The effect of locally changing pressure due to dilatancy on the shear resistance can be illustrated with equation A.3 and equation A.4. Total stress σ of the soil body stays constant during shearing while water pressure u will drop due to dilatancy. This will lead to increasing effective stress σ' . As a result, the shear resistance of the soil will increase with the same rate as the pressure drop according to Coulomb's shearing theory represented in equation A.4. This means that more shearing is needed by the blade to further cut the sea-floor material (Schriek, 2021).

$$\sigma' = \sigma - u \quad (A.3)$$

$$\tau = \sigma' \cdot \tan(\varphi) \quad (A.4)$$

The cutting force required can be represented by the horizontal force equilibrium (S. Miedema, 2014). This is schematized in Figure A.2. Forces due to under pressure are represented by W_1 and W_2 in equation A.5.

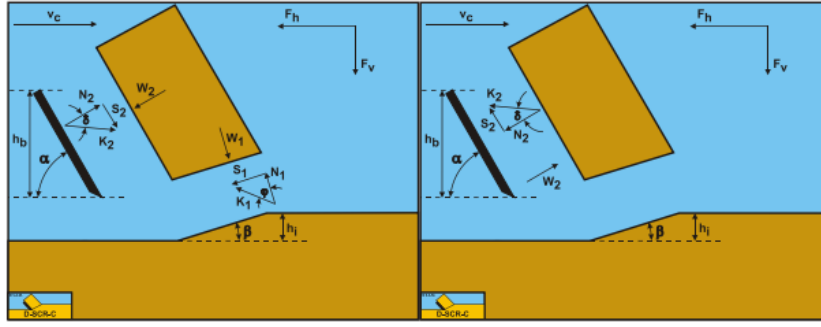


Figure A.2: Horizontal force equilibrium for cutting sand (S. Miedema, 2014). A: forces on sand; B: forces on blade

$$F_H = \frac{W_2 \cdot \sin(\varphi) \cdot \sin(\alpha + \delta) + W_1 \cdot \sin(\delta) \cdot \sin(\beta + \varphi)}{\sin(\alpha + \beta + \delta + \varphi)} \quad (\text{A.5})$$

Where:

- α = Blade angle [degrees]
- δ = external friction angle [degrees]
- φ = internal friction angle [degrees]
- β = shear angle [degrees]

With forces W_1 and W_2 for non-cavitating cutting given in equation A.6 and equation A.7. For non-cavitating cutting, the amount of under pressure is dependent dilatancy Δe , permeability k and cutting velocity v_{cut} . Dimensionless coefficients C_1 and C_2 represent non-cavitating cutting. These can be estimated by numerical groundwater calculations or by blade-soil interaction estimations (Schrieck, 2021).

$$W_1 = C_1 \cdot \rho \cdot g \cdot w \cdot h^2 \cdot \frac{v_{cut}}{k} \cdot \Delta e \quad (\text{A.6})$$

$$W_2 = C_2 \cdot \rho \cdot g \cdot w \cdot h^2 \cdot \frac{v_{cut}}{k} \cdot \Delta e \quad (\text{A.7})$$

With coefficients W_1 and W_2 for cavitating cutting given in equation A.8 and equation A.9. For cavitating cutting, the amount of pressure drop is dependent on the hydrostatic water pressure and atmospheric pressure.

$$W_1 = \rho_w \cdot g \cdot w \cdot h \cdot (z + 10) \cdot \frac{1}{\sin(\alpha)} \quad (\text{A.8})$$

$$W_2 = \rho_w \cdot g \cdot w \cdot h \cdot (z + 10) \cdot \frac{1}{\sin(\beta)} \quad (\text{A.9})$$

Where:

- C_1 = Dimensionless coefficient, non-cavitating [-]
- C_2 = Dimensionless coefficient, non-cavitating [-]
- ρ_w = Water density [kg/m³]
- g = Gravitational acceleration [m/s²]
- w = Cutting width [m]
- h = Cutting depth [m]
- z = Dredging depth [m]
- V_{cut} = Cutting velocity [m/s]
- k = permeability [m²/s]
- e = void ratio [-]

Hence, controlling the cutting velocity, and cutting depth to remain in the non-cavitation zone by the operator of the TSHD will lead to the most efficient cutting of the sea-bed material. In addition, permeable blades (Schrieck, 2021) and blades with water jets (S. Miedema, 2019) exist to neutralize pore under pressures.

Cutting Clay

The cutting theory of **clay** can also be based on coulomb shear failure. Clay behaves differently compared to sand due to its cohesion (Schrieck, 2021). Grains will not disentangle individually, but will fall apart in fragments called clay balls or clay fragments. Clay failure can also be illustrated by Coulomb's shear failure theory. In clay compression tests, shear failure will occur at twice the cohesive strength of the soil. However, compression failure of clay does not fully represent cutting clay by blade. Compression failure of clay is in the same order of magnitude as the blade cutting failure but tends to be on the optimistic side (Schrieck, 2021).

$$F_{cut} = 2 \cdot c \cdot b \cdot h \quad (A.10)$$

Where:

- F_{cut} = Cutting force [kN]
- c = Cohesion [kPa]
- b = Cutting width [m]
- h = Cutting depth [m]

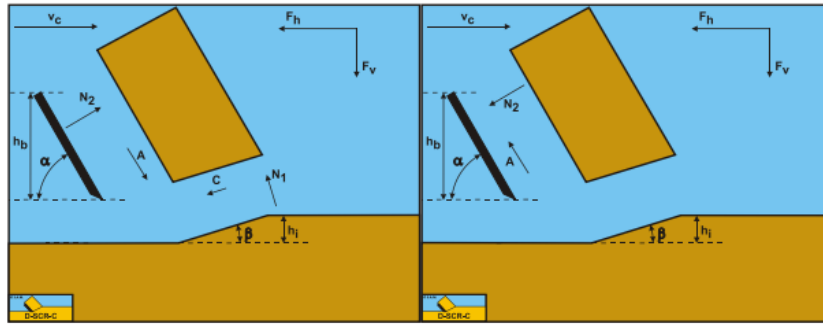


Figure A.3: Horizontal force equilibrium for cutting clay (S. Miedema, 2014). A: forces on clay; B: forces on blade

The required horizontal cutting force that needs to be delivered by the blade can be extracted from the horizontal force balance, shown in Figure A.3. From the force balance, adhesion A and cohesion C are the main clay properties determining the horizontal cutting force required. Pore pressures do not play a role in cutting clay since dilatancy is mainly countered by the cohesion ability of clay. Clay will not disentangle in individual grains, but in clay fragments.

$$\frac{F_H}{C \cdot w \cdot h} = \frac{\sin(\alpha)}{\sin(\beta) \cdot \sin(\alpha + \beta)} + \frac{A}{C} \cdot \frac{h_i}{h_b} \cdot \frac{\sin(\beta)}{\sin(\alpha) \cdot \sin(\alpha + \beta)} \quad (A.11)$$

$$E_{spec} = \frac{F_H}{h \cdot w} \quad (A.12)$$

In this theory of S. Miedema (2014), the shear plane angle will be varied and the lowest corresponding horizontal force can be considered. This will be the required horizontal force for the weakest shear plane and is the normative cutting force that needs to be delivered by the blade.

In practice, clays can only be cut due to its cohesive behaviour. The magnitude of clay balls that occur after the clay has passed the knife can be reduced by reducing cutting depth.

Cutting Rock

The cutting theory of **rock** is also based on the coulomb shear failure theory. Rock cutting is dominated by the internal shear strength and the internal and external friction angles. The cutting forces required to cut rock can be estimated by the cutting theory of Miedema. Permeability of rock is very low. Potential cavitation under-pressures can be neglected in relation to the compressive strength of the rock. The cutting forces are therefore dominated by the shear strength and the internal and external friction angles of the material.

Two common failure modes exist under atmospheric cutting of rock; brittle tensile failure, and brittle shear failure. Brittle failure occurs when $UCS/BTS > 15$ (S. A. Miedema, 2016). The kind of brittle failure; tensile or shear depends on the material tensile strength, compressive strength and cohesion.

According to the theory of S. A. Miedema (2016), the cutting of rock can be based on the flow model as shown in Figure A.4. This is based on the shear resistance of the material along the failure plane. Therefore the governing stresses F_h leading to failure will include the blade angle and the internal and external friction angles of the material. According to expert judgment, the average blade angle during excavation is assumed to be 45 degrees.

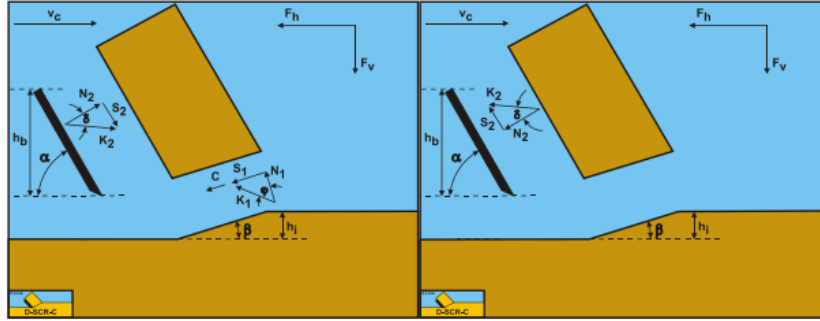


Figure A.4: Horizontal force equilibrium for cutting rock (S. A. Miedema, 2016).

Exerting a horizontal force, created by the blade will lead to compressive and tensile forces in the rock. Tensile forces are created due to the cohesive behaviour of rock. Therefore, rock fractures (equivalent to rock failure) can occur due to compressive failure or tensile failure. The existence of compressive and tensile forces in grains are illustrated in Figure A.5.

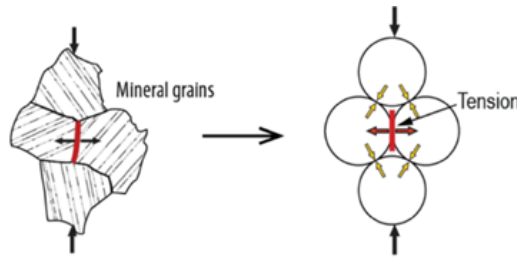


Figure A.5: Compressive and tensile forces under compressive loading (obtained from Nicksair & Martin (2014))

Brittle shear failure occurs when the minimal principle (tensile) stress is smaller than the maximum tensile stress that the material can bear. This means that the material will purely fail based on shear stress exceedance due to maximum compressive strength (maximum compressive forces that the material can take). This is shown in Figure A.6. The cutting force can be calculated based on the failure envelope of the Mohr circle. The governing equations for the horizontal cutting force is given in equation A.13 and A.14.

Brittle shear failure:

$$F_h = \frac{c \cdot h_i \cdot w \cdot \cos(\varphi) \sin(\alpha + \delta)}{1 + \cos(\alpha + \delta + \varphi)} \quad (\text{A.13})$$

$$c = \frac{UCS}{2} \cdot \left(\frac{1 - \sin(\varphi)}{\cos(\varphi)} \right) \quad (\text{A.14})$$

Where:

- F_h = Cutting force [kN]
- c = Cohesion [kPa]
- w = Cutting width [m]
- h = Cutting depth [m]
- UCS = Unconfined compressive strength [kPa]

- BTS = Brazilian tensile strength [kpa]

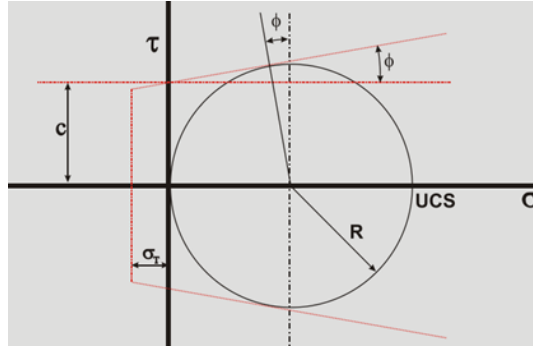


Figure A.6: Mohr circle: brittle shear failure obtained from S. A. Miedema, 2016

If the minimal principle stress is bigger than the maximum tensile stress that the material can withstand, brittle tensile failure will occur. This means that the material will fail based on the tensile forces that are created by pushing the blade against the rock (maximum tensile forces that the material can take). The Mohr circle will be adjusted to just touch the maximum tensile stress, in order to obtain the shear strength for failure. This is shown in Figure A.7. The corresponding cohesion value of this adjusted Mohr circle is c_m , known as the mobilized cohesive shear strength (based on maximum tensile strength σ_T). The governing equations for the horizontal cutting force is given in equation A.15 and A.16.

Brittle tensile failure:

$$F_h = \frac{2 \cdot c_m \cdot h_i \cdot w \cdot \cos(\varphi) \sin(\alpha + \delta)}{\cos\left(\frac{\pi}{4}\right) + \cos(\alpha + \delta + \varphi)} \quad (\text{A.15})$$

$$c_m = \frac{\sigma_T}{\left(\frac{\sin\left(\frac{\alpha + \delta - \varphi}{2}\right)}{\cos\left(\frac{\alpha + \delta + \varphi}{2}\right)} - 1\right) \cdot \left(\frac{1 - \sin(\varphi)}{\cos(\varphi)}\right)} \quad (\text{A.16})$$

$$\sigma_T \approx BTS \quad (\text{A.17})$$

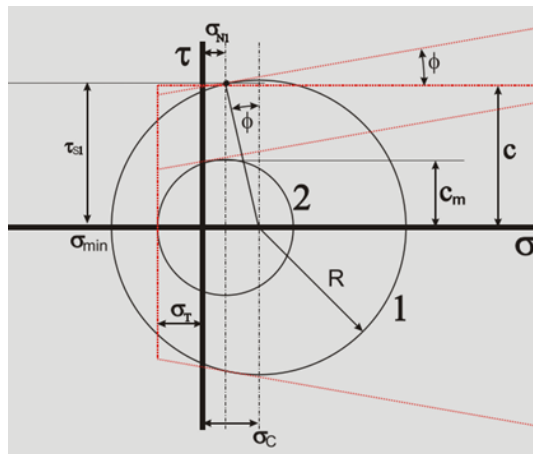


Figure A.7: Mohr circle: brittle tensile failure obtained from S. A. Miedema, 2016

Jetting

The theory of **jetting** is described by S. Miedema (2019). The process of jetting can be represented by high pressure water ejection from nozzles which are mounted on the draghead and reach into the sea-floor material. The high pressure water jet penetrates and creates a scour hole in the sea-floor material, transporting all the fluidized or eroded material to the suction tube of the draghead. Jetting is efficient because it requires less energy compared to cutting by blade (S. Miedema, 2019).

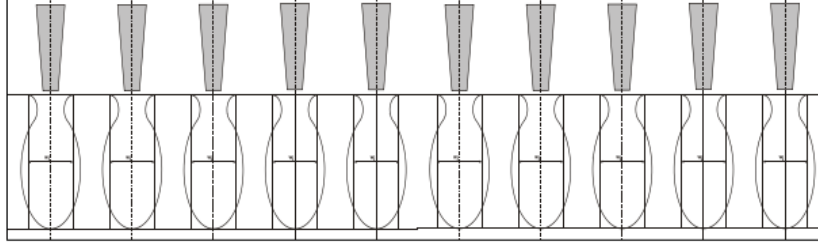


Figure A.8: Jetting scour holes created by multiple jet nozzles (S. Miedema, 2019).

This theory makes the analogy between jetting and non-cavitating cutting at zero meters of water depth. The water jet will shear the particles and disentangle them to individual particles just as the principle of cutting by blade (non-cavitation). The situ production can be estimated with equation A.18.

$$Q_{situ} = \frac{P_{jet}}{E_{spec}} \quad (A.18)$$

Where:

- Q_{situ} = Situ production [m³/s]
- P_{jet} = Power of jet pumps [kW]
- E_{spec} = Specific energy situ material [kJ/m³]

The power of the jet is based on the pump power of the jet pump. The pump and the pipeline connected with the jet determine the flow-rate and flow velocity of the water coming out of the nozzle. This process can be represented by equation A.19 (S. Miedema, 2019).

$$P_{jet} = \Delta p \cdot \left(\frac{2 \cdot \Delta p}{\rho_w} \right)^{0.5} \cdot \frac{\pi}{4} \cdot (\alpha \cdot D)^2 \quad (A.19)$$

Where:

- P_{jet} = Power jets [kW]
- Δp = Pressure difference over jet nozzle [kPa]
- ρ_w = Density of water [kg/m³]
- α = Contraction coefficient [-]
- D = Nozzle diameter [m]

The jet pumps, the amount of jets and the nozzle contraction determine the pressure difference over the nozzle in equation A.19.

Jetting can be used in material with relatively high permeability where the high pressure water can reach a significant jetting depth, equivalent to the blade cutting depth. Jetting has less effect in low permeable materials due to limited penetration ability.

A.2. Sailing: Holtrop & Mennen method

The Trailing Suction Hopper Dredger for the hydraulic work method and the barge for the mechanical work method transports the dredged material by sailing full form the dredging site to the placement site, after which it sails back empty from the placement site back to the dredging site. Large distances between dredging and placement site will enhance the importance of sailing velocities in the dredging cycle. Sailing velocities can therefore affect production per cycle significantly if distances are large. This section will explain how to determine the full and empty sailing velocity of Trailing Suction Hopper Dredgers and Split-Hopper Barges.

The velocity of a vessel is related to the installed power and the resistance forces that are exerted on the vessel's hull for sailing at a given velocity. This is related through the following relation in equation A.20. This equation is valid based on physical principles of "work" and "power".

$$P \cdot \eta_T = R_{total} \cdot V_{vessel} \quad (A.20)$$

Where:

- P = installed power [kW]
- η_T = total efficiency factor [-]
- R_{total} = total resistance force [kN]
- V_{vessel} = vessel velocity [m/s]

Since resistance R_{total} is dependent on the sailing velocity squared means that the required power for providing forward motion of the ship will increase with velocity cubed (Woud and Stapersma, 2002). This is illustrated in equation A.21.

$$P \cdot \eta_T = (C_1 \cdot V_{vessel}^2) \cdot V_{vessel} = C_1 \cdot V_{vessel}^3 \quad (A.21)$$

Vessel resistance

Various methods exist for estimating the total resistance force of vessels. A straightforward method is the Van Der Kaa method (Van der Kaa, 1978), obtained from lecture notes "Ports and Waterways" (van Koningsveld et al., 2021). This method is based on estimating the resistance force by including pressure resistance and frictional Resistance as shown in equation A.22.

$$R_{total} = \frac{1}{2} \cdot \rho_w \cdot V_{vessel}^2 \cdot C_F \cdot S + \frac{1}{2} \cdot \rho_w \cdot V_{vessel}^2 \cdot C_p \cdot A_s \quad (A.22)$$

The total resistance depends on a pressure resistance term, dependent on the drag coefficient C_p , wetted cross-section A_s and vessel velocity. The frictional resistance term depends on friction factor C_F , wetted surface area S and vessel velocity.

A more detailed empirical method is of Holtrop and Mennen (1982). This is a empirical method based on test data which estimates the resistance force including frictional resistance R_F , appendage resistance R_{app} , wave resistance R_w , pressure resistance of bulbous bow R_B , pressure resistance of transom stern R_{TR} and model-ship correlation resistance R_A , as shown in equation A.23.

$$R_{total} = R_F(1 + k_1) + R_{app} + R_w + R_B + R_{TR} + R_A \quad (A.23)$$

Equation A.24 represents the frictional forces acting on the vessel. The friction coefficient C_F is based on the ITTC (2002) expression. S_T represents the wet surface area of the vessel. The $(1 + k_1)$ terms represent a form factor which represents the viscous resistance of the hull geometry in relation to the ordinary friction resistance R_F of a flat plate.

$$R_F(1 + k_1) = (0.5 \cdot \rho_w C_F \cdot S_T \cdot V_{vessel}^2) \cdot (1 + k_1) = (0.5 \cdot \rho_w \cdot 0.075 \times \frac{\rho \times V_{vessel}^2 \times S}{(\log_{10}(Re) - 2)^2} \cdot S_T \cdot V_{vessel}^2) \cdot (1 + k_1) \quad (A.24)$$

Equation A.25 represents the resistance of the appendages. These are objects which are mounted on the vessel frame; rudders, propellers, keels. S_{app} represents the wetted surface area of the appendage

and $(1 + k_2)$ represents the form factor for appendage resistance. All the appendage resistance form factors need to be added up, including their wetted surface area.

$$R_{app} = 0.5 \cdot \rho_w \cdot V_{vessel}^2 \cdot S_{app} \cdot (1 + k_2)_{eq} \cdot C_F \quad (A.25)$$

Equation A.26 represents the wave resistance. Wave resistance occurs due to the displacement of water and the waves that are created by the forward motion of the vessel. The waves that the ship creates by displacing water and its forward motion requires energy (Roh and Lee, 2018). In equation A.26, ∇ represents water displacement and F_n represents the Froude number.

$$R_w = c_1 c_2 c_5 \nabla \rho_w g \cdot \exp(m_1 F_n^d + m_2 \cos(\lambda F_n^2)) \quad (A.26)$$

Equation A.27 represents the pressure resistance of the bulbous bow, taking into account the pressure created at the bow due to the forward motion of the vessel (Roh and Lee, 2018). This equation depends on bow emergence P_b , transverse area of the bulb A_{BT} and the Froude number F_{ni} .

$$R_B = 0.11 \cdot \exp(-3P_b^{-2}) \cdot F_{ni}^3 \cdot A_{BT}^{1.5} \rho_w g / (1 + F_{ni}^2) \quad (A.27)$$

Equation A.28 represents the pressure resistance of the transom stern. Low pressure area behind the stern is created due to turbulence of water that flows from the stern away from the vessel (Roh and Lee, 2018). This low pressure area creates a resistance force along the vessel. This equation depends on the immersed area of the transom A_T and the velocity V squared.

$$R_{TR} = 0.5 \cdot \rho_w \cdot V_{vessel}^2 \cdot A_T \cdot c_6 \quad (A.28)$$

Equation A.30 represents the scaling effects between theory and practise, including hull roughness and still-air resistance (Roh and Lee, 2018). This equation depends on the wetted surface area S and velocity V squared.

$$R_A = 0.5 \cdot \rho_w \cdot V_{vessel}^2 \cdot S \cdot C_A \quad (A.29)$$

For the other coefficients in these of equations is referred to the publication of Holtrop and Mennen (1982). For further physical interpretation of the resistance factors is referred to the publications of Roh and Lee (2018) and Carlton (1994).

Every term of the total resistance depends in some way on the vessel velocity. For R_{app} , R_{TR} , R_A through the velocity term V_{vessel}^2 . For R_w and R_B indirectly through the Froude number F_n and Froude number F_n^2 . This shows that the resistance will increase for increasing ship velocity, which is convenient with equation A.21. The result of calculating the total resistance force curve at various ship velocities is illustrated in Figure A.9.

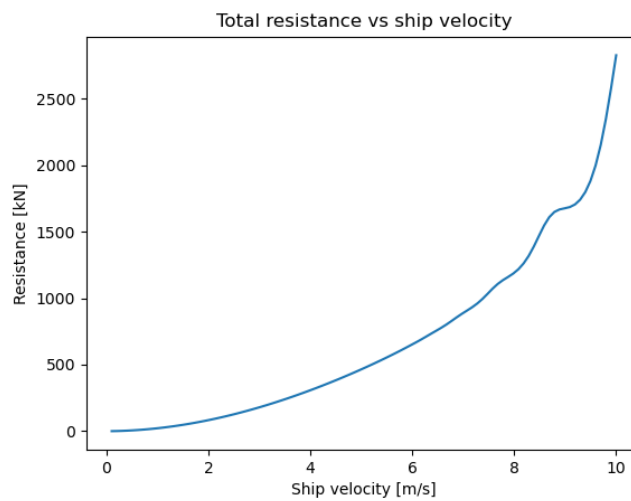


Figure A.9: Vessel resistance for arbitrary ship using the Holtrop & Mennen method.

The velocity of the vessel sailing full and empty can be determined based on the installed power of the ship, the drive-train efficiency and the total resistance estimated by (Holtrop and Mennen, 1982). Hence that the real-life average velocity during the whole sailing phase is lower than the predicted values due to acceleration, deceleration and turning of the vessel. However, it is assumed that these contributions are negligible due to the small time-frames where acceleration and deceleration are occurring during the total duration of the sailing activities.

Vessel power

The power to drive the vessel forward, overcoming resistance at a certain vessel velocity, comes from the engine. However, the drive-system setup of a vessel comes with losses in efficiency due to the complex interaction of the different drive-system components such as gearbox, drive shafts, bearings and propeller. This means that the exact installed engine power will not end up to be exerted on the water by the propeller. A general drive-system is illustrated in Figure A.10.

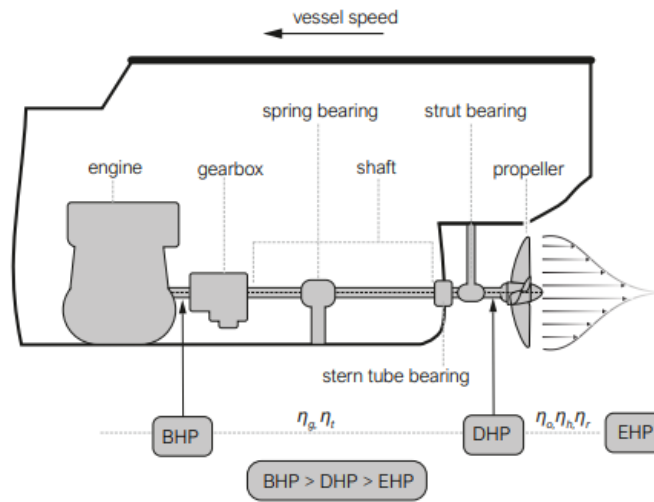


Figure A.10: Drive-system vessel including efficiency factors obtained from (van Koningsveld et al., 2021).

This figure shows the following definitions. The 'Effective Horse Power' (EHP) is the power that is exerted on the water to drive the ship forward. The 'Delivered Horse Power' (DHP), is the power that is delivered to the propeller from the engine. The installed engine power is known as 'Brake Horse Power' (BHP).

$$P_e = \eta_g \eta_t \eta_o \eta_r \eta_h \cdot P_b \quad (\text{A.30})$$

Equation A.30 shows the relations between effective horse power (EHP) and the brake horse power (BHP). The difference between these two factors come from efficiency of the drive-train. Where the main question is; how much of the installed engine power can be effectively delivered onto the water by the propeller? The power that can be delivered on to the water is less than the installed power of the engine due to energy losses in the drive-system (BHP to DHP) and efficiency of the propeller (DHP to EHP). The efficiency factors in Figure A.10 and equation A.30 take these energy losses into account. In practise, these efficiency coefficients are given by the maritime ship builder and come with the ship specifications. If no ship specific information is available to the reader, empirical estimations can be used based on ship characteristics. This is illustrated below.

The efficiency factor of η_g represents the gearing efficiency (van Koningsveld et al., 2021). The assumed value for η_g is given below.

- $\eta_g = 0.96$ [-]

The efficiency factor of η_t represents the transmission efficiency (van Koningsveld et al., 2021). The assumed value for η_t is given below.

- $\eta_t = 0.98$ [-]

The efficiency factor of η_o represents the open water propeller efficiency (van Koningsveld et al., 2021). This is the ratio between produced propeller thrust and the power absorbed by the water. The open water efficiency can be seen as the amount of thrust that the propeller can transfer to the water to bring the water in motion. This value needs to be determined based on open water diagrams or vessel design or towing tank reports.

The range of operating values for η_o are given below

- $\eta_o = 0.55 - 0.70$ [-]

The efficiency factor of η_r represents the relative rotative propeller efficiency (van Koningsveld et al., 2021). This term represents the ratio of absorbing power of the propeller for operating in a uniform flow field over operating in a wake field for the same flow velocity (Carlton, 1994). According to Holtrop and Mennen (1982), the values for the relative rotative propeller efficiency for twin-screw vessels can be estimated by equation A.31. In this expression $l.c.b$ is the longitudinal center of buoyancy and C_p is a prismatic coefficient representing the under water volume of the vessel.

$$\eta_r = 0.9737 - 0.111 \cdot (C_p - 0.0225 \cdot l.c.b) - 0.06325 \cdot \frac{P}{D} \quad (A.31)$$

The range of operating values for η_r are given below.

- $\eta_r = 0.98 - 1.02$ [-]

The efficiency factor of η_h represents the hull efficiency (van Koningsveld et al., 2021). The hull efficiency depends on the wake fraction w and the thrust deduction t . The wake fraction is mainly the effect of the interaction of the hull of the ship and the water. A boundary layer is created around the hull due to friction of water that flows along the hull, which is the largest at the stern of the ship (Woud and Stapersma, 2002). This causes that the water that flows into the propeller has a lower velocity than the actual ship velocity. This is considered to be the wake fraction. The thrust deduction factor is defined as the difference between propeller thrust and resistance over the total thrust (Woud and Stapersma, 2002). The physical interpretation of the thrust deduction factor is that the propeller action creates flow towards the propeller due to pressure differences. This creates extra resistance along the hull besides the normal towing resistance (Carlton, 1994).

The hull efficiency can be determined with equation A.32.

$$\eta_h = \frac{1 - t}{1 - w} \quad (A.32)$$

This relation include the thrust deduction factor t and the wake fraction w . A first estimation of the wake fraction and the thrust deduction factor can according to (Carlton, 1994) are presented in equation A.33 and equation A.33.

$$w = 0.5 \cdot C_B - 0.05 \quad (A.33)$$

$$t = 0.27 \cdot C_B \quad (A.34)$$

According to (Holtrop and Mennen, 1982), the values of the wake fraction and thrust deduction factor can be estimated with equation A.35 and equation A.35 for twin-screw vessels

$$w = 0.3095 \cdot C_B + 10 \cdot C_V C_B - 0.23 \cdot \frac{D}{\sqrt{BT}} \quad (A.35)$$

$$t = 0.325 \cdot C_B - 0.1885 \cdot \frac{D}{\sqrt{BT}} \quad (A.36)$$

Typical values for the hull efficiency for single-screw vessels are in the range of 1.1-1.3 (MAN, 2023). For twin-screw vessels with a single skeg the values for the hull efficiency are the range of 0.95-1.15 (MAN, 2023). The higher the block coefficient the higher the hull efficiency will be (MAN, 2023).

Fuel consumption

Fuel consumption of a vessel that is sailing is based on the power that is needed from the engine and the specific engine fuel consumption. Once these variables are known, the amount of fuel can be determined. The power demand of the vessel can be integrated over time to get the energy required. Following the energy required, and the energy source of the engines, the amount of liters of fuel can be determined that is needed for the transport stage of the dredging cycle. These values will differ between sailing full and sailing empty.

Estimating sailing velocity

For purpose of this thesis, the Holtrop & Mennen method is used to make a estimation about the sailing velocities of TSHD's (Vox Amalia) for hydraulic production and for barges (Pieter Caland & Cornelis Lely) for mechanical production. This method is performed for both sailing full and sailing empty. For both of these operations, efficiency factors and resistance forces differ.

The following steps are needed to estimate vessel velocity based on Holtrop & Mennen method:

1. Estimate resistance forces R_{total} at various sailing speeds. As shown in Figure A.9. Ship characteristics for input is provided from Van Oord databases.
2. Fit a approximation to obtain the resistance force. This is shown in Figure A.11.

$$F = C_1 \cdot V_s^2 \quad (\text{A.37})$$

3. Estimate the efficiency η_{total} from literature and in-house knowledge on efficiency factors.
4. Calculate the sailing speeds based on the fitted approximation of the resistance forces and the installed power and corresponding vessel efficiency.

$$V_{\text{estimated}} = \left(\frac{P_{\text{installed}} \cdot \eta_{\text{total}}}{C_1} \right)^{\frac{1}{3}} \quad (\text{A.38})$$

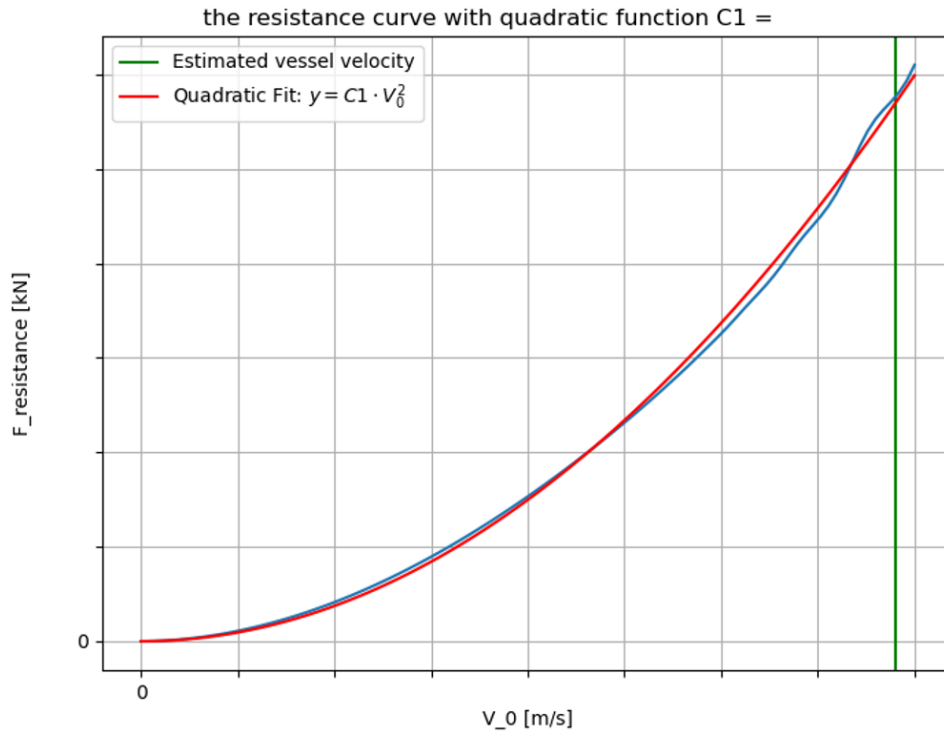


Figure A.11: Estimate resistance with $F = C_1 \cdot V_s^2$

A.3. Hydraulic production

The dredging cycle of a TSHD represents the cycle of the dredging vessel for continuously transporting material from the dredging site to the placement site. The dredging cycle is illustrated in Figure A.12. The dredging cycle can be seen as a series of events that consist of dredging the material at the dredging site, sailing full to the placement site, placing the material at the placement site and sailing back to the dredging site. The dredging cycle is repeated until a certain amount of material is moved from A to B. The amount of material that needs to be moved is often agreed upon with the client in a contract.

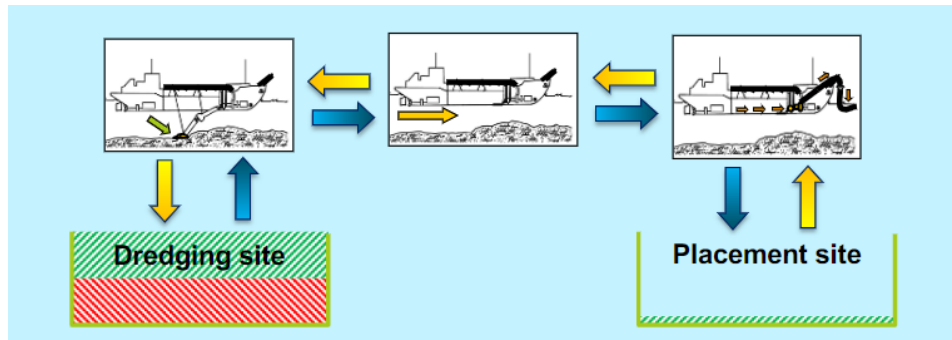


Figure A.12: Dredging cycle obtained from Dredging Technology (CIEM5300)

This section will provide estimations of each part of the dredging cycle for; trailing production, sailing empty, discharge production and sailing empty. Estimations are based on available literature and expert judgement from Van Oord. Outcomes of the estimations will be in terms of energy used and duration of the dredging cycle. The estimations provided in this section are coded numerically and used to estimate the duration and costs of a complete dredging cycle in context of the case-study. The calculations for trailing production and discharge production for using the Amalia are computed in the last section of this chapter "Model operations".

A.3.1. Trailing Production

The production of a TSHD is defined as the volume of material that can be transported from the sea-floor to the hopper per unit of time. Two processes play a role in the production of a TSHD; the cutting production of the blade and the suction production of the pumps. These processes require energy which needs to be provided by the vessel's thrust force and the on-board pumps. The more energy that is available, the more material can be transported per unit of time. Besides the available power of the pumps, other aspects play a crucial role for determining production such as, dredging depth, pipeline geometry, and in-situ soil conditions. This section will cover the working principles of soil cutting, pump-pipeline interaction and fuel consumption. These aspects are used to obtain a model which estimates production rates and production costs.

Soil cutting

Soil cutting is described by Appendix A. Soil cutting determines the quantity of soil that is available for hydraulic transport. The soil is cut by cutting teeth or jet-system which are mounted on the drag-head of the TSHD.

Soil cutting production is defined as the volume of soil that is cut per unit of time. This is dependent on soil cutting velocity, cutting depth and the geometry of the draghead. The cutting production can be calculated by equation A.39.

$$Q_{prod, cut} = h \cdot w \cdot v_{cut} \quad [m^3/s] \quad (A.39)$$

Where:

- $Q_{prod, cut}$ = Cutting production $[m^3/s]$
- h = Cutting depth $[m]$
- w = Cutting width $[m]$
- v_{cut} = Cutting velocity $[m/s]$

Equation A.39 represents the production of the volume of **in-situ** material that is cut per unit of time. In-situ material is mixed with water to achieve the desired mixture density for hydraulic transport.

Hydraulic production

Hydraulic production can be defined as the amount of transported cubic meters per unit of time for a given density. Another method is to compute the amount of kilo's of solids that are produced per unit of time, as indicated in equation A.40.

$$Q_{prod,solids} = v_{mixture} \cdot A_{pipe} \cdot \frac{\rho_{mix} - \rho_w}{\rho_{solids} - \rho_w} \cdot \rho_{solids} \quad [kg/s] \quad (A.40)$$

Where:

- $Q_{prod,solids}$ = Solids production [m³/s]
- A_{pipe} = Pipe surface [m²]
- ρ_{mix} = Density of mixture [kg/m³]
- ρ_w = Density of water [kg/m³]
- ρ_{solids} = Density of solids [kg/m³]

The mixture velocity $v_{mixture}$ comes from the mixture velocity at the working point which is established from equilibrium between driving forces and resistance forces for pump-pipeline interaction. Important is to aim for optimizing overall production by matching soil cutting production and hydraulic production.

Suction: working point

Suction production is the process of transporting dredged material from the sea-floor to the hopper. This process is governed by hydraulic transport of the soil-water mixture by centrifugal pumps. Centrifugal pumps have the capacity to create a under pressure on the pump inlet side and create a overpressure on the pump exit side (Schrieck, 2021) (VBKO, 1998a) (VBKO, 1998c). The pressure variation over the pump-pipeline system enables to transport the soil-water mixture from the sea-floor to the hopper.

Intermezzo: Working principle centrifugal pump

A centrifugal pump is a machine that uses centrifugal acceleration to move a fluid. This machine is mainly used in the dredging world for hydraulic transport of sediment material in and out of the hopper during loading and unloading.

The rotating impeller creates a centrifugal force field that results a radial pressure build-up. The rotation of the fluid at the end of the impeller causes a velocity head. This radial pressure build-up and velocity head created by the pump are translated into pressure head (Schrieck, 2021). This results in a under pressure at the inlet and a over pressure at the outlet of the pump. The pressure difference over the pump leads to the ability of the pump to move fluids. The under pressure at the inlet is known as "vacuum". This is the ability of the pump to create a under pressure to suck a mixture towards the pump inlet. The pressure buildup at the edge of the pump is known as the 'pump head'. This is the ability of the pump to push a mixture away from the pump. The "vacuum" and "pump head" are part of the driving forces in the energy system for moving the soil-water mixture in the pipeline.

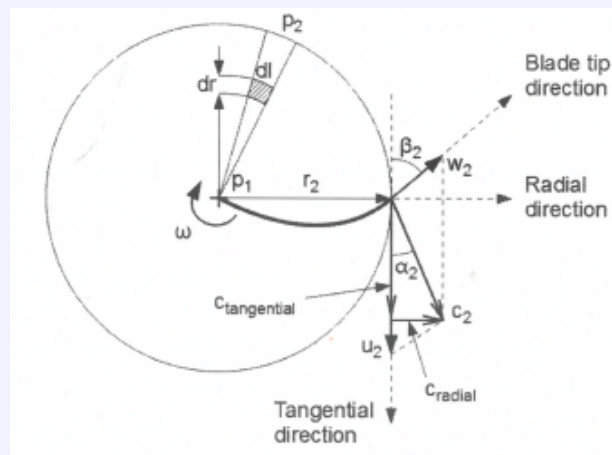


Figure A.13: Pump velocity vectors, obtained from (Schrieck, 2021)

The physics of a centrifugal pump is explained briefly below according to Schrieck (2021) and VBKO (1998a).

The pump and pipeline will result in a energy system. The flow-rate resulting from the equilibrium between driving forces and resistance forces will determine the amount of material that can be transported by the pump through the pipeline. The "working point" is defined as the point where driving forces equal resistance forces. Two different energy systems can be considered, before the pump and after the pump. The driving force before the pump consist of the hydrostatic pressure of the water column and the vacuum that the pump creates (Schrieck, 2021) (VBKO, 1998a). The driving forces behind the pump is the pump head (Schrieck, 2021) (VBKO, 1998a).

The energy equation **before** the pump is written in equation A.41. The energy balance before the pump is governed by the suction ability of the centrifugal pump. The under pressure created by the pump should never descend under the threshold of vapour pressure, where cavitation will occur. Pump cavitation will cause pump impellor damage, due to collapsing of vapour bubbles. The system before the pump represent the pipeline system and physical processes affecting the mixture, transporting it from the sea-floor up to the pump inlet.

$NPSH_a$ = Net Pressure Suction Head available. $NPSH_r$ = Net Pressure Suction Head required.

These principles govern the equilibrium before the pump. The net pressure suction head available is the pressure available minus the pipeline resistance. This is considered to represent the pressure that exists before the pump inlet and could be seen as the pressure that could be lost up to the pump inlet.

The net pressure suction head required is the required pressure that needs to exist before the pump inlet to overcome pressure losses due flow through the pump inlet.

$$NPSH_a = NPSH_r \quad (A.41)$$

The expression for $NPSH_a$ is given in Equation A.42. The driving forces in this equation are the pre-suction pressure of the water column at suction head and the atmospheric pressure. The resistance forces consist of line-losses, required vapour pressure at pump inlet, and losses due to lifting of the mixture. Hence, the dynamic pressure term is excluded from the line-losses, because this pressure will still exist at the pump inlet.

$$NPSH_a = (\rho_w \cdot g \cdot z) + P_{atm} - P_{vapour} - \left(\alpha + \xi + \lambda \frac{L}{D} \right) \frac{\rho_m v_s^2}{2} - \rho_m \cdot g \cdot (z - k) \quad [\text{Pa}] \quad (A.42)$$

Where:

- ρ_w = density water [kg/m³]
- g = gravitational acceleration [m/s²]
- z = water column height at suction head [m]
- P_{atm} = atmospheric pressure [Pa]
- P_{vapour} = vapour pressure [Pa]
- α = inlet losses at suction head [-]
- ξ = losses due to pipe geometry change [-]
- λ = friction coefficient [-]
- L = pipeline length [m]
- D = pipeline diameter [m]
- v_s = mixture suction velocity [m/s]
- k = pump axis below water level [m]

The expression for $NPSH_r$ is given in Equation A.43. The amount of revolutions per minute (RPM) of the pump blades affect the pump inlet pressure loss. The pressure loss at different pump RPM can be estimated with the "affinity rules" for $NPSH_r$. These affinity rules are pre-described by the pump manufacturer. Equation A.43 explains that increasing flow-rate, pump RPM, or mixture density will increase the pump inlet pressure loss.

$$NPSH_r = \left(N_3 \cdot Q^2 + N_2 \cdot Q \cdot \frac{n}{n_0} + N_1 \cdot \left(\frac{n}{n_0} \right)^2 \right) \cdot 1000 \cdot \frac{\rho_m}{\rho_w} \quad [\text{Pa}] \quad (A.43)$$

Where:

- $N_1 N_2 N_3$ = calibration constants [-]
- Q = flow-rate [m³/s]
- n = current RPM
- n_0 = nominal base RPM
- ρ_m = mixture density [kg/m³]
- ρ_w = water density [kg/m³]

Figure A.14 represents the $NPSH_a$ and $NPSH_r$ evolutions for different mixture velocities at fixed mixture density and fixed pump RPM. The resulting working point for a certain mixture density and pump RPM will be at mixture velocity where net pressure suction head available and required are equal. From Figure A.14 can be observed that $NPSH_a$ decreases for increasing mixture velocity, due to the quadratic increase of friction losses in the pipeline. The $NPSH_r$ term increases for increasing mixture velocity, due to pump inlet losses which are more pronounced at high mixture velocities. The equilibrium in Figure A.14 is the velocity for which the pump is on its operational limit between non-cavitating and cavitating flow.

Hence, mixture density changes from time to time in reality. This could cause sudden changes in mixture density or mixture velocity. These sudden changes could lead to cavitation when operating at

the theoretical limit. In reality, it is wise to work at a safety margin from the operational limit. This is not considered in the hydraulic production model presented in this thesis.

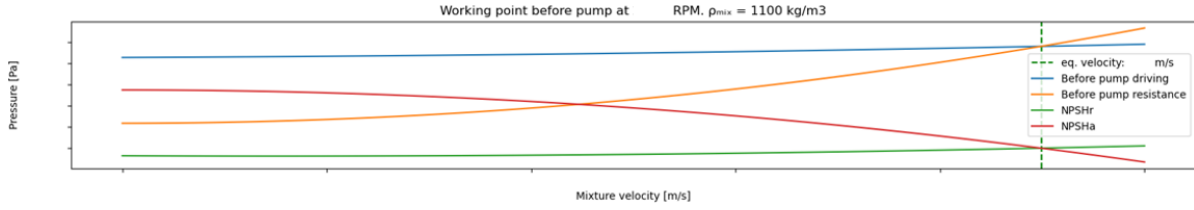


Figure A.14: Trailing: working point before pump

The energy equation **after** the pump is written in equation A.44. The energy balance after the pump is governed by the driving pressure created by the centrifugal pump and the resistance occurring in the pipeline. The system after the pump represent the pipeline system and physical processes affecting the mixture from the pump outlet to discharge in the hopper.

$$H_{pump} = Resistance \quad (A.44)$$

The driving pressure is created by the centrifugal acceleration, as described in the intermezzo. The amount of revolutions per minute (RPM) of the pump blades affect the pressure that can be created by the centrifugal pump, as can be seen from equation A.46. The relation between RPM and the absolute pressure head that can be created is known as "Affinity Rules" for pump head. These affinity rules are pre-described by the pump manufacturer. Equation A.45 explains that increasing flow-rate, pump RPM, or mixture density will increase the pump head.

$$H_{pump} = \left((F_3 \cdot Q^2) + \left(F_2 \cdot Q \cdot \frac{n}{n_0} \right) + \left(F_1 \cdot \left(\frac{n}{n_0} \right)^2 \right) \right) \cdot 1000 \cdot \frac{\rho_m}{\rho_w} \quad [\text{Pa}] \quad (A.45)$$

Where:

- $F_3 F_2 F_1$ = calibration constants [-]
- Q = flow-rate [m³/s]
- n = current RPM
- n_0 = nominal base RPM
- ρ_m = mixture density [kg/m³]
- ρ_w = density water [kg/m³]

The expression for resistance after the pump is given by equation A.46. This expression consists mainly of line losses due to friction and lifting of the mixture from the pump to the hopper. The dynamic pressure term is included in the friction term, because pump head is utilized to create dynamic pressure of the mixture.

$$Resistance = \left(1 + \alpha + \xi + \lambda \frac{L}{D} \right) \cdot \rho_m \cdot \frac{v_s^2}{2} + (\rho_m \cdot g \cdot (k + a)) \quad [\text{Pa}] \quad (A.46)$$

Where:

- ρ_w = density water [kg/m³]
- g = gravitational acceleration [m/s²]
- P_{atm} = atmospheric pressure [Pa]
- P_{vapour} = vapour pressure [Pa]
- α = inlet losses at suction head [-]
- ξ = losses due to pipe geometry change [-]
- λ = friction coefficient [-]
- L = pipeline length [m]

- D = pipeline diameter [m]
- v_s = mixture suction velocity [m/s]
- k = pump axis below water level [m]
- a = discharge height above water-line [m]

From equation A.45 and equation A.46 can be observed that ρ_m is present in every term. As a result, the mixture density will not affect the equilibrium between driving pressure and resistance. Only the absolute pressure belonging to the equilibrium point is affected by mixture density.

Figure A.15 represents the H_{pump} and $Resistance$ terms for different mixture velocities at a fixed mixture density and fixed pump RPM. The resulting working point for a certain mixture density and pump RPM will be where the driving pressure (pump head) is in balance with the pressure drop due to pipeline resistance terms. The resistance line increases quadratically due to the velocity increase of the mixture. The pump head decreases for increasing mixture velocity due to reduced pump efficiency (Schrieck, 2021) which is accounted for in the affinity rules of equation A.45.

Hence, the pump head in Figure A.15 is based on the “unlimited power” assumption. This means that there are no drive-train limitations in providing the torque and mechanical power for the pump to achieve high flow-rates. In reality, drive-train limitations will limit the pump head at high flow-rates or high densities. The effect of drive-train limitations is perfectly described by Schrieck (2021) and VBKO (1998a).

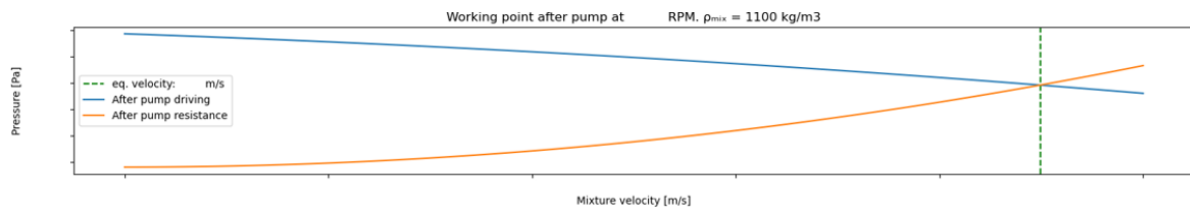


Figure A.15: Trailing: working point after pump

The principle of **RPM Scaling** is important for determining the ultimate working point of the complete pump-pipeline system. The optimal working points for the systems before and after the pump are initially different. This is due to the fact that the systems are different in driving-resistance configuration. However, a different work point before and after the pump is physically **not** justified. Conservation of mass needs to be satisfied in the whole system. To bring the flow-rates together, RPM scaling must be used. Flow-rates can be adjusted by changing the pump RPM in equation A.43 and equation A.45.

The working points in terms of mixture velocity of all possible pump RPM configurations are calculated and plotted in Figure A.16. The working points before the pump is plotted in red, according to equation A.41 and the working point after the pump is plotted in blue, according to equation A.44. The observed result is that the mixture velocity after the pump increases for increasing RPM. This is the result of the amplifying effect of RPM on the equilibrium between H_{pump} and $Resistance$. Before the pump, mixture velocity decreases for increasing pump RPM. This is caused by the suppressing effect of RPM on the equilibrium between $NPSH_r$ and $NPSH_a$.

As a result of RPM scaling, the working point can be found for which conservation of mass is satisfied along the complete system. This is the point where the mixture velocity before and after the pump are equal. This point is indicated by the dashed green lines in Figure A.16. Hence, when pipeline diameters before and after the pump are not equal, flow-rate is used instead of mixture velocity to obtain conservation of mass.

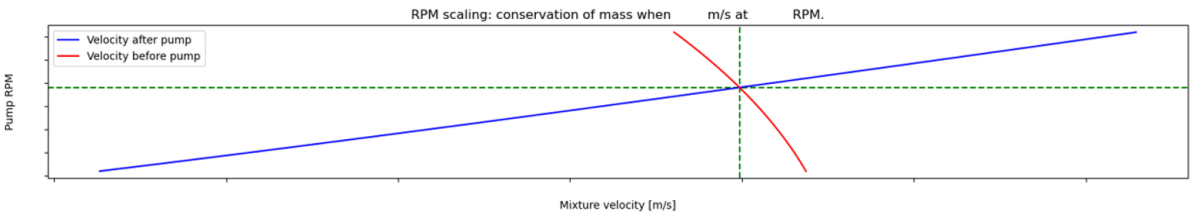


Figure A.16: Trailing: RPM scaling for $\rho_m = 1100kg/m^3$

A.3.2. Sailing

The sailing velocity for hydraulic production is estimated for the Vox Amalia hopper in this section. The estimation is based on the theory described in section Holtrop & Mennen. The input parameters and the calculation to obtain the sailing velocity is provided in this section. The characteristic vessel parameters are extracted from the Vox Amalia design report.

Amalia full:

- $h = \text{[]}$ [m]
- $T = \text{[]}$ [m]
- $T_f = \text{[]}$ [m]
- $C_b = \text{[]}$ [-]
- $C_{stern} = \text{[]}$ [-]
- $1 + k_2 = \text{[]}$ [-]
- $P = \text{[]}$ [kW]
- $D_{propeller} = \text{[]}$ [m]
- $\eta_o = \text{[]}$ [-]
- $\eta_r = \text{[]}$ [-]
- $\eta_h = \text{[]}$ [-]
- $\eta_g = \text{[]}$ [-]
- $\eta_t = \text{[]}$ [-]
- $L_{wl} = \text{[]}$ [m]
- $B = \text{[]}$ [m]

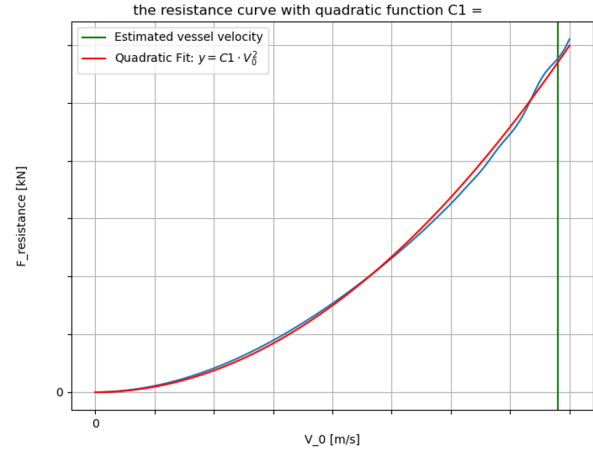


Figure A.17: Resistance estimation Amalia full.

$$V_s = \left(\frac{P_{\text{installed}} \cdot C_1}{\eta_{\text{total}}} \right)^{\frac{1}{3}} = \left(\frac{\text{[]} \cdot \text{[]}}{\text{[]}} \right)^{\frac{1}{3}} = \text{[]} \text{ [knots]} \quad (\text{A.47})$$

Amalia empty:

- $h = \text{[]}$ [m]
- $T = \text{[]}$ [m]
- $T_f = \text{[]}$ [m]
- $C_b = \text{[]}$ [-]
- $C_{stern} = \text{[]}$ [-]
- $1 + k_2 = \text{[]}$ [-]
- $P = \text{[]}$ [kW]
- $D_{propeller} = \text{[]}$ [m]
- $\eta_o = \text{[]}$ [-]
- $\eta_r = \text{[]}$ [-]
- $\eta_h = \text{[]}$ [-]
- $\eta_g = \text{[]}$ [-]
- $\eta_t = \text{[]}$ [-]
- $L_{wl} = \text{[]}$ [m]
- $B = \text{[]}$ [m]

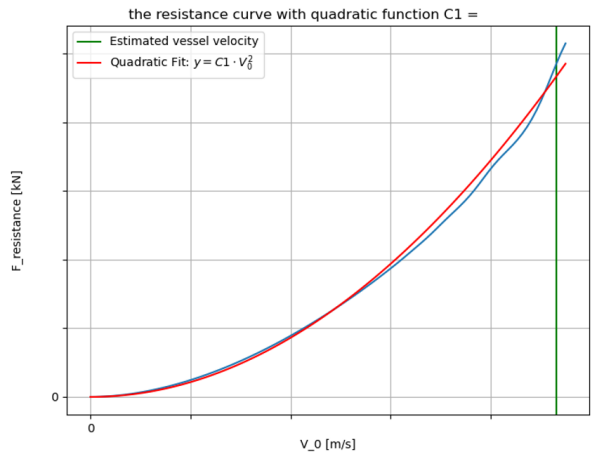


Figure A.18: Resistance estimation Amalia empty.

$$V_s = \left(\frac{P_{\text{installed}} \cdot C_1}{\eta_{\text{total}}} \right)^{\frac{1}{3}} = \left(\frac{\text{[]} \cdot \text{[]}}{\text{[]}} \right)^{\frac{1}{3}} = \text{[]} \text{ [knots]} \quad (\text{A.48})$$

A.3.3. Discharge production

The pipeline discharge method requires hydraulic transport, because the material is pumped from the hopper to the placement site via pipeline. The length of the pipeline in this application can reach several

kilometers. This requires severe pump capacity to pump the mixture over these distances. This method is often used in shallow water area's where the hopper can not operate and sail safely. The objective during discharging is to get the slurry mixture out of the hopper as efficient as possible.

The pipeline discharge method is the most efficient method when using a spraying pontoon in order to minimize segregation of the mixture at the reclamation site. Minimizing segregation is essential for obtaining favourable consolidation properties regarding compressibility and permeability of soil in a reclamation.

Hydraulic production

The principles for estimation of hydraulic production is based on the same theory based for discharging and trailing. This is highlighted again in equation A.49.

$$Q_{prod,solids} = v_{mixture} \cdot A_{pipe} \cdot \frac{\rho_{mix} - \rho_w}{\rho_{solids} - \rho_w} \cdot \rho_{solids} \quad [kg/s] \quad (A.49)$$

The mixture velocity $v_{mixture}$ comes from the mixture velocity at the working point which is established after RPM scaling. For land reclamation purposes, pumping out the exact same slurry density from the hopper is essential and favours the building quality of the material.

Discharge: working point

The discharging from the hopper to the reclamation site is governed by 2 centrifugal pumps in a series connection. Two pumps are in this configuration due to the high discharge lengths possible. A series connection of two pumps have different effects on the working points before and after the pump, according to company experts. The suction is governed only by the first pump. The discharge head is increased by two pumps in series connection and can be added up.

The energy equation **before** the pump is written in equation A.50.

$$NPSH_a = NPSH_r \quad (A.50)$$

The expression for $NPSH_a$ is given in Equation A.51. The driving forces in this equation are the pre-suction pressure of the hopper mixture column at suction head and the atmospheric pressure. The friction forces consist of line-losses, required vapour pressure at pump inlet and losses due to lifting of the mixture from the hopper bottom to the pump axis slightly above. Hence, dynamic pressure term is excluded from the line-losses term, because this pressure will still exist at the pump inlet.

$$NPSH_a = (\rho_m \cdot g \cdot z) + P_{atm} - P_{vapour} - \left(\alpha + \xi + \lambda \frac{L}{D} \right) \frac{\rho_m v_s^2}{2} - \rho_m \cdot g \cdot (z - k) \quad [Pa] \quad (A.51)$$

Where:

- ρ_w = density water [kg/m³]
- g = gravitational acceleration [m/s²]
- z = mixture column height in hopper pipeline inlet [m]
- P_{atm} = atmospheric pressure [Pa]
- P_{vapour} = vapour pressure [Pa]
- α = inlet losses at suction head [-]
- ξ = losses due to pipe geometry change [-]
- λ = friction coefficient [-]
- L = pipeline length [m]
- D = pipeline diameter [m]
- v_s = mixture suction velocity [m/s]
- k = pump axis below hopper mixture level [m]

The expression for $NPSH_r$ is given in Equation A.52.

$$NPSH_r = \left(N_3 \cdot Q^2 + N_2 \cdot Q \cdot \frac{n}{n_0} + N_1 \cdot \left(\frac{n}{n_0} \right)^2 \right) \cdot 1000 \cdot \frac{\rho_m}{\rho_w} \quad [\text{Pa}] \quad (\text{A.52})$$

Where:

- $N_1 N_2 N_3$ = calibration constants [-]
- Q = flow-rate [m³/s]
- n = current RPM
- n_0 = nominal base RPM
- ρ_m = mixture density [kg/m³]
- ρ_w = water density [kg/m³]

A.19

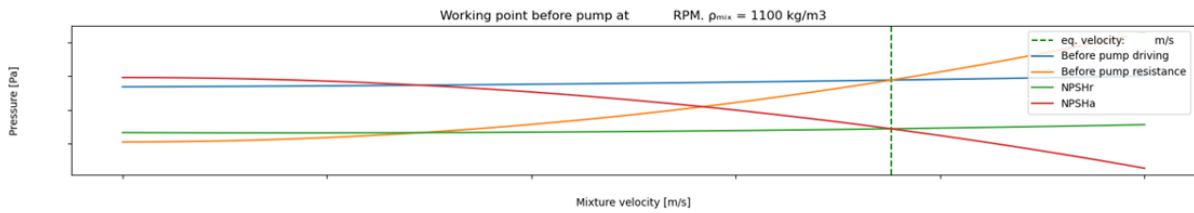


Figure A.19: Discharge: working point before pump

The energy equation **after** the pump is written in equation A.53. The energy balance after the pump is governed by the driving pressure created by two centrifugal pumps in series connection and the resistance occurring in the pipeline. The system after the pump represent the pipeline system and physical processes affecting the mixture from the pump outlet to the discharge in the reclamation. Discharge lengths of pipeline could reach the order of kilometers.

$$H_{pump} = Resistance \quad (\text{A.53})$$

The series connection of two pumps results in a multiplication of H_{pump} by 2, as shown in equation A.54.

$$H_{pump} = \left((F_3 \cdot Q^2) + \left(F_2 \cdot Q \cdot \frac{n}{n_0} \right) + \left(F_1 \cdot \left(\frac{n}{n_0} \right)^2 \right) \right) \cdot 1000 \cdot \frac{\rho_m}{\rho_w} \cdot 2 \quad [\text{Pa}] \quad (\text{A.54})$$

Where:

- $F_3 F_2 F_1$ = calibration constants [-]
- Q = flow-rate [m³/s]
- n = current RPM
- n_0 = nominal base RPM
- ρ_m = mixture density [kg/m³]
- ρ_w = density water [kg/m³]

The expression for resistance after the pump is given by equation A.55. This expression consists of line losses due to friction and lifting of the mixture from the pump outlet to the water level where the discharge pipeline is floating. The frictional resistance of the pipeline is dominant due to the generally long discharge lengths.

$$Resistance = \left(1 + \alpha + \xi + \lambda \frac{L}{D} \right) \cdot \rho_m \cdot \frac{v_s^2}{2} + (\rho_m \cdot g \cdot (a)) \quad [\text{Pa}] \quad (\text{A.55})$$

Where:

- ρ_w = density water [kg/m³]
- g = gravitational acceleration [m/s²]
- P_{atm} = atmospheric pressure [Pa]
- P_{vapour} = vapour pressure [Pa]
- α = inlet losses at suction head [-]
- ξ = losses due to pipe geometry change [-]
- λ = friction coefficient [-]
- L = pipeline length [m]
- D = pipeline diameter [m]
- v_s = mixture suction velocity [m/s]
- k = pump axis below water level [m]
- a = discharge height above water-line [m]

Figure A.20 represents the H_{pump} and $Resistance$ terms for different mixture velocities at fixed mixture density and fixed pump RPM. From the figure can be seen that the driving pressure H_{pump} is twice as high compared to the working point after pump when trailing in Figure A.15. This is the effect of two pumps in series connection. Similarly, drive-train limitations will limit the H_{pump} in reality.

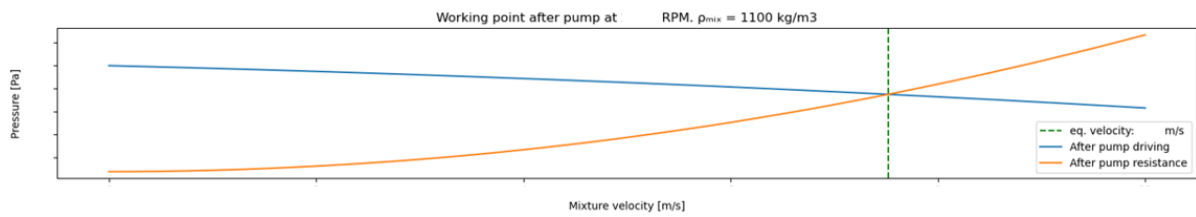


Figure A.20: Discharge: working point after pump

The principle of **RPM Scaling** is used to find the working point for which conservation of mass is satisfied. The working point is generally lower for discharging due to the high line frictions that occur while discharging over long pipeline lengths. The working points in terms of mixture velocity for all possible pump RPM configurations are calculated and plotted in Figure A.21.

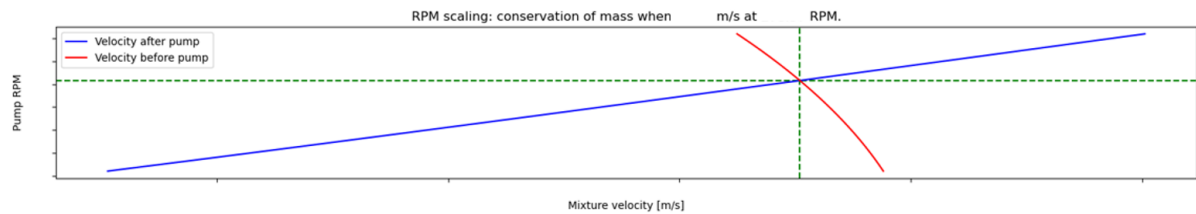


Figure A.21: Discharge: RPM scaling for $\rho_m = 1100$ kg/m³

A.3.4. Power Utilization

The effect of **Power Utilization** of the complete dredging cycle is important for estimation of fuel consumption of the vessel. Based on the required power and the energy utilized along the complete dredging cycle, fuel consumption can be estimated. This section will explain a method for estimating power consumption and required energy from the vessel drive-train during soil cutting, and during hydraulic transport while trailing or discharging.

Power for sailing operations of the ship is provided by the main engines. Power is provided from a separate engine for driving the dredging pumps during trailing and discharge.

Intermezzo: Pump limitations by drive system

During hydraulic transport, a drive-system needs to deliver power for the centrifugal pump to rotate the impeller. The pump shaft power that needs to be delivered by the drive-system is the product of required torque and angular velocity (VBKO, 1998a) or RPM. There are different drive-systems that can be considered; diesel engines, electric motors and hydraulic motors, which each its characteristical properties (Schrieck, 2021).

$$P_{\text{pump}} = T \cdot \omega = T \cdot \frac{2\pi \cdot n}{60} \quad (\text{A.56})$$

The H-V curves, provided in section A.3, are in reality affected by limitations of the drive-system. The drive-system can maintain torque at increasing RPM until the needed torque for spinning the pump impeller can not anymore be delivered, as a result, the pressure head will decrease. The drive-system will eventually reach the smoke-limit, where no torque can be created anymore. This is the physical limit of the drive-system driving the centrifugal pump.

Power soil cutting

During trailing, the soil is cut by the draghead of the TSHD. The power required from the main engines to drive the ship forward and to provide the cutting force of the drag head to cut the sea-floor material is relevant here.

According to experts, the vessel velocity during trailing is often 2 knots (1 m/s). The power required for cutting the material at two knots depends on the force needed to provide the shear for soil failure. The shear force needed can be calculated from the formulations of S. A. Miedema (2016) in section A.1.

$$P_{\text{cut}} = F_{\text{cut}} \cdot v_{\text{trailing}} \quad [\text{kW}] \quad (\text{A.57})$$

$$P_{\text{trailing}} = (C_1 \cdot v_{\text{trailing}}^2) \cdot v_{\text{trailing}} \quad [\text{kW}] \quad (\text{A.58})$$

The energy required for both cutting the material and sailing the vessel at 2 knots comes from the thrust of the propellers connected to the main engine. This can be calculated according to equation A.59.

$$E_{\text{trailing+cut}} = (P_{\text{trailing}} + P_{\text{cut}}) \cdot \frac{t_{\text{trailing}}}{3600} \quad [\text{kWh}] \quad (\text{A.59})$$

Power hydraulic transport

The pump engine serves as the primary power source for hydraulic slurry transport through the pumps. This section details the engine's power demand and outlines how to calculate its energy requirements effectively.

The required power needed for pump operations is dependent on the pump head and flow-rate which correspond with the working point found while trailing. An efficiency factor of 80% is accounting for in-efficiencies between pump-drive system, according to company experts.

$$P_{\text{hydraulic transport}} = \frac{H_{\text{pump}}(n) \cdot Q_{\text{equilibrium}}}{\eta} \quad [\text{kW}] \quad (\text{A.60})$$

Where:

- $\eta = 0.8$

Torque is defined as the rotational force required to overcome resistance and rotate the impeller. The torque is affected when flow-rate increases or when density of the mixture increases, as more rotational force is required to spin the pump impeller.

$$T_{\text{hydraulic transport}} = \frac{P_{\text{hydraulic transport}} \cdot 60}{2 \cdot \pi \cdot n} \quad [\text{kNm}] \quad (\text{A.61})$$

The utilized power over the time-frame of hydraulic transport transforms into energy. The energy needed for hydraulic transport operations directly corresponds to the energy that needs to be delivered by the engine.

$$E_{\text{hydraulic transport}} = \frac{P_{\text{hydraulic transport}} \cdot t_{\text{hydraulic transport}}}{3600} \quad [\text{kWh}] \quad (\text{A.62})$$

$$t_{\text{hydraulic transport}} = \frac{V_{\text{hopper}}}{Q_{\text{equilibrium}}} \quad [\text{sec}] \quad (\text{A.63})$$

The power needed is different in discharging compared to trailing. During discharging, two pumps in series connection are used for hydraulic transport of the slurry compared to only one pump while trailing. This will lead to increased power, torque and energy demand during discharging. Here, it is assumed that the two pumps have equal effect on the slurry. The calculations for power, torque and energy are the same for trailing and discharging. However, the absolute values for the variables in the equations below will be different due to two pumps in series, compared to one pump while trailing.

Similarly, the torque (T) and energy (E) demand from the two pumps on the engine will double. This makes that discharging will likely cost more energy than trailing, which is intuitive.

The power and torque demand on the engine from the pump during discharge and trailing are visualized in Figure A.22. In addition, the working area of the engine is defined in this plot as well. Operating at the boundary of the engine's working area means utilizing its full potential, maximizing power and torque output. The values which require higher power and torque in Figure A.22, correspond with discharging due to two pumps in series, the values in the lower regions of the plot correspond with trailing. The envelope in brown represents the working area of the drive for 2 pumps in series.

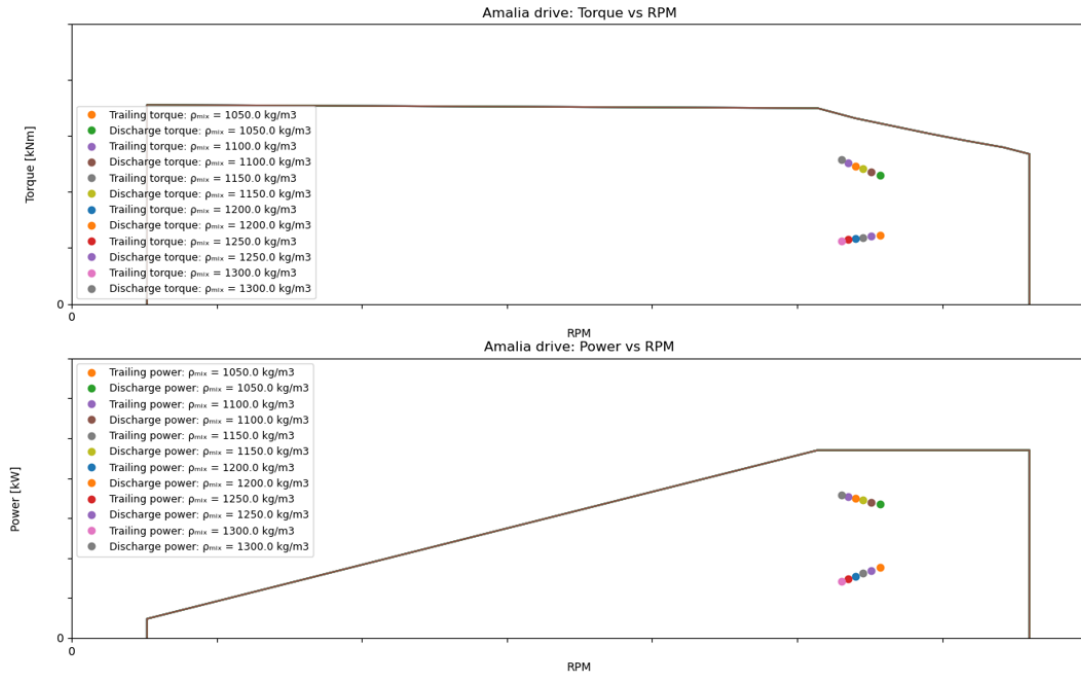


Figure A.22: Pump + Drive analysis Vox Amalia: power and torque

It can be observed that torque demand increases for increasing density while discharging and the torque demand decreases for increasing density while trailing. This is due to the rate of change of pump head relative to flow-rate. Flow rates are dropping relatively more between densities while trailing compared to discharging (see Figure A.36 and Figure A.37). The ratio between flow rate drop and pump head increase between trailing and discharging results in the difference between a decreasing power and torque rate for trailing and a increasing power and torque rate for discharging in Figure A.22. Because torque is based on power, the same pattern is visible in the torque plot.

Power sailing

During sailing, power is demanded by the propellers from the main engines. The power utilization and total energy usage can be calculated by equation A.64 and equation A.65

$$P_{\text{sailing}} = (C_1 \cdot v_{\text{sailing}}^2) \cdot v_{\text{sailing}} \quad [\text{kW}] \quad (\text{A.64})$$

$$E_{\text{sailing}} = \frac{P_{\text{sailing}} \cdot t_{\text{sailing}}}{3600} \quad [\text{kWh}] \quad (\text{A.65})$$

The sailing velocity and the corresponding energy needed, differ for sailing full and sailing empty. The coefficient for C_1 are obtained from the fitting principle in the Holtrop & Mennen method, as described in section A.2.

A.4. Mechanical production

The production of a BHD is defined as the volume of material that can be transported from the sea-floor to the barge per unit of time. BHD production is heavily dependent on the soil cutting production, the bulking behaviour of the cut material and the ability of the BHD to move the material (lift, swing, lower, release).

The complete cycle of mechanical production can be distinguished in the BHD sub-cycle and the barge cycle, as shown in Figure A.23. The BHD sub-cycle transfers the material from the sea-floor to the barge. The barge cycle transports and dumps the material at the placement site. The dredging cycle is repeated until a certain amount of material is moved from A to B. The discharging method of the barge is bottom-door-dumping. The amount of barges used in the complete process is heavily affecting the mechanical production rates.

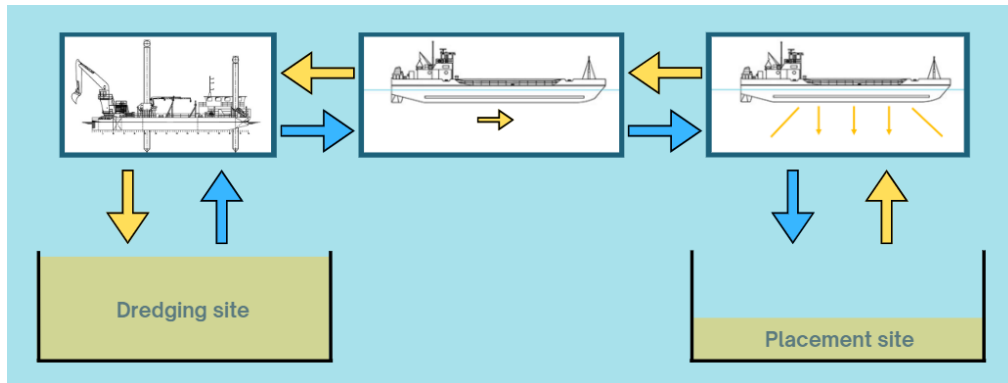


Figure A.23: Mechanical production: BHD & Barge cycle

This section will provide estimations of each part of the dredging cycle for; BHD sub-cycle, sailing full, discharging and sailing empty. Estimations are based on available literature and expert judgement from Van Oord. Outcomes of the estimations will be in terms of energy used and duration of the dredging cycle. The estimations provided in this section are coded numerically and used to estimate the duration and costs of a complete dredging cycle in context of the case-study. The calculations for BHD production and discharge production are computed in the last section of this chapter "Model operations".

A.4.1. Loading production

This section will provide an method to estimate the loading production, by analysing the BHD sub-cycle. This sub-cycle consists of; soil cutting, lifting, swinging, releasing, swinging and lowering. The configuration between the barge and excavator during loading is visualized in Figure A.24. It can be observed that material is excavated in the circular effective area and is transferred to the barge next to the BHD pontoon.

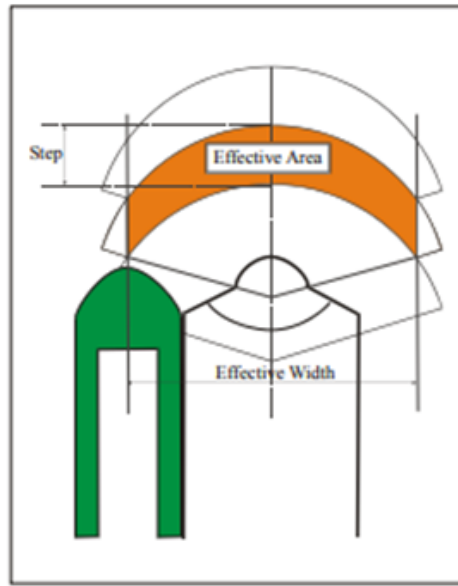


Figure A.24: BHD & Barge configuration. Obtained from Vlasblom, [2005b](#)

Soil cutting

The loading of a barge is performed by a backhoe. The backhoe extracts material from the sea-floor by using blades mounted on its excavator bucket, which cut through the material on the seabed.

The required cutting depth to fill up the bucket is an important parameter in the calculation of the cutting forces. The volume of in-situ material that is excavated is less than the volume of slurry that ends up in the bucket, due to the filling degree of the bucket and the bulking ability of the material from in-situ conditions to excavated conditions in the bucket. This means that the compact sea-floor material changes into a less compacted state in the bucket. This explains why a smaller quantity of material is required than the bucket's actual volume to fully fill it. The cutting depth can be calculated with equation A.66.

$$L_{\text{cut}} \cdot w_{\text{bucket}} \cdot h_{\text{bucket}} = \frac{V_{\text{bucket}} \cdot \text{filling degree}}{\text{bulking}} \quad (\text{A.66})$$

Where:

- L_{cut} = digging path [m]
- w_{bucket} = bucket width [m]
- h_{bucket} = cutting depth [m]
- V_{bucket} = bucket volume [m³]
- filling degree [-]
- bulking [-]

Intermezzo: Bulking

The principle of bulking is important in dredging practices. During soil cutting and the process of mixing soil with water, the in-situ material experiences a volume increase as it transitions from a densely packed to a loosely packed soil structure, as shown in Figure A.25. Bulking can occur on micro (re-orientation of individual grains) and macro scale (re-orientation between sheared soil fragments) according to Schrieck (2021). The bulking factor represents the volume increase of material from its pre-dredging state to its post-dredging state and is directly related to the material's porosity and density. Bulking is important for both, hydraulic and mechanical production work methods.

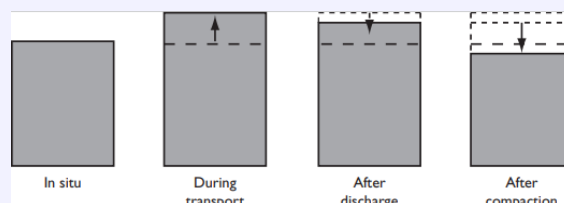


Figure A.25: Bulking: change of pore volume of soil sample in different stages of dredging cycle. Obtained from Van 't Hoff and Van Der Kolff, 2012

The amount of bulking is important for land reclamation purposes for estimation of the quantity of material needed, the amount of dredging cycles needed for transport and the final density of the material in the fill. Bulking values are relatively low for sand and clay, but high for rock. Specific bulking values differ for each type of material to be dredged due to unique soil structures.

Table A.1: Typical bulking values for various types of soil. Obtained from Vlasblom (2005b) and Schrieck (2021).

Soil type	Bulking value
Sand	1 - 1.35
Clay	1.1 - 1.3
Gravel	1.05 - 1.4
Rock	1.5 - 2.0

The digging path of the BHD is based on the depth at which the material is excavated. This can be extracted from Figure A.26. For example, at 16 meters depth, the possible digging path is 6 meters. The bucket width is constant.

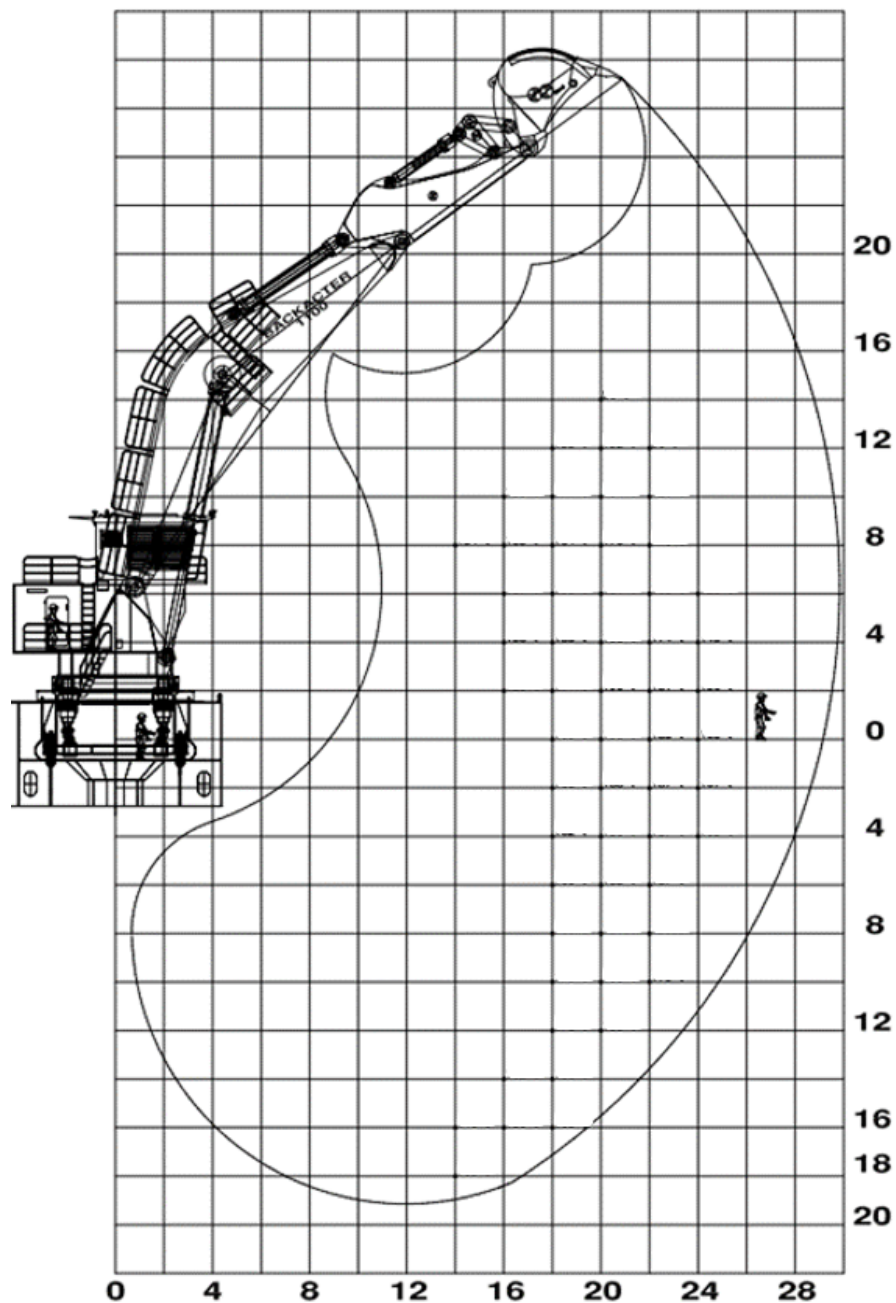


Figure A.26: Excavation graph Goliath: determine the digging path and cutting capability at any depth

The cutting force required to fail the in-situ material at depth needs to be delivered by the excavator. This is based on the excavation graphs of excavators, as shown in Figure A.26. This figure shows the cutting force that an excavator can deliver at positions relative to the excavator axis. The potential cutting forces differ due to the available power that can be exerted by the excavator in any digging orientation. If the required cutting force cannot be delivered by the excavator, other equipment, a smaller bucket size needs to be chosen or the cutting depth needs to be decreased. This will be an iterative process.

Lifting

Lifting checks need to be performed after cutting and filling of the excavator bucket. Lifting checks are essential for determining the amount of material that can be moved by the excavator in one sub-cycle. The lifting capability decreases in the upper operation area in Figure A.27. To fill the barge, the excavator needs to lift the material from the sea-floor to a couple of meters above the water line in order to overcome the freeboard of the barges at its most undeeep configuration.

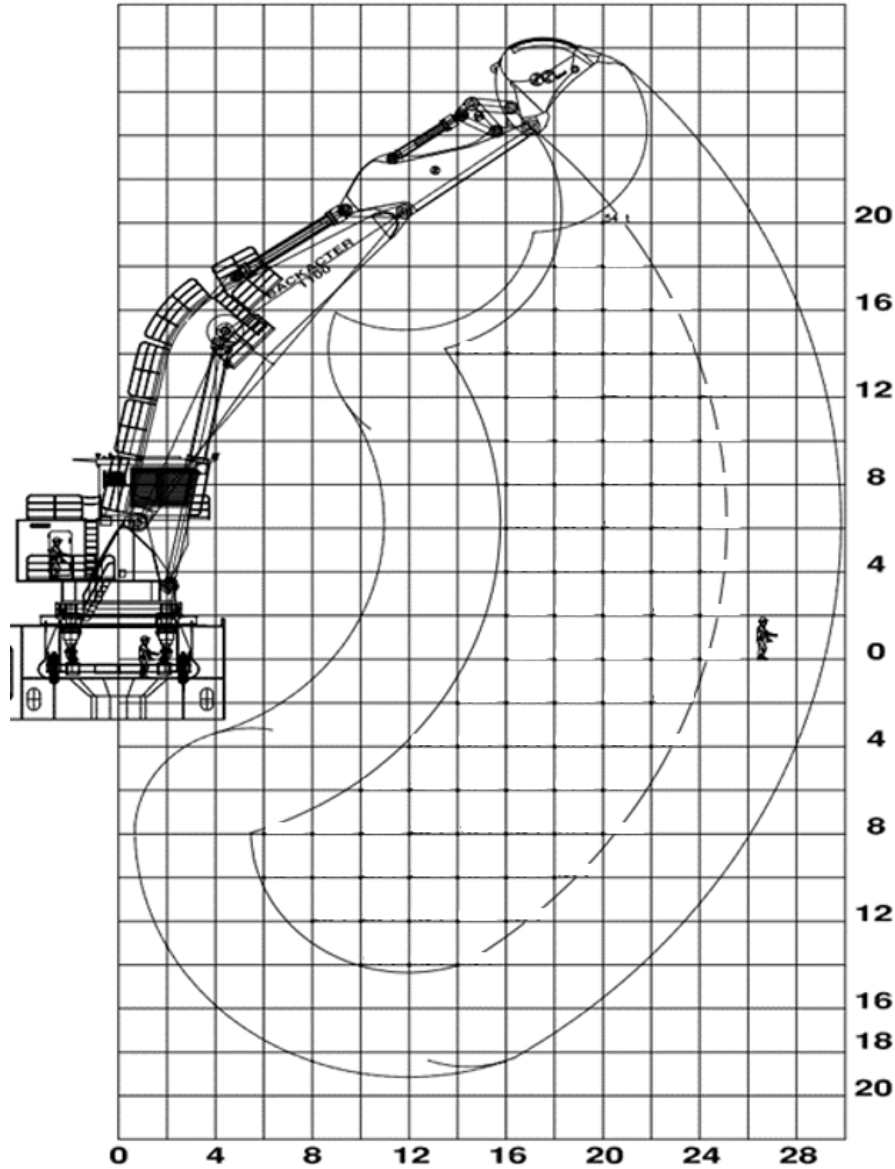


Figure A.27: Excavation graph Goliath: lifting capability of BHD at any depth

The lifting capacity in the graphs consists of the weight of the slurry material in the bucket. The weight of the bucket itself is excluded. Bucket slurry weight can not exceed this value, as lifting will not be possible. If the bucket contents can not be lifted, a smaller bucket size could be mounted or the cutting depth could be reduced. This will be a iterative process.

Sub-Cycle duration

The duration components of the BHD sub-cycle are shown in equation A.67.

$$t_{\text{total}} = t_{\text{swing}} + t_{\text{lowering}} + t_{\text{cut}} + t_{\text{lift}} + t_{\text{swing}} + t_{\text{release}} \quad [\text{sec}] \quad (\text{A.67})$$

Equation A.67 can be translated into equation A.68, based on internal research of De Wit, 2013. Where all the sub-cycle components other from t_{cut} are represented by t_{other} .

$$t_{\text{total}} = t_{\text{other}} + t_{\text{cut}} \quad [\text{sec}] \quad (\text{A.68})$$

There are no clear methods for determining the duration of this total sub-cycle. It is assumed that $t_{\text{other}} = 60 \text{ sec}$, based on the work of De Wit (2013) and expert judgement of the company.

The cutting duration t_{cut} is estimated based on total installed power of the excavator and the cutting force that needs to be delivered to shear the sea-floor material. The duration of cutting and corresponding cutting power required can be calculated from equation A.69. The required power for cutting needs to be lower than the installed power. The duration for cutting can therefore be obtained by using the required cutting force and the assumption that all the installed power is used while cutting. This makes the cutting duration the only unknown variable.

$$P = F_{\text{cut}} \cdot V_{\text{cut}} = F_{\text{cut}} \cdot \frac{L_{\text{cut}}}{t_{\text{cut}}} \quad (\text{A.69})$$

Density estimation

Bucket density is dependent on the amount of material that is excavated and their properties affecting the filling degree of the bucket and the bulking. The bulking and the filling degree of the bucket are material specific.

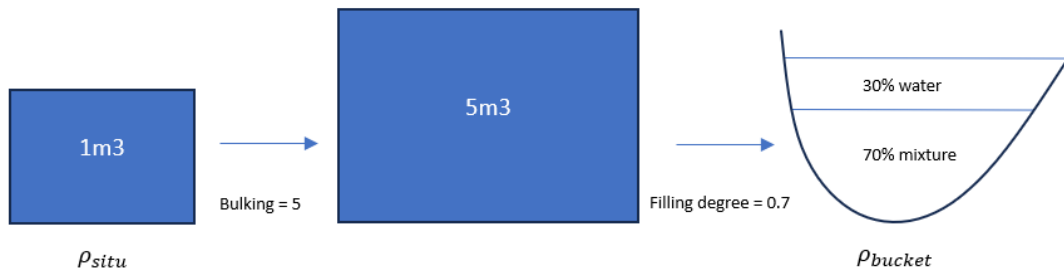


Figure A.28: Bulking and filling degree effects on bucket density

The conversion between ρ_{situ} and ρ_{bucket} can be calculated with equation A.70. All the effects from volume increase resulting from the bulking and the filling degree of the bucket are assumed to be filled with water.

$$\rho_{\text{bucket}} = \left(\frac{\rho_{\text{situ}} \cdot 1 + (\text{bulking} - 1)\rho_w}{\text{bulking}} \right) \cdot \text{filling degree} + (1 - \text{filling degree})\rho_w \quad [\text{kg/m}^3] \quad (\text{A.70})$$

The density of the bucket will end up to be the same density as the barge, due to the fact that overflow capacity of the barge is not used.

Density of the bucket is crucial since the volume reduction of the material due to consolidation in a land reclamation depends on the initial density. The effect of bulking on the bucket density according to equation A.70 is shown in Figure A.29.

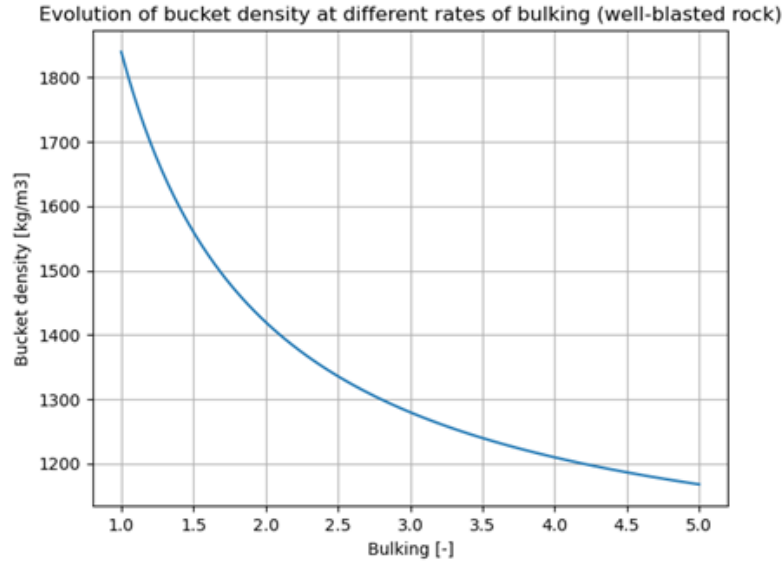


Figure A.29: Bulking effects on bucket density; keeping filling degree constant at 0.7.

Loading production

The production of a backhoe during loading is dependent on two sub-processes. First, the duration of loading the barge.

The amount of cycles needed to fill up a barge is needed to determine the barge loading time. This can be calculated with equation A.71. The volume of material in the bucket per dredging cycle is based on the dredged volume and the volume increase due to bulking and the bucket filling degree.

$$V_{\text{bucket}} = \frac{L_{\text{cut}} \cdot h_{\text{cut}} \cdot w_{\text{bucket}}}{\text{filling degree}} \cdot \text{bulking} \quad [m^3] \quad (\text{A.71})$$

Second, the duration of moving the barge when the effective area is fully excavated, as indicated in Figure A.24. The pontoon needs to be moved backwards with a 'step', in order to excavate new material. The movement of one step of the pontoon takes around 10 minutes (VBKO, 1998b).

$$t_{\text{moving}} \approx 10 \text{ min} \quad (\text{A.72})$$

The effective volume per step comprises of a circular trajectory with a swing motion of 140 degrees, a digging length of 6 meters and a layer depth of 1 meter. The volume of the effective area can be calculated with equation A.73.

$$V_{\text{effective-area}} = L_{\text{cut}} \cdot H_{\text{layer}} \cdot \left(\frac{140^\circ}{360^\circ} \cdot \pi \cdot r_{\text{excavator}}^2 \right) \cdot \left(\frac{\text{bulking}}{\text{filling degree}} \right) \quad (\text{A.73})$$

The amount of pontoon movements during the loading of one barge can be calculated with equation A.76.

$$n_{\text{movements}} = \frac{V_{\text{barge}}}{V_{\text{effective area}}} \quad [-] \quad (\text{A.74})$$

The total loading duration can then be calculated by multiplying the amount of cycles needed with the duration for one dredging cycle plus the amount of pontoon movements multiplied with the movement duration, as illustrated in equation A.75.

$$t_{\text{loading}} = (n_{\text{cycles}} \cdot t_{\text{total}}) + (n_{\text{movements}} \cdot t_{\text{moving}}) \quad [\text{sec}] \quad (\text{A.75})$$

Together with the bucket density, the total production of solids during loading can be calculated according to equation A.76.

$$Q_{\text{solids}} = \frac{\rho_{\text{bucket}} - \rho_w}{\rho_{\text{solids}} - \rho_w} \cdot \rho_{\text{solids}} \quad (\text{A.76})$$

A.4.2. Sailing

The sailing velocity for mechanical production is estimated for the Pieter Caland barge in this section. The estimation is based on the theory described in section Holtrop & Mennen. The input parameters and the calculation to obtain the sailing velocity is provided in this section. The characteristic vessel parameters are extracted from the technical reports of the Pieter Caland and Cornelis Lely. As no information was available on the open water efficiency η_o of these vessels, the open water efficiency of the ZSH5.0 project is assumed. This vessel has been assumed to have a similar open-water efficiency.

Pieter Caland / Cornelis Lely full:

- $h = \square$ [m]
- $T = \square$ [m]
- $T_f = \square$ [m]
- $C_b = \square$ [-]
- $C_{stern} = \square$ [-]
- $1 + k_2 = \square$ [-]
- $P = \square$ [kW]
- $D_{propeller} = \square$ [m]
- $\eta_o = \square$ [-]
- $\eta_r = \square$ [-]
- $\eta_h = \square$ [-]
- $\eta_g = \square$ [-]
- $\eta_t = \square$ [-]
- $L_{wl} = \square$ [m]
- $B = \square$ [m]

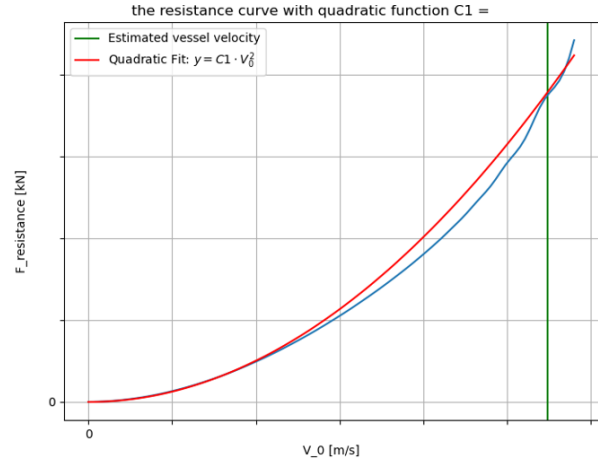


Figure A.30: Resistance estimation Pieter Caland / Cornelis Lely full.

$$V_s = \left(\frac{P_{\text{installed}} \cdot C_1}{\eta_{\text{total}}} \right)^{\frac{1}{3}} = \left(\frac{\square \cdot \square}{\square} \right)^{\frac{1}{3}} = \square \text{ [knots]} \quad (\text{A.77})$$

Pieter Caland / Cornelis Lely empty:

- $h = \square$ [m]
- $T = \square$ [m]
- $T_f = \square$ [m]
- $C_b = \square$ [-]
- $C_{stern} = \square$ [-]
- $1 + k_2 = \square$ [-]
- $P = \square$ [kW]
- $D_{propeller} = \square$ [m]
- $\eta_o = \square$ [-]
- $\eta_r = \square$ [-]
- $\eta_h = \square$ [-]
- $\eta_g = \square$ [-]
- $\eta_t = \square$ [-]
- $L_{wl} = \square$ [m]
- $B = \square$ [m]

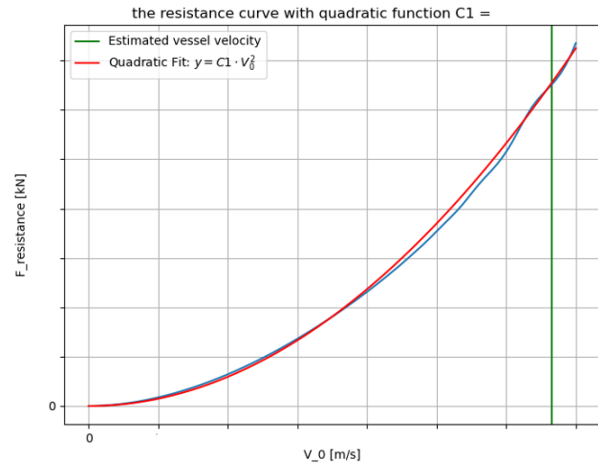


Figure A.31: Resistance estimation Pieter Caland / Cornelis Lely empty

$$V_s = \left(\frac{P_{\text{installed}} \cdot C_1}{\eta_{\text{total}}} \right)^{\frac{1}{3}} = \left(\frac{\square \cdot \square}{\square} \right)^{\frac{1}{3}} = \square \text{ [knots]} \quad (\text{A.78})$$

A.4.3. Discharge production

The discharge method of the barge at the site will be bottom-door-dumping. The bottom-door dumping method is the fastest discharging method (Schrieck, 2021). The sediment mixture flows out by opening of the bottom doors of the barge. This method is often used for underwater deposition in a dumping area or early stages of a reclamation.

The physical process of bottom-door dumping is based on gravity. The material can first be fluidized by the hopper jets to provide a more efficient dumping process by reducing friction resistance of the mixture. Once the bottom doors are opened, gravity will be the driving force for getting the material out of the hopper. Hence, it is assumed that there will be no concentration differences in between the inside of the barge and the material that is discharged onto the sea-floor.

Power utilization depends on the installed power on the barge. The duration of bottom-door-opening is around 30 minutes according to company experts.

A.4.4. Power utilization

Power BHD

Power utilization of a BHD is difficult to estimate. The amount of power used relative to total installed power is estimated for each component of the BHD sub-cycle by expert judgement from the company.

- $P_{\text{swing}} = \square\%$
- $P_{\text{lowering}} = \square\%$
- $P_{\text{cut}} = \square\%$
- $P_{\text{lift}} = \square\%$
- $P_{\text{release}} = \square\%$

The power utilized for lifting the slurry by the excavator is considered to be $\square\%$ when lifting the maximum lifting capacity. When lower weights are lifted, the power utilization will be between $\square\%$ of the installed power. This relation is assumed to be linear. The normative lifting force at maximum height above the waterline is obtained from Figure A.26. The power utilization for a arbitrary slurry weight in the bucket can be calculated with equation A.79.

$$P_{\text{lift}} = 0.5 + \left(\frac{0.5}{F_{\text{lift, normative}}} \right) \cdot \left(\frac{V_{\text{bucket}} \cdot \rho_{\text{bucket}}}{1000} \right) \quad [\text{kW}] \quad (\text{A.79})$$

The average power consumption in kiloWatts during the BHD sub-cycle can be calculated as in equation A.80 and A.81. Energy consumed during the BHD sub-cycle can be calculated with equation A.82

$$P_{\text{avg, other}} = \left(\frac{P_{\text{swing}} + P_{\text{lowering}} + P_{\text{cut}} + P_{\text{lift}} + P_{\text{release}}}{5} \right) \cdot P_{\text{installed}} \quad [\text{kW}] \quad (\text{A.80})$$

$$P_{\text{avg, cut}} = P_{\text{cut}} \cdot P_{\text{installed}} \quad [\text{kW}] \quad (\text{A.81})$$

$$E_{\text{loading}} = \left(P_{\text{avg, other}} \cdot \frac{t_{\text{other}}}{3600} \right) + \left(P_{\text{avg, cut}} \cdot \frac{t_{\text{cut}}}{3600} \right) \quad [\text{kWh}] \quad (\text{A.82})$$

Power barge

For the barge, power is demanded by the propeller from the main engines during sailing. The power utilization and total energy usage during sailing can be calculated by equation A.83 and equation A.84.

$$P_{\text{sailing}} = (C_1 \cdot v_{\text{sailing}}^2) \cdot v_{\text{sailing}} \quad [\text{kW}] \quad (\text{A.83})$$

$$E_{\text{sailing}} = \frac{P_{\text{sailing}} \cdot t_{\text{sailing}}}{3600} \quad [\text{kWh}] \quad (\text{A.84})$$

The sailing velocity and the corresponding energy needed, differ for sailing full and sailing empty. The coefficient for C_1 are obtained from the fitting principle in the Holtrop & Mennen method, as described in section A.2.

For bottom-door-opening during discharging of the barge, the power can be calculated with equation A.85 and A.86.

$$P_{\text{discharge}} \approx \boxed{} \quad [\text{kW}] \quad (\text{A.85})$$

$$E_{\text{discharge}} = P_{\text{discharge}} \cdot t_{\text{duration}} \quad [\text{kWh}] \quad (\text{A.86})$$

A.5. Costs

Costs for dredging and reclamation operations contribute to total project costs. Costs for dredging operations can be sub-divided in; fuel costs and weekly fixed costs. The main costs for reclamation operations are the expenses for installing and buying the ground improvement methods of surcharge and PVD's. Only the main costs components are used in this thesis, since other costs are very project specific, not accessible and fall under company secrets.

Fuel costs

The fuel consumption can be calculated based on the energy that is needed to complete one dredging cycle, the fuel type, the engine efficiency. This section will explain how fuel costs can be estimated for TSHD and BHD operations.

Table A.2: Power and Fuel Consumption of Equipment

ID	Vessel	Power Installed (main + auxiliary) [kW]	Engine Consumption [g/kW]
1	Vox Amalia	<input type="text"/>	<input type="text"/>
2	Goliath	<input type="text"/>	<input type="text"/>
3	Pieter Caland	<input type="text"/>	<input type="text"/>
4	Cornelis Lely	<input type="text"/>	<input type="text"/>

Fuel costs TSHD

The fuel consumption can be calculated based on the energy that is needed to complete one dredging cycle, the fuel type, the engine efficiency, and the amount of cycles needed to fill up the hopper. The complete energy components needed for TSHD operations is shown in equation A.87. The expression for individual energy components can be found in the section of Hydraulic Production.

The TSHD engines (Amalia) consumes at a rate of g/kWh. This means that grams of are needed to generate 1 kWh from the engine. This conversion includes engine efficiencies in terms of heat loss. Fuel consumption in tons of fuel can be calculated with equation A.88.

$$E_{\text{cycle}} = E_{\text{trailing+cut}} + E_{\text{trailing, hydraulic}} + E_{\text{sailing, full}} + E_{\text{discharge, hydraulic}} + E_{\text{sailing, empty}} \quad [\text{kWh}] \quad (\text{A.87})$$

$$\text{Fuel consumption} = \frac{\text{Fuel consumption}}{1000000} \cdot \frac{E_{\text{cycle}}}{1000000} \cdot \text{cycles needed} \quad [\text{grams}] \quad (\text{A.88})$$

Costs of is extracted from the internal fuel database and costs USD/ton. Multiplying the fuel consumption in tons by the fuel price gives the costs for TSHD operations. The complete fuel costs for filling up a reclamation depends on the amount of total cycles needed.

$$\text{Fuel costs} = \text{Fuel consumption} \cdot \text{Fuel price} \quad [\text{EUR}] \quad (\text{A.89})$$

Fuel costs BHD

The fuel consumption can be calculated based on the energy that is needed to complete one dredging cycle, the fuel type, the engine efficiency, and the amount of cycles needed to fill up a barge. The complete energy components needed for BHD+barge operations is shown in equation A.90. The expression for individual energy components can be found in the section of Mechanical Production.

The excavator engine (Goliath) consumes at a rate of g/kWh. This means that grams of MGO are needed to generate 1 kWh from the engine. This conversion includes engine efficiencies in terms of heat loss. The engines of the barges (Pieter Caland & Cornelis Lely) consume MGO at a rate of g/kWh. Fuel consumption in tons of fuel can be calculated with equation

A.91. This is performed by taking the average engine consumption between loading by BHD and sailing and discharge by barge.

$$E_{\text{cycle}} = E_{\text{loading}} + E_{\text{sailing, full}} + E_{\text{discharge}} + E_{\text{sailing, empty}} \quad [\text{kWh}] \quad (\text{A.90})$$

$$\text{Fuel consumption} = \boxed{} \cdot \frac{E_{\text{cycle}}}{1000000} \cdot \text{cycles needed} \quad [\text{tons}] \quad (\text{A.91})$$

Costs of $\boxed{}$ is extracted from the internal fuel database and costs $\boxed{}$ USD/ton. Multiplying the fuel consumption in tons by the fuel price gives the costs for BHD and barge operations. The complete fuel costs for filling up a reclamation depends on the amount of total cycles needed.

$$\text{Fuel costs} = \text{Fuel consumption} \cdot \boxed{} \quad [\text{EUR}] \quad (\text{A.92})$$

CIRIA costs

Cost estimation of dredging equipment can be estimated with the guidelines of CIRIA (2009). The method of CIRIA (2009) provide a standardized method for estimating costs of dredging equipment. A standardized method is especially valuable in joint-venture projects where each party does not want to give up their competitive market position in terms of costs. This method includes costs of dredging equipment in terms of maintenance & repairs and depreciation & interest. CIRIA (2009) uses technical, statistical and economic data for these estimates.

Costs that are not included in the CIRIA (2009) estimation method are summarized below.

- Production operations
- (de)Mobilisation
- Crew
- Fuel
- Insurance
- Wear and tear due to dredged materials

The CIRIA (2009) guidelines uses the standard value V . The standard value is considered to be the new price of purchase of the equipment considered. Depreciation & Interest and Maintenance & Repair is considered to be a function of the standard value. The standard value of equipment is determined according to a regression method based on cost data supplied by IADC, and is based on technical characteristics of the dredging vessel.

Service life N is used to define the period of utilization of the asset, before the asset is not used anymore due to technical or economical reasons. CIRIA, 2009 assumes that the residual value for the TSHD will be $\boxed{}\%$ of the standard value at the end of the service lifetime of $\boxed{}$ years.

Depreciation and Interest ($D+i$) is used to represent the value of the asset in the future. The value of the asset will reduce when it is utilized along its service lifetime, which is depreciation. Depreciation is represented by the annuity method (CIRIA, 2009). Depreciation is calculated based on the expected residual value at the end of service lifetime and the utilization hours of the equipment per week during the service lifetime. Interest is used to represent the value of the money that you invest right now after the service life of the asset. The interest rate represents the return on capital when the money is kept in the bank. An interest rate of seven percent is assumed (CIRIA, 2009), which is considered to be the yearly average yield of the S&P500 since the year 1800 (McKinsey, 2022). The total depreciation & interest percentage is 0.292% of the standard value per week, considering a hopper.

Maintenance and repair ($M+R$) is used to describe the costs of all the maintenance to keep the asset performing properly. The absolute value of maintenance and repair costs depend on the service hours of the equipment, which is assumed to be $\boxed{}$ hours per week. CIRIA (2009) assumes this to be a percentage of the initial value of the asset.

Hopper Costs

The Amalia weekly rates can be determined with Figure A.32. According to CIRIA (2009), the operational hours of a TSHD are hours per week (during operational weeks per year), the lifetime years and the residual value after lifetime is .



Figure A.32: TSHD weekly cost , obtained from (CIRIA, 2009).

$V =$ (A.93)

Where:

- V = standard value
- W = Lightweight vessel
- P = Power dredge pumps
- J = Power jet pumps on draghead
- S = Propulsion power

The standard value of the Amalia can be calculated from equation A.93 by using the The Amalia characteristics. These are obtained from the Van Oord database. By using the characteristics below, the standard value of the Amalia is EUR.

Where:

- W = [tons]
- P = [kW]
- J = [kW]
- S = [kW]

The computed standard value for the Amalia can be used to calculate the weekly depreciation + interest rates (D+i) and the maintenance + repairs rates (M+R). According to Figure A.32, D+i = % of

standard value V per year and M+R = % of standard value V per year. The weekly cost rates are calculated in equation A.94.

Costs = [EUR/week] (A.94)

Pipeline Costs

The weekly rates of using floating pipeline of 500 meters can be determined with Figure A.33. According to CIRIA (2009), the lifetime is years and the residual value of % at the end of lifetime. The yearly utilization period is weeks. The pipelines consist of 11.8 meter of pipeline. It is assumed that D+i = % of standard value V.

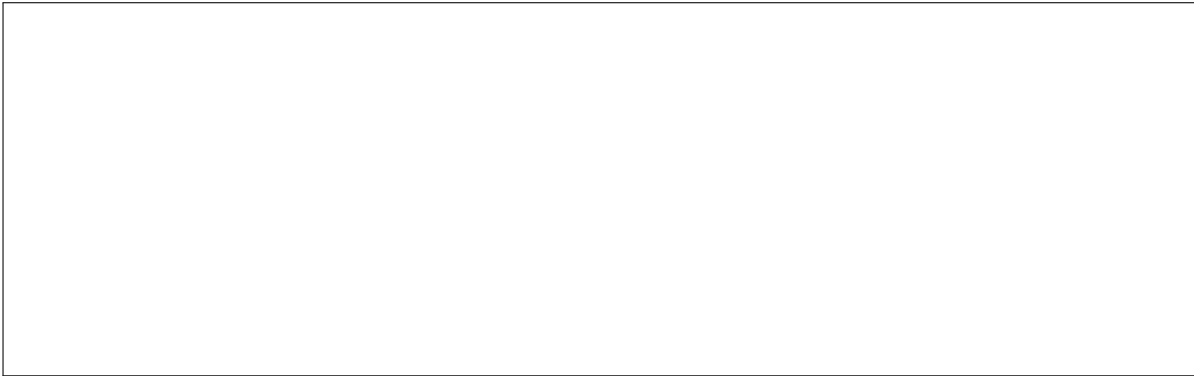


Figure A.33: Pipeline weekly cost , obtained from (CIRIA, 2009).

Units pipeline needed = $\frac{500}{11.8} = 42.37$ (A.95)

The standard value V for the pipelines will result in EUR, when utilizing floating pipelines with a diameter of 1000 mm. The total weekly costs are calculated in equation A.96.

Costs = [EUR/week] (A.96)

Backhoe Costs

The Goliath weekly rates can be determined with Figure A.34. According to CIRIA (2009), the operational hours of a BHD are hours per week (during operational weeks per year), the lifetime years for the pontoon and years for the excavator, and the residual value after lifetime is respectively % and % of standard value V.



Figure A.34: BHD weekly cost , obtained from (CIRIA, 2009).

$$V = \boxed{\hspace{10em}} \quad (\text{A.97})$$

- W = Lightweight vessel
- $S + S_b$ = Propulsion power

The standard value of the Pieter Caland and Cornelis Lely can be calculated from equation A.99 by using the characteristics of these **identical** barges. These are obtained from the Van Oord database. By using the characteristics below the standard value each Pieter Caland and Cornelis Lely is EUR.

Where:

- $W = \text{}$ [tons]
- $S + S_b = \text{}$ [kW]

The computed standard value for the barges can be used to calculate the weekly depreciation + interest rates ($D+i$) and the weekly maintenance + repairs rate ($M+R$). According to CIRIA (2009), $D+i = \text{}\%$ of standard value V per year and $M+R = \text{}\%$ of standard value V per year. The total weekly cost rates are calculated in equation A.100.

$$\text{Costs} = \text{} \quad [\text{EUR/week}] \quad (\text{A.100})$$

Hence, when two barges work simultaneously, weekly costs need to be multiplied by two.

A.6. Production Estimation calculations

In this section, all theory explained in this appendix is applied to the case-study. The duration, energy utilization, costs and production of one dredging cycle is calculated according to hydraulic and mechanical production principles explained above. Estimations for sailing full and sailing empty for the hydraulic and mechanical method is already computed above. These values are obtained and processed in this section for $t_{\text{sailing full}}$ and $t_{\text{sailing empty}}$. Production costs, including weekly cost rates of CIRIA and fuel costs for each hydraulic and mechanical methods are used for cycle cost estimations in this section.

A density range is used for hydraulic and mechanical work methods to indicate how different target hopper-densities affect the production rates and costs coming for one dredging cycle.

The total cycle production can be calculated according to equation A.101. Duration of sailing full and sailing empty are constant for each density configuration in the hydraulic and mechanical calculations.

$$\text{Cycle Production} = \frac{V_{\text{hopper}}}{t_{\text{trailing}} + t_{\text{sailing,full}} + t_{\text{discharge}} + t_{\text{sailing,empty}}} \quad [\text{m}^3/\text{s}] \quad (\text{A.101})$$

A.6.1. Hydraulic production

The hydraulic production is estimated for the Trailing Suction Hopper Dredger Vox Amalia and the soil parameters obtained from the case-study. The configuration of the Vox Amalia, including the parameters to calibrate the pump operations is given below for trailing and discharging. All parameters below are obtained through the Van Oord database and are applied to the case-study of this thesis. Values differ before and after the pump due to different pipeline geometries in the vessel.

Trailing parameters

Trailing production is determined based on the vessel and pump characteristics below. These parameters are obtained from Van Oord databases. The dredging depth z is obtained from the case-study. During trailing, the vessel is sailing at 2 knots. The fuel type of the vessel consists of and the engine consumes fuel at a rate of grams per kilowatt-hours (kWh).

The following parameters are used for the soil cutting model of rock. These parameters are obtained from the Scandinavia soil report, and can be representative for the soil material used in the case-study. The theory for rock cutting of S. A. Miedema (2016) is used for cutting production.

Table A.3: Rock cutting parameters

Parameter	Value
α	45 [°]
δ	22 [°]
φ	33 [°]
UCS	1480 [kPa]

Table A.4: Working point before pump

Parameter	Value
N_1	<input type="text"/> [-]
N_2	<input type="text"/> [-]
N_3	<input type="text"/> [-]
z	<input type="text"/> [m]
k	<input type="text"/> [m]
α	<input type="text"/> [-]
ξ	<input type="text"/> [-]
L	<input type="text"/> [m]
D	<input type="text"/> [m]
λ	<input type="text"/> [-]

Table A.5: Working point after pump

Parameter	Value
F_1	<input type="text"/> [-]
F_2	<input type="text"/> [-]
F_3	<input type="text"/> [-]
a	<input type="text"/> [m]
α	<input type="text"/> [-]
ξ	<input type="text"/> [-]
L	<input type="text"/> [m]
D	<input type="text"/> [m]
λ	<input type="text"/> [-]

The outcomes of the trailing working point can be seen in Figure A.36. The working points defines the flow-rate at which the material from the sea-floor can be loaded to the hopper. Together with the hopper

volume, the duration for loading can be determined as presented in equation A.102. For each of the densities considered, the working point where conservation of mass is satisfied can be obtained from the point where the density line intersects with the blue line. It can be observed that the working points for higher densities are achieved at lower mixture velocities. This is intuitive, since more energy is lost in the system by pumping heavier material. In addition, RPM drops when dredging higher mixture densities, this might not be intuitive since one would expect more power is needed to pump heavier material. The occurrence of RPM drop happens in this model because the suction side of the pump is dominating the ability of the system to conserve mass due to the effect of RPM on $NPSH_r$.

$$t_{\text{loading}} = \frac{V_{\text{hopper}}}{Q_{\text{mixture}}} \quad (\text{A.102})$$

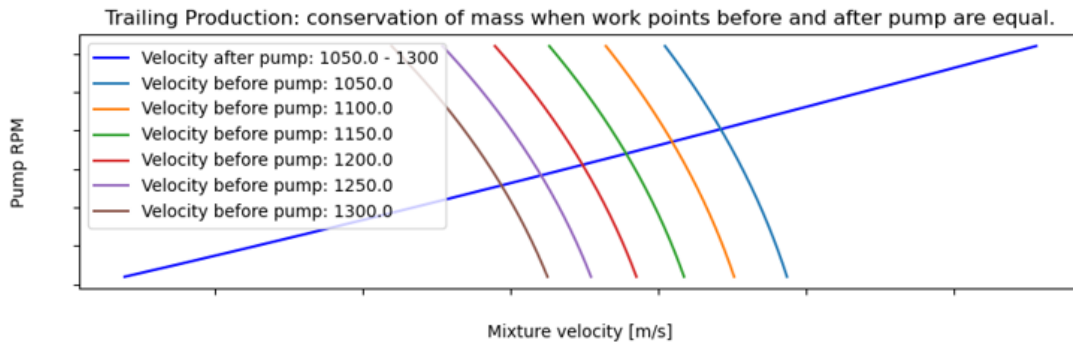


Figure A.36: Hydraulic production: trailing

Discharge parameters

The trailing production is determined based on the vessel and pump characteristics below. These parameters are obtained from Van Oord databases. The line length L after the pump is added by 500 meters for the utilization of 500 meters of floating pipeline in the case-study.

Table A.6: Working point before pump

Parameter	Value
N_1	<input type="text"/> [-]
N_2	<input type="text"/> [-]
N_3	<input type="text"/> [-]
z	<input type="text"/> [m]
k	<input type="text"/> [m]
α	<input type="text"/> [-]
ξ	<input type="text"/> [-]
L	<input type="text"/> [m]
D	<input type="text"/> [m]
λ	<input type="text"/> [-]

Table A.7: Working point after pump

Parameter	Value
F_1	<input type="text"/> [-]
F_2	<input type="text"/> [-]
F_3	<input type="text"/> [-]
a	<input type="text"/> [m]
α	<input type="text"/> [-]
ξ	<input type="text"/> [-]
L	<input type="text"/> [m]
D	<input type="text"/> [m]
λ	<input type="text"/> [-]

The outcomes of the discharge working point can be seen in Figure A.37. The working points define the flow-rate at which the material can be discharged. Together with the hopper volume, this determines the discharge duration as presented in equation A.103. For each of the densities considered, the working point where conservation of mass is satisfied can be obtained from the point where the density lines intersect with the blue line. It can be observed that the working points for higher densities are achieved at lower mixture velocities, although the absolute spread is less compared to the working points for trailing.

$$t_{\text{discharge}} = \frac{V_{\text{hopper}}}{Q_{\text{mixture}}} \quad (\text{A.103})$$

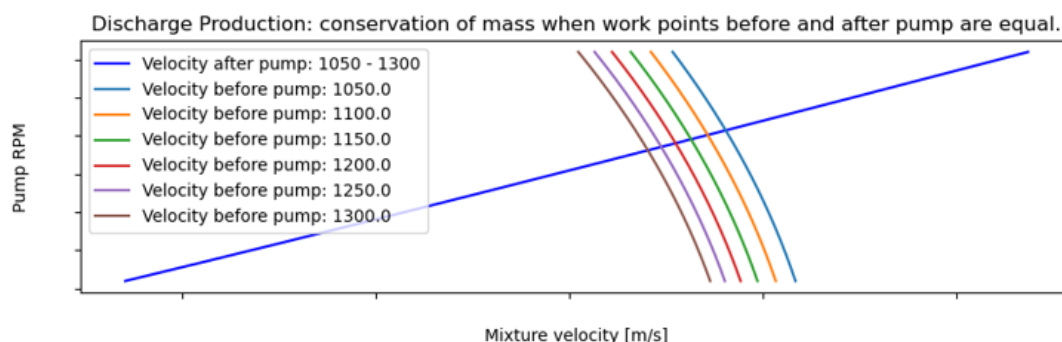


Figure A.37: Hydraulic production: discharge

Results

The final results of cycle computations for hopper densities reaching from 1050 kg/m³ to 1300 kg/m³ are obtained from the model in Table A.8. The outcomes of trailing duration and discharge duration are combined with the results for the velocity sailing full and empty and power consumption obtained from the Holtrop & Mennen method to make a estimation of a single cycle duration and costs. One can observe that dredging higher density slurries lead to more costs, duration and more energy utilization. This is intuitive since dredging higher densities takes more effort compared to dredging lower densities. In contrast, higher densities leads to more mass transported in one cycle.

Table A.8: Vox Amalia - Production analysis of one dredging cycle

Density [kg/m ³]	Flow [m ³ /min]	Cycle duration [min]	Production [ton/min]	Energy [kWh]	Costs [EUR]	Costs [EUR/ton]
1050						
1100						
1150						
1200						
1250						
1300						

A.6.2. Mechanical production




The mechanical production is estimated for the Backhoe Dredger and barge; Goliath and Pieter Caland. The soil parameters for production are obtained from the case-study. The configuration of the Goliath and Pieter Caland are obtained from the Van Oord database. The fuel type of the either the backhoe and barges consists of . The engine consumption of the backhoe and barges are respectively; and grams per kilowatt-hours (kWh).

The following parameters are used for the soil cutting model of rock. These parameters are obtained from the Scandinavia soil report and are representable for the soil material used in the case-study.

Table A.9: Rock cutting parameters

Parameter	Value
α	45 [°]
δ	22 [°]
φ	33 [°]
UCS	1480 [kPa]

Table A.10: Backhoe configuration parameters

Parameter	Value
$P_{\text{installed}}$	3800 [kW]
w_{bucket}	 [m]
L_{cut}	 [m]
V_{bucket}	 [m3]
H_{layer}	1 [m]
$r_{\text{excavator}}$	180 - 330 [m]
Dredging depth	16 [m]
Lifting height	9-10 [m]
Filling degree	0.7 [-]
Bulking values	1.5 - 5 [-]

The calculations are performed for different target densities which can be achieved with bulking values between 1.5 - 5. Production analysis is performed for the target densities in the table below. The outcomes of loading duration by BHD and discharge duration by barge are combined with the results for the velocity sailing full and empty and power consumption obtained from the Holtrop & Mennen method to make a estimation of a single cycle duration and costs. One can observe that production rates and flow are very low compared to the production rates and flow from the hydraulic work method. This is due to the relatively low production rates of the excavator while loading, and the relatively small barge volume. The costs of the mechanical method are high, due to the high cycle duration. The benefit of this method is that higher hopper densities can be obtained. In contrast, higher densities leads to more mass transported in one cycle.

Table A.11: Goliath & Pieter Caland - Production analysis of one dredging cycle

[illegible]

B

Reclamation Engineering

This section will explain the estimation principles for *Reclamation Engineering*. The effects of different materials, reclamation design requirements, consolidation principles, ground improvement methods and reclamation costs will be covered. The theory of Gibson is explained as well as the modifications needed to make this approach suitable to reclamation practices. This section ends off with the loading steps required by external loading to make the reclamation comply with design requirements.

B.1. Reclamation process

A land reclamation is defined as "reclaiming land from oceans, seas riverbeds or lakebeds". A land reclamation consists of filling of an area with soil and can also be named a "Hydraulic Fill" according to Van 't Hoff and Van Der Kolff (2012). The boundaries of reclamation area are often enclosed by bunds. Bunds protect the reclamation area from erosive forces coming from ocean waves, and provide stability for the fill material. Reclamations are often open in the first phase where vessels can sail in to place their material through bottom-door placement. Reclamations will be closed when filling proceeds whereby hydraulic discharge techniques will be used until the filling is finished. This is illustrated in Figure B.1. Filling of the reclamation is gradual and can be approximated with the placement of time dependent layers. Production governs the filling rate of the reclamation. The amount of material that is needed to obtain the design height is estimated with consolidation models.

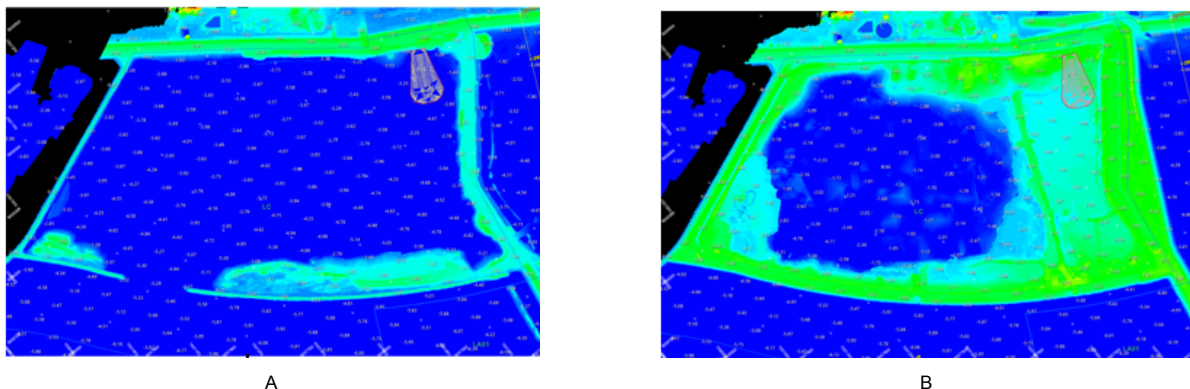


Figure B.1: Phase A: Open reclamation. Phase B: Closed reclamation.

After the placement of the first layer of slurry, consolidation starts. This governs the process of drainage of water due to compaction of the slurry under gravity, also called "self-weight" consolidation. The process of consolidation helps the soil body to compact and gain strength. While the self-weight consolidation has been started for the first layer, a second layer is introduced on top of the first layer. This layer makes the load on top of the first layer higher, which induces extra pressure on the lower layers,

increasing excess pore pressure, increasing consolidation rates. This process is repeated until all layers are placed which are needed to fill up the reclamation. Important here is to place enough material to maintain the design level of the reclamation after consolidation. It could be that 78 meters of material is placed which reduces to 11 meters after self-weight consolidation, while the design level is 10 meters. Then the long term consolidation can only be 1 meter. Therefore, knowledge on self-weight consolidation behaviour of the material is very important when designing a land reclamation.

After the consolidation has reached some strength, a capping crust layer is placed with a spraying pontoon. This capping layer has a squeezing effect, by introducing a load on the still soft top layer, which gets squeezed and gains strength. After placement of the capping layer, machines (PVD rigs, bulldozers and dump trucks) can access the reclamation and place the ground improvement methods such as surcharge and Pre-fabricated vertical drains.

After placement of the ground improvement methods, long term consolidation takes place. During this process, the soil compacts further and gains strength to eventually comply with the design requirements of the client. Airports, port storage facilities or industrial applications often require high strength from the soil which bears the loads of these applications. The duration until a hydraulic fill can bear such loads can take up to years and decades when using "complex" materials (Van Rijn, 2019), or require intensive artificial ground improvement.

B.2. Fill material

Sands are characterized by high permeability and low compressibility, typically considered as favourable engineering properties in engineering works. Reclamation works including sands consolidate and gain strength fast. The drainage of excess pore pressure is fast due to high permeability. Compressibility is less, therefore less absolute material is needed to comply with the design level. Silt particles can be up to 100 times smaller than sand, while clay particles can be up to 1000 times smaller than sand particles. This has huge impacts on engineering properties and consolidation of slurry consisting of such material. Materials with high fines content are characterized by low permeability and high compressibility, typically unfavourable engineering properties in reclamation works. Reclamation works including high fines content consolidate slowly and gain strength slowly due to the low permeability. Consolidation timeframes can take years up to decades to gain sufficient strength. High compressibility results in the fact that a lot of material is needed to comply with design levels because of extensive settlements. These typical engineering properties that come with the types of soil open up the knowledge gap as indicated in the literature review.

Sands, silts and clay material can be used as filling material for reclamations, each with their own characteristic behaviour. The soil used in reclamations is not purely sand, silt or clay, but a mixture is often present in practice. Mixtures of material can have big effects on its behaviour and properties in a hydraulic fill (Fan et al., 2022). Every material behaves differently, this is why soil classification is important in estimating consolidation behaviour.

Sands or finer material can dominate in the microstructure of soil mixtures, as illustrated in Figure B.2. Each of these occurring skeleton structures has an effect on soil compressibility and permeability. Course grains dominate compressibility ability in cases where the coarse grains are still in contact throughout the soil skeleton. Small grains dominate compressibility when the course grains are not longer in contact with each other (Fan et al., 2022). The presence of fines in the pore spaces of sand grains does lead to smaller permeability. Permeability decreases already with a factor of 20 for fines content between 12-50% (Fan et al., 2022).

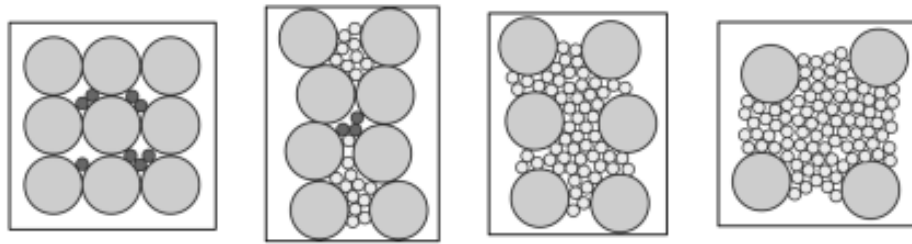


Figure B.2: Soil skeleton: coarse and fine material mixture, obtained from Fan et al., 2022

Besides the type of material itself, also the initial density has a crucial effect on the consolidation behaviour. The absolute consolidation duration for "complex" materials with higher initial densities is smaller, because less volumes of water need to drain compared to materials that have very low initial density and more mass is placed in a shorter amount of time which induces higher excess pore pressures. This means that the initial density in the fill plays a significant role on consolidation duration, besides the classification of the soil mixture. Hydraulic and mechanical placement methods can be used to induce different initial densities in a hydraulic fill.

According to company experts, dredging companies aim to minimize segregation of coarse and fines particles during placement when working with complex material. The effects of segregation and no segregation on density in soils is shown in Figure B.3. Several engineering properties of the soil are linked to density, such as shear strength and compressibility. Minimizing segregation during placement will create higher initial density of the fill material leading to lower compressibility (less settlements) and higher shear strength of the material placed in the fill, according to company experts.

Another downside of segregation is the fact that all the soft material will stay on top. This material will remain fluid for long due to low excess pore pressures and low permeability, which complicates the accessibility of equipment to the reclamation. This is often solved with capping the soft material with a sand crust, which will lead to significant delays and additional costs.

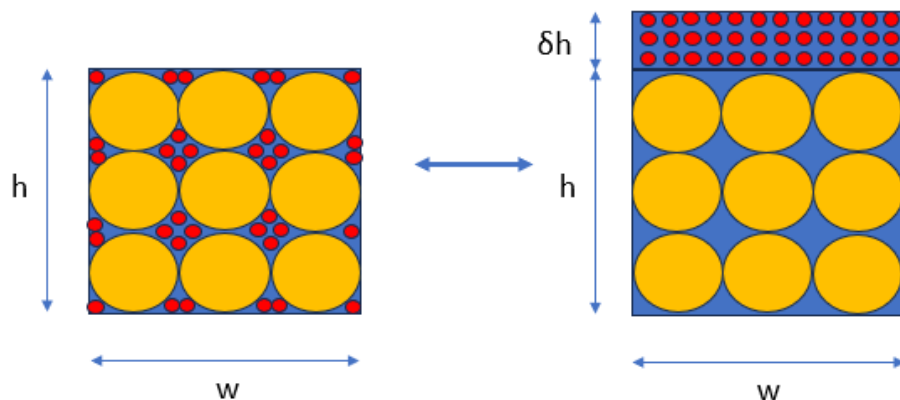


Figure B.3: Density differences for segregating and non-segregating material

The work method that is chosen will highly affect the ability of the fill material to segregate. When placing materials, placement of high energy and low energy placement can be distinguished when using hydraulic dredging. Generally, high energy placement methods, rainbowing and landline pumping, will lead to high segregation while having a high production rate. Low energy placement methods, a spraying pontoon, will lead to low segregation at the cost of having a lower production rate. However the usage of a low energy placement method does not always lead to limitations in production when multiple spraying pontoons are used simultaneously. Mechanical placement by Backhoes in the fill is hard to classify, but could be considered as a low energy placement method according to Christian

Hoffmann (Geo-technical specialist Van Oord). Therefore the work method is crucial for reducing segregation in a fill. Low energy placement techniques are advantageous when working with complex soils and considering the optimal geo-technical properties of a fill.

Intermezzo: Geotechnical tender objectives

The goal of the Geotechnical tender phase is to link and scale up in-situ soil classifications and lab tests to the behaviour of the material in the fill. This is done to make reliable predictions on consolidation behaviour of when the dredged material is present in the fill. This intermezzo will briefly describe the tender considerations from Geo-technical perspective

During the tender, the client provides information of the soil that is present in the dredging area. The client performed field tests across the dredging areas, in the form of CPT's and Vane tests. Also standard lab tests are performed to get the basic soil classifications. Hence, no state-of-the-art tests are performed typically by the client. The tender needs to be based on the information that is available. Field and lab tests are conducted on materials across the dredging area to obtain their geotechnical properties. By doing this, a good estimation can be made about the in-situ properties of the material at different locations within the dredging area. Based on the soil characteristics, different execution strategies are considered. During this step, the dredging company is exploring strategies to come to the most efficient project execution. The objective is to create a fill which has engineering properties which comply with the boundaries set by the client.

The fill behaviour will be estimated by running consolidation test cases for different fractions of segregation. The objective is to minimize segregation of sand and fines, due to the favourable engineering properties that come with no segregation. Test cases in the form of consolidation simulations will be performed for different cases of segregation to get a best case and worst case scenario for consolidation durations. A convenient method for coupling consolidation properties to fines content is obtained from the mining industry, where they have more experience in dealing with similar challenges when investigating the consolidation of their "complex" mining tailings slurries. This method, which describes the compressibility and permeability ability based on the percentage of fines in the mix is considered to be a good approximation for estimating the consolidation behaviour for different amounts of segregation (C. Hoffmann, Geotechnical specialist Van Oord). Based on this information, small strain consolidation estimations are performed for different cases of segregation.

Compressibility and permeability data from all soil samples provided by the client during the tender phase are plotted against the fines content present in each specific area across the dredging site. By doing this, a similar plot is obtained as in Figure B.4, obtained from Fan et al. (2022). Plots of permeability and compressibility based on fines content will have significant scattering, because in natural soils, more factors affect the permeability and compressibility besides the fines content. This paper comes from the mining industry where they have created soils with varying fines content artificially, based on the combination of sand particles and non-plastic powder.

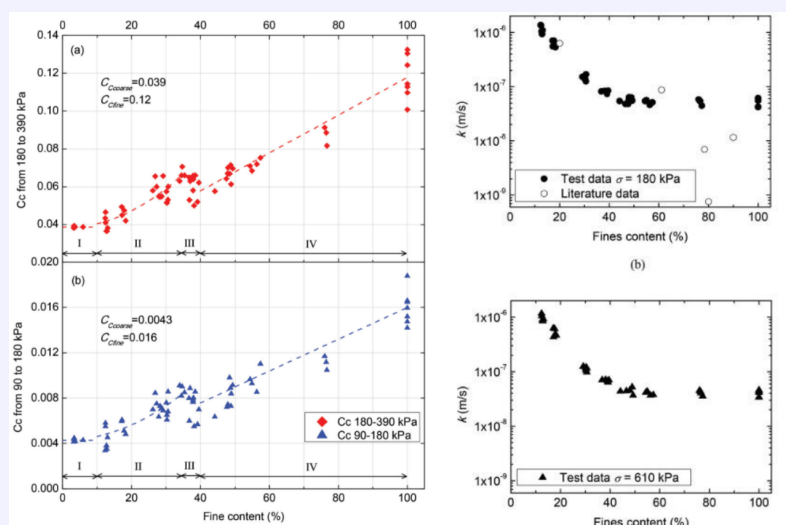


Figure B.4: Compressibility and permeability coupled to fines content. Obtained from Fan et al., 2022

Coupling the permeability and compressibility ability to fines content is convenient because the amount of fines define the amount of segregation that occurs. It is not true that the compressibility and permeability are solely dependent on fines content. Other physical factors contribute to this as well. However, using this parameter is convenient for all stakeholders in the project to understand the challenges that come when building with complex materials.

B.3. Consolidation

The process of consolidation can be described as the compaction of a soil body due to the drainage of water. Drainage of water from the soil body is driven by an excess pore pressure gradient inside the pores of the slurry like material. Excess pore pressure exists due to the weight of the soil particles that pressurizes the voids between the soil particles. Subsequently, the water flows out of the porous material and then the individual soil grains can re-arrange in a more compact state. This is called consolidation. By consolidation of the soil, the density of the material goes up, which favours engineering properties such as compressibility and shear strength resistance.

The small strain and large strain consolidation models are the two main approaches for modeling consolidation behaviour of soils according to the literature review. In the context of intermezzo B.2, the large-strain model can add value to consolidation estimations when "complex" materials are used. It will contribute by estimating the self-weight consolidation stage of these "complex" materials. The physical principles that are fundamentals for these consolidation models are essential in this thesis. Understanding the models will give insights in the parameters that need to be extracted from the production module which are affecting the consolidation behaviour in the reclamation module.

B.3.1. Large-strain consolidation

The Large strain theory of Gibson can deal with consolidation when concentrations are high enough in order that the soil particles just touch. This is the moment where effective stresses start to develop between particles. The Gibson equation can be used for high and low initial densities for estimation of the consolidation behaviour. Therefore this equation is perfect to handle the physical behaviour of the material when consolidating under its own weight. Here, the material that is disposed in the fill has low densities when using a Trailing Suction Hopper Dredger. This approach of Gibson can also be used when having higher densities as an initial concentration in the fill which is the case when using a Backhoe Dredger. Figure B.5 depicts the physical behaviour of material when starting from an homogeneous initial concentration over the column.

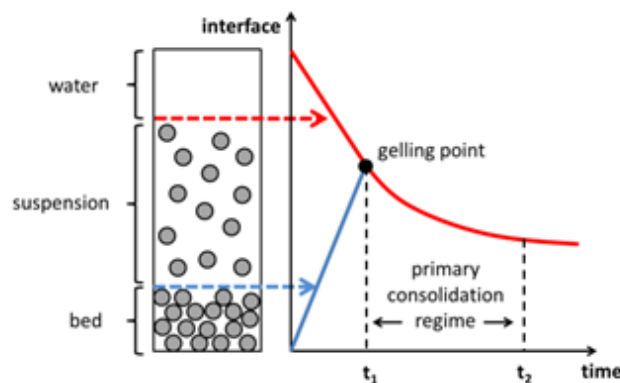


Figure B.5: Sedimentation and consolidation of a slurry, obtained from Chassagne, 2021

The Gibson approach of consolidation can deal with these large strains because it accounts for non-linearities in permeability and compressibility ability of the material at different volume fractions of solids. In addition, the Darcy equation for outflow of water through a porous medium is modified to account for the soil particles that are settling. This makes that the Gibson equation can handle materials that have large deformations. The Gibson equation can be seen as the basis of consolidation theories. Simplifying the Gibson equation will eventually lead to the small strain consolidation theory of Terzaghi. This derivation is perfectly shown in the work of Chassagne (2021). The derivation, calibration and validation of the Gibson theory is shown in the section below.

Gibson derivation

The Gibson equation is based on continuity and a modified version of Darcy's law (Gibson, 1967). The derivation of the governing equation is excellently described by Chassagne (2021) and Merckelbach (2000). The derivation that is showed below summarizes the steps in the derivation, based on the

derivation of Chassagne (2021). Volume solid fraction is a measure for the amount of solids in the total volume. This is an essential parameter as the governing equation of Gibson is written out in this variable in Merckelbach (2000) and Chassagne (2021). The original Gibson equation is written out in terms of void ratio. The volume fraction of solids ϕ_s is related to void ratio e . The definition of ϕ_s is given in equation B.1.

$$\phi_s = \frac{V_s}{V} \quad (\text{B.1})$$

This quantity of volume fraction of solids will differ over depth in the water column that is considered. The ϕ_s profile over depth will change as well over time due to consolidation. Therefore ϕ_s is a function of depth and time.

The continuity equation is basically conservation of mass. Here, the difference between inflow and outflow of ϕ_s equals the difference of quantity ϕ_s in the considered volume, as shown in Figure B.6. The amount of inflow and outflow is based on $v_s \phi_s$, which illustrates that the settling velocity of the particles transport the particles in and out of the control volume.

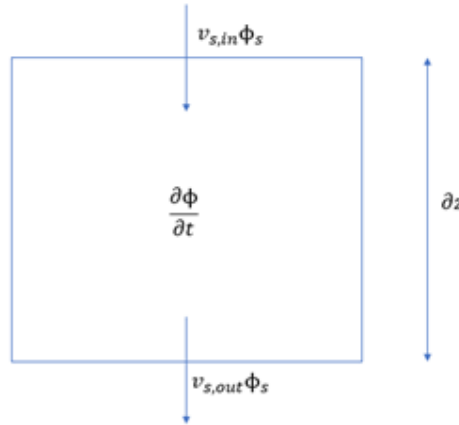


Figure B.6: Control volume: continuity equation

This lead to the continuity equation as shown below, which stands for the conservation of mass.

$$\frac{\partial \phi_s}{\partial t} - \frac{\partial (v_s \phi_s)}{\partial z} = 0 \quad (\text{B.2})$$

Darcy's law describes the flow of water through a porous medium, which contains a soil structure that is static and not moving. In this application, water flows out of the soil structure, because of the soil structure that is settling. This approach needs a modification of the Darcy equation that relates the flux of out-flowing water to the settling soil particles. This is done by fixing the reference frame to the settling particles. By doing this, Darcy can again be applied as the particles appear to be non-moving because of the reference frame that is moving down with the settling particles. The modified Darcy equation is shown in equation B.3.

$$J_{w/s} = (1 - \phi_s) v_{w/s} \quad (\text{B.3})$$

Equation B.3 shows that the flux of water outflow is equal to the volume fraction of water times the velocity of water within the pores relative to the settling particles.

The outflow of water according to Darcy, which is dependent on permeability, viscosity and pressure gradient is shown below in equation B.4. Permeability here can not be treated as a constant but is dependent on the volume fraction of solids in the control volume.

$$J_{w/s} = -\frac{k}{\eta} \nabla P \quad (\text{B.4})$$

Equations B.3 and B.4 show that the pressure gradient that is unknown is dependent on the settling velocity of particles.

$$J_w = -J_s \quad (\text{B.5})$$

Equation B.5 is indicating that the flux of solids is minus the flux of water. This means that when the flux of solids is pointing downwards, the flux of water is in the opposite direction, pointing upwards to conserve mass.

$$J_s = \phi_s v_s \quad (\text{B.6})$$

$$J_w = (1 - \phi_s) v_w \quad (\text{B.7})$$

$$v_w = v_{w/s} + v_s \quad (\text{B.8})$$

By using the relations of equation B.5, B.6, B.7 and B.8, which assume conservation of flux, v_s can be related to $v_{w/s}$. This means that the flux of water flowing out is related to the velocity of which the particles are settling. By doing this, equation B.9 is created, which relates the velocity of the solids to the velocity of the water in the reference frame of the settling particles.

Combining equation B.9, B.3 and B.4 leads to equation B.10, which is also the "modified" version of the Darcy equation which describes the settling velocity of the particles due to a pressure gradient.

$$(1 - \phi_s) v_{w/s} = -v_s \quad (\text{B.9})$$

$$-v_s = -\frac{k}{\eta} \frac{\partial P_e}{\partial z} \quad (\text{B.10})$$

A definition for the pressure gradient needs to be found in the modified Darcy equation, which is related to the settling velocity of particles when looking at equation B.9 and B.10. Only hydrostatic pressure is occurring when the water is not moving. So when particles are settling and the water is moving, extra pressures are created. This is the excess pore pressure. This gradient of excess pore pressure is defined as the gradient of total pressure minus the gradient of hydrostatic pressure, as shown in equation B.11.

This excess pore pressure gradient is generated due to the settling velocity of the particles. The following interpretation can be used; the particles that settle due to gravity create an excess pore pressure gradient. This excess pore pressure gradient leads then to the flow of water in the opposite direction of the particles that settle. Due to the fact that the settling of particles is very slow, forces due to acceleration of the particles can be neglected.

$$\nabla P_e = \nabla P_w - \nabla P_{hyd} \quad (\text{B.11})$$

We can rewrite equation B.11 by using the relation between total stress, effective stress and total pressure as in equation B.12. This leads to equation B.13.

$$P_w = \sigma_{zz} - \sigma_{sk} \quad (\text{B.12})$$

$$\nabla P_e = \nabla(\sigma_{zz} - \sigma_{sk}) - \nabla P_{hyd} \quad (\text{B.13})$$

Consolidation is assumed to be slow and we have nearly hydrostatic pressure. This means that the estimation for the total stress at height z can be approximated by the weight of water plus the weight of the solids at height z .

$$d\sigma_{zz}(z) = -[(1 - \phi_s(z))\rho_w + \phi_s(z)\rho_s]g dz \quad (\text{B.14})$$

Substituting this estimation for the total stress in equation B.13 leads an expression for excess pore pressure gradient as shown in equation B.15.

$$\frac{\partial P_e}{\partial z} = \frac{\partial \sigma_{sk}}{\partial z} + (\rho_s - \rho_w)g\phi_s \quad (\text{B.15})$$

The excess pore pressure that is defined here leads to the outflow of water from the soil body while the particles are settling slowly. This pressure gradient is considered to be the driving force in the Darcy equation B.4.

Combining continuity, Darcy, and the expression for the excess pore pressure leads to the Gibson equation as shown below in equation B.16. This is basically an advection-diffusion equation.

$$\frac{\partial \phi_s}{\partial t} = \frac{\partial}{\partial z} \left(K \frac{(\rho_s - \rho_w)}{\rho_w} \phi_s^2 + \frac{K}{g\rho_w} \phi_s \frac{\partial \sigma_{sk}}{\partial z} \right) \quad (\text{B.16})$$

The Gibson equation estimates the vertical distribution of volume fraction of solids over time. This is dependent on the hydraulic conductivity K , and the vertical effective stress σ_{eff} . Both of these parameters are non-linear in the context of large strain consolidation and depend both on the volume fraction of solids that exist in the control volume that is considered. This is elaborated on in the next section of constitutive relations.

The Gibson equation represented in equation B.16 is based on a Eulerian reference frame, where an estimation is made on the volume solid fraction in a fixed control volume based on inflow and outflow. The Lagrangian approach follows a particle through space and time, instead of a fixed location in space when using Eulerian reference frame. The utilization of a Lagrangian reference frame is convenient because the upper boundary of the consolidating soil layer is followed over time. This makes it possible to propose boundary conditions on top of the consolidating layer. The Lagrangian version of the Gibson equation is shown in equation B.17.

$$\frac{d\phi_s}{dt} = \phi_s \frac{\partial}{\partial z} \left(\frac{k}{\eta} (\rho_s - \rho_w)g\phi_s + \frac{k}{\eta} \frac{\partial \sigma_{sk}}{\partial z} \right) \quad (\text{B.17})$$

Calibration

Material properties such as permeability k and compressibility σ_{sk} change based on the volume fraction of solids. One can imagine that permeability does depend on volume fraction of solids. If the volume fraction of solids somewhere in the column is low, big void spaces should be present where the water can permeate through, which corresponds with high permeability. If the volume fraction of solids is high, small amount of pores exist where water can permeate through, which corresponds with low permeability. The same is the case with compressibility. A very compacted soil will have high inter particle forces due to the high packing density of the individual soil particles. In this context, the effective stress between particles will be high when the soil is highly compacted at high volume fractions of solids. The effective stress will be lower for low compacted soils at low volume fraction of solids, so less pressure is applied between the individual soil particles. Another way of thinking is that the more compact the

soil particles are, the higher effective stress is needed for further compaction. This illustrates that the absolute value of effective stress depends on the volume fraction of the solids. Compressibility and permeability are not constant over space and time because the volume fraction of solids is changing significantly, due to high volume changes of particles as a result of consolidation. The relations between permeability and compressibility and the volume fraction of solids are called ‘constitutive relations’.

The constitutive relations are an input of the Gibson equation as it needs an expression for k and σ_{sk} at different volume fractions of solids. These constitutive relations need to be ‘captured’ by lab tests. There are a lot of tests available to capture the constitutive relations and most of them are reviewed by Ahmed et al. (2023).

The constitutive relations are fitted with exponential power laws. An example of calibrated power-laws is shown in Figure B.7. These power-laws describe permeability and effective stresses at different volume fraction of solids. The non-linearities are distinct in this figure. The values in the graphs are intuitive as permeability decreases heavily when the volume fraction of solids is high and the particles are more compacted. Effective stresses increase when volume fraction of solids are high, which is intuitive. Higher inter-particle forces occur when the packing density of these particles is higher.

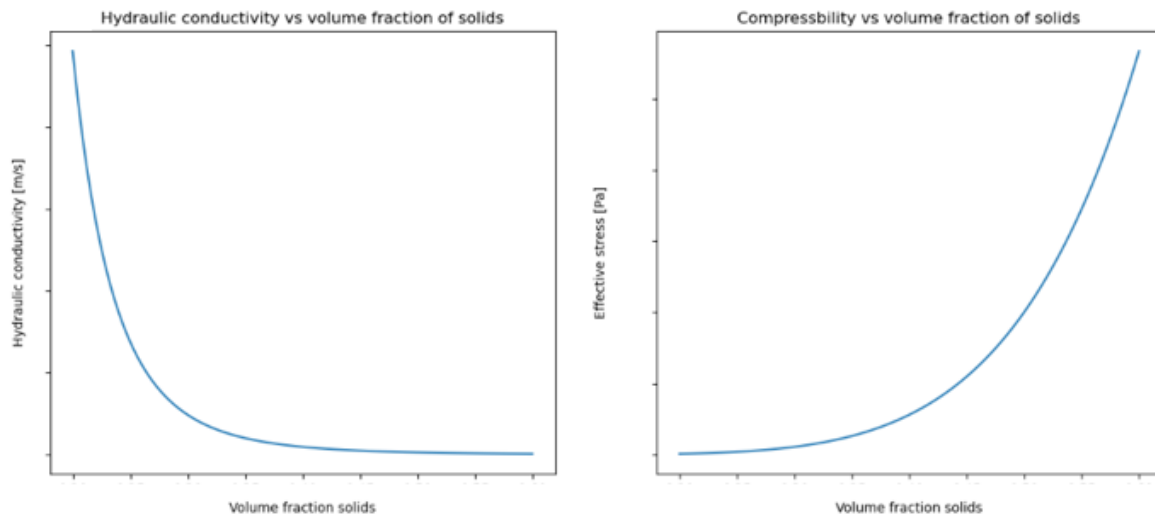


Figure B.7: Constitutive relations from Merckelbach fitting from NMR data

In literature, several expressions exist for obtaining the power-laws. This thesis uses the expressions of Merckelbach (2000) for the power-law estimations, as this method is proven to establish reliable results in combination with NMR calibration (Chassagne, 2021) Myouri (In prep). This thesis will explore the calibration options by using state-of-the-art Nuclear Magnetic Resonance tests and the ‘Analytical Solution’ method based on the Merckelbach / Gibson theories. Another empirical method for estimating the constitutive relations based on index properties of Carrier and Beckman (1984) is tested as well.

Merckelbach

Merckelbach proposes a physical theory on the constitutive relation characteristics, called the fractal approach. This theory justifies power laws that can be fitted for permeability and compressibility by lab tests to get a formulation of the constitutive relations. These power laws are shown in equation B.18 and B.19. Once the power-laws are obtained, they can be applicable to various initial densities and initial heights in consolidation simulations.

$$\sigma_{sk}(z, t) = K_{\sigma}[\phi_s(z, t)]^n - K_{\sigma_0} \quad (\text{B.18})$$

$$K(z, t) = K_k[\phi_s(z, t)]^{-n} \quad (\text{B.19})$$

$$n = \frac{2}{3 - D} \quad (\text{B.20})$$

Where K_σ , K_{σ_0} , and n are parameters that are fitted to the experimental data. The work of Merckelbach (2000) and Chassagne (2021) is referred to if the reader of this document wants more details of the fractal approach theory in context of large strain consolidation.

The constitutive relations of Merckelbach can be captured by performing lab tests (NMR) and can be obtained by the analytical solution of the Gibson equation.

Nuclear Magnetic Resonance (NMR)

NMR is a test which can be used to measure water content of the material in the settling column. This water content inside the pores of the solids can be measured by making the settling column prone to a magnetic field. The water content fraction ϕ_w and also density can be measured by molecular spinning of water molecules when prone to a magnetic field. From this method, density profiles can be obtained along the height of the settling column over time. The constitutive relations can be found by fitting the NMR data. Compressibility (K_σ for Merckelbach) is fitted on the final profile of consolidation data. Permeability (K_k for Merckelbach) is defined by a back calculation, fitting the water/suspension interface over time with the Gibson model. Hence, permeability and compressibility are not directly measured for every volume fraction of solids. These parameters follow from the density profiles obtained by the NMR.

The constitutive relations that are extracted from the NMR samples can be used afterwards by the Gibson model for scaled up problems. The samples from the NMR work for bigger column heights and for different initial concentrations.

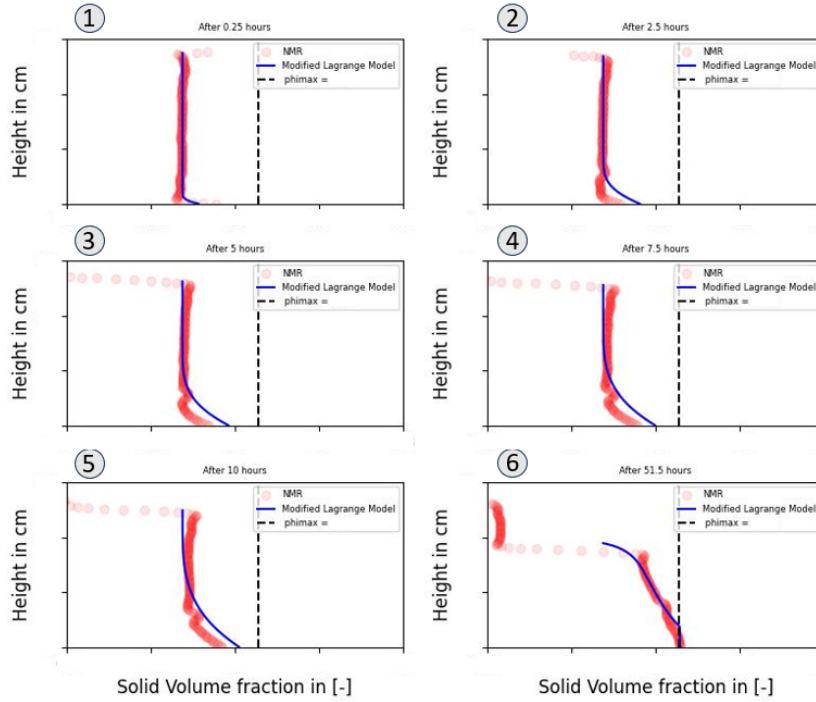


Figure B.8: Gibson equation fitted to density profile data obtained by Nuclear Magnetic Resonance (NMR) calibration

The calibration parameters found for the sample tested used in the case-study of this thesis is summarized in Table B.1.

Analytical Solution

The second method is based on the theory of Merckelbach (2000) and derivation in the book of Chassagne (2021). For calibration based on the analytical solution, data on the slurry / water interface height

Table B.1: Scandinavia material: NMR calibration parameters

Parameter	Value
K_k	5.0e-10
n	2.65
K_σ	2.1e+04
ϕ_{\max}	0.456

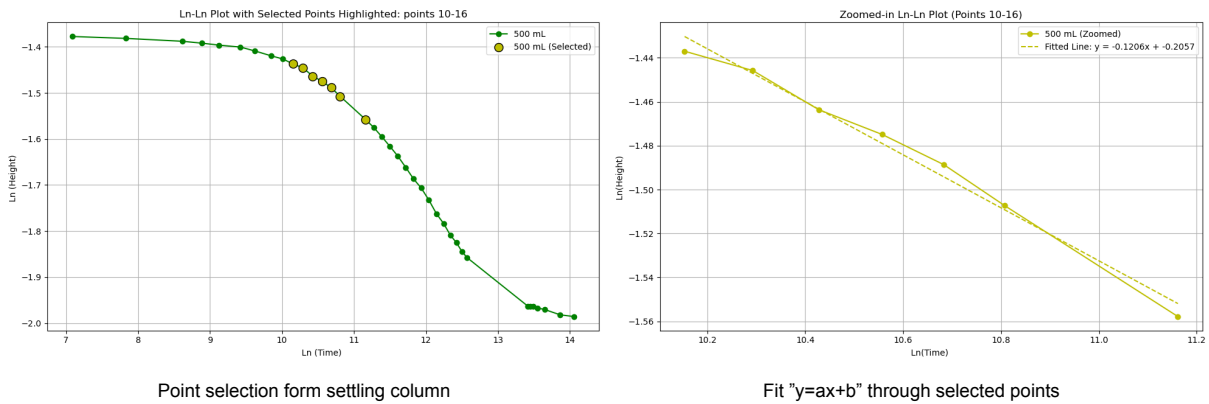
evolution in time needs to be measured from a settling column. These measurements in combination with analytical solutions for the Gibson equation are used to estimate the power-law constants K_σ and K_k . These power-law constants are the input parameters of the power laws that are used to describe the constitutive relations in the work of Merckelbach (2000).

The analytical solution can be obtained under the assumption that $\frac{\partial \sigma_{sk}}{\partial z} = 0$. This assumption reduces the Gibson equation of expression B.16 to the expression in equation B.21.

$$\frac{\partial \phi_s}{\partial t} = K_k \cdot \frac{\rho_s - \rho_w}{\rho_w} \cdot (2 - n) \cdot \phi_s^{1-n} \cdot \frac{\partial \phi_s}{\partial z} \quad (\text{B.21})$$

The method of characteristics can be utilized to reduce the expression to B.22. This expression contains the height evolution depending on the initial height, initial volume fraction of solids, n , permeability coefficient K_k and time. The transient slurry / water interface settling column data can be fitted to a linear line in the form of $y = ax + b$, by applying Ln-Ln scaling to this expression. Linear parts in the Ln-Ln plot can be fitted and used for estimating K_k and n .

$$\ln(h(t)) = \ln \left(\left(\phi_0 \cdot H \cdot \frac{2 - n}{1 - n} \right) \cdot \left(K_k \cdot \frac{\rho_s - \rho_w}{\rho_w} \cdot (n - 2) \right)^{\frac{1}{2-n}} \right) + \frac{1}{2 - n} \cdot \ln(t) \quad (\text{B.22})$$

**Figure B.9:** Calibration of numerical Gibson solution: point selection and fitting method

After obtaining the expression of K_k and n , only the expression for K_σ is left to be determined. This parameter can be found based on the end height of consolidation by using the value for n and equation B.23. Combining these expressions will result in a equation with only one unknown, K_σ .

$$h_\infty = \frac{n}{n - 1} \cdot \phi_0 \cdot H \cdot \left(\frac{K_\sigma}{(\rho_s - \rho_w) \cdot g \cdot \phi_0 \cdot H} \right)^{\frac{1}{n}} \quad (\text{B.23})$$

Hence, neglecting the term of K_σ to obtain K_k in equation B.22 and then estimating K_σ based on these parameters does **not** comply with the physical and mathematical rules in this derivation. However, it is a method to obtain a first estimate of the Merckelbach power-law constants from only the data obtained from a settling column.

Carrier & Beckham

Carrier and Beckman (1984) propose other power laws to capture the constitutive relations. The Carrier & Beckham method proposes a relation between engineering properties of clays and index properties. For the relations between effective stress and void ratio, 98 samples are used coming from Oedometer, Consolidometer tests and field measurements consisting of dredged materials and remoulded clays. This data is extracted from all kinds of papers that are published in the past. This makes this method of obtaining the constitutive relations highly empirical. Carrier and Beckman (1984) proposes the following relations:

$$e = \alpha \left(\frac{\sigma_{sk}}{P_{atm}} \right)^{\beta} + \epsilon \quad (B.24)$$

Where:

- $\alpha = 0.0208 \cdot (PI) [1.192 + (\text{act})^{-1}]$
- $\beta = -0.143$
- $\epsilon = 0.027 \cdot (PL) - 0.0133 \cdot (PI) [1.192 + (\text{act})^{-1}]$

The proposed relation and its empirical parameters, depend on void ratio, plastic index (PI), plastic limit (PL) and the activity (act) of clay. Activity is defined as the plasticity index (PI) divided by the percentage of clay fraction (fraction of material under 2 micron). This relation can be used to estimate the properties of normally consolidated natural clays and of dredged materials & mining waste, which are hydraulically disposed in a fill.

For the relation between permeability and void ratio 61 samples are used from Constant Head Different test, Oedometer tests (back calculations), numerical solutions (back calculations) consisting of dredged materials and remoulded clays. Carrier & Beckham propose the following relation:

$$k = \mu \frac{(e - \delta)^v}{1 + e} \quad (B.25)$$

Where:

- $\mu = \left(\frac{0.389}{PI} \right)^{4.29}$
- $\delta = 0.027 \cdot (PL - 0.242 \cdot PI)$
- $v = 4.29$

The proposed relation and its empirical parameters depend on void ratio, plastic index (PI) and plastic limit (PL). The permeability model proposed by Carrier and Beckman (1984) is stated to be reliable between permeability values of 10^{-10} and 10^{-5} . This method determining constitutive relations of slurries by index properties is already used by other dredging companies.

Validation

The proposed calibration strategies are used to study their reliability for estimating the interface of a settling column of 500 mL. This settling column analysis is performed in the Geo-Lab of Deltares. For calibration and the settling column, the physical material of the Scandinavia is used. Lab tests are performed to estimate the index properties of the sample in the Geotechnical lab of Delft University of Technology.

B.3.2. Small-Strain consolidation

The derivation of the Terzaghi consolidation model is based on the explanation of Verruijt (2012). The derivation of the Terzaghi model comes with assumptions. The most important assumptions are listed below.

- Soil is saturated
- Darcy's law of flow through a soil body is valid
- Constant permeability and volume compressibility (small strains)

- Incompressibility of soil and water
- Consolidation and water flow is 1D vertical
- Total stress is applied instantaneously and is constant over time

Equation B.26 represents the strain of a volume of soil. Strain represents the change in height of a soil element over its original initial length. Strain is also related to the coefficient of compressibility m_v of the soil and the effective stress σ' , because excess pore water pressure p will flow out of the soil due to the total stress σ that is applied. Eventually, all the load is carried by the soil skeleton, the effective stress.

$$\epsilon = -m_v \sigma' \quad (\text{B.26})$$

Strain can be rewritten in terms of total stress and excess pore water pressure by substituting equation B.27 in equation B.26, leading to equation B.28.

$$\sigma' = \sigma - p \quad (\text{B.27})$$

$$\epsilon = -m_v (\sigma - p) \quad (\text{B.28})$$

Lets consider a soil body of volume V , visualized in Figure B.10. Particles and water are considered to be incompressible. Volume changes of this soil body can occur via the vertical outflow q_z of water from the soil.

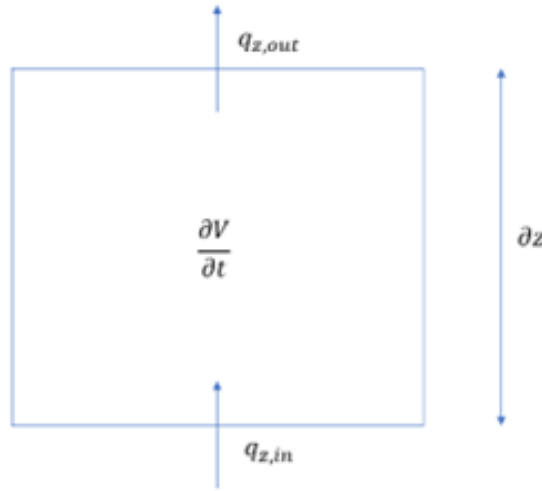


Figure B.10: Continuity of soil body: vertical flow of water

Continuity is represented in equation B.29.

$$\Delta V = - \left(\frac{\partial q_z}{\partial z} \right) V \Delta t \quad (\text{B.29})$$

The strain will therefore be proportional to the change in the change in volume due to outflow of water. This represented in equation (B.30).

$$\Delta \epsilon_{vol} = \frac{\Delta V}{V} = - \left(\frac{\partial q_z}{\partial z} \right) \Delta t \quad (\text{B.30})$$

Equation (B.30) can be rewritten into equation (B.31).

$$\frac{\partial \epsilon_{vol}}{\partial t} = - \frac{\partial q_z}{\partial z} \quad (\text{B.31})$$

$$q_z = -\frac{k}{\gamma_w} \frac{\partial p}{\partial z} \quad (\text{B.32})$$

Equation (B.32) is known as the Darcy equation. This equation represents the outflow of water based on a pressure gradient and a constant permeability ability k of the soil. When substituting equation (B.28) and (B.32) into equation (B.31) gives equation (B.33). Equation (B.33) represents the volume change based on the outflow of water and the total stress gradient.

$$\frac{\partial p}{\partial t} = \frac{\partial \sigma}{\partial t} + \frac{k}{\gamma_w m_v} \frac{\partial^2 p}{\partial z^2} \quad (\text{B.33})$$

Assuming that the total stress is constant over time will change equation (B.33) into equation (B.34). This equation can be considered to be the Terzaghi small strain consolidation equation. The coefficient of consolidation, C_v , represents constant soil properties.

$$\frac{\partial p}{\partial t} = C_v \frac{\partial^2 p}{\partial z^2} \quad (\text{B.34})$$

Constitutive model

D-settlement uses approximations of constitutive models in combination with consolidation models of Terzaghi or Darcy. From the consolidation models, effective stresses per time-step are calculated. The constitutive models use these effective stresses to estimate the settling behaviour (Deltares, 2016), based on consolidation characteristics measured in the Oedometer. The constitutive model of NEN-Bjerrum describes the effects of primary settlements (outflow of water) and the settlements due to creep (deformations due to viscous behaviour of soil particles). The D-settlement manual of Deltares (2016) is referred to if the reader wants more extensive explanation of the constitutive model and its implications on settlement calculations. The classical small strain consolidation theory of Terzaghi is often used in combination with a constitutive model to explain primary settlements due to drainage of excess pore pressure and secondary settlements due to creep.

NEN-Bjerrum is based on the Creep-Isotache pattern. This model uses a linear strain assumption to estimate parameters as $RR/CR/C_a$. The NEN-Bjerrum model is most suited when considering cases of loading and unloading (*D-Settlement manual*, 2016). This model distinguishes between primary settlements Δh_{prim} and a creep contribution Δh_{sec} . This model is appropriate if one wants a good prediction for long-term settlements including creep.

For drained conditions, three main contributions exist.

$$\frac{\Delta h_{prim}}{h_0} = RR \cdot \log \left(\frac{\sigma'}{\sigma'_0} \right) \quad (\text{B.35})$$

$$\frac{\Delta h_{prim}}{h_0} = RR \cdot \log \left(\frac{\sigma'_p}{\sigma'_0} \right) + CR \cdot \log \left(\frac{\sigma'}{\sigma'_p} \right) \quad (\text{B.36})$$

$$\frac{\Delta h_{sec}}{h_0} = C_a \cdot \log \left(\frac{t}{t_0} \right) \quad (\text{B.37})$$

$$\Delta h_{total} = \Delta h_{prim} + \Delta h_{sec} \quad (\text{B.38})$$

Where CR is based on the compression index above the pre-consolidation pressure and the initial void ratio e_0 . RR is based on the reloading/reloading/swelling index below pre-consolidation pressure and the initial void ratio e_0 . Both can contribute to the primary settlements. The creep component includes a time-dependent effect which corresponds with the simulation time.

$$CR = \frac{C_c}{1 + e_0} \quad (\text{B.39})$$

$$RR = \frac{C_r}{1 + e_0} \quad (\text{B.40})$$

Coefficient C_c corresponds to the compressibility index. Coefficient C_r corresponds to the reloading index below pre-consolidation pressure, as indicated in Figure B.11. Coefficient C_a is defined as the secondary compression index. These coefficients are extracted from experimental data from the Oedometer. These parameters are used as the input of D-Settlement.

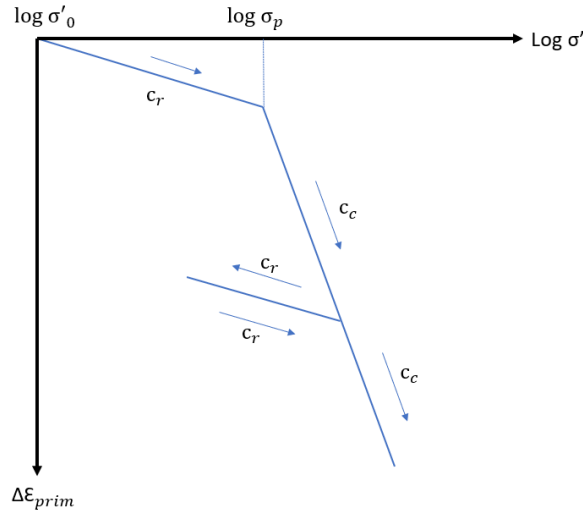


Figure B.11: NEN-Bjerrum method obtained from Deltares, 2016

Calibration

Calibration of the small strain Terzaghi model is often done based on experimental data coming from an Oedometer. In a Oedometer test, the deformation of soil under certain loading is captured by the relation between effective stress and vertical strain (Chassagne, 2021). A sample is placed in an Oedometer cell, where the sample is drained at the top and undrained at the bottom. Vertical load can be applied at the top of the sample and the water can drain from the top of the sample (Verruijt, 2012). By loading of the sample, the excess pore water pressure of the sample increases. This generated excess pore water pressure will drain from the sample, and the effective stress will go up, leading to compaction of the soil sample (consolidation). The sample is loaded in steps to measure the deformation behaviour at different loading steps over time. By doing this, experimental data is generated on the relation between effective stress and strain, but also on the relation between settlement and time.

From the Oedometer, data is generated according to Figure B.11. From these settlement over effective stress graph, parameters for NEN-Bjerrum constitutive models can be determined as well as the coefficient of consolidation C_v . For exact methods to extract this parameters from Oedometer data is referred to the work of Verruijt (2012).

The value for the coefficient of consolidation can be calculated from the constitutive powerlaws of Merckelbach (2000), according to the work of Chassagne (2021). This is shown in equation B.41.

$$C_v = n \cdot \frac{K_k \cdot K_\sigma}{g \cdot \rho_w} \quad (\text{B.41})$$

B.4. Design requirements

According to the hydraulic fill manual (Van 't Hoff and Van Der Kolff, 2012), several requirements are important when designing a land reclamation.

The reclamation should adhere to a certain bearing capacity and slope stability for bearing loads of the use-case of the clients. Slope stability requirements often only occur during the construction stage of the reclamation where slopes of placed material near the pipe outlet could occur. Slope stability also occurs at the containment bunds for containing the fill material in the reclamation. Instabilities can occur when the weight of the loading force of the soil body exceeds the shear strength of the sub-soil. This can occur when the soil is not consolidated yet and has not yet developed sufficient shear strength to bear the loads. For this thesis, the effect of bund stability and the fill material stability during construction are neglected.

Additionally, the reclamation should show not too much deformation under loading of the reclamation area by the client's use-case. Settlements are essential since these provide instabilities or failure of the facilities of the client. Furthermore, settlements must be taken into account in the design stage to be compensated for in order to achieve the design level after consolidation of the material. According to the hydraulic fill manual, settlements requirements are more pronounced when using "complex" materials due to their high deformation ability over a long period of time.

Finally, the reclamation area should be resistant against liquefaction effects. This design requirement of often more strict in earthquake areas. Liquefaction occurs when high excess pore water pressures are generated due to sudden or shearing of the soil body. The excess pore pressures created by the shearing can increase to the point where the effective stress in the soil drops to zero. This will cause the soil to lose its shear strength and behave like a fluid. As a result, the soil body liquefies and will fail. According to the hydraulic fill manual, liquefaction requirements are based on a high relative density for which the soil has major resistance against shearing. Another mitigation strategy may be increasing the drainage capacity of the soil.

Due to time-constraints, this thesis only considers the effect of settlements under loading conditions of the use-case of the client. The settlements requirements used for the case-study of this thesis are presented in Table B.2. It is necessary that within the duration available for application of ground improvement methods, the reclamation is pre-loaded and drained in order to comply with the pre-written settlements under the final Uniformly Distributed Load (UDL) set by the use-case of the client. This load is applied on top of the pavement layer of the reclamation at the moment of hand-over of the asset to the client. For this thesis, the quantity of pre-loading and PVD's required to remain within the design settlement requirements are determined by using small-strain consolidation model D-Settlement (Deltares, 2016).

Load condition	Requirement
75 kPa UDL	200 mm over 50 years

Table B.2: Settlement requirements under loading

Settlement value [mm]	Time
50	2 years
100	5 years
150	20 years
200	50 years

Table B.3: Settlement requirements

B.5. Ground improvement methods

Ground improvement methods (GIM) are used for accelerating the consolidation of the fill material. This is done by increasing the drainage capacity of fill material. Ground improvement methods can be used to increase permeability, density and shear strength of the fill material and to decrease excessive settlements during the reclamation life-cycle (Van 't Hoff and Van Der Kolff, 2012).

This section covers the main ground improvement methods according to the Hydraulic Fill Manual (Van 't Hoff and Van Der Kolff, 2012). Methods considered are surcharge and pre-fabricated vertical drains (PVD). Hence, ground improvement methods can only be used after capping by a crust when the fill is accessible to equipment.

Prefabricated vertical drains

Reclamations consisting of material with reduces permeability can take ages to drain the excess pore pressures. The long drainage times are due to the low permeability characteristics of the soil, but also due to the long drainage paths. Pre-fabricated vertical drains can be used to accelerate the drainage of low permeable material by reducing the drainage path (Van 't Hoff and Van Der Kolff, 2012). PVD's create a reduction of the drainage path since water takes the shortest path through a porous medium from high pressure to low pressure area's. This principle is illustrated in Figure B.12. This method significantly increases the rate of consolidation, and therefore settlements and shear strength of the material in the fill.

PVD's are made of high permeable material and can be made form of plastics or sand columns and can reach up to 60 meters deep. It is evident that the drains need to be connected with a high permeable medium to enhance the draining from PVD tubes or sand columns. The drains are often placed with a triangular grid with grid spacing of 1 to 3 meters (Van 't Hoff and Van Der Kolff, 2012). This means that drainage path can be reduced to 1.5 meters, instead of over the whole height of the filled material.

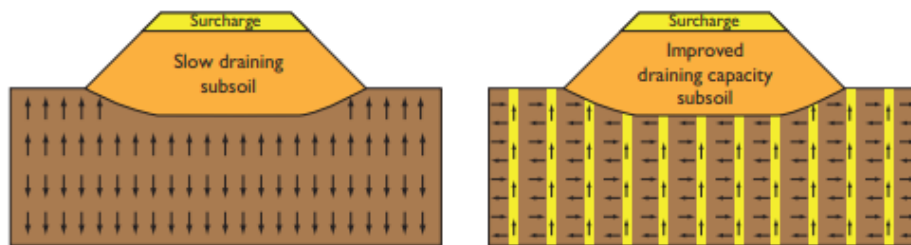


Figure B.12: Effect of Pre-fabricated vertical drains (PVD), obtained from Van 't Hoff and Van Der Kolff, 2012

In this thesis, the PVD's are placed in triangular setup with equal center-to-center distance. The center-to-center distance will differ for each case, depending on the time available to drain. Shorter available drainage times will require shorter center-to-center distance to further shorten the drainage path. Center-to-center distances are often minimal 1.2 meters, due to practical placement constraints. The global triangular setup is illustrated in Figure B.13 A.

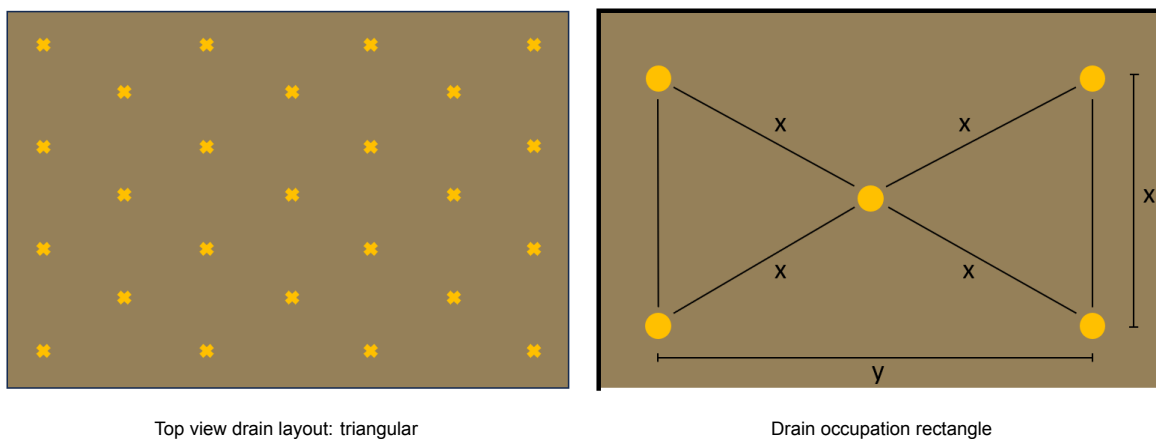


Figure B.13: Pre-fabricated Vertical Drain layout

A calculation approach can be proposed to calculate the total length of PVD's used across the whole

reclamation, based on a given center-to-center distance. The calculation is based on the surface area occupied by a rectangular formation of 5 drains, as illustrated in Figure B.13. The area occupied by 5 drains can be calculated according to equation B.42. Here the variable x is the center-to-center distance between the drains.

$$A_{\text{rectangular}} = y \cdot x = 2 \cdot \sqrt{x^2 - (0.5 \cdot x^2)} \cdot x \quad (\text{B.42})$$

The total amount of drains installed can be calculated by dividing the whole reclamation area by the rectangular drain area occupied by 5 drains. Next, the height of the fill over which the drain needs to span needs to be multiplied with the amount of drains needed across the whole reclamation area. This is how the total length of drains can be calculated and is shown in equation B.43.

$$L_{\text{PVD}} = \frac{A_{\text{reclamation}}}{A_{\text{PVD}}} \cdot H_{\text{fill}} \cdot 5 \quad (\text{B.43})$$

Surcharge

Applying surcharge to a fill is mostly done to directly enhance consolidation and indirectly enhance settlements (Van 't Hoff and Van Der Kolff, 2012). Using surcharge will lead to a sudden increase of total stress and excess pore pressure which increases the hydraulic gradient over the fill mass. This will enhance drainage capacities. Surcharge is often used in combination with PVD's to enhance consolidation.

Surcharge is a temporary load which is used to only enhance settlements. After the consolidation under the effect of surcharge, surcharge load is removed when a certain degree of compaction is achieved. The thickness of the surcharge can vary between 2 and 10 meters and mostly depends on the excess pressure that needs to be created in the fill layer underneath. Very low permeable fill material will need more surcharge to reach a certain compaction state than high permeable fill material.

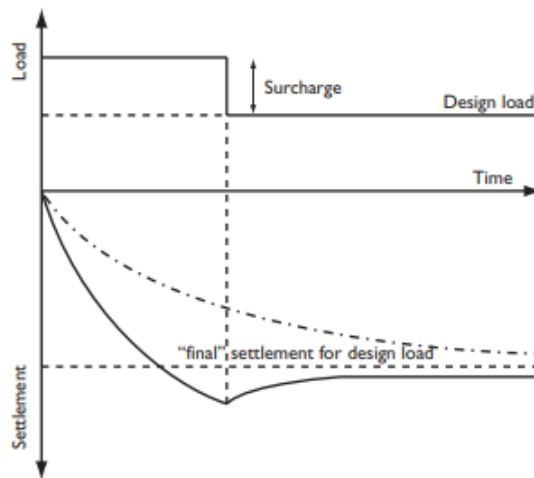


Figure B.14: Effect of surcharge over time, obtained from Van 't Hoff and Van Der Kolff, 2012

The amount of surcharge needed depends on the UDL load in the design requirements and the crust height. The quantity of material needed for surcharge can be calculated with equation B.44.

$$V_{\text{surcharge}} = A_{\text{reclamation}} \cdot (H_{\text{crust}} + H_{\text{surcharge}}) \quad (\text{B.44})$$

B.6. Costs

Costs coming in from PVD's and surcharge. Costs based on internal data of Van Oord (surcharge) and previous contracts with third parties for PVD installation.

ID	Method	Costs
1	Surcharge	<input type="text"/> [EUR/m ³]
2	PVD	<input type="text"/> [EUR/m]
3	PVD installation	<input type="text"/> [EUR]

Table B.4: Costs of ground improvement methods

The costs for surcharge can be calculated once the required surcharge volume and crust volumes are known. The costs for important sand can be calculated with equation B.45.

$$C_{\text{sand}} = \text{} \cdot V_{\text{surcharge}} \quad (\text{B.45})$$

The costs for PVD's can be calculated once the height is known of the fill material after self-weight consolidation. The costs can be calculated with equation B.46.

$$C_{\text{PVD}} = \text{} \cdot L_{\text{PVD}} + \text{} \quad (\text{B.46})$$

B.7. Large-Strain consolidation: numerical computations

For this thesis, a numerical solution to Gibson's large-strain theory is obtained from I.Myouri and C.Chassagne, called *Consoil*. The fundamentals of this code adhere to Gibson's theory of large-strain consolidation according to the derivation in this appendix. This section will cover the working principles and results that can be obtained from the numerical approach of Consoil in combination with the NMR calibration method. In addition, modifications needed for the consoil numerical method to be applicable for land reclamation construction are illustrated as well. Finally, the potential use-cases of the model are discussed.

Working principles of numerical method

The numerical approach received, simulates the large-strain consolidation of one homogeneous layer of slurry with an initial concentration over the height, C_0 . The initial profile converts from a homogeneous profile to a consolidated profile as illustrated from step 1 to 2 in Figure B.19. What can be observed are high deformations and the Gibsonian's consolidation profile. This profile consists of low concentrations (equivalent to the initial concentration) of solids on the top layer which is increasing non-linearly to high concentrations at the bottom of the column. This is convenient because the particles in the bottom layer carry more weight compared to the material on the top, resulting higher effective stresses and therefore more compaction after self-weight consolidation. The profiles corresponding from self-weight consolidation of a slurry and its corresponding density profile at the end of consolidation is shown in Figure B.15.

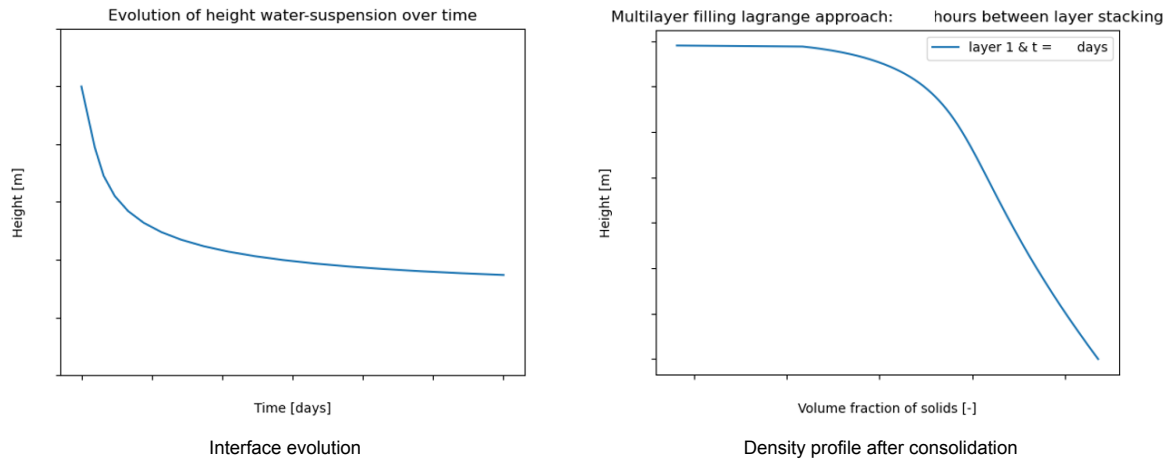


Figure B.15: Gibson consolidation of one layer

However, remarkable differences can be spotted when testing the material used in this thesis from **Scandinavia** using the Nuclear Magnetic Resonance (NMR) analysis for calibration. This material densifies according to Gibson's theory until it reaches a point where no densification takes place anymore under effect of the samples own weight. This is a remarkable observation which could indicate that the sample is only compacting up to a certain point where the particles can not continue compacting. This behaviour can be replicated by using Gibson's theory, imposing a maximum value of the volume fraction of solids that can be reached Myouri ([In prep](#)). This is demonstrated in Figure B.16.

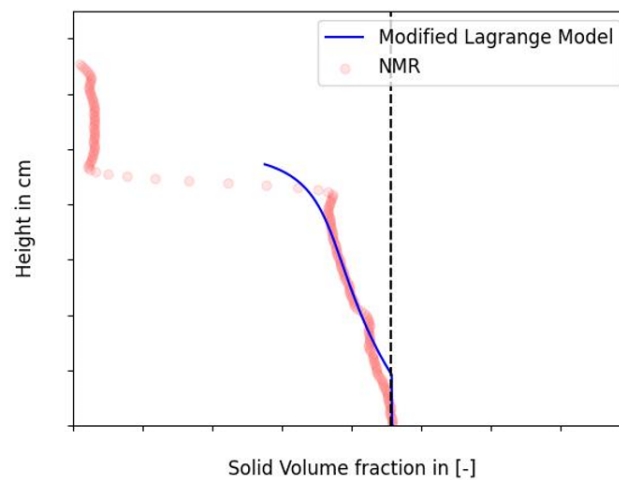


Figure B.16: Starting signs of maximum densification on lowest 2 cm observed from NMR during consolidation

This maximum densification behaviour can be numerically modelled by the "modified Gibson" approach Myouri ([In prep](#)). This numerical approach forces a maximum solid volume fraction in each cell. As a result, the behaviour of the sample observed by the NMR can be replicated with this method. This can be seen in the blue line at the bottom of Figure B.16. Simulating the consolidation behaviour including maximum densification with the modified Gibson approach is illustrated in Figure B.17.

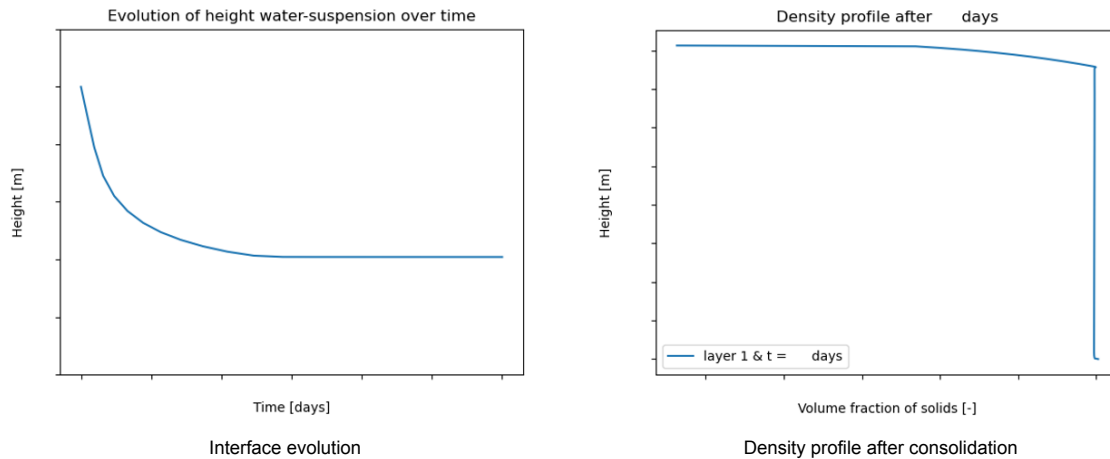


Figure B.17: Modified Gibson consolidation of one layer

The effects of the maximum densification behaviour demonstrated in Figure B.17 are distinct, compared to ordinary Gibson behaviour in Figure B.15. One can see here that the maximum densification profile is outconsolidated faster. This phenomena occurs because the bottom of the column has consolidated already to the maximum volume fraction on solids. Therefore, the part of the column that is at maximum densification is "shut-down" and does not consolidate further. As a result, the absolute settlements of the modified Gibson behaviour (59 cm) will be less compared to the profile of the ordinary Gibson behaviour (66 cm) where the bottom layers of the column can compact further than a maximum value.

Numerical modifications: layer stacking

The application of land reclamation construction can not be represented with one thick layer from which self-weight consolidation is starting after the filling stage. The numerical approach of the large-strain *Consoil* model (I.Myouri) is modified to make the numerical approach applicable to the construction of a land reclamation with layers stacking per unit of time.

The main modification is the introduction of transient layer stacking of layers. Including this application in the current numerical approach is performed in two stages. First the "freezed" layer approach was implemented, after which a "continuous" layer approach was implemented. This is illustrated in Figure B.18 A. In this figure, a clear difference can be observed between the two approaches. The "freezed" approach utilizes the principle of copying the large-strain behaviour of one layer over a certain timeframe. The result of this one-layer consolidation is stacked on top of each other. With this approach, the lower layers are "freezed" and no further self-weight consolidation occurs there, which results in **linear** increase of the water-suspension interface over time, as can be observed in Figure B.18 A.

In reality, every new layer places extra weight on the lower layers, which induces extra consolidation of the lower layers. This should make the freezing layer approach not completely fit-for-purpose. This approach can rather be seen as a first step in simulating the self-weight consolidation during the filling stages. A continuous approach, which includes the increased weight per unit of time on already existing material in the fill is suitable to be representable for the consolidation of the fill material over its complete height. The effects of the two approaches is illustrated in Figure B.18. Here, clearly the linear vs non-linear increase of water-suspension interface over time can be observed for the two approaches. Applying the continuous approach significantly increases the accuracy of the amount of material that is needed from Production.

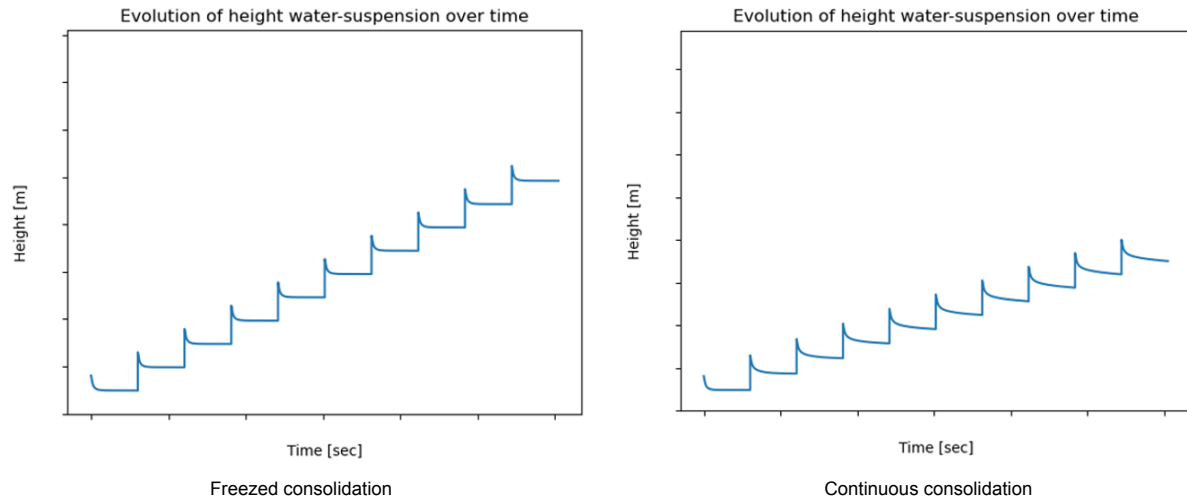


Figure B.18: Layer-stacking approach: Freezing layer stacking vs continuous layer stacking

The working principle of the "continuous" approach is illustrated in Figure B.19. First, a homogeneous layer is subjected to self-weight consolidation from step 1 to step 2. A new homogeneous layer is introduced on top of the already consolidated material between step 2 and step 3 and subjected to a new round of consolidation between step 3 and 4. This strategy obtains the continuous approach and is repeated until all the required layers are placed. All new layers introduced have equivalent height and concentration. The time-frame between two consecutive layer placements is controlled by duration for which Production can deliver the material. This will be different for different dredging work methods.

In the numerical code, this "continuous" process is applied by repeating the consolidation simulation for the amount of layers needed. After consolidation over the layer stacking duration, the final consolidation profile of the volume fraction of solids over height is obtained and a new homogeneous layer of the initial volume fraction of solids is added on top, adding again 1 meter of material to the existing body. This is the working principle behind the adjusted numerical approach (Figure B.19). This "continuous" approach is incorporated in the original numerical approach by repeating the consolidation simulation of 1 layer after the placement of every layer, including the profile of the volume fraction of solids of the last simulation with a new homogeneous layer on top as a input for the new simulation. The principle of continuous layer stacking is shown in Figure B.19. This is the basis behind the working principle of the adjusted numerical approach. In addition, the numerical approach includes the scaling of the simulation time-frames for the last layer, which enables the possibility to simulate a long time-frame for self-weight consolidation.

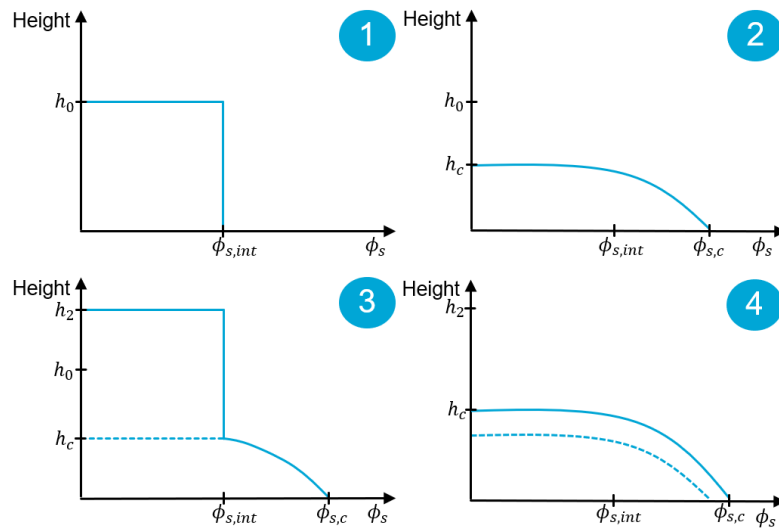


Figure B.19: Layer stacking approach

The density developments of the continuous layer approach are presented in Figure B.20. From this figure can be observed that the soil gets more dense at the bottom over time due to the ever growing weight on the bottom particles by new layers. This means that the bottom particles are getting more compressed after each layer increment over time. This process happens over the complete height. Rate of increase of volume fraction of solids at the bottom slows down over time. This is intuitive when taking the constitutive relations into account, which indicate an increase of effective stress and a decrease of permeability at higher volume fractions of solids. This slows down the consolidation process when the volume fraction of solids are getting high. The volume fraction of solids profile shifts to the right over the whole height when a new layer is placed. This process happens at the expense of profile height. This approach is consistent and conserves mass at all times in the numerical approach.

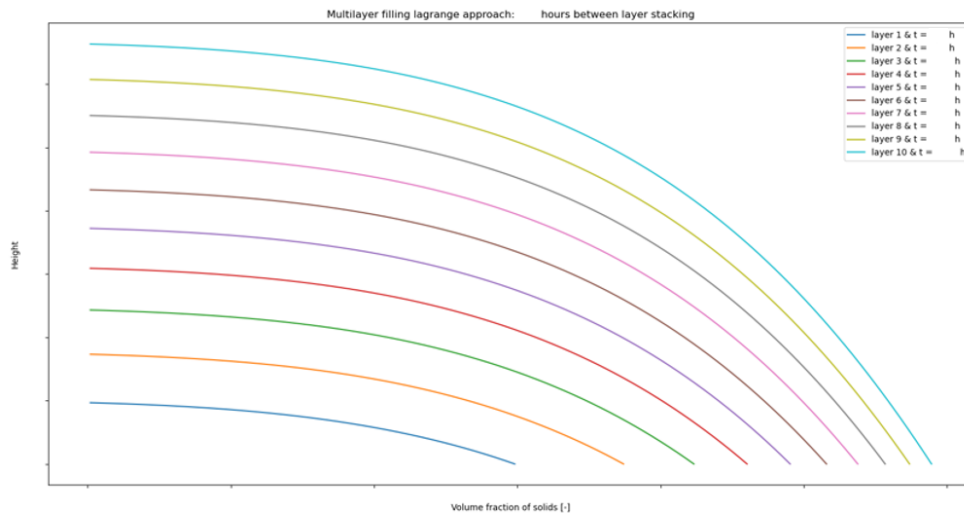


Figure B.20: Density profiles over time after consolidation with continuous consolidation layer stacking

Numerical modifications: adapted meshing

Scaling up simulations for large-scale land reclamation projects is a computationally intensive process, often requiring several days on a standard laptop. To accelerate the computation, an advanced meshing technique was implemented in combination with a numerical approach utilizing non-linear time-stepping. This method employs smaller time steps during the early stages of consolidation, where the rate of change is high, and progressively increases the time step as the consolidation rate decreases. By using advanced meshing, the time discretization is kept relatively low at the start of the computation and gradually increases as larger time steps are applied, maintaining an approximately constant absolute Δt . This technique significantly improved computational efficiency, reducing the simulation time for 80 layers of consolidation from several days to approximately one day.

Model use-cases

This adapted model could serve several use-cases in the process of estimating land reclamation developments:

- Estimation of amount of material needed from production.
- Estimation duration of filling until sufficient material is placed.
- Estimation of required bund height to contain all the filled material in the fill.
- Estimation on the soil property development under self-weight consolidation.

B.8. Small-Strain consolidation: numerical computations

The transfer between large-strain and small-strain models enables the application of ground improvement methods in the last stage of consolidation. Ground improvement methods in terms of surcharge and PVD's are considered in this thesis. The effects of external loading and PVD's on a soil body can be simulated by D-settlement, using Terzaghi's small strain consolidation theory.

In the small strain domain, several steps are required to prepare the asset for handover to the client. The construction process begins with the installation of the crust layer, followed by the temporary placement of the surcharge layer. Once the surcharge is removed, a pavement layer is installed, providing a foundation for the client to build upon. These steps are highlighted in Table B.5.

Step	Load	Density [kg/m3]	Duration [days]
1	Crust	1800	Design lifetime
2	Place surcharge	1800	30 days after crust placement
3	Strip surcharge	-1800	90 days before handover
4	Pavement	2200	Design lifetime + 45
5	UDL	75 kPa	Design lifetime

Table B.5: Loading steps in small strain domain based on expert judgement

The crust layer is installed to provide sufficient bearing capacity for equipment accessing the reclamation area. The required crust height is determined using Terzaghi's bearing capacity equation, specifically calculated for a PVD rig operating under undrained conditions. Undrained conditions are assumed because the equipment load is a short-term, dynamic load, during which the excess pore pressure generated by the weight cannot dissipate within the time the force is applied. The bearing capacity calculation is presented in equation B.47. These calculations are based on the specifications of a Hitachi EX 750 rig and are performed using software developed by Van Oord for crust height determination. Here, input parameters are the density and undrained shear strength of the fill material. In addition the density and friction angle of the sand crust are used as well as the water table level. In this calculation, punch through failure and shear failure are considered.

$$q_u = cN_{cs}d_c i_c + qN_{qs}d_q i_q + \frac{1}{2}\gamma BN_{\gamma}s_{\gamma}d_{\gamma}i_{\gamma} \quad (\text{B.47})$$

Where:

- q_u = ultimate bearing capacity [kPa]
- c = cohesion [kPa]
- q = overburden pressure [kPa]
- γ = unit weight of the soil [kN/m²]
- D_f = depth of the foundation [m]
- B = width of the foundation [m]
- N_c, N_q, N_γ = bearing capacity factors [-]
- s_c, s_q, s_γ = shape factors, adjusting for non-rectangular foundations
- d_c, d_q, d_γ = depth factors, accounting for the foundation depth
- i_c, i_q, i_γ = inclination factors, modifying for inclined loads

The input of the company software is provided in Table B.6 and Table B.7 below. These values are based on the data from the It can be seen that for a crust height H of 2 meters, the factors of safety for both single track and total width are above the recommended factor of safety of respectively 2.5 and 1.5. This means that a crust of 2 meters will provide enough bearing capacity for the Hitachi EX 750 rig to install the PVD's.

Table B.6: Capacity for reclamation - input

Input values soil properties	Symbol	Value
<input type="text"/>	<input type="text"/>	<input type="text"/>
<input type="text"/>	<input type="text"/>	<input type="text"/> m
<input type="text"/>	<input type="text"/>	<input type="text"/>
<input type="text"/>	<input type="text"/>	<input type="text"/>
<input type="text"/>	<input type="text"/>	<input type="text"/>
<input type="text"/>	<input type="text"/>	<input type="text"/>
<input type="text"/>	<input type="text"/>	<input type="text"/>
<input type="text"/>	<input type="text"/>	<input type="text"/>
<input type="text"/>	<input type="text"/>	<input type="text"/>

Table B.7: Capacity for reclamation - output

Output	Symbol	Value
<input type="text"/>	<input type="text"/>	<input type="text"/>
<input type="text"/>	<input type="text"/>	<input type="text"/>
<input type="text"/>	<input type="text"/>	<input type="text"/>
<input type="text"/>	<input type="text"/>	<input type="text"/>
<input type="text"/>	<input type="text"/>	<input type="text"/>
<input type="text"/>	<input type="text"/>	<input type="text"/>

The loading scheme over time is based on expert judgment input. The sand crust height is placed on top of the maximal densified material in the fill (the soft part is drained off). This happens when the filled material has consolidated until a soft layer exists on top which is equivalent to the calculated crust height. This is quantified as small strain day 0 ($t=0$). After day 0, the PVD's and surcharge are fully installed at day 30. The surcharge is stripped off after 30 - 60 days beyond installation, depending on the time available to finish the project. A pavement layer is placed 45 days before handover, to facilitate a rigid layer which can bear the facilities of the client. The absolute duration for which it is possible to use the surcharge determines the quantity of surcharge and PVD's needed to force the soil profile into its desired state, complying with the design requirements after handover.

The loading time-frame can be seen in Figure B.21 and its corresponding settlement can be seen in Figure B.22. Here, the first peak shows the crust height, corresponding to 2 meters of 18 kN/m². After 30 days the surcharge is placed on top of the crust which corresponds to a layer of 5.5 meters of 18 kN/m². After stripping off the surcharge, the pavement layer is placed, which is a 1 meter layer of 22 kN/m². After handover, the UDL design load is placed on top of the pavement layer, which is a load of 75 kPa. Under this load the long term settlements must remain within the design requirements.

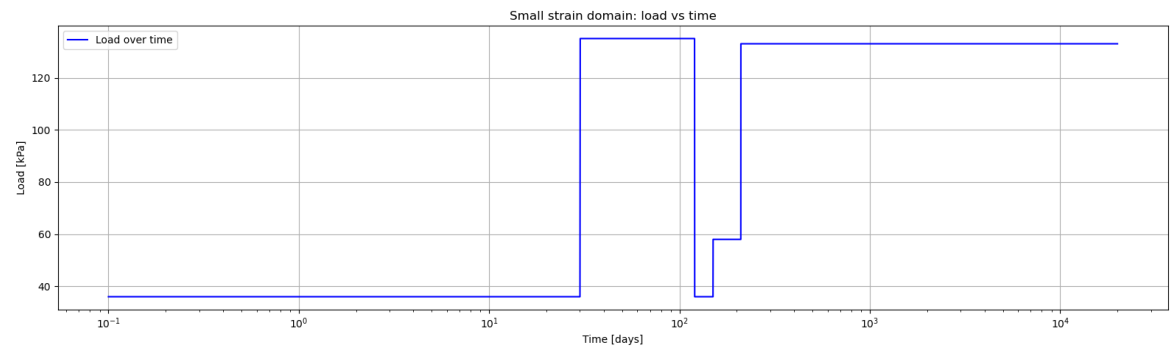


Figure B.21: Pre-loading steps in small strain domain

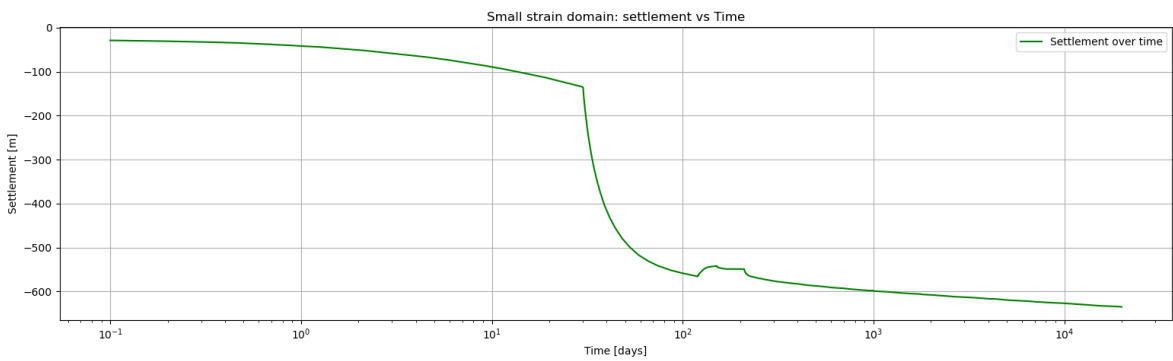
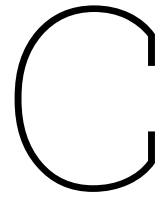


Figure B.22: Settlements due to pre-loading steps in small strain domain



Soil sample analysis

The aim of this appendix is to illustrate the laboratory experiments conducted on the physical samples received from the **Scandinavia** project. Laboratory studies are performed to provide input values for the calibration options and to evaluate the numerical solution in combination with a calibration method to settling column data based on physical material.

This section will first elaborate on the settling column tests performed, including numerical computations based on NMR. Next, the Attenberg limit tests that are performed are elaborated on. Furthermore, the Carrier & Beckham calibration method is analysed as well as the Analytical Solution method on the numerical outcomes of the large-strain consolidation.

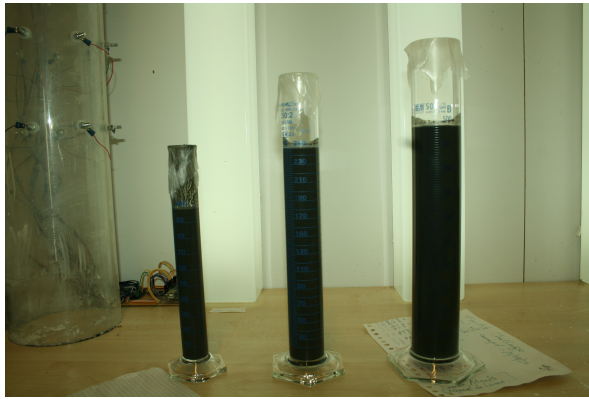
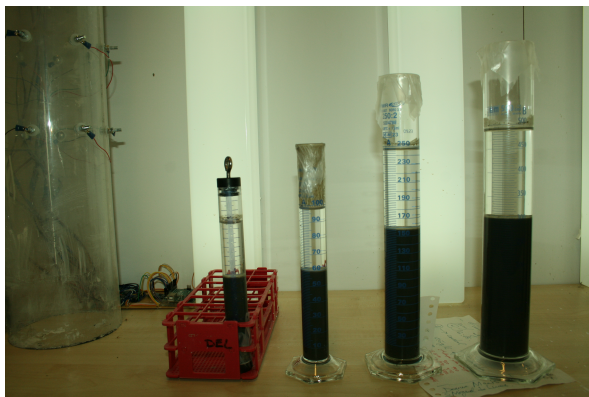
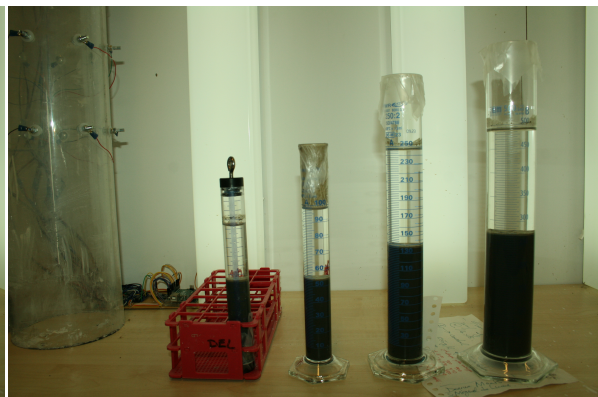
C.1. Laboratory experiments

For this thesis, settling column tests are performed to get insights into the real-life consolidation behaviour of the material received. Index tests are performed in the lab to obtain the Attenberg limits and the grain-size distribution which are a classification of the engineering properties of the soil samples received.

C.1.1. Settling column tests

Settling column tests are performed with a initial concentration of 660 g/L. The settling columns are left to settle for over 15 days. A high definition camera is capturing the settling columns at increasing time-interval steps. More pictures just after placement because a lot of interface changes are expected and less pictures at the end because less interface changes are expected. 4 settling columns can be spotted. The smallest, most left column is a replica of the settling column which is tested in the NMR. The other settling columns consists of volumes of 100, 250 and 500 mL, from left to right respectively.

A camera failure led to a hole in the data between day 4 and 8. This was over the weekend, so the problem was spotted after several days. The interface over time of the columns is plotted in Figure C.4.

 $t = 0$ hours $t = 6.7$ hours $t = 17.9$ hours $t = 39.9$ hours $t = 74.7$ hours $t = 202.5$ hours

The density starts with 1411 kg/m³ at time is zero. After which is consolidates to 1573 kg/m³ after 39.9 hours and finally ends up around 1736 kg/m³ after 202.5 hours. Between $t = 202.5$ and the end of the measurements at $t = 355.9$ hours, no severe changes have been observed. Therefore, this material consolidates quite quickly.

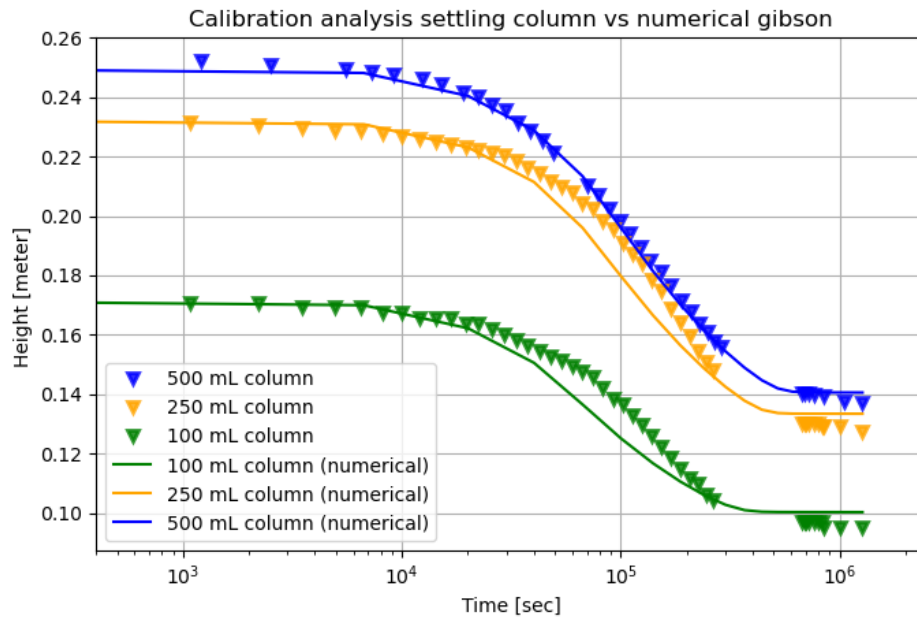


Figure C.4: Settling column data

From this plot can be seen that the fits of the 100 and 250 mL columns are less accurate. This can be explained by the fact that the calibration tube of the NMR started a minor leaking during measurements. K_σ and n are fitted on the last profile. However the fitting of K_k is based on the interface evolution. Since the NMR interface is losing mass, the interface might go down faster than in reality. Therefore, the estimation based on the NMR of K_k is less accurate.

Additionally, the determination of the density of the settling column was harder due to the leaks. The DMA35 density meter was used to aim for 1300 kg/m³ in the suspension prior to starting the settling columns. However the NMR showed that the density was way higher, around 1411 g/L. Therefore, it can be said that some errors between the settling column data can come from the fact that not every column started from the same initial density. The effects of the leakage on the 500 mL column is less visible.

Utilizing the NMR in a ordinary procedure, without losing mass due to leakage will result to a perfect fit most of the time. This is indicated in the work of Myouri ([In prep](#)).

C.1.2. Grain size distribution

The grain size distribution is measured from the physical sample of the Scandinavia project in figure C.5. It was found that the grain-size of 8.06% was under 2 micron, which corresponds to clay. 74.41% of the grain-sizes were between 2 and 63 micron and correspond to silt. 17.53 % was found to be above 63 micron and corresponds to sandy material.

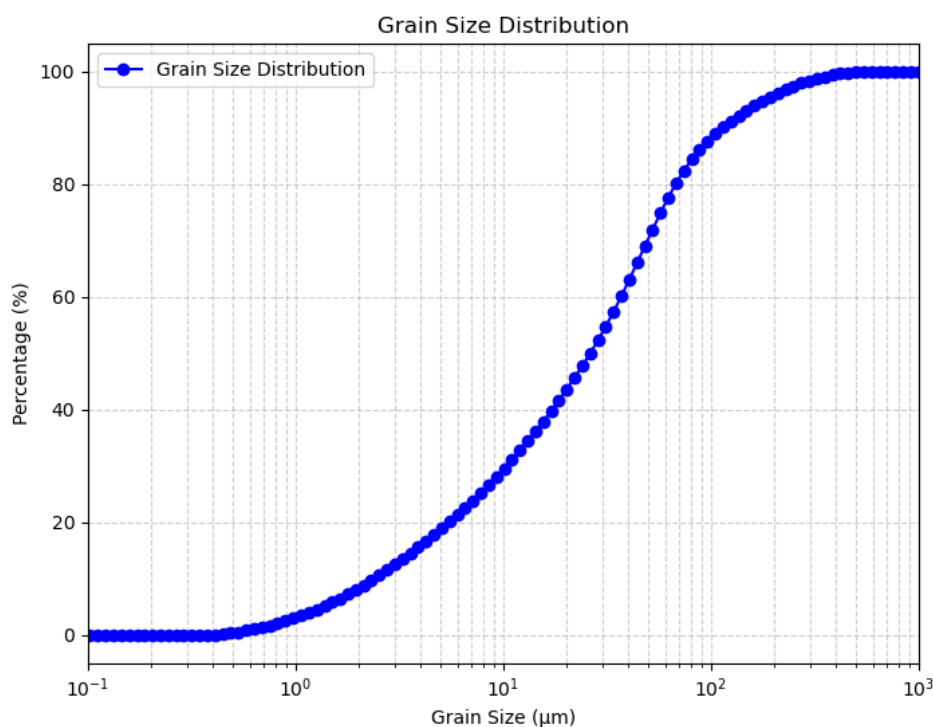


Figure C.5: Grain-size distribution physical sample

C.1.3. Attenberg limits

The liquid limit and the plastic limit of the material is tested to obtain the input parameters of the Carrier & Beckham calibration method.

The liquid limit is obtained with a Cone Penetrometer. The material is first air-dried after it is re-wetted. The Cone Penetrometer is used to obtain a range of penetrations around the 20 mm mark, in this case ranging from 16 mm of penetration and 24. After each sample is penetrated, it is put in the oven to determine its correspondent moisture content. The liquid limit is obtained as the value for which the cone penetrates the material exactly 20 mm. This value is obtained by using a linear fit through data points as shown in Figure C.8.

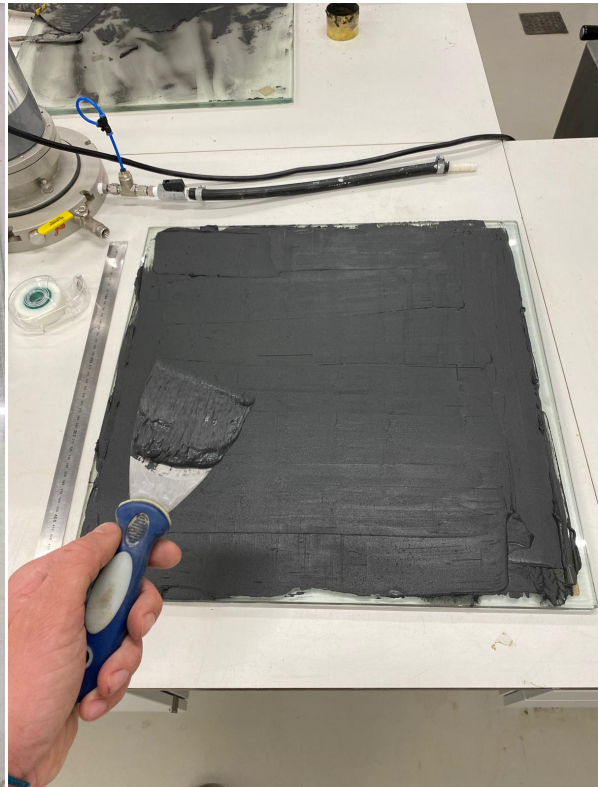
The plastic limit is obtained with manually with rolling of material between the fingers. The reaches its plastic limit when it crumbles due to the rolling between the fingers. Then enough moisture has drained the material that is crumbles. This samples are dried and the corresponding moisture content is determined which corresponds to the crumbling. This data ended up with ranged between a moisture content of 17% to 24 %, with an average of 20 %.

The Attenberg limits obtained from the laboratory are:

- Plastic Index = 20%
- Liquid Limit = 39.2%



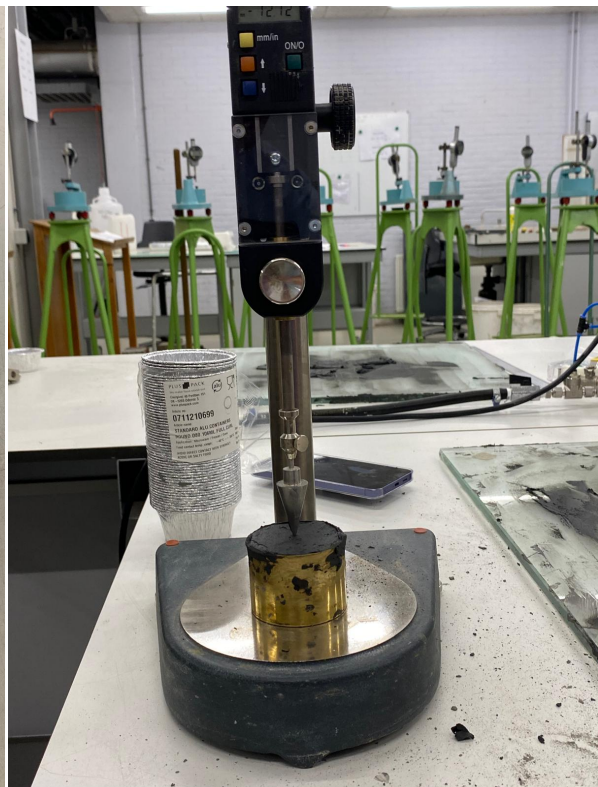
Scandinavia material dry



Scandinavia material wetted



Scandinavia material plastic limit test



Scandinavia material liquid limit test

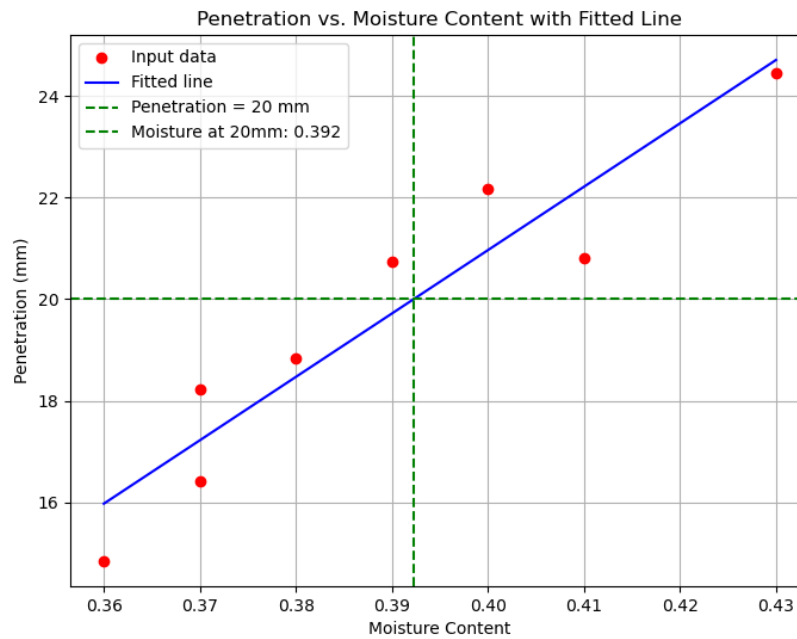


Figure C.8: Liquid limit determination

C.2. Calibration tests

C.2.1. Carrier & Beckham calibration

As explained in Appendix B, the Carrier & Beckham method is calibrated with the Attenberg limits and the activity of the material obtained from laboratory tests. The activity can be determined as the plastic index divided by the fraction of the soil sample smaller than 2 micron and can be calculated according to equation C.1 (Carrier and Beckman, 1984).

$$\text{Activity} = \frac{\text{Plasticity Index}}{\text{Fraction smaller than } 2\mu\text{m}} \quad (\text{C.1})$$

The results are compared to the settling column data of 500 mL based on the physical sample received. From Table C.1 can be spotted that the Root Mean Squared Error (RMSE) is high for the index properties. This is confirmed by Figure C.9, where it can be seen that the Carrier & Beckham fit is not giving reliable results and underestimates consolidation behaviour significantly. The numerical result based on the index properties of the bulk material tested in the Scandinavia project is overestimating the consolidation behaviour.

Due to the high uncertainty that comes with determination of the Attenberg limits in the laboratory, it is decided to perform a analysis whether to see if the Carrier & Beckham method is able to obtain a good fit based on varying values of plastic limit and liquid limit. This analysis is performed in Table C.1. Eleven combinations are evaluated by its root mean squared error compared to the settling column data.

According to Table C.1 and Figure C.9, a good fit of the settling column data can be obtained. This is obtained for a plastic limit of 13% and a liquid limit of 32%.

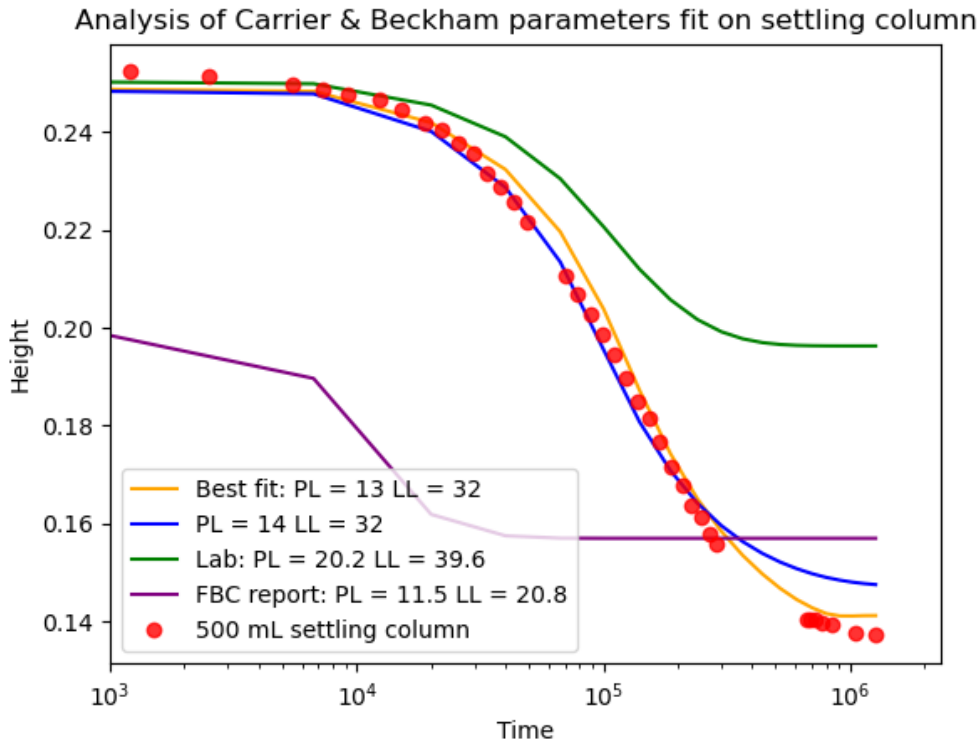


Figure C.9: Carrier & Beckham fit to settling column 500 mL.

Index	Plastic limit [%]	Liquid limit [%]	Plasticity index [%]	Activity [-]	RMSE
1	10	20	10	1.240	0.03806
2	12	26	14	1.736	0.02161
3	13	32	19	2.357	0.00313
4	14	26	12	1.488	0.02801
5	14	32	18	2.233	0.00615
6	14	36	22	2.729	0.01876
7	18	32	14	1.736	0.04053
8	18	40	22	2.729	0.03289
9	22	26	4	0.496	0.08724
10	22	36	14	1.736	0.06237
11	22	40	18	2.233	0.05370
12 (Lab)	20.2	39.6	19.4	2.406	0.04236
13 (FBC report)	11.5	20.8	9.3	1.154	0.03384

Table C.1: Carrier & Beckham constitutive relation analysis

C.2.2. Analytical solution calibration

As explained in Appendix B, the Analytical Solution method can calibrate the constitutive relations based on only settling column data. Several sets of points of the settling column data are fitted with a linear line to obtain K_k and n . The final height of the column is then used together with K_k and n to obtain the parameter for K_σ . With these Merckelbach (2000) coefficients, the power-laws corresponding to the constitutive relations can be obtained.

For every set of points, the numerical solution is computed and compared to the settling column data of the physical sample. Three fits are presented in Figure C.10 and Figure C.11. Their corresponding power-law coefficients are presented in Table C.2. From every fit can be observed that the initial stage

of consolidation is over-estimated, while the later stage of consolidation is predicted more accurately. This can be due to the fact that the settling column initial concentration is high whereas the assumption of $K_\sigma = 0$ is not valid.

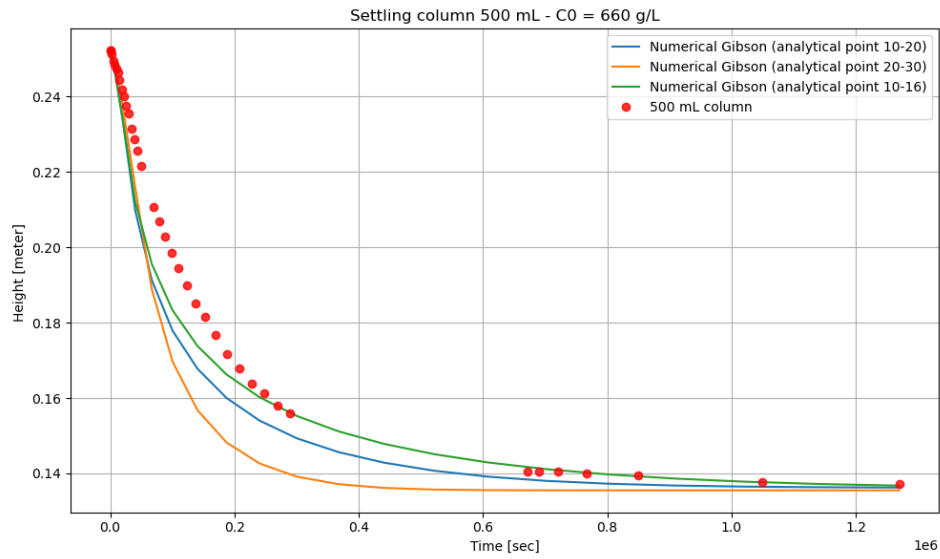


Figure C.10: Calibration of numerical Gibson model: Linear scale

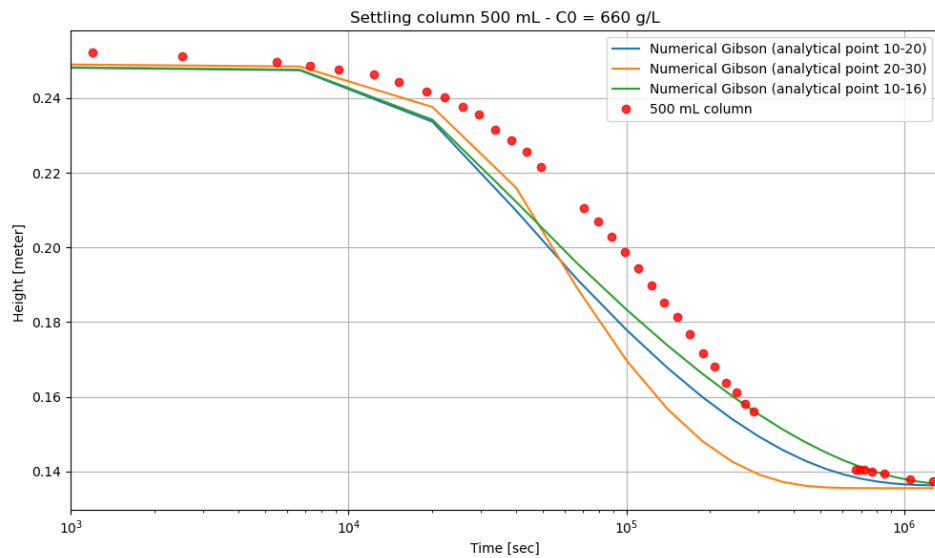


Figure C.11: Calibration of numerical Gibson model: Log scale

Selected points	K_k	K_σ	n	D_f
10-16	2.3287e-14	2.0784e07	10.29	2.806
10-20	1.6981e-13	6.1634e06	9.19	2.783
20-30	2.5159e-11	2.3944e05	6.28	2.682

Table C.2: Analytical solution parameters obtained from point selection

C.3. Discussion: calibration method testing

One of objectives of this thesis is to analyse the calibration method of the large-strain consolidation model by capturing the constitutive relations. In this analysis presented in appendix C and highlighted in section 3, compares sophisticated calibration methods to more standard approaches that require less information for calibration. This section discusses the considered calibration methods, focusing on their applicability and accuracy in combination with the numerical large-strain consolidation approach to settling column data from the laboratory.

The Nuclear Magnetic Resonance (NMR) method has been proven to fit the data found in the settling column properly. This method obtains a high accuracy because its able to find the water content at each height of the calibration column. Due to back-calibration, the parameters can be found to fit the power-laws of the constitutive relations proposed by Merckelbach, 2000. It can be observed that the uncertainty in this method increases in the tail of the settling column data. The NMR fit of the 500 mL column is corresponding well. However, the 100 mL and 250 mL fits are less accurate (appendix c). This is due to a sudden leakage that occurred during the NMR measurement procedure at TU/e. As a result, this could lead to inaccuracies in the estimation of K_k . However, the work of Myouri (In prep) proves that the NMR calibration method provides strong matches with the observed consolidation behaviour observed in the laboratory. Another explanation could be the fact that the settling columns did not have the same initial density due to inaccuracies coming with the usage of the DMA50 density meter when setting up the settling columns. Nevertheless, the NMR method is able to detect the density profiles over time of the sample tested, it was able to detect the maximum densification behaviour for the material tested in this thesis. This behaviour is likely to occur due to particles reaching a densification limit for which particles are further incompressible. Therefore, it is not right to assume that every material will behave according to the perfect Gibsonian profiles. Sophisticated calibration methods need to be utilized to be certain of the expected densification behaviour of the material; according to ordinary Gibson or the modified Gibson approach. Detecting this behavior can significantly impact the simulation outcomes in terms of the volume of material required and the duration of consolidation, which has the potential to significantly affect project costs.

The Analytical Solution method seems to over-estimate the consolidation data in the first half of consolidation of the settling column, while the tail of the settling column data is fitted perfectly by this method. This could be due to the fact that the initial concentration of the settling column was high whereas the assumption K_σ is completely valid. The relatively steep consolidation at the beginning half of the column suggests that this method could work well when materials are used at more diluted concentrations. This method requires only consolidation data from a settling column, which makes this method less demanding than a NMR method. However, this calibration method is straightforward and was often used at Deltares to obtain the calibration parameters for the power-laws of the constitutive relations. It seems that the Analytical Solution method does not obtain perfectly fitting approximations of the consolidation observed in the laboratory, but is capable of giving a first estimate of the consolidation behaviour of the material when almost no information is available. However, this method assumes that the profile of the material obtains a ordinary Gibson profile which has been proven not to be always the case. This method can be improved by using a Ultra-sonic High Concentration Meter (Chassagne, 2021) to measure the density profile after consolidation enabling a more accurate estimation of whether the material follows ordinary Gibson or modified Gibson behavior.

The Carrier & Beckham method does not provide a reliable solution for the consolidation behavior observed in the laboratory. This method shows poor correspondence with the observed data, likely due to the empirical nature of its power-law calibration constants. These constants are derived from index properties, which are prone to high uncertainty during testing. The poor estimations may stem from measurement errors in the laboratory tests of index properties for the material used in this study. However, back-fitting the observed behavior in the settling column with the calibration constants allows for the generation of a relatively accurate profile. It remains unclear whether the uncertainty associated with this method arises from measurement errors in the laboratory for obtaining the Attenberg limits or is due to empirical constraints of this method. Additionally, the method assumes that the density profiles obtains a ordinary Gibsonian profiles, which may not fully applicable to estimate the behaviour of materials obtaining maximum densification. A re-evaluation of this method's applicability using a bigger dataset to validate is recommended to make a better assessment of this calibration method.